University of Windsor
Scholarship at UWindsor

Electronic Theses and Dissertations | Theses, Dissertations, and Major Papers

9-26-2018

Towards Putting the 'P' in Perovskite: Exploring the Reactivity of Phosphonium Salts with Group 14 Halides

Emily Helen Omahen
University of Windsor

Follow this and additional works at: https://scholar.uwindsor.ca/etd

Recommended Citation

Omahen, Emily Helen, "Towards Putting the 'P' in Perovskite: Exploring the Reactivity of Phosphonium Salts with Group 14 Halides" (2018). *Electronic Theses and Dissertations*. 7552.
https://scholar.uwindsor.ca/etd/7552

This online database contains the full-text of PhD dissertations and Masters' theses of University of Windsor students from 1954 forward. These documents are made available for personal study and research purposes only, in accordance with the Canadian Copyright Act and the Creative Commons license—CC BY-NC-ND (Attribution, Non-Commercial, No Derivative Works). Under this license, works must always be attributed to the copyright holder (original author), cannot be used for any commercial purposes, and may not be altered. Any other use would require the permission of the copyright holder. Students may inquire about withdrawing their dissertation and/or thesis from this database. For additional inquiries, please contact the repository administrator via email (scholarship@uwindsor.ca) or by telephone at 519-253-3000ext. 3208.

Towards Putting the 'P' in Perovskite: Exploring the Reactivity of Phosphonium Salts with Group 14 Halides

By

Emily Helen Omahen

A Thesis
Submitted to the Faculty of Graduate Studies
through the Department of Chemistry and Biochemistry
in Partial Fulfillment of the Requirements for
the Degree of Master of Science
at the University of Windsor

Windsor, Ontario, Canada

2018

© 2018 Emily Helen Omahen

Towards Putting the 'P' in Perovskite: Exploring the Reactivity of Phosphonium Salts with Group 14 Halides

by

Emily Helen Omahen

APPROVED BY:

_____

C. Weisener
Great Lakes Institute for Environmental Research

_____

J. Rawson
Department of Chemistry & Biochemistry

_____

C. Macdonald, Advisor
Department of Chemistry & Biochemistry

September 18th, 2018

DECLARATION OF ORIGINALITY

I hereby certify that I am the sole author of this thesis and that no part of this thesis has been published or submitted for publication.

I certify that, to the best of my knowledge, my thesis does not infringe upon anyone's copyright nor violate any proprietary rights and that any ideas, techniques, quotations, or any other material from the work of other people included in my thesis, published or otherwise, are fully acknowledged in accordance with the standard referencing practices. Furthermore, to the extent that I have included copyrighted material that surpasses the bounds of fair dealing within the meaning of the Canada Copyright Act, I certify that I have obtained a written permission from the copyright owner(s) to include such material(s) in my thesis and have included copies of such copyright clearances to my appendix.

I declare that this is a true copy of my thesis, including any final revisions, as approved by my thesis committee and the Graduate Studies office, and that this thesis has not been submitted for a higher degree to any other University or Institution.

ABSTRACT

Inorganic/organic hybrid perovskites have emerged as synthetic materials that exhibit light-harvesting properties. Although perovskites with alkylammonium cations have been previously reported, a perovskite family with phosphonium cations has not been investigated. Firstly, a library of phosphonium salts was made with the intention of further reaction with the group 14 halides towards creating a perovskite crystal. The composition of these salts were elucidated via NMR spectroscopy, and the crystal structures of three of the phosphonium salts were determined. The phosphonium iodide salts were then reacted with the lead, tin, and germanium iodides and bromides to discover if variant perovskitic structures are obtained. The reaction of lead(II) iodide with various phosphonium salts produced a charge-balanced network of PbI_3^- fragments connecting in a face-sharing octahedral motif. These phosphonium-templated iodoplumbates were found to possess semi-conducting properties, as suggested by the results of UV-Vis and their high thermal stability was confirmed by TGA experiments. Three novel crystal structures were isolated from reaction of phosphonium salts with tin(II) and tin(IV) iodide, each of them producing an iodostannate anion with a unique geometry. In a reaction with SnI_4 an unpredictable oxidation of starting material produced a potentially Lewis acidic tin(IV) cation. Finally, the reaction of phosphonium salts with germanium(II) halides produced charge-balanced compounds with an ABX_3 general formula that did not crystallize in a perovskitic manner. Germanium(IV) iodide formed a series of co-crystals when reacted with the phosphonium iodide salts. These species were found to form Ge-I···I halogen-bonding interactions.

ACKNOWLEDGEMENTS

Some of the best journeys we take in life are often the ones that are unexpected. I never planned on going to graduate school, but after the conclusion of my undergraduate degree I had a gut feeling that it was something I should pursue. I am certainly glad I chose to take this path, as I have grown a lot over the past two years as a chemist and a person. It wasn't easy to juggle graduate studies, teaching, and being an elite athlete and I would like to thank all of the people who supported me on this journey and made the completion of this degree possible.

Firstly, I would like to thank my supervisor, Dr. Chuck Macdonald, for his support and guidance throughout my graduate studies as well as during my undergraduate degree. I joined the Macdonald Research Group as an Outstanding Scholar in my second year, and ever since then Chuck has been instrumental in my development as a chemist and moreover as a researcher. Not only did he answer the questions I had with regards to my projects, he also taught me how to ask the questions that needed an answer, and ultimately that is what research is about. I would also like to thank my other committee members, Dr. Weisener and Dr. Rawson, for taking the time to read this thesis.

I would like to thank Justin Binder and Dr. Stephanie Kosnik for taking me under their wings when I was an undergrad and being outstanding mentors. Not only did they train me in all the areas I needed to be a good chemist, but they were always available to troubleshoot research problems with me and find a solution. Thank you to Ala'aeddeen Swidan and Brad Jacobs for being there to bounce ideas off, in both

chemistry and in life, and for their constant life chats. I'd also like to thank the other members of the Macdonald Group, past and present, for all the laughs that we have had in the office, most of the time at the expense of each other. Thanks to Max, Louae, and Balakey for being the most comical group of 410 students around.

I'd also like to thank the friends I have made during my time as part of the department. To Nadia Stephaniuk, thank you for being the best roommate I could have asked for. You have always brought positive energy to any situation, even when I needed to rant. To Dominique Leckie, thank you for being someone I can depend on to talk about anything from chemistry to life choices. To Lara Watanabe, thank you for also being someone that I can chat with, vent to about thesis things, and talk about the crazy East Coast weather with. To Adit and Dan, thanks for helping to make my first chemistry conference such a lit time. These people have truly made my experience in graduate school one to remember.

There are also so many people outside the department that I'd like to thank. Last May, I was seriously considering dropping out of the program, and without these people I would not have been able to persevere and write this thesis. To my coach, Brett Lumley, thank you for your guidance on and off the track throughout the course of my degree. Thank you for being so accommodating when I had deadlines or experiments to run, and helping me balance being an elite athlete with being a graduate student. Not only have you made me a better athlete, but you have also made me a better person. To Ben Warnock, who is pretty much my big brother, thank you for constantly pushing me to achieve my goals and being a great inspiration for overcoming adversity. To Mayce Mirza, Joanne Yu, Matthew

McLaughlin, and Leslie Hernandez, thank you for never allowing me to give up on my studies and, in a broader sense, my overall life goals. Each of you has inspired me in your own way to keep "reaching for the stars" (as cheesy as that sounds) and to keep going after my passion. You are all success stories in your own way and I feel privileged that I was able to watch each of you achieve your goals. I hope one day I may be as successful as you.

I would also like to thank my loving and supportive parents and sister. Although I may not always show it, I truly appreciate all the times you let me take the car to go to lab, all the times you let me pack the leftovers for lunch, and for the constant nagging that pushed me to finish my thesis. Thank you for inspiring me to never give up on my dreams. Finally, I would like to thank my amazing boyfriend, Randall Beardy, who is literally my beacon of sunshine. Thank you for your constant optimism and wisdom. You have supported me from the beginning of this Master's degree and your belief in me has never wavered. You keep saying that I am a superstar, and in the past I didn't quite believe you, but now I do. Thank you.

TABLE OF CONTENTS

DECLARATION OF ORIGINALITY iii

ABSTRACT iv

ACKNOWLEDGEMENTS v

LIST OF TABLES xi

LIST OF FIGURES xii

LIST OF SCHEMES xv

LIST OF ABBREVIATIONS/SYMBOLS xvi

LIST OF APPENDICES xviii

CHAPTER 1: An Introduction to Inorganic/Organic Hybrid Perovskites 1

1.1 Introduction 1

1.2 References 26

CHAPTER 2: Synthesis of Novel Phosphonium Salts 42

2.1 Introduction 42

2.2 Results & Discussion 44

2.2.1 Synthesis of Monophosphonium Salts 44

2.2.2 Synthesis of Diphosphonium Salts 56

2.2.3 Chapter Conclusions 70

2.3 Experimental 71

2.4 References 77

CHAPTER 3: Phosphonium-Templated Iodoplumbates 83

3.1 Introduction 83

3.2 Results & Discussion 84

3.3 Experimental 95

3.4 References 98

CHAPTER 4: Synthesis of a Novel Iodotin Trianion 104

4.1 Introduction 104

4.2 Results & Discussion 105
4.2.1 Reactions of Phosphonium Salts with Tin(II) Halides 105
4.2.2 Reactions of Phosphonium Salts with Tin(IV) Iodides 114
4.2.3 Chapter Conclusions 127
4.3 Experimental 128
4.4 References 132

CHAPTER 5: Phosphonium-Templated Halogermanates 139
5.1 Introduction 139
5.2 Results & Discussion 140
5.2.1 Reactions with Germanium(II) Halides 140
5.2.2 Reactions with Germanium(IV) Iodide 152
5.2.3 Chapter Conclusions 168
5.3 Experimental 168
5.4 References 174

CHAPTER 6: Conclusions & Future Work 181
6.1 Conclusions 181
6.2 Future Work 183
6.3 References 185

APPENDICES 190
Appendix A: Crystallographic Data and Refinement Parameters from Chapter 2 190
A1: Tetramethylphosphonium Iodide 190
A2: Trimethylphosphonium Iodide 191
A3: [(Diphenylphosphino)methyl]methyldiphenylphosphonium iodide 192
Appendix B: Crystallographic Data and Refinement Parameters from Chapter 3 193
B1: Tetramethylphosphonium Lead Triiodide 193
B2: Tri(n-butyl)phosphonium Lead Triiodide 194
B3: Methyltriphenylphosphonium Lead Triiodide 195
B4: Bis(trimethylphosphonio)ethane Lead Triiodide 196
Appendix C: Crystallographic Data and Refinement Parameters from Chapter 4 197
C1: $[HPMe_3]_4[I][SnI_5]$ 197
C2: $[(O{=}PMe_3)_3SnI_3]_2[SnI_6]$ 198
C3: $[PMePh_3][SnI_5]$ 199

Appendix D: Crystallographic Data and Refinement Parameters from Chapter 5 200
D1: Trimethylphosphonium Triiodogermanate 200
D2: Tetramethylphosphonium Tribromogermanate 201
D3: [PPh_4][I](GeI_4).....202
D4: [$PMePh_3$][I](GeI_4)$_2$ 203
D5: [$C_8H_{22}P_2$][I]$_2$(GeI_4) 204
VITA AUCTORIS 205

LIST OF TABLES

Table 2.1: Summary of the ^{1}H NMR Spectrum of $[HP(n\text{-}bu)_3][I]$**……...52**

Table 2.2: Summary of the $^{13}C\{^{1}H\}$ NMR Spectrum of $[HP(n\text{-}bu)_3][I]$**…….53**

Table 2.3: Selected Metrical Parameters of Compound 2.3.8**……63**

Table 2.4: Summary of ^{1}H NMR Shifts in Dimethylated dppp**……66**

Table 2.5: Summary of the ^{1}H NMR Spectrum of Bis(methyldiisopropylphosphonio)propane Iodide**……...……..70**

Table 4.1: Summary of the Key Metrical Parameters in $[(O{=}PMe_3)_3SnI_3][SnI_6]$**……..119**

Table 4.2: Summary of the ^{1}H NMR Spectrum of $[PMePh_3][I] + SnI_4$**……..123**

Table 4.3: Summary of the ^{13}C NMR Spectrum of $[PMePh_3][I] + SnI_4$**……..……..124**

Table 5.1: Summary of the $^{13}C\{^{1}H\}$ NMR Spectrum of the Reaction of $[PMePh_3][I] + GeI_2$**…….146**

Table 5.2: Summary of the ^{1}H NMR Spectrum of $[PPh_4][Br] + GeBr_2$**……152**

Table 5.3: Summary of the $^{13}C\{^{1}H\}$ NMR Spectrum of $[PPh_4][Br] + GeBr_2$**…….……152**

Table 5.4: Summary of the ^{1}H NMR Spectrum of $[PPh_4][I](GeI_4)$**……..152**

Table 5.5: Summary of the $^{13}C\{^{1}H\}$ NMR Spectrum of $[PPh_4][I](GeI_4)$**……..156**

Table 5.6: A Summary of the Key Metrical Parameters in $[PPh_4][I](GeI_4)$**…….158**

LIST OF FIGURES

Figure 1.1: The Main Group Elements in the s-block and p-block of the periodic table……...……2

Figure 1.2: The Tetrahedral Structure of White Phosphorus…….……3

Figure 1.3: The Fragmentation Method of Assigning Oxidation Numbers: Heterolytic Cleavage of Hydrogen Bromide……...…4

Figure 1.4: Lewis Structure of Hydrogen Peroxide……..6

Figure 1.5: Lewis Structure of Dichloromethane……..6

Figure 1.6: Lewis Structure of the Phosphonium Ion……...7

Figure 1.7: Phosphorus' Most Common Oxidation States……8

Figure 1.8: A Survey of Possible Oxidation States for Group 14…..……...……9

Figure 1.9: The General Perovskite Crystal Structure…….10

Figure 1.10: The Distortion of Perovskite at High Pressures…….12

Figure 1.11: Jahn-Teller Elongation and Compression…….……14

Figure 1.12: The Goldschmidt Tolerance Factor Equation…….……...15

Figure 1.13: A Functioning Perovskite Solar Cell……...17

Figure 1.14: The Black Polymorph of $CsSnI_3$…….18

Figure 1.15: Methylammonium and Formamidinium Cations……20

Figure 1.16: Methylammonium Germanium Iodide Perovskite……..20

Figure 1.17: Trimethylsulfonium Lead Triiodide……...21

Figure 1.18: Outline of Potential Phosphorus-Containing Perovskites Explored in this Thesis……26

Figure 2.1: Common Phosphine Ligands……42

Figure 2.2: Crystal Structure of $[PMe_4][I]$…….……46

Figure 2.3: ^{1}H NMR Environments of $[HPMe_3][I]$……48

Figure 2.4: $^{31}P\{^{1}H\}$ and ^{31}P NMR Spectra of $[HPMe_3][I]$…….49

Figure 2.5: Crystal Structure of $[HPMe_3][I]$……50

Figure 2.6: ^{1}H Environments in Tri(n-butyl)phosphonium iodide……..52

Figure 2.7: ^{13}C Environments in Tri(n-butyl)phosphonium iodide**…….53**

Figure 2.8: ^{13}C Environments in Tri(n-butyl)methylphosphonium iodide**……..54**

Figure 2.9: ^{1}H NMR Environments in Tri(n-butyl)methylphosphonium iodide**….56**

Figure 2.10: [Diphenylphosphino)methyl]methyldiphenylphosphonium iodide**...60**

Figure 2.11: Crystal Structure of Compound 2.3.8**…….62**

Figure 2.12: ^{1}H NMR Environments of bis(methyldiphenylphosphonio)propane iodide**……...……66**

Figure 2.13: ^{13}C NMR Environments of Dimethylated Dppp**……67**

Figure 2.14: Bis(methyldiisopropylphosphonio)propane Iodide**……68**

Figure 2.15: ^{1}H NMR Environments of Bis(methyldiisopropylphosphonio)propane iodide**……...69**

Figure 3.1: Monophosphoniums Reacted with PbI_2**……84**

Figure 3.2: The $[PbI_3]_\infty$ Chains of $[PMe_4][PbI_3]$**…….87**

Figure 3.3: Face-Sharing Octahedra of Monophosphonium-Templated Iodoplumbates**……...……..88**

Figure 3.4: Crystal Packing of the Monophosphonium-Templated Iodoplumbates**.....89**

Figure 3.5: Face-Sharing Octahedra of the $[PbI_3]_\infty$ Chain in $[P_2C_8H_{22}][Pb_2I_6]$**…..90**

Figure 3.6: The Crystal Packing of $[P_2C_8H_{22}][Pb_2I_6]$**……..91**

Figure 3.7: UV-Vis Spectra of the Phosphonium-Templated Iodoplumbates**…….92**

Figure 3.8: TGA Curves of the Phosphonium-Templated Iodoplumbates**……..93**

Figure 4.1: Unit Cell Contents of $[HPMe_3][I][SnI_5]$**……107**

Figure 4.2: Crystal Structure of $[HPMe_3][I][SnI_5]$**……108**

Figure 4.3: ^{1}H and ^{13}C NMR Environments of $[PPh_4][I]$**……..110**

Figure 4.4: $^{31}P\{^{1}H\}$ NMR Spectrum of the Product Mixture of $[HPMe_3][I]$ + SnI_4**……116**

Figure 4.5: Crystal Structure of $[(O=PMe_3)_3SnI_3][SnI_6]$**……..117**

Figure 4.6: Crystal Packing of $[(O=PMe_3)_3SnI_3][SnI_6]$ Normal to (001)**…….120**

Figure 4.7: The Equation for the Gutmann-Beckett Method**……121**

Figure 4.8: Crystal Structure of $[PMePh_3][SnI_5]$**……..……125**

Figure 5.1: Crystal Structure of $[HPMe_3][GeI_3]$**……142**

Figure 5.2: Unit Cell Contents of $[HPMe_3][GeI_3]$ Normal to (100)**……..143**

Figure 5.3: ^{13}C NMR Environments in $[PMePh_3][I]$**……146**

Figure 5.4: Crystal Structure of $[PMe_4][GeBr_3]$**……148**

Figure 5.5: Unit Cell Contents of $[PMe_4][GeBr_3]$ Normal to (100)**…….149**

Figure 5.6: Unit Cell Contents of $[PMe_4][GeBr_3]$ Normal to (001)**…….150**

Figure 5.7: Crystal Structure of $[PPh_4][I](GeI_4)$**……157**

Figure 5.8: A Halogen Bond Interaction**……...159**

Figure 5.9: Halogen Bonding Interaction in $[PPh_4][I](GeI_4)$**…….160**

Figure 5.10: Crystal Structure of $[PMePh_3][I](GeI_4)$**……161**

Figure 5.11: Crystal Structure of $[C_8H_{22}P_2][I]_2(GeI_4)$**……..165**

Figure 5.12: Halogen Bonding Interaction in $[C_8H_{22}P_2][I]_2(GeI_4)$**……...166**

Figure 5.13: Unit Cell Contents of $[C_8H_{22}P_2][I]_2(GeI_4)$ Normal to (001)**…….167**

LIST OF SCHEMES

Scheme 2.1: Protonation of Phosphine**……...43**

Scheme 2.2: Alkylation of Phosphine**…….....43**

Scheme 2.3: Novel Synthesis of Tetramethylphosphonium Iodide**……...44**

Scheme 2.4: Novel Synthesis of Trimethylphosphonium Iodide**...……47**

Scheme 2.5: Protonation of Dmpe**……..57**

Scheme 2.6: Methylation of Dmpe**…….58**

Scheme 2.7: Methylation of Dppp**……64**

Scheme 4.1: Reaction Scheme of the Synthesis of $[HPMe_3]_4[SnI_5][I]$**……..…..106**

Scheme 4.2: Reaction of $[PMePh_3][I]$ with SnI_4**……..122**

Scheme 5.1: Reaction of $[HPMe_3][I]$ with GeI_2**……...140**

Scheme 5.2: Reaction of $[PMe_4][I]$ with $GeBr_2$**……...…147**

Scheme 5.3: Reaction of $[PPh_4][Br]$ with $GeBr_2$**…….…….151**

Scheme 5.4: Reaction of $[PMe_4][I]$ with GeI_4**……..……153**

Scheme 5.5: Reaction of $[PPh_4][I]$ with GeI_4**……...……155**

Scheme 5.6: Reaction of Bis(trimethylphosphonio)ethane Iodide with GeI_4**…...163**

LIST OF ABBREVIATIONS/SYMBOLS

Å	Angstrom
AVC	antisolvent vapor-assisted crystallization
Bu	Butyl
CB	conduction Band
CSD	Cambridge Structural Database
Cy	Cyclohexyl
δ	chemical shift (NMR)
d	doublet (NMR)
DCM	Dichloromethane
DFT	Density Functional Theory
dippp	bis(diisopropylphosphino)propane
DMF	dimethyl formamide
dmpe	bis(dimethylphosphino)ethane
DMSO	Dimethylsulfoxide
dppm	bis(diphenylphosphino)methane
dppp	bis(diphenylphosphino)propane
ESD	estimated standard deviation
eV	Electronvolt
FA	Formamidinium
FTO	Fluorine-doped tin oxide
HOMO	highest occupied molecular orbital
IR	Infrared
IUPAC	International Union of Pure and Applied Chemistry
ITC	inverse temperature crystallization
J_{XY}	coupling constant between nuclei x and y
LUMO	lowest unoccupied molecular orbital
m	multiplet (NMR)
M	nondescript metal
MA	Methylammonium
Me	Methyl
MeCN	Acetonitrile
mmol	Millimole
NMR	Nuclear Magnetic Resonance
PCE	power conversion efficiency
Ph	Phenyl
PL	photoluminescence
ppm	parts per million
PSC	perovskite solar cell
q	quartet (NMR)

R	organic substituent
RP	Ruddlesden-Popper
s	singlet (NMR)
sept	septet(NMR)
t	triplet (NMR)
TGA	thermogravimetric analysis
THF	Tetrohydrofuran
UV	Ultraviolet
VB	valence band
Vis	Visible
VSEPR	Valence Shell Electron-Pair Repulsion Theory
X	Halogen
1D	one-dimensional
3D	three-dimensional

LIST OF APPENDICES

Appendix A: Crystallographic Tables from Chapter 2**……190**

Appendix B: Crystallographic Tables from Chapter 3**……192**

Appendix C: Crystallographic Tables from Chapter 4**……195**

Appendix D: Crystallographic Tables from Chapter 5**……197**

CHAPTER 1: An Introduction to Inorganic/Organic Hybrid Perovskites

1.1 Introduction

1.1.1 An Overview of Main Group Chemistry

Main group chemistry is arguably one of the most fascinating fields in modern science. It focuses on the study of elements contained in the s-block and p-block[1], which makes it a very rich and diverse topic. The main group elements are comprised of metals, nonmetals and metalloids included in groups 1, 2, and 13-18.[1] Metals and nonmetals can be roughly distinguished by electronegativity, or the tendency of an atom in a bond to attract electrons toward itself.[1] In general, metals have an electronegativity of less than 2.0 whereas nonmetals have electronegativities greater than 2.2.[1] Furthermore, metals are able to conduct heat and electricity, while nonmetals are insulators. In the periodic table, metallic character increases going down a column and decreases going from left to right across a period.[1] Some of the main group elements do not fit in either of the nonmetal or metal categories, however. These elements are termed "metalloids" and have intermediate electronegativities to the metals and nonmetals. Metalloids also display limited electrical conductivity, however this increases with temperature.[1] Figure 1.1 provides a pictorial representation of the main group elements as they appear in the periodic table and their classifications as metals, nonmetals, or metalloids. Given the wide scope of elements that belong to the main group, it is no surprise that main group chemistry also has a wealth of real-world applications.

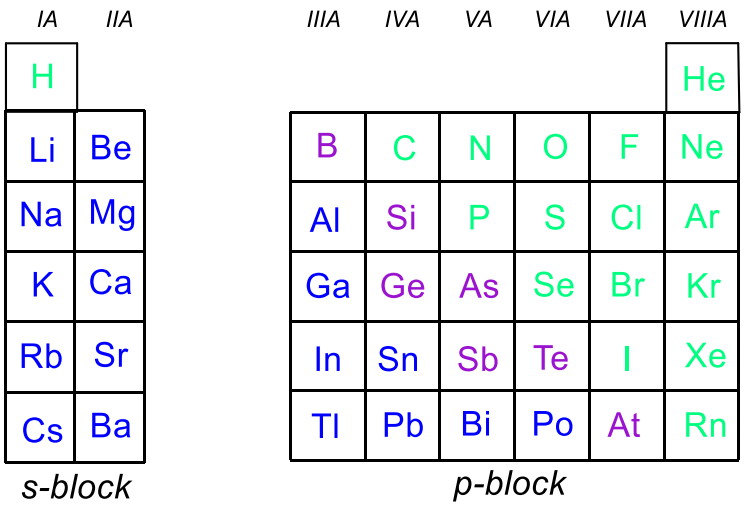

Figure 1.1: The Main Group Elements in the s-block and p-block of the periodic table. Elements with green text are nonmetals, elements with purple text are metalloids, and elements with blue text are metals.[1]

The chemistry in the Macdonald Research Group here at the University of Windsor primarily revolves around main group elements in low oxidation states and atypical bonding environments. Our research focuses on phosphorus in various oxidation states and contributes to the current chemical bonding knowledge of elements ranging from group 13 to the halogens. This thesis will deal with elements in groups 15 and 14.

In the Periodic Table of Elements, the Group 15 elements are sometimes called the 'pnictogens', which is derived from the Greek word *pniktos*, which means "to strangle".[2] This group contains the elements nitrogen, phosphorus, arsenic, antimony, and bismuth. These elements occur naturally in various states and forms. Nitrogen occurs in nature as a non-metal gas and makes up 78.1% of our atmosphere.[1] Phosphorus is a non-metal solid that has several allotropes, arsenic and antimony are metalloid solids, and bismuth is a solid metal. The pnictogens possess 5 valence electrons and commonly occur in the +5 or

+3 oxidation states.[1] The behaviour of the pnictogens in each unique oxidation state varies. A more detailed discussion of oxidation states will follow in section 1.1.2.

As previously stated, phosphorus occurs in various allotropes. An allotrope can be defined as one of two or more physical forms in which an element can exist.[3] One of the allotropes, white phosphorus, has a chemical formula of P_4 and exists as a solid, liquid, or gas.[1] Its tetrahedral structure is shown in Figure 1.2. White phosphorus is extremely pyrophoric; however it is widely used as a reagent in inorganic synthesis. Red phosphorus, another allotrope, is rather inert in comparison to white phosphorus and has a structure in the solid state that is very difficult to model.[4] Black phosphorus is the most stable allotrope and has a rhombohedral form in the solid state.[1]

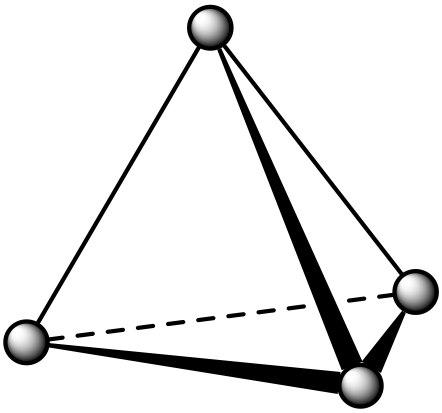

Figure 1.2 The Tetrahedral Structure of White Phosphorus.[1] The silver balls represent phosphorus atoms.

Group 14 is arguably one of the most fascinating groups of the periodic table. It is comprised of the elements carbon, silicon, germanium, tin, and lead. Carbon is a nonmetal, silicon and germanium are metalloids, and tin and lead are metals. Group 14 elements are often termed the 'tetrels' because they contain four valence electrons.[1] This thesis deals

with germanium, tin, and lead, and these tetrels typically exist in the +2 or +4 oxidation states. Whether a group 14 element exists in the +2 or +4 oxidation state helps one gain an understanding of its chemical behaviour.

1.1.2 Oxidation and Valence States

In order to predict the type of bonding an element may take part in and thus in order to understand its reactivity, one must have a grasp on the concept of oxidation states. Parkin[5] defines an oxidation state to be the charge an atom would have if all ligands were heterolytically cleaved from it. Thus, for each ligand removal, the electrons would be given to the most electronegative atom. For example, in hydrogen bromide the electron pair used for bonding would be given to bromine if the molecule underwent heterolytic cleavage. Thus, hydrogen would have a +1 oxidation state and bromine would have a -1 oxidation state. This is called the Fragmentation Method of Assigning Oxidation Numbers[5] and it is illustrated in Figure 1.3.

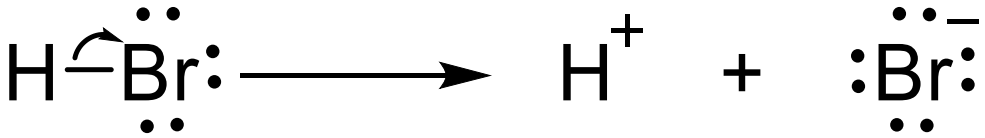

Figure 1.3: The Fragmentation Method of Assigning Oxidation Numbers[5]:Heterolytic Cleavage of Hydrogen Bromide.

Therefore, the oxidation state of an atom can be expressed by subtracting the charge on each of the ligands from the total charge of the compound. In the hydrogen bromide example, the total charge of the compound is 0, so the oxidation state of hydrogen would therefore be 0- (-1), which is +1. Although this model is useful in determining oxidation

states in redox reactions, it is not always appropriate for assigning the oxidation states of p-block and transition metal compounds due to chemically unintuitive results.

Valence state is another model that is used to rationalize the potential reactivity and bonding of a particular atom. According to Parkin[5], the valence state of an atom is simply the number of electrons an atom uses in bonding (or chemistry). On rare occasions the valence state and absolute value of the oxidation state of an atom may be equal, however it is merely by coincidence that this occurs. Beryllium hydride is a good example of when the oxidation state and valence state are equal by coincidence. Beryllium has an oxidation state of +2 in this compound since hydrogen is more electronegative and adopts the electrons upon heterolytic bond cleavage. By the valence state model, beryllium has an equal valence state of 2 because it uses two electrons to make bonds with the hydrogen ligands.

The oxidation state and valence state of an atom fails to be equivalent in three different situations as described by Parkin[5]. The first situation occurs when a homonuclear bond is present, as in hydrogen peroxide. Hydrogen peroxide is electrically neutral, meaning that all of the oxidation states on each atom must balance out to zero. Since hydrogen has a +1 oxidation state in this compound, oxygen must have a -1 charge. In comparison, the valence model suggests that oxygen is bivalent (valence state of 2) since two electrons are involved in bonding for each atom.

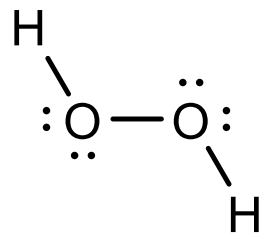

Figure 1.4: Lewis Structure of Hydrogen Peroxide.

Another situation where the oxidation state and valence state are not equivalent is when two of the ligands that dissociate from the atom of interest have equal and opposite charges[5]. A clear example occurs in the common electrically neutral solvent, dichloromethane. The carbon atom has a valence state of 4 since it uses 4 electrons to bind its ligands, however its oxidation state is 0 because hydrogen (+1) and chlorine (-1) have oxidation states that cancel each other out. Lastly, when the overall molecule is charged and the ligand that dissociates from the atom in question is a cation, it is impossible for that atom to have identical valence and oxidation states.[5] This situation is illustrated by the phosphonium (PH_4^+) ion. Phosphorus is pentavalent but has an oxidation state of -3 due to the proton ligand dissociation. Since the three situations presented above are quite common, examples of when the valence state is equal to the absolute value oxidation number are few and far between.

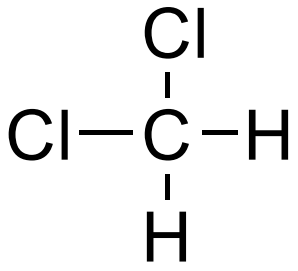

Figure 1.5: Lewis structure of Dichloromethane.

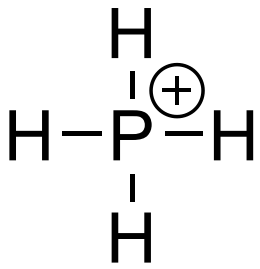

Figure 1.6: Lewis Structure of the Phosphonium Ion.

A model that is related, but not identical, to the valence state model is employed to unambiguously assign oxidation states to p-block elements. This model, proposed by Ellis and Macdonald[6], defines the oxidation state of an atom by the number of lone pairs associated with it. This model is preferred over the valence state model because it can consistently determine oxidation states as well as give insight into the chemical behaviour and structure of compounds with the same oxidation state.

Ellis and Macdonald's[6] oxidation state model is related to Parkin's[5] valence state model in that it assumes that for a given atom of interest, the atom is less electronegative than the than the other atoms to which it is bonded. A clear example occurs in the compound PF_5. Since fluorine is more electronegative than phosphorus, the central phosphorus atom has an oxidation state of +5. Another example in which the pnictogen centre is less electronegative than the ligands it is bound to occurs in trimethylphosphine, which is used as a reagent in this thesis. In this compound (PMe_3), the phosphorus atom adopts a +3 oxidation state due to the carbon atoms (-4 oxidation state) being more electronegative than both the phosphorus centre and the hydrogens (+1 oxidation state) bound to the carbons. Thus, it is most common to observe phosphorus in either a +3 or +5 oxidation state, however phosphorus has been observed by the Macdonald Group in the +1

state.[7–10] It is uncommon to have a negative or even-numbered oxidation state on phosphorus since this implies paramagnetism. An illustration of phosphorus in its common oxidation states with various coordination environments is shown below in Figure 1.7.

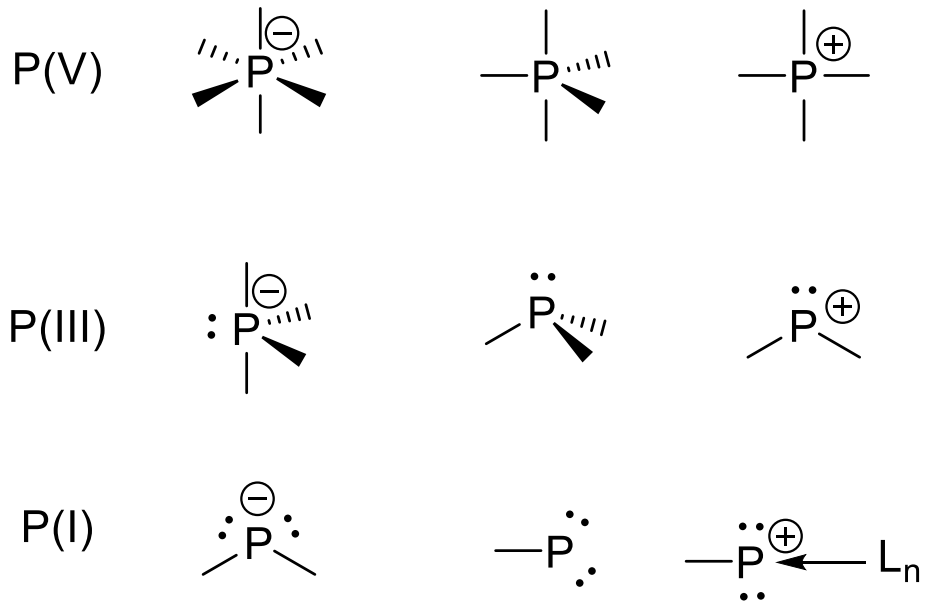

Figure 1.7: Phosphorus' Most Common Oxidation States.[6,7]

In addition to phosphorus, the group 14 elements germanium, tin, and lead will be prominent in this thesis, and thus their oxidation states should be discussed. The group 14 elements can adopt a much wider range of possible oxidation states than phosphorus. Based on Ellis and Macdonald's model[6], they can be assigned an oxidation state ranging from -4 to +4. Some of these oxidation states are more prevalent in nature than others. It is uncommon to find any of the group 14 elements in the +3 or +1 oxidation state because this indicates paramagnetism.[1] The most stable oxidation state for carbon, silicon, germanium, and tin is +4, whereas the most stable oxidation state for lead is +2.[1] It should be noted that tin and germanium can also be found in the +2 oxidation state. An illustration

of possible examples of zero and positive oxidation states for the group 14 elements is presented in Figure 1.8.

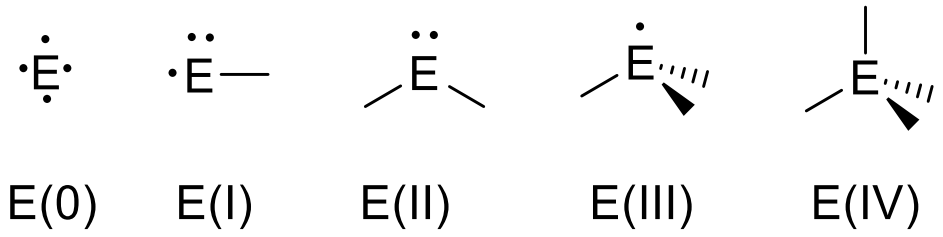

Figure 1.8: Prototypical examples of structures associated with various oxidation states for Group 14.[1]

The prominence of lower oxidation states as one descends group 14 can be explained by the inert pair effect.[1] The inert pair effect refers to the tendency of valence electrons in the outermost s-orbital to remain unionized.[11] In other words, the ns^2 electrons in the atom become more like core electrons and do not participate in bonding. This can be explained by the increase in ionization energy caused by a larger effective nuclear charge.

The Macdonald Group has taken advantage of the variance in elemental behavior with different oxidation states in our research. We have synthesized compounds that can be suitable for applications ranging from metathesis[10] to inorganic dyes[12] and thus we feel that we can make valuable contributions to a rapidly-growing family of compounds: the organic-inorganic hybrid perovskites.

1.1.3 Perovskites

Perovskites are undoubtedly one of the most fascinating topics of research in inorganic chemistry today. The perovskite mineral, calcium titanium oxide ($CaTiO_3$) was

discovered in 1839 by Gustav Rose in Russia and was named after Lev Perovski, a Russian minerologist.[13] After this discovery, all other materials that adopt the general formula of ABO_3 or ABX_3 are termed "perovskites". In these formulae, 'A' represents a large cation and 'BO_3' or 'BX_3' represents a polyatomic anion[13], with 'X' denoting a halogen atom. The crystal structure of a perovskite can be described as corner-sharing octahedra with a central cation. This motif can be best thought of as repeating cubic units with a cation in the center of each cube, as illustrated in Figure 1.6. In this diagram, the central blue sphere represents the 'A' cation, the pink spheres on the corners represent the 'B' cations within the polyatomic anions, and the green spheres on the edges of the cube represent the 'O' or 'X' anions. It is worthwhile to note that in the crystal structure of a perovskite, the 'B' cations become hexacoordinate as opposed to tricoordinate as suggested by the general formula. It is possible to obtain distorted perovskites in which the cubic structure appears buckled if the central 'A' cation is too large.

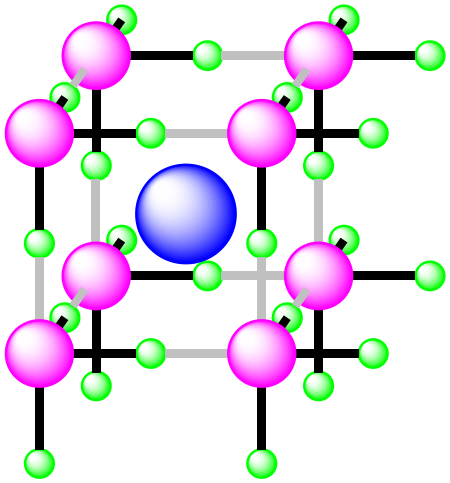

Figure 1.9: The General Perovskite Crystal Structure where the blue sphere represents the 'A' cation, the pink spheres represent the 'B' cations, and the green spheres represent the 'O' or 'X' anions.

The most common perovskite minerals are found within the Earth's crust. In fact, two out of the three primary components of Earth's lower mantle adopt a perovskite crystal structure. Bridgmanite or silicate perovskite, (Mg, Fe)SiO_3 and $CaSiO_3$, are two perovskites found below the Earth's surface.[14] There is also evidence of this perovskite in outer space, as (Mg, Fe)SiO_3 has been observed in the Tenham meteorite.[15] These minerals do not always exhibit the same motif adopted by an ideal perovskite, however. As the pressure increases from the surface to the Earth's lower mantle, the crystal structure of these perovskites become increasingly distorted.[16] This distortion was evaluated at increasing pressures in $YAlO_3$, $CaSnO_3$ and $GdFeO_3$ perovskites and it was discovered that the corner octahedra tilt slightly at higher pressures.[17] This is demonstrated in Figure 1.10, where an ABO_3 perovskite with slight distortion is depicted.

A transmission electron microscopy (TEM) study of magnesium-bearing bridgmanite has found that this perovskite undergoes phase transitions at higher temperatures and pressures in the Earth's lower mantle.[18] A phase transition from orthorhombic to tetragonal to cubic crystal systems was observed as the temperature increased moving closer to the Earth's core.[18] This provides further evidence that structural transitions in perovskites occur with increasing temperature and pressure.

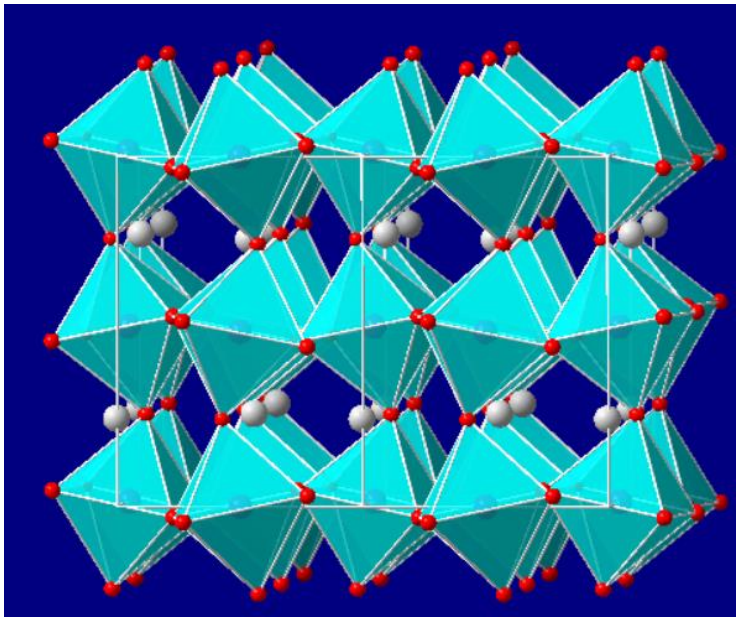

Figure 1.10: The Distortion of Perovskite at High Pressures.[19] The turquoise octahedra with red spheres on the vertices represent the BO_3^- anions and the grey spheres represent the A cations.

Although the most common perovskites found on Earth contain oxygen, there are naturally occurring perovskites that form from transition metals and halides. $MgCNi_3$, one of the transition-metal perovskites that has received a lot of attention due to its superconducting abilities, adopts the same cubic perovskite structure as seen in the oxide perovskites.[20] Another example of a transition-metal perovskite is Cs_3AuO.[21] This compound is very unique because its formula does not match the traditional structural formula for a perovskite. The three cesium atoms each have a +1 charge, the oxygen has a -2 charge, and the gold atom has a -1 charge. Interestingly, the anionic character of the gold varies with the alkali metal chosen, as a complimentary study of Rb_3AuO yielded a higher ionization energy in gold.[21] Neighborite, a well-studied perovskite with the formula $NaMgF_3$, is a naturally-occurring halogen-containing perovskite. It is reminiscent of

$MgSiO_3$ in that it also transitions from an orthorhombic to cubic crystal system as the temperature and pressure increases.[22]

In addition to the unique characteristics of their crystal structure, perovskites also have fascinating properties from both a theoretical and practical standpoint. Perovskites are good candidates for various applications in materials science because of their superconductivity, ionic conductivity, and magnetoresistance.[23] These properties indicate that perovskites could potentially be used in microelectronics, telecommunications, and even photoelectronics.[23]

Perovskites exhibit interesting properties due to their inherently flexible bond angles and the resulting deviations from the ideal octahedral structure that can take place. These deviations include slight tilting of the corner octahedrons (as previously discussed), displacement of the central "A" cation from the cube, and also the Jahn-Teller distortions of the corner octahedra.[24] Jahn-Teller distortion describes the spontaneous breaking of symmetry that occurs in a molecular system in order to lower its overall energy.[25] This typically occurs in octahedral or tetrahedral transition metal complexes[26] and has been observed in perovskites containing Cu^{2+} and Mn^{3+}.[24] Since perovskites exhibit a corner-sharing octahedral crystal structure[13], Jahn-Teller distortions will occur as either elongation or compression[26] as depicted in Figure 1.11. Elongation occurs when d-orbitals that have a z-component, namely the d_z^2, d_{xz}, and d_{yz} orbitals, decrease in energy, whereas compression occurs when the d-orbitals without a z-component (d_{xy}, $d_{x^2-y^2}$ orbitals) decrease in energy.[26]

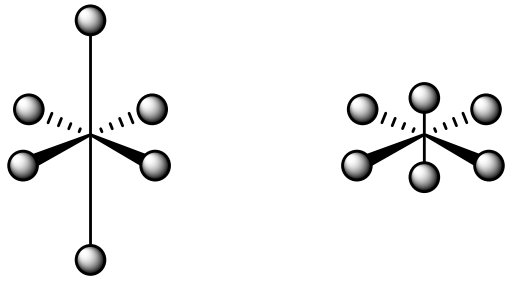

Figure 1.11: Jahn-Teller Elongation (left) and Compression (right).[26]

It is useful to quantify the distortion an ABO_3 or ABX_3 molecular system might experience in order to determine whether it will, in fact, form a perovskite. The Goldschmidt tolerance factor, *t*, for perovskites serves as an indication of the stability and amount of distortion of the crystal structure from the ideal cubic shape.[27,28] It describes how compatible an ion is to making the traditional perovskite crystal structure. An equation representing the relationship between the ionic radii and tolerance factor is depicted in Figure 1.12. R_A represents the ionic radius of the central cation, R_B represents the ionic radius of the cation within the polyatomic anion, and $R_{O\ or\ X}$ represents the ionic radius of oxygen or any halide. Materials with a calculated tolerance factor of 0.9-1.0 will have an ideal cubic structure and form a perovskite.[29] A tolerance factor of 0.71-0.9 indicates a material that adopts a distorted perovskite structure with tilted octahedra[29], which was previously visualized in Figure 1.7. Non-perovskite structures occur when the tolerance factor is greater than 1 or less than 0.71; the former case usually forms a hexagonal crystal system whereas the latter case usually forms an orthorhombic system.[29]

$$t = \frac{(R_A + R_B)}{[\sqrt{2}(R_{O\ or\ X} + R_B)]}$$

Figure 1.12: The Goldschmidt Tolerance Factor Equation[28].

Although the naturally-occurring perovskites have interesting crystal properties and a potential for useful applications, they have proven to be tedious to synthesize in the laboratory. The original perovskite, $CaTiO_3$, can be made in the laboratory setting by mixing $CaCO_3$ and TiO_2 in the solid state using a mortar and ethanol slurries for 3h. This product is then pressed into pellets and calcined in air at elevated temperature for 12h, and then broken up to repeat the process again.[30] $MgCNi_3$ perovskite is similarly synthesized using solid-state starting materials, which are ground together, made into a pellet, and heated at elevated temperature under a mixture of argon and hydrogen gas.[20] Once again, the pellet is broken up and the mixing-heating process is repeated before the final perovskite product is obtained. An even longer process is in place to synthesize the anionic gold perovskite, Rb_3AuO, which must remain untouched for six weeks after initial reaction before excess solid rubidium can be removed.[21]

The lengthiness of the oxide perovskites' syntheses is tolerated because of their remarkable properties such as superconductivity. Superconductivity refers to the phenomenon in which a material poses zero resistance to conducting electricity.[31] This property was first discovered in layered copper oxide perovskites at high temperatures[32] and further observed in barium oxide perovskites.[33,34] Non-traditional perovskitic structures have also demonstrated useful properties. The Ruddlesden-Popper (RP) phase of perovskite[35,36] has a general formula of $A_{n+1}B_nX_{3n+1}$ or $A_{n-1}A_2'B_nX_{3n-1}$, where A, A', and B are cations, X is an anion such as oxygen, and n is the number of layers of octahedra in

the crystal structure.[37] The RP phase perovskite $LaSr_3Fe_3O_{10}$ can be used as a rechargeable metal-air battery since the oxygen in the crystal lattice is easily removed.[38] The discovery of these properties in the oxygen-containing perovskites motivated the synthesis of more perovskitic materials that have their own unique properties and applications.

1.1.4 Organic-Inorganic Hybrid Perovskites

Inorganic-organic hybrid perovskites are most well studied because they can work as light-harvesting materials in solar cells. The use of solar cells has grown exponentially in recent years due to their ability to convert light energy from the sun directly to electrical energy.[39] Traditionally, rooftop solar cells are comprised of crystalline silicon and have power conversion efficiencies (PCEs) reaching up to 25%.[27,39,40] Other common types of solar cells include cadmium telluride (CdTe), gallium arsenide (GaAs), and copper indium gallium diseluride (CIGS), which all have PCEs exceeding 20%.[27,40] Perovskites have recently joined these materials in the ranks of possible materials for solar cells, as they have a comparable PCE of 20.1%[40] and are inexpensive in comparison to silicon and CdTe.[23]

In a perovskite solar cell (PSC), the perovskite layer absorbs light and electrons jump from the valence band (VB) to the conduction band (CB), leaving holes in the valence band. These holes allow electrical current to flow through the cell, which can power an electronic device.[39] The energy gap between the valence band and the conduction is called the bandgap and it represents the minimum energy required to excite an electron from the VB to the CB so electrical current may flow.[41] The band gap is equivalent to the HOMO/LUMO gap in molecular orbital theory, where the HOMO is the VB and the

LUMO is the CB.[42] Figure 1.13 depicts a functioning perovskite solar cell.[39] It should be noted that FTO (Fluorine-doped Tin Oxide) is a type of electrically conductive glass that is used to construct a wide range of optoelectronic devices.

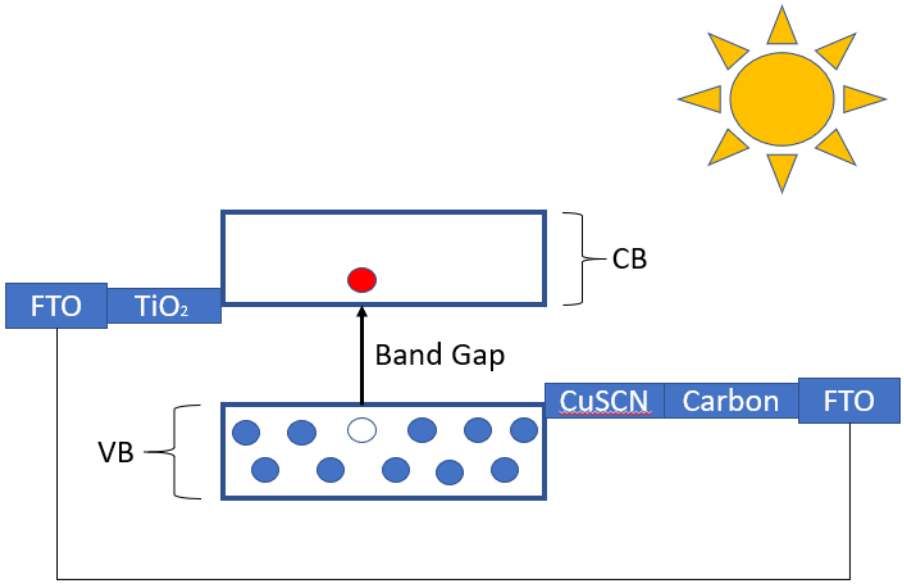

Figure 1.13: A Functioning Perovskite Solar Cell[39], showing the VB, the CB, and the band gap. The blue circles represent electrons in the VB, the red circle represents an excited electron that has gone to the CB, and the white circle represents a hole in the VB.

In recent years, main group halometallate perovskites have been extensively studied because of their ability to be used in solar cells as well as other important applications. Lead halide perovskites with the general formula of $APbX_3$ have been used as LEDs[43–45], lasers[46,47], photodetectors[48–51], and in facilitated water-splitting[52,53]. The Kanatzidis group[54–57] has pioneered the synthesis of main group halometallate perovskites. Their first perovskite synthesized was $CsSnI_3$[54] and it has the same structural formula (ABX_3) as the perovskites discussed above.[13] This perovskite undergoes complex transitions between two different polymorphs upon increases in pressure and temperature

in a similar fashion to bridgmanite[16,17] and neighborite[22]. One polymorph of $CsSnI_3$, depicted in Figure 1.14, is black in colour and functions as a p-type semiconductor.[54] P-type semiconductors are characterized by an electron hole in the crystalline lattice.[58] A neighboring electron fills the hole and leaves another hole adjacent to it. Thus, the hole is constantly moving from atom to atom. This occurs in the direction opposite to that of the electron flow. It is important to note that although the electrons move in p-type semiconductors, the atoms themselves stay stationary. In the $CsSnI_3$ perovskite, the hole is due to tin vacancies in the perovskite structure.[54] This black polymorph of $CsSnI_3$ has a narrow bandgap of 1.3eV[54], making it suitable for semiconducting applications. The black polymorph also exhibited near-IR photoluminescence (PL) at room temperature, making it a desirable candidate for non-invasive investigation of artefacts and paintings[59], optical amplifiers[60], fibre-optic and laser systems[61], and biomedical applications.[62]

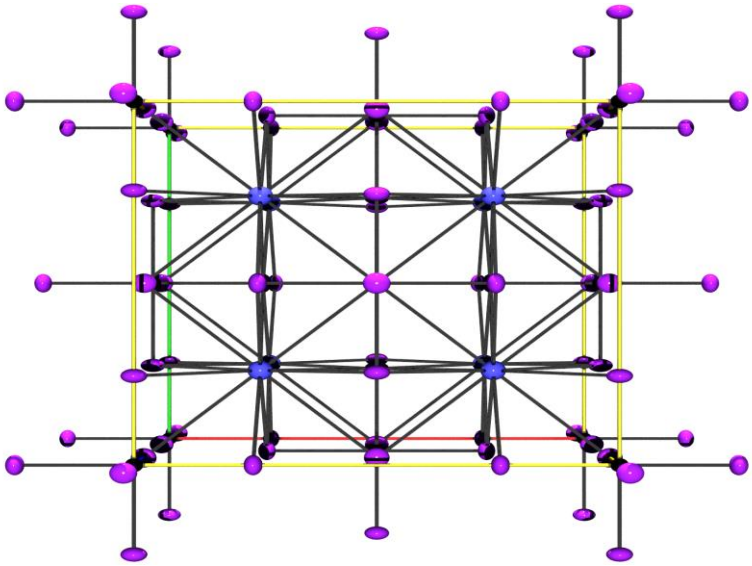

Figure 1.14: The Black Polymorph of $CsSnI_3$.[54] The purple spheres represent iodine, the blue spheres represent cesium, and the grey spheres represent tin. The bonds drawn between Cs-I are meant to show that the cesium cation is in a 12-fold coordination sphere.

The other polymorph of $CsSnI_3$ has greatly contrasting properties in comparison to its black polymorph. It is yellow in colour and has a chemical formula of $Cs_2Sn_2I_6$. As its formula suggests, it does not exhibit the same corner-sharing octahedra as a typical perovskite, but rather it forms infinite 1D [$Sn_2I_6^{2-}$] chains.[54] Its bandgap of 2.55eV is much larger than that of the black polymorph, making it a wide-bandgap semiconductor. This substantial difference in bandgap between the two phases can be explained by the structural changes that occur when the black polymorph is exposed to air.[54]

Group 14 halide perovskites are not limited to inorganic ions, like Cs^+. Organic cations such as methylammonium (MA) and formamidinium (FA), pictured in Figure 1.15, have been shown to yield hybrid inorganic-organic perovskite materials which have important photophysical properties. The structural formula for these compounds is AMI_3, where "A" is one of the organic cations mentioned above and "M" is either tin or lead. Not surprisingly, these perovskites exhibited similar temperature-dependent phase transitions to those found in the oxide perovskites[16,17,22] and $CsSnI_3$[54]. Four different phase transitions (α, β, γ, and δ)[55] were exhibited in all four compounds made from the combination of the cations with tin(II) or lead(II) iodide. These materials are classified as medium bandgap semiconductors with bandgaps ranging from 1.2-1.7eV.[55] Materials with bandgaps in this range are sought after for solar cell applications due to their optimal PCE.[63] Near-IR PL is also observed in these perovskites, making them attractive candidates for energy conversion applications.[64]

Figure 1.15: Methylammonium (MA) and Formamidinium (FA) Cations.

Kanatzidis and his colleagues went on to create more organic halometallate perovskites with the general formula of $AGeI_3$[56]. A wider variety of ammonium ions were used to synthesize this family of perovskites, and their structure with a methylammonium A-site cation is depicted in Figure 1.16. Akin to the perovskites made of tin and lead that were previously synthesized[55], these perovskites also displayed a direct band gap which highlights the semiconducting properties they have. Interestingly, a gradual change in size of the organic cation was found to influence the packing of the $[GeI_3]^-$ anions, which lead to differences in the crystal structures among the $AGeI_3$ perovskite family.

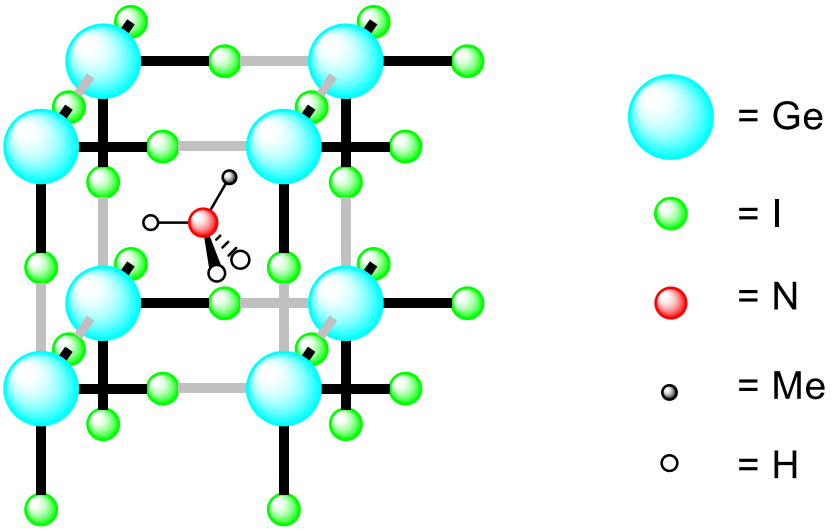

Figure 1.16: Methylammonium Germanium Iodide Perovskite.[56]

A trimethylsulfonium lead triiodide perovskite, $(CH_3)_3SPbI_3$, synthesized by the Kanatzidis group[57] is the newest member of the main group halometallate perovskite family. This perovskite, which is depicted in Figure 1.17, also undergoes a change in crystal system as the temperature changes, losing symmetry as temperature decreases. This perovskite is unique in that it forms a 1D network of face-sharing PbI_6 octahedra due to the sulfonium cation being too large to accommodate a 3D network of octahedra.[57] Trimethylsulfonium lead triiodide has a very large bandgap (3.1eV)[57] in comparison to those of the aforementioned perovskites, and thus it is classified as a wide-bandgap semiconductor. Although its optoelectronic properties are still being investigated, this perovskite shows promise due to its stability in air at ambient temperatures. It surpasses the other perovskites in this respect, as the black polymorph of $CsSnI_3$[54], $MAPbI_3$[55,65], and the trigonal polymorph of $FAPbI_3$[55] all decompose to some degree in air at room temperature.

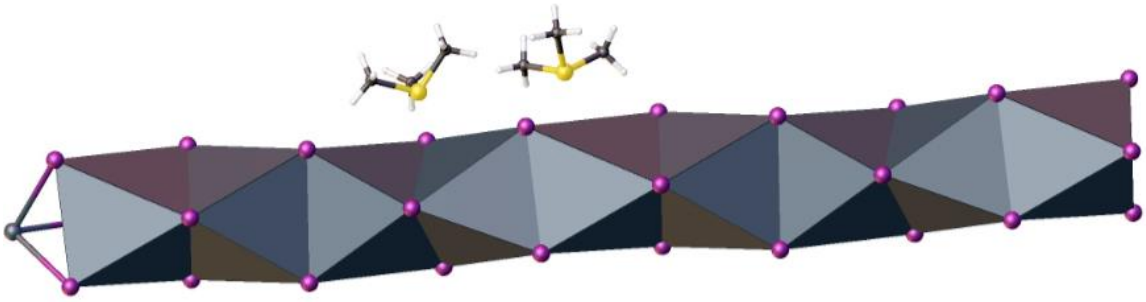

Figure 1.17: Trimethylsulfonium Lead Triiodide.[57] The grey polyhedra represent the face-sharing octahedral motif of this 1D perovskite.

The main group perovskites made by Kanatzidis represent the cutting edge of a synthetic boom in this research area. Other groups have synthesized perovskites of this

nature with different halides apart from iodine[27,29,66–75], and each of these compounds exhibit unique properties based on the combination of cations and anions used.

Fascinatingly, each inorganic-organic hybrid perovskite has a unique bandgap that can be tuned by changing the composition of the perovskite. The general formula for perovskitic materials (ABX_3) suggests that there is a lot of potential for variation in their composition. The X-site anion, which is occupied by a halogen in these perovskites, was the most common component that researchers tried to tune to date. For example, single crystals of methylammonium lead halide perovskites ($MAPbX_3$) were studied with UV-Visible spectroscopy and it was found that the bandgap narrows as X is changed from iodide to bromide to chloride.[76] Furthermore, the effects of changing the halide (X) between iodide, bromide, and chloride in a mixed-halogen $MAPbI_2X$ perovskite were examined by Mosconi et al.[68] using DFT calculations. It was found that the perovskites in which the X anion is bromide had a higher bandgap than those that contained chloride or iodide.[68] Noh et al.[77] further examined the tunability of the bandgap of $MAPbI_{3-x}Br_x$ by changing the ratio of Br:I. They were able to achieve bandgaps of 1.6-2.2eV, which covers almost the entire visible spectrum.[77]

Notably, fluoride is absent from the inorganic-organic halide perovskites. Chung et al.[54] showed that fluoride incorporation in $CsSnI_3$ perovskite greatly enhanced the PCE, thus chemists working with organic cations sought to incorporate fluorine in their mixed-halide perovskites. Fluorine afforded low stability in these systems,[68] thus Ogale and coworkers[78] used the tetrafluoroborate (BF_4^-) anion as a source of fluorine in a $MAPbI_3$ perovskite. This anion is similar in size to iodide, thus it was readily integrated into the perovskite structure. It was discovered that $MAPbI_{3-x}(BF_4)_x$ displays enhanced electrical

conductivity in comparison to $MAPbI_3$[78], which is further evidence that tuning the X-site can have a significant effect on the properties of a perovskite.

The B-site cations also play a role in the conductive properties of perovskitic materials. Using the $MAPbI_3$ perovskite, researchers have investigated the effect of gradually incorporating other metal cations in the B-site with lead. Navas et al.[79] doped the Pb^{2+} in this perovskite with Sn^{2+}, Cd^{2+}, Sr^{2+}, and Ca^{2+} cations and analyzed the effect by studying the change in bandgap. It was found that $MAPbI_3$ doped with tin(II) was the only perovskite that had a higher bandgap than that of the parent structure. The presence of the other cations narrowed the bandgap, with $MAPbI_3$ doped with Sr^{2+} having the smallest bandgap.[79] Tin has also been controllably exchanged for lead in $FASnI_3$ and it was discovered that the bandgap decreases as the lead content increases.[80] Trivalent cations such as Bi^{3+}, Au^{3+}, and In^{3+} have also been incorporated in $MAPbBr_3$ by Bakr and coworkers.[81] They found that Bi(III) incorporation lowered the bandgap in comparison to the parent compound, but Au(III) and In(III) had no appreciable effect on the bandgap.[81]

Kanatzidis and his colleagues have made perovskites with various nitrogen-containing organic cations with lead, tin, and germanium iodides.[55,56] In general, the tin(II) compounds have smaller bandgaps than those containing Pb(II). Germanium-templated perovskites with the general formula of $AGeI_3$ were also studied and it was found that their bandgaps are wider than those of any Sn(II) or Pb(II) perovskites.[56] The variance in bandgaps with different B-site cations show that this component of the perovskite could also respond to external stimuli and therefore play a role in the conduction of electrons.

The A-site cation is the final component in the perovskite formula that may be tuned. Originally, this cation was thought to have no orbital or electronic contribution to the final electronic structure of perovskite.[82–84] However, Hu et al.[85] demonstrated that changing the values of *a*, *b*, and *c* in $Cs_aFA_bMA_cPbBr_zI_{3-z}$ by tuning the ratio of FA: (MA+Cs) changed the onset of absorption in comparison to the parent compound $FAPbBr_zI_{3-z}$. Furthermore, DFT calculations performed by Filip and colleagues[86] showed that the bandgap of metal halide perovskites decreases with the X-B-X bond angle in the perovskite. The X-B-X bond angle can be adjusted by tilting the octahedra, which is achieved by changing the size of the A cation due to steric hindrance.[86,87] Many studies suggest that a larger A-site cation such as FA may be better than MA in terms of stability, efficiency, and narrowing the bandgap[27,88–100], however it is more difficult to incorporate such a cation into the perovskitic structure due to steric considerations.

In addition to their attractive optoelectronic properties and tunability, perovskites are relatively facile to synthesize. Perovskites can be made in bulk as crystals or by deposition of thin films.[27] This thesis will focus on synthesizing perovskite crystals, therefore the methods used to create perovskite crystals will be discussed. One of the most common ways to grow perovskite crystals is to heat a saturated perovskite precursor solution containing an organic halide salt and lead(II) halide. The reaction mixture is left to cool and halide perovskite crystals crash out of solution.[86,101–104] Perovskite crystals as large as 1cm in size have been reported using this method[102]. Another conventional method of growing crystals, slow evaporation, is also used to grow perovskite crystals. In this method, crystals are grown when an organic solvent such as DMF or ethanol is slowly evaporated from the perovskite precursor solution.[92,105,106]

There are also several novel crystal-growth methods that have been used to grow perovskite crystals in bulk. Antisolvent vapor-assisted crystallization (AVC)[107] is a method used to grow crystals as well as thin films. In AVC, an appropriate antisolvent is made to slowly diffuse into a perovskite precursor solution. The solvothermal method[73] is another facile way to grow perovskite crystals. It is done by heating the precursor solution in a closed vial to prevent solvent from evaporating. Solvothermal synthesis has been used to make mixed-halide perovskites. Lastly, perovskite crystals can be created via inverse temperature crystallization (ITC)[108]. ITC takes advantage of the decrease in solubility of the perovskite at elevated temperatures in certain solvents. One other avenue taken to create perovskites is mixing the ammonium halide salt and the lead halide in the solid state to create a powder.[27]

1.1.5 Scope of Thesis

The previous section summarizes the most recent advances in the synthesis and investigation of main group halometallate perovskites. Although there exists a large family of these perovskites, the A-site cation is largely limited to cesium[54] and alkylammonium species[55,56]. Since phosphonium is isolobal to ammonium[1], it is possible that a perovskite structure similar to those observed by Kanatzidis and colleagues[54–56] can be made with phosphorus. To date, there has been one instance of a phosphonium-containing perovskite, which was synthesized by Kociok-Köhn.[109] Trimethylphosphonium trichlorogermanate(II) adopts a distorted perovskite structure in the crystalline state and was inadvertently synthesized as an attempted crystallization of an adduct of trimethylphosphine-germanium(II) chloride.[109]

Kociok-Köhn's discovery[109] serves as encouragement that a perovskite structure may be created using other phosphoniums and group 14 halides. Given that trimethylphosphonium formed a distorted perovskite structure, it is probable that a larger phosphonium cation like the ones synthesized in this thesis will not crystallize in a perovskitic manner. Nevertheless, it is still worthwhile to explore the products of these reactions as novel structures. The second chapter of this thesis describes the synthesis and characterization of novel phosphonium salts of various size for reaction with the group 14 halides. Chapters 3,4, and 5 outline the results of the reactions of the different phosphonium salts with lead, tin, and germanium halides, respectively. Chapter 6 provides a summary of the work in this thesis as well as future considerations for this research.

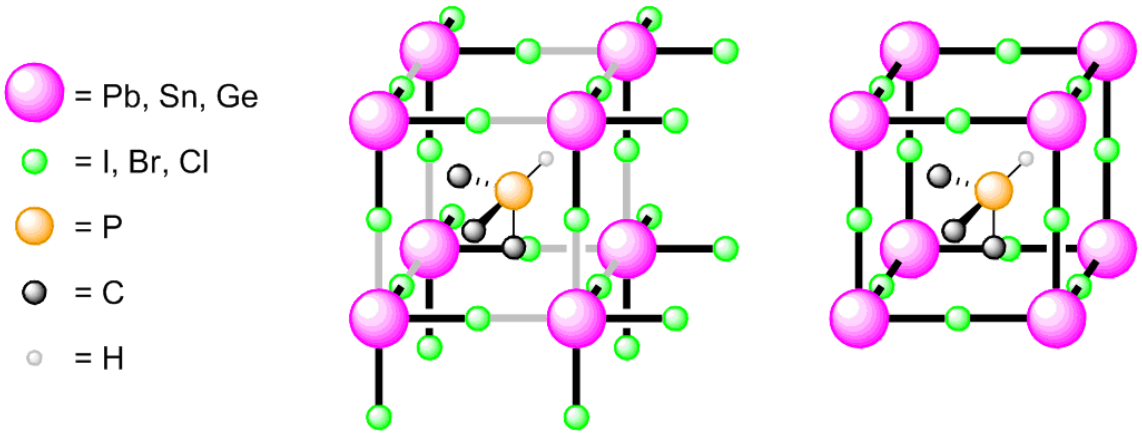

Figure 1.18: Outline of Potential Phosphorus-Containing Perovskites Explored in this Thesis.

1.2 References

(1) Henderson, W. *Main Group Chemistry*, 3rd ed.; Abel, E. W., Ed.; The Royal Society of Chemistry: Cambridge, 2000.

(2) Arduengo, A. J.; Stewart, C. A.; Davidson, F.; Dixon, D. A.; Becker, J. Y.; Culley,

S. A.; Mizenx, M. B. The Synthesis, Structure, and Chemistry of 10-Pn-3 Systems: Tricoordinate Hypervalent Pnictogen Compounds'^13. **1987**, *109* (4).

(3) McNaught, A. D.; Wilkinson, A.; International Union of Pure and Applied Chemistry. *Compendium of Chemical Terminology : IUPAC*, 2nd ed.; Blackwell Science, 1997.

(4) Hartl, H. New Evidence Concerning the Structure of Amorphous Red Phosphorus. *Angew. Chemie Int. Ed. English* **1996**, *34* (2324), 2637–2638.

(5) Parkin, G. Valence, Oxidation Number, and Formal Charge: Three Related but Fundamentally Different Concepts. *J. Chem. Educ.* **2006**, *83* (5), 791.

(6) Ellis, B. D.; Macdonald, C. L. B. Stable Compounds Containing Heavier Group 15 Elements in the +1 Oxidation State. *Coord. Chem. Rev.* **2007**, *251* (7–8), 936–973.

(7) Ellis, B. D.; Carlesimo, M.; Macdonald, C. L. B. Stabilised Phosphorus(I) and Arsenic(I) Iodide: Readily-Synthesised Reagents for Low Oxidation State Main Group Chemistry. *Chem. Commun. (Camb).* **2003**, *64* (15), 1946–1947.

(8) Ellis, B. D.; Macdonald, C. L. B. Phosphorus(I) Iodide: A Versatile Metathesis Reagent for the Synthesis of Low Oxidation State Phosphorus Compounds. *Inorg. Chem.* **2006**, *45* (17), 6864–6874.

(9) Dube, J. W.; MacDonald, C. L. B.; Ragogna, P. J. Accessing the Coordination Chemistry of Phosphorus(I) Zwitterions. *Angew. Chemie - Int. Ed.* **2012**, *51* (52), 13026–13030.

(10) Binder, J. F.; Swidan, aeddeen; Tang, M.; Nguyen, J. H.; B Macdonald, C. L.

Remarkably Stable Chelating Bis-N-Heterocyclic Carbene Adducts of Phosphorus(I) Cations. *Chem. Commun. Chem. Commun* **2015**, *51* (51), 7741–7744.

(11) Nevil Vincent Sidgwick. *The Electronic Theory Of Valency*, 1st ed.; Woodward, Ed.; Oxford University Press: London, 1927.

(12) Macdonald, C. L. B.; Binder, J. F.; Swidan, A.; Nguyen, J. H.; Kosnik, S. C.; Ellis, B. D. Convenient Preparation and Detailed Analysis of a Series of NHC-Stabilized Phosphorus(I) Dyes and Their Derivatives. *Inorg. Chem.* **2016**, *55* (14), 7152–7166.

(13) Navrotsky, A. Energetics and Crystal Chemical Systematics among Ilmenite, Lithium Niobate, and Perovskite Structures. *Chem. Mater.* **1998**, *10* (10), 2787–2793.

(14) Wolf, A. S.; Jackson, J. M.; Dera, P.; Prakapenka, V. B. The Thermal Equation of State of (Mg, Fe)SiO_3 Bridgmanite (Perovskite) and Implications for Lower Mantle Structures. *J. Geophys. Res. Solid Earth* **2015**, *120* (11), 7460–7489.

(15) Tomioka, N.; Fujino, K. Natural (Mg,Fe)SiO_3-Ilmenite and -Perovskite in the Tenham Meteorite. *Science* **1997**, *277* (5329), 1084–1086.

(16) Vanpeteghem, C. B.; Zhao, J.; Angel, R. J.; Ross, N. L.; Bolfan-Casanova, N. Crystal Structure and Equation of State of $MgSiO_3$ Perovskite. *Geophys. Res. Lett.* **2006**, *33* (3), L03306.

(17) Zhao, J.; Ross, N. L.; Angel, R. J. New View of the High-Pressure Behaviour of $GdFeO_3$-Type Perovskites. *Acta Cryst* **2004**, *60*, 263–271.

(18) Wang, Y.; Guyot, F.; Liebermann, R. C. Electron Microscopy of (Mg,Fe)SiO_3

Perovskite: Evidence for Structural Phase Transitions and Implications for the Lower Mantle. *J. Geophys. Res.* **1992**, *97* (B9), 12327.

(19) Sasaki, S.; Prewitt, C. T.; Bass, J. D. Orthorhombic Perovskite $CaTiO_3$ and $CdTiO_3$: Structure and Space Group. *Acta Crystallogr. C* **1987**, *39* (43), 1668–1674.

(20) Kumar, A.; Jha, R.; Tandon, R. P.; Awana, V. P. S. Superconductivity and Ferromagnetism in the Non-Oxide Perovskite $MgCNi_3$. In *AIP Conference Proceedings*; 2012; Vol. 1447, pp 875–876.

(21) Feldmann, C.; Jansen, M. Gradual Anionic Character of Gold in Ternary Perovskite Type Oxides. *J. Chem. Soc. Chem. Commun.* **1994**, No. 9, 1045.

(22) Chen, J.; Liu, H.; Martin, C. D.; Parise, J. B.; Weidner, D. J. Crystal Chemistry of $NaMgF_3$ Perovskite at High Pressure and Temperature. *Am. Mineral.* **2005**, *90* (10), 1534–1539.

(23) Hodes, G. Perovskite-Based Solar Cells. *Science (80-.).* **2013**, *342* (6156), 317–318.

(24) Lufaso, M. W.; Woodward, P. M. Jahn-Teller Distortions, Cation Ordering and Octahedral Tilting in Perovskites. *Acta Crystallogr. Sect. B Struct. Sci.* **2004**, *60* (1), 10–20.

(25) Jahn, H. A.; Teller, E. Stability of Polyatomic Molecules in Degenerate Electronic States. I. Orbital Degeneracy. *Proc. R. Soc. A Math. Phys. Eng. Sci.* **1937**, *161* (905), 220–235.

(26) Housecroft, C.; Sharpe, A. G. *Inorganic Chemistry*, 3rd ed.; Prentice Hall, 2008.

(27) Zhao, Y.; Zhu, K. Organic–inorganic Hybrid Lead Halide Perovskites for Optoelectronic and Electronic Applications. *Chem. Soc. Rev.* **2016**, *45* (3), 655–689.

(28) Goldschmidt, V. M. Die Gesetze Der Crystallochemie. *Naturwissenschaften* **1926**, No. 14, 477–485.

(29) Li, Z.; Yang, M.; Park, J. S.; Wei, S. H.; Berry, J. J.; Zhu, K. Stabilizing Perovskite Structures by Tuning Tolerance Factor: Formation of Formamidinium and Cesium Lead Iodide Solid-State Alloys. *Chem. Mater.* **2016**, *28* (1), 284–292.

(30) Yashima, M.; Ali, R. Structural Phase Transition and Octahedral Tilting in the Calcium Titanate Perovskite CaTiO3. *Solid State Ionics* **2009**, *180* (2–3), 120–126.

(31) Bardeen, J.; Cooper, L. N.; Schrieffer, J. R. Theory of Superconductivity. *Phys. Rev.* **1957**, *108* (5), 1175–1204.

(32) Bednorz, J. G.; Miiller, K. A. Possible High T c Superconductivity in the Ba -La-Cu-0 System. *Z. Phys. B -Condensed Matter* **1986**, *64*, 189–193.

(33) Cava, R. J.; Batlogg, B.; Van Dover, R. B.; Murphy, D. W.; Sunshine, S.; Siegrist, T.; Remeika, J. P.; Rietman, E. A.; Zahurak, S.; Espinosa, G. P. Bulk Superconductivity at 91 K in Single-Phase Oxygen-Deficient Perovskite $Ba_2YCu309$ — B. **1987**, *58* (16).

(34) Rao, C. N. R. Solid-State Chemistry of High-Temperature Oxide Superconductors: The Experimental Situation. *J. Solid State Chem.* **1988**, *74* (1), 147–162.

(35) Ruddlesden, S. N.; Popper, P. New Compounds of the K_2NIF_4 Type. *Acta Crystallogr.* **1957**, *10* (8), 538–539.

(36) Ruddlesden, S. N.; Popper, P. The Compound SrsTi$_2$0$_7$ and Its Structure. *SHORT Commun. Acta Cryst* **1958**, *11*.

(37) Beznosikov, B. V.; Aleksandrov, K. S. Perovskite-like Crystals of the Ruddlesden-Popper Series. *Crystallogr. Reports* **2000**, *45* (5), 792–798.

(38) Takeguchi, T.; Yamanaka, T.; Takahashi, H.; Watanabe, H.; Kuroki, T.; Nakanishi, H.; Orikasa, Y.; Uchimoto, Y.; Takano, H.; Ohguri, N.; et al. Layered Perovskite Oxide: A Reversible Air Electrode for Oxygen Evolution/Reduction in Rechargeable Metal-Air Batteries. *J. Am. Chem. Soc.* **2013**, *135* (30), 11125–11130.

(39) Patwardhan, S.; Cao, D. H.; Hatch, S.; Farha, O. K.; Hupp, J. T.; Kanatzidis, M. G.; Schatz, G. C. Introducing Perovskite Solar Cells to Undergraduates. *J. Phys. Chem. Lett.* **2015**, *6* (2), 251–255.

(40) Green, M. A.; Emery, K.; Hishikawa, Y.; Warta, W.; Dunlop, E. D. Solar Cell Efficiency Tables (Version 45). *Prog. Photovoltaics Res. Appl.* **2015**, *23* (1), 1–9.

(41) Ünlü, H. A Thermodynamic Model for Determining Pressure and Temperature Effects on the Bandgap Energies and Other Properties of Some Semiconductors. *Solid. State. Electron.* **1992**, *35* (9), 1343–1352.

(42) Griffith, J. S.; Orgel, L. E. Ligand-Field Theory. *Q. Rev. Chem. Soc.* **1957**, *11* (4), 381.

(43) Era, M.; Morimoto, S.; Tsutsui, T.; Saito, S. Organic-Inorganic Heterostructure Electroluminescent Device Using a Layered Perovskite Semiconductor (C6H5C2H4NH3)2PbI4. *Appl. Phys. Lett.* **1994**, *65* (6), 676.

(44) Tan, Z.-K.; Moghaddam, R. S.; Lai, M. L.; Docampo, P.; Higler, R.; Deschler, F.; Price, M.; Sadhanala, A.; Pazos, L. M.; Credgington, D.; et al. Bright Light-Emitting Diodes Based on Organometal Halide Perovskite. *Nat. Nanotechnol.* **2014**, *9* (9), 687–692.

(45) Gil-Escrig, L.; Longo, G.; Pertegás, A.; Roldán-Carmona, C.; Soriano, A.; Sessolo, M.; Bolink, H. J. Efficient Photovoltaic and Electroluminescent Perovskite Devices. *Chem. Commun.* **2015**, *51* (3), 569–571.

(46) Zhu, H.; Fu, Y.; Meng, F.; Wu, X.; Gong, Z.; Ding, Q.; Gustafsson, M. V.; Trinh, M. T.; Jin, S.; Zhu, X.-Y. Lead Halide Perovskite Nanowire Lasers with Low Lasing Thresholds and High Quality Factors. *Nat. Mater.* **2015**, *14* (6), 636–642.

(47) Xing, G.; Mathews, N.; Lim, S. S.; Yantara, N.; Liu, X.; Sabba, D.; Grätzel, M.; Mhaisalkar, S.; Sum, T. C. Low-Temperature Solution-Processed Wavelength-Tunable Perovskites for Lasing. *Nat. Mater.* **2014**, *13* (5), 476–480.

(48) Dou, L.; Yang, Y. (Micheal); You, J.; Hong, Z.; Chang, W.-H.; Li, G.; Yang, Y. Solution-Processed Hybrid Perovskite Photodetectors with High Detectivity. *Nat. Commun.* **2014**, *5*, 5404.

(49) Fang, H.; Li, Q.; Ding, J.; Li, N.; Tian, H.; Zhang, L.; Ren, T.; Dai, J.; Wang, L.; Yan, Q. A Self-Powered Organolead Halide Perovskite Single Crystal Photodetector Driven by a DVD-Based Triboelectric Nanogenerator. *J. Mater. Chem. C* **2016**, *4* (3), 630–636.

(50) Wang, Z.; Yu, R.; Pan, C.; Li, Z.; Yang, J.; Yi, F.; Wang, Z. L. Light-Induced

Pyroelectric Effect as an Effective Approach for Ultrafast Ultraviolet Nanosensing. *Nat. Commun.* **2015**, *6*, 8401.

(51) Zheng, F.; Saldana-Greco, D.; Liu, S.; Rappe, A. M. Material Innovation in Advancing Organometal Halide Perovskite Functionality. *J. Phys. Chem. Lett.* **2015**, *6* (23), 4862–4872.

(52) Luo, J.; Im, J.-H.; Mayer, M. T.; Schreier, M.; Nazeeruddin, M. K.; Park, N.-G.; Tilley, S. D.; Fan, H. J.; Gratzel, M. Water Photolysis at 12.3% Efficiency via Perovskite Photovoltaics and Earth-Abundant Catalysts. *Science (80-.).* **2014**, *345* (6204), 1593–1596.

(53) Chen, Y.-S.; Manser, J. S.; Kamat, P. V. All Solution-Processed Lead Halide Perovskite-$BiVO_4$ Tandem Assembly for Photolytic Solar Fuels Production. *J. Am. Chem. Soc.* **2015**, *137* (2), 974–981.

(54) Chung, I.; Lee, B.; He, J.; Chang, R. P. H.; Kanatzidis, M. G. All-Solid-State Dye-Sensitized Solar Cells with High Efficiency. *Nature* **2012**, *485* (7399), 486–489.

(55) Stoumpos, C. C.; Malliakas, C. D.; Kanatzidis, M. G. Semiconducting Tin and Lead Iodide Perovskites with Organic Cations: Phase Transitions, High Mobilities, and Near-Infrared Photoluminescent Properties. *Inorg. Chem.* **2013**, *52* (15), 9019–9038.

(56) Stoumpos, C. C.; Frazer, L.; Clark, D. J.; Kim, Y. S.; Rhim, S. H.; Freeman, A. J.; Ketterson, J. B.; Jang, J. I.; Kanatzidis, M. G. Hybrid Germanium Iodide Perovskite Semiconductors: Active Lone Pairs, Structural Distortions, Direct and Indirect

Energy Gaps, and Strong Nonlinear Optical Properties. *J. Am. Chem. Soc.* **2015**, *137* (21), 6804–6819.

(57) Kaltzoglou, A.; Stoumpos, C. C.; Kontos, A. G.; Manolis, G. K.; Papadopoulos, K.; Papadokostaki, K. G.; Psycharis, V.; Tang, C. C.; Jung, Y.-K.; Walsh, A.; et al. Trimethylsulfonium Lead Triiodide: An Air-Stable Hybrid Halide Perovskite. *Inorg. Chem.* **2017**, *56* (11), 6302–6309.

(58) Harris, D. C. *Quantitative Chemical Analysis*, 8th ed.; W H Freeman & Co., 2010.

(59) Romani, A.; Clementi, C.; Miliani, C.; Favaro, G. Fluorescence Spectroscopy: A Powerful Technique for the Noninvasive Characterization of Artwork. *Acc. Chem. Res.* **2010**, *43* (6), 837–846.

(60) Kuriki, K.; Koike, Y.; Okamoto, Y. Plastic Optical Fiber Lasers and Amplifiers Containing Lanthanide Complexes. *Chem. Rev.* **2002**, *102* (6), 2347–2356.

(61) Kido, J.; Okamoto, Y. Organo Lanthanide Metal Complexes for Electroluminescent Materials. *Chem. Rev.* **2002**, *102* (6), 2357–2368.

(62) Hemmilä, I.; Webb, S. Time-Resolved Fluorometry: An Overview of the Labels and Core Technologies for Drug Screening Applications. *Drug Discov. Today* **1997**, *2* (9), 373–381.

(63) Shockley, W.; Queisser, H. J. Detailed Balance Limit of Efficiency of P-n Junction Solar Cells. *J. Appl. Phys.* **1961**, *32* (3), 510–519.

(64) Slooff, L. H.; Bende, E. E.; Burgers, A. R.; Budel, T.; Pravettoni, M.; Kenny, R. P.; Dunlop, E. D.; Büchtemann, A. A Luminescent Solar Concentrator with 7.1%

Power Conversion Efficiency. *Phys. status solidi - Rapid Res. Lett.* **2008**, *2* (6), 257–259.

(65) Misra, R. K.; Aharon, S.; Li, B.; Mogilyansky, D.; Visoly-Fisher, I.; Etgar, L.; Katz, E. A. Temperature- and Component-Dependent Degradation of Perovskite Photovoltaic Materials under Concentrated Sunlight. *J. Phys. Chem. Lett.* **2015**, *6* (3), 326–330.

(66) Gonzalez-Carrero, S.; Schmidt, L. C.; Rosa-Pardo, I.; Martínez-Sarti, L.; Sessolo, M.; Galian, R. E.; Pérez-Prieto, J. Colloids of Naked $CH_3NH_3PbBr_3$ Perovskite Nanoparticles: Synthesis, Stability, and Thin Solid Film Deposition. *ACS Omega* **2018**, *3* (1), 1298–1303.

(67) Chen, Y.; Chen, T.; Dai, L. Layer-by-Layer Growth of $CH_3NH_3PbI_{3-x}Cl_x$ for Highly Efficient Planar Heterojunction Perovskite Solar Cells. *Adv. Mater.* **2015**, *27* (6), 1053–1059.

(68) Mosconi, E.; Amat, A.; Nazeeruddin, M. K.; Grätzel, M.; De Angelis, F. First-Principles Modeling of Mixed Halide Organometal Perovskites for Photovoltaic Applications. *J. Phys. Chem. C.* **2013**, *117* (27), 13902–13913.

(69) Yang, W. S.; Noh, J. H.; Jeon, N. J.; Kim, Y. C.; Ryu, S.; Seo, J.; Seok, S. I. High-Performance Photovoltaic Perovskite Layers Fabricated through Intramolecular Exchange. *Science (80-.).* **2015**, *348* (6240), 1234–1237.

(70) Kojima, A.; Teshima, K.; Shirai, Y.; Miyasaka, T. Organometal Halide Perovskites as Visible-Light Sensitizers for Photovoltaic Cells. *J. Am. Chem. Soc.* **2009**, *131*

(17), 6050–6051.

(71) Fan, Z.; Sun, K.; Wang, J. Perovskites for Photovoltaics: A Combined Review of Organic–inorganic Halide Perovskites and Ferroelectric Oxide Perovskites. *J. Mater. Chem. A* **2015**, *3* (37), 18809–18828.

(72) Luo, B.; Pu, Y.-C.; Lindley, S. A.; Yang, Y.; Lu, L.; Li, Y.; Li, X.; Zhang, J. Z. Organolead Halide Perovskite Nanocrystals: Branched Capping Ligands Control Crystal Size and Stability. *Angew. Chemie Int. Ed.* **2016**, *55* (31), 8864–8868.

(73) Park, N.-G. Perovskite Solar Cells: An Emerging Photovoltaic Technology. *Mater. Today* **2015**, *18* (2), 65–72.

(74) Schmidt, L. C.; Pertegás, A.; González-Carrero, S.; Malinkiewicz, O.; Agouram, S.; Mínguez Espallargas, G.; Bolink, H. J.; Galian, R. E.; Pérez-Prieto, J. Nontemplate Synthesis of $CH_3NH_3PbBr_3$ Perovskite Nanoparticles. *J. Am. Chem. Soc.* **2014**, *136* (3), 850–853.

(75) Zhang, F.; Zhong, H.; Chen, C.; Wu, X.; Hu, X.; Huang, H.; Han, J.; Zou, B.; Dong, Y. Brightly Luminescent and Color-Tunable Colloidal $CH_3NH_3PbX_3$ (X = Br, I, Cl) Quantum Dots: Potential Alternatives for Display Technology. *ACS Nano* **2015**, *9* (4), 4533–4542.

(76) Butler, K. T.; Frost, J. M.; Walsh, A. Band Alignment of the Hybrid Halide Perovskites CH3NH3PbCl3, $CH_3NH_3PbBr_3$ and $CH_3NH_3PbI_3$. *Mater. Horizons* **2015**, *2* (2), 228–231.

(77) Noh, J. H.; Im, S. H.; Heo, J. H.; Mandal, T. N.; Seok, S. Il. Chemical Management

for Colorful, Efficient, and Stable Inorganic–Organic Hybrid Nanostructured Solar Cells. *Nano Lett.* **2013**, *13* (4), 1764–1769.

(78) Nagane, S.; Bansode, U.; Game, O.; Chhatre, S.; Ogale, S. $CH_3NH_3PbI_{(3-x)}(BF_4)_X$: Molecular Ion Substituted Hybrid Perovskite. *Chem. Commun.* **2014**, *50* (68), 9741.

(79) Navas, J.; Sánchez-Coronilla, A.; Gallardo, J. J.; Cruz Hernández, N.; Piñero, J. C.; Alcántara, R.; Fernández-Lorenzo, C.; De Los Santos, D. M.; Aguilar, T.; Martín-Calleja, J. New Insights into Organic-Inorganic Hybrid Perovskite $CH_3NH_3PbI_3$ Nanoparticles. An Experimental and Theoretical Study of Doping in Pb^{2+} Sites with Sn^{2+}, Sr^{2+}, Cd^{2+} and Ca^{2+} †. *Nanoscale* **2015**, *7*, 6216.

(80) Eperon, G. E.; Ginger, D. S. B-Site Metal Cation Exchange in Halide Perovskites. *ACS Energy Lett.* **2017**, *2* (5), 1190–1196.

(81) Abdelhady, A. L.; Saidaminov, M. I.; Murali, B.; Adinolfi, V.; Voznyy, O.; Katsiev, K.; Alarousu, E.; Comin, R.; Dursun, I.; Sinatra, L.; et al. Heterovalent Dopant Incorporation for Bandgap and Type Engineering of Perovskite Crystals. *J. Phys. Chem. Lett.* **2016**, *7* (2), 295–301.

(82) Motta, C.; El-Mellouhi, F.; Kais, S.; Tabet, N.; Alharbi, F.; Sanvito, S. Revealing the Role of Organic Cations in Hybrid Halide Perovskite $CH_3NH_3PbI_3$. *Nat. Commun.* **2015**, *6* (1), 7026.

(83) Ke, W.; Fang, G.; Wan, J.; Tao, H.; Liu, Q.; Xiong, L.; Qin, P.; Wang, J.; Lei, H.; Yang, G.; et al. Efficient Hole-Blocking Layer-Free Planar Halide Perovskite Thin-Film Solar Cells. *Nat. Commun.* **2015**, *6* (1), 6700.

(84) Yin, W.-J.; Shi, T.; Yan, Y. Unique Properties of Halide Perovskites as Possible Origins of the Superior Solar Cell Performance. *Adv. Mater.* **2014**, *26* (27), 4653–4658.

(85) Hu, C.; Bai, Y.; Xiao, S.; Zhang, T.; Meng, X.; Ng, W. K.; Yang, Y.; Wong, K. S.; Chen, H.; Yang, S. Tuning the A-Site Cation Composition of FA Perovskites for Efficient and Stable NiO-Based P–i–n Perovskite Solar Cells. *J. Mater. Chem. A* **2017**, *5* (41), 21858–21865.

(86) Filip, M. R.; Eperon, G. E.; Snaith, H. J.; Giustino, F. Steric Engineering of Metal-Halide Perovskites with Tunable Optical Band Gaps. *Nat. Commun.* **2014**, *5*, 5757.

(87) Amat, A.; Mosconi, E.; Ronca, E.; Quarti, C.; Umari, P.; Nazeeruddin, M. K.; Grätzel, M.; De Angelis, F. Cation-Induced Band-Gap Tuning in Organohalide Perovskites: Interplay of Spin–Orbit Coupling and Octahedra Tilting. *Nano Lett.* **2014**, *14* (6), 3608–3616.

(88) Jeon, N. J.; Noh, J. H.; Yang, W. S.; Kim, Y. C.; Ryu, S.; Seo, J.; Seok, S. Il. Compositional Engineering of Perovskite Materials for High-Performance Solar Cells. *Nature* **2015**, *517* (7535), 476–480.

(89) Hu, M.; Liu, L.; Mei, A.; Yang, Y.; Liu, T.; Han, H. Efficient Hole-Conductor-Free, Fully Printable Mesoscopic Perovskite Solar Cells with a Broad Light Harvester $NH_2CHNH_2PbI_3$. *J. Mater. Chem. A* **2014**, *2* (40), 17115–17121.

(90) Eperon, G. E.; Stranks, S. D.; Menelaou, C.; Johnston, M. B.; Herz, L. M.; Snaith, H. J. Formamidinium Lead Trihalide: A Broadly Tunable Perovskite for Efficient

Planar Heterojunction Solar Cells. *Energy Environ. Sci.* **2014**, *7* (3), 982.

(91) Koh, T. M.; Fu, K.; Fang, Y.; Chen, S.; Sum, T. C.; Mathews, N.; Mhaisalkar, S. G.; Boix, P. P.; Baikie, T. Formamidinium-Containing Metal-Halide: An Alternative Material for Near-IR Absorption Perovskite Solar Cells. *J. Phys. Chem. C* **2014**, *118* (30), 16458–16462.

(92) Pang, S.; Hu, H.; Zhang, J.; Lv, S.; Yu, Y.; Wei, F.; Qin, T.; Xu, H.; Liu, Z.; Cui, G. $NH_2CH{=}NH_2PbI_3$: An Alternative Organolead Iodide Perovskite Sensitizer for Mesoscopic Solar Cells. *Chem. Mater.* **2014**, *26* (3), 1485–1491.

(93) Zheng, L.; Zhang, D.; Ma, Y.; Lu, Z.; Chen, Z.; Wang, S.; Xiao, L.; Gong, Q. Morphology Control of the Perovskite Films for Efficient Solar Cells. *Dalt. Trans.* **2015**, *44* (23), 10582–10593.

(94) Wang, F.; Yu, H.; Xu, H.; Zhao, N. HPbI 3 : A New Precursor Compound for Highly Efficient Solution-Processed Perovskite Solar Cells. *Adv. Funct. Mater.* **2015**, *25* (7), 1120–1126.

(95) Seol, D.-J.; Lee, J.-W.; Park, N.-G. On the Role of Interfaces in Planar-Structured HC(NH 2) 2 PbI 3 Perovskite Solar Cells. *ChemSusChem* **2015**, *8* (14), 2414–2419.

(96) Philippe, B.; Park, B.-W.; Lindblad, R.; Oscarsson, J.; Ahmadi, S.; Johansson, E. M. J.; Rensmo, H. Chemical and Electronic Structure Characterization of Lead Halide Perovskites and Stability Behavior under Different Exposures—A Photoelectron Spectroscopy Investigation. *Chem. Mater.* **2015**, *27* (5), 1720–1731.

(97) Kim, J.; Lee, S.-C.; Lee, S.-H.; Hong, K.-H. Importance of Orbital Interactions in

Determining Electronic Band Structures of Organo-Lead Iodide. *J. Phys. Chem. C* **2015**, *119* (9), 4627–4634.

(98) Eperon, G. E.; Bryant, D.; Troughton, J.; Stranks, S. D.; Johnston, M. B.; Watson, T.; Worsley, D. A.; Snaith, H. J. Efficient, Semitransparent Neutral-Colored Solar Cells Based on Microstructured Formamidinium Lead Trihalide Perovskite. *J. Phys. Chem. Lett.* **2015**, *6* (1), 129–138.

(99) Boix, P. P.; Agarwala, S.; Koh, T. M.; Mathews, N.; Mhaisalkar, S. G. Perovskite Solar Cells: Beyond Methylammonium Lead Iodide. *J. Phys. Chem. Lett.* **2015**, *6* (5), 898–907.

(100) Binek, A.; Hanusch, F. C.; Docampo, P.; Bein, T. Stabilization of the Trigonal High-Temperature Phase of Formamidinium Lead Iodide. *J. Phys. Chem. Lett.* **2015**, *6* (7), 1249–1253.

(101) Weber, D. $CH_3NH_3PbX_3$, a Pb(II)-System with Cubic Perovskite Structure. *Zeitschrift für Naturforsch. B* **1978**, *33*, 1443–1445.

(102) Dang, Y.; Liu, Y.; Sun, Y.; Yuan, D.; Liu, X.; Lu, W.; Liu, G.; Xia, H.; Tao, X. Bulk Crystal Growth of Hybrid Perovskite Material $CH_3NH_3PbI_3$. *CrystEngComm* **2015**, *17* (3), 665–670.

(103) Wasylishen, R. E.; Knop, O.; Macdonald, J. B. Cation Rotation in Methylammonium Lead Halides. *Solid State Commun.* **1985**, *56* (7), 581–582.

(104) Baikie, T.; Fang, Y.; Kadro, J. M.; Schreyer, M.; Wei, F.; Mhaisalkar, S. G.; Graetzel, M.; White, T. J. Synthesis and Crystal Chemistry of the Hybrid Perovskite

(CH_3NH_3)PbI_3 for Solid-State Sensitised Solar Cell Applications. *J. Mater. Chem. A* **2013**, *1* (18), 5628.

(105) Zhuo, S.; Zhang, J.; Shi, Y.; Huang, Y.; Zhang, B. Self-Template-Directed Synthesis of Porous Perovskite Nanowires at Room Temperature for High-Performance Visible-Light Photodetectors. *Angew. Chemie Int. Ed.* **2015**, *54* (19), 5693–5696.

(106) Bi, C.; Shao, Y.; Yuan, Y.; Xiao, Z.; Wang, C.; Gao, Y.; Huang, J. Understanding the Formation and Evolution of Interdiffusion Grown Organolead Halide Perovskite Thin Films by Thermal Annealing. *J. Mater. Chem. A* **2014**, *2* (43), 18508–18514.

(107) Shao, Y.; Xiao, Z.; Bi, C.; Yuan, Y.; Huang, J. Origin and Elimination of Photocurrent Hysteresis by Fullerene Passivation in CH3NH3PbI3 Planar Heterojunction Solar Cells. *Nat. Commun.* **2014**, *5* (1), 5784.

(108) Saidaminov, M. I.; Abdelhady, A. L.; Murali, B.; Alarousu, E.; Burlakov, V. M.; Peng, W.; Dursun, I.; Wang, L.; He, Y.; Maculan, G.; et al. High-Quality Bulk Hybrid Perovskite Single Crystals within Minutes by Inverse Temperature Crystallization. *Nat. Commun.* **2015**, *6* (May), 1–6.

(109) Kociok-Köhn, G.; Winter, J. G.; Filippou, A. C. Trimethylphosphonium Trichlorogermanate(II). *Acta Crystallogr. Sect. C Cryst. Struct. Commun.* **1999**, *55* (3), 351–353.

CHAPTER 2: Synthesis of Novel Phosphonium Salts

2.1 Introduction

2.1.1 Phosphines

Phosphines are arguably the most versatile class of ligands ever studied.[1] These species are commonly used as neutral ligands in transition metal and organometallic chemistry. Phosphines can coordinate to metals that are in various oxidation states and they can also be used in catalysis.[2] They have the general formula of PR_nH_{3-n},[3] where R is usually an organic derivative, and adopt a trigonal pyramidal geometry. The value of n in the general formula for a phosphine dictates whether it is primary (n=1), secondary (n=2) or tertiary (n=3) phosphine. In this chapter, tertiary phosphines will be used as precursors to phosphonium salts.

Tertiary phosphines are the most common types of phosphines in chemistry today, with triphenylphosphine and trimethylphosphine, pictured in Figure 2.1, being the most routine.[3] The triarylphosphines occur as white air-stable solids, whereas the trialkylphosphines are colourless liquids that readily oxidize to $O=PR_3$ in air.[3] Phosphines may also occur as bi- or triphosphines which typically serve as chelating ligands. A common diphosphine, dmpe, and a triphosphine, triphos, are also displayed in Figure 2.1.

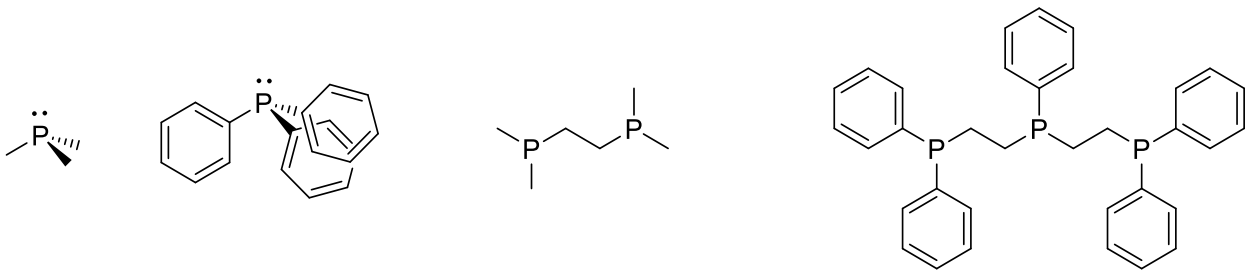

Figure 2.1: Common Phosphine Ligands. From left to right: trimethylphosphine, triphenylphosphine, dmpe, and triphos.

Phosphines are classified by the Tolman electronic parameter and the cone angle. The Tolman electronic parameter gives insight into the π-acidity of a phosphine, whereas the cone angle measures the steric bulk of a ligand.[1,4,5] For the purposes of this thesis, it is important to consider the size of the phosphine being used to make a phosphonium salt because the phosphonium cation will occupy the A-site of a perovskite.

2.1.2 Phosphonium Salts

Phosphonium salts are a family of phosphorus-containing compounds that have a PR_4^+ cation. The R-groups in the cation can consist of hydrogen, such as in $[PH_4^+][I^-]$, or an organic moiety such as in the quaternary phosphonium salts.[6] This chapter will focus on the creation of phosphonium salts through protonation (Scheme 2.1) and alkylation (Scheme 2.2) of tertiary phosphines. Protonation involves the use of an inorganic acid such as hydroiodic acid, whereas alkylation employs an alkylating agent such as iodomethane.

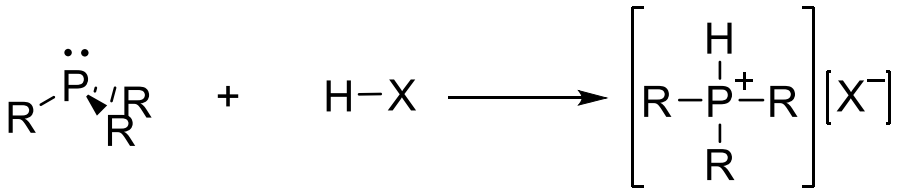

Scheme 2.1: Protonation of Phosphine[6]

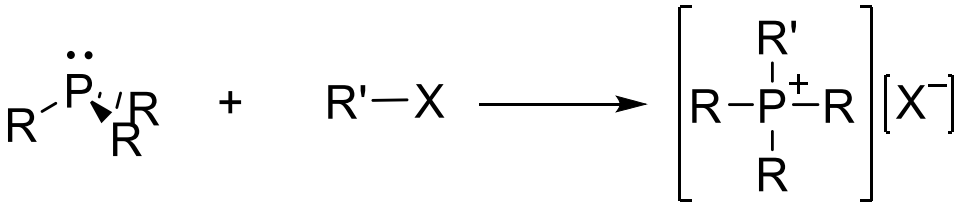

Scheme 2.2: Alkylation of Phosphine[6]

The following chapter demonstrates that the above two methods of synthesizing phosphonium salts can be used with multiple organic mono- and diphosphines. The structural elucidation of each phosphonium salt via NMR spectroscopy is presented along with the crystal structures of three of the synthesized salts.

2.2 Results & Discussion

2.2.1 Synthesis of Monophosphonium Salts

Tetramethylphosphonium Iodide

Given the success of forming perovskites from methylammonium species,[7–10] it seemed fitting to start building the phosphonium salt library with one that contains methyl substituents. Trimethylphosphine (PMe_3) and iodomethane (MeI) were reacted in a 1:1 ratio in toluene at room temperature under inert atmosphere. MeI was added to the Schlenk flask in a dropwise fashion, and a white precipitate formed. After 24h, this white precipitate was isolated and characterized as tetramethylphosphonium iodide ($[PMe_4][I]$) by NMR and CHN-Elemental Analysis. Interestingly, although this phosphonium salt has been prepared before,[11] it had not been crystallographically characterized.

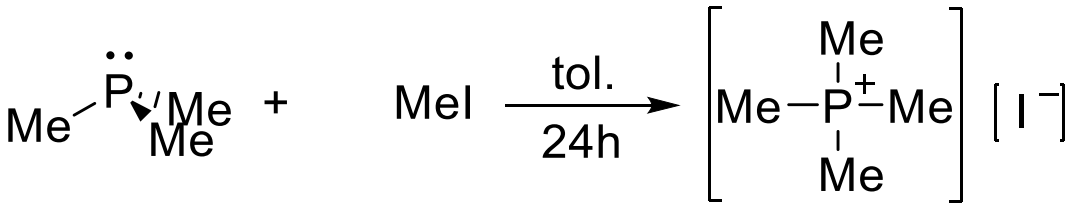

Scheme 2.3: Novel Synthesis of Tetramethylphosphonium Iodide.

Our synthesis of $[PMe_4][I]$ is more facile and higher-yielding than the synthesis described by Herrmann and Kuhn.[11] Previously, this salt was made by reacting calcium

phosphide and iodomethane in a methanol-water solution at 0°C for 3h.[11] This mixture is then heated at reflux for 48h, the solvents are removed in vacuo, then the resulting residue is mixed with ethanol and heated to boiling again. The residue obtained from exposing the hot-filtered solution to reduced pressure is then recrystallized from anhydrous ethanol. In addition to the being more convenient, our synthetic protocol has a 78% yield, whereas the reported synthesis[11] generates a 53% yield. Furthermore, NMR spectroscopy of the crude product from the previous literature method reveals the presence of three other byproduct phosphonium cations[11], whereas the NMR spectrum of our synthesis contains only the target phosphonium. The $^{31}P\{^{1}H\}$ NMR of our product displayed one singlet at 23.6 ppm, suggesting that there was no unreacted starting material or byproduct in the product mixture. The ^{1}H NMR shows one doublet at 1.84 ppm which represents the methyl proton environment coupling to the phosphorus. Hermann and Kuhn[11] found a doublet at 1.93 ppm for the methyl protons of this phosphonium, which is similar to the chemical shift we observed. The differences in chemical shift can be explained by the difference in solvents used: Kuhn et al.[11] used D_2O, whereas we used CD_3CN. The $^{2}J_{PH}$ is 15 Hz, which is the same as the coupling constant reported by Herrmann and Kuhn[11] for this salt. The ^{13}C NMR of our product also matches well with the previously reported synthesis of $[PMe_4][I]$. The single methyl environment in the cation appears as a doublet at 9.98 ppm in our spectrum and 9.2 ppm in Khun et al.'s.[11] The one-bond coupling constants between carbon and phosphorus match closely as well, with ours at 56.3Hz and the previously-reported coupling constant at 56Hz.[11] As previously stated, the differing solvents could be a cause for the small discrepancy in chemical shift between the two different characterizations of $[PMe_4][I]$.

Although [PMe_4][I] has been made before, it has not been crystallographically characterized and we were fortunate to obtain crystalline material from an acetonitrile solution. Crystals suitable for X-Ray diffraction were selected, and the crystal structure of [PMe_4][I] was elucidated. It is depicted in Figure 2.2.

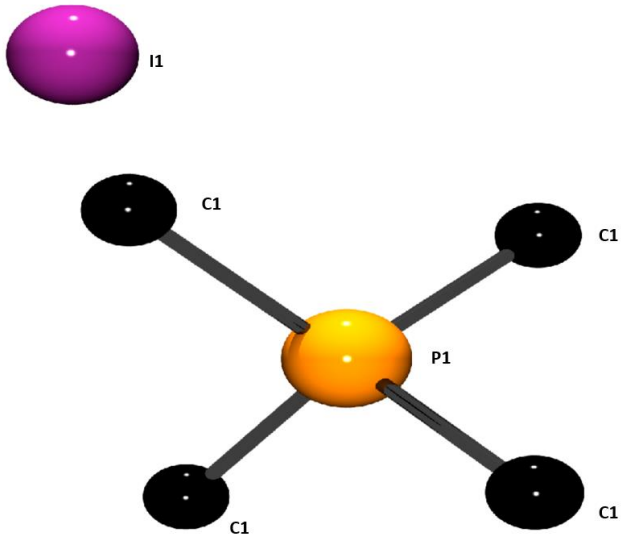

Figure 2.2: Crystal structure (ball and stick) of [PMe_4][I] with selected bond lengths (Å) and angles (º): P1-C1, 1.761(7)Å; C1-P1-C1', 109.5(3)˚, Hydrogen atoms not bound to phosphorus are omitted for clarity.

Although a CSD search gives many examples of species that contain a tetramethylphosphonium ion, there is only one example of a tetramethylphosphonium salt with a single halide. Tetramethylphosphonium fluoride ([PMe_4][F]) has been crystallographically characterized by Kornath et al.[12] and thus the metrical parameters of the phosphonium cations in this structure and our structure may be compared. In comparison to the analogous tetramethylphosphonium fluoride salt,[12] which have P-C bond lengths averaging at 1.778(13)Å, the P-C bond lengths in tetramethylphosphonium iodide are similar at 1.761(7)Å. The bond angles in the cation at 109.5(3)˚ are similar to those

previously reported,[12] indicating that the methyl groups are tetrahedrally arranged about the phosphine, as anticipated.

Trimethylphosphonium Iodide

Given the successful synthesis of $[PMe_4][I]$ via the alkylation of trimethylphosphine, the protonation of trimethylphosphine to create $[HPMe_3][I]$ was attempted. Trimethylphosphine was reacted with hydroiodic acid solution in a 1:1 ratio to create the phosphonium iodide salt. This compound has been reported by Bellachioma as a product of the hydrolysis of $[PMe_3I][I]$, however it has not been fully characterized.[13] The phosphine was dissolved in toluene and the hydroiodic acid solution was added dropwise under stirring to ensure that the reaction went to completion. A white precipitate formed immediately upon addition of the brown HI solution. After pumping off the toluene, the white solid was dissolved in acetonitrile to yield colourless crystals.

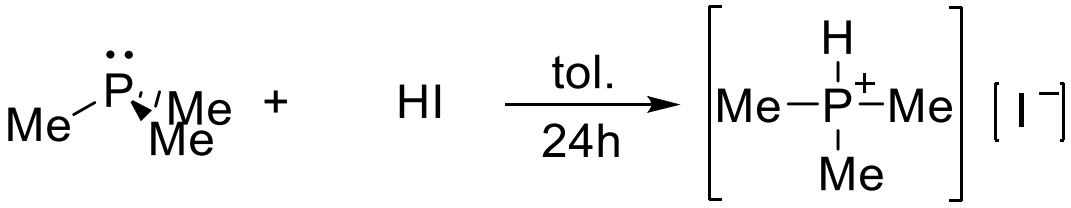

Scheme 2.4: Novel Synthesis of Trimethylphosphonium Iodide.

The successful synthesis of trimethylphosphonium iodide ($[PMe_3][I]$) was confirmed by NMR spectroscopy and X-Ray crystallography. The $^{31}P\{^1H\}$ NMR gave good evidence for creation of the trimethylphosphonium cation as the chemical shift obtained was similar to that of previously reported trimethylphosphonium cations. The spectrum exhibited one phosphorus environment, which was a singlet. The chemical shift of the synthesized compound is 2.09 ppm, which is very close to the shift for

trimethylphosphonium iodide of -0.44 ppm reported by Bellachioma.[13] To observe the phosphorus coupling to protons, a ^{31}P NMR without proton decoupling was run. The splitting pattern showed a doublet of decets, which corresponds with the predicted pattern for trimethylphosphonium iodide.

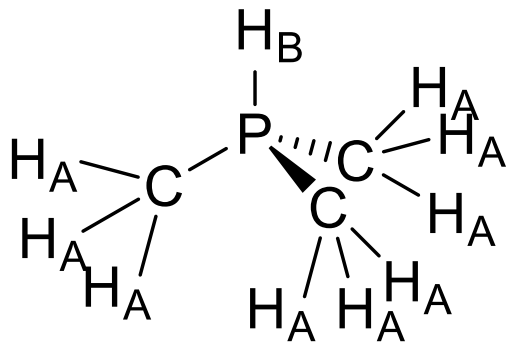

Figure 2.3: ^{1}H Environments of $[HPMe_3][I]$.

The doublet of decets exhibited in the ^{31}P NMR is due to the phosphorus coupling to the H_A and H_B environments of $[PMe_3][I]$ as depicted in Figure 2.3. Phosphorus exhibits stronger coupling (510Hz) to the lone proton in environment B because it is only one bond away. Weaker coupling (15.9Hz) is exhibited to the methyl protons because they are two bonds away. The chemical shift for phosphonium iodide in this spectrum is 1.18 ppm, which is in close correspondence with the shift found by Bellachioma.[13] A comparison between the $^{31}P\{^{1}H\}$ and ^{31}P NMR spectra is displayed in Figure 2.4.

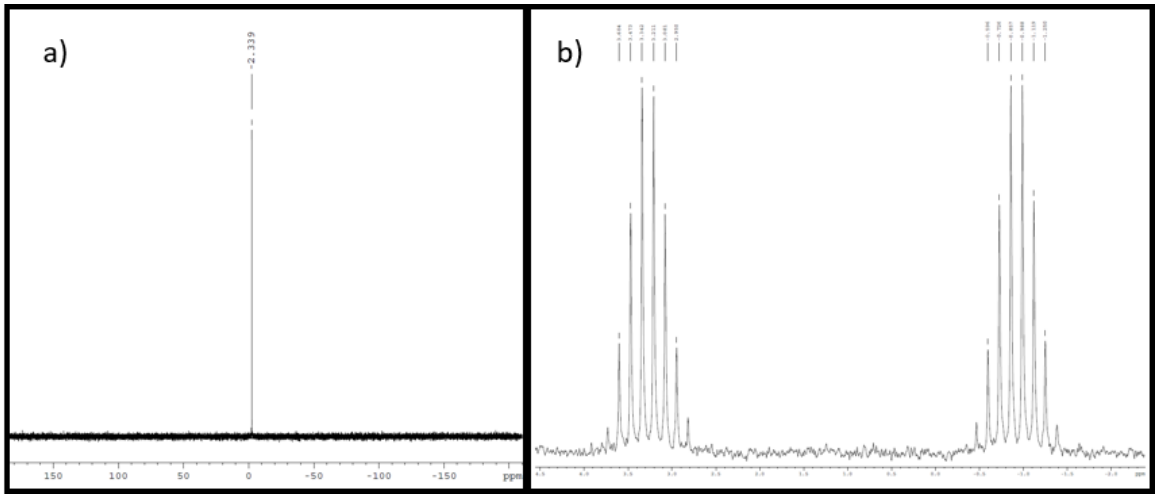

Figure 2.4: The a) $^{31}P\{^{1}H\}$ and b) ^{31}P NMR Spectra of $[HPMe_3][I]$.

The proton NMR spectrum further confirmed that phosphonium iodide was synthesized. Two signals corresponding to environment A and environment B, as shown in Figure 2.3, were displayed on the spectrum. A doublet of decets that is displayed at 6.42 ppm corresponds to the H_B environment. The large coupling constant of 513 Hz is due to H_B coupling to the phosphorus one bond away, while the smaller coupling constant of 5.7Hz is due to H_B coupling to the methyl protons of environment A. The doublet of doublets resonance displayed at 1.85 ppm (*cf.* 1.99 ppm)[13] corresponds to the H_A environment. H_A exhibits coupling to phosphorus two bonds away (16.5Hz *cf.* 15.7 Hz)[13] and the proton from environment H_B which is three bonds away (6.3Hz *cf.* 5.5Hz).[13]

Although trimethylphosphonium iodide has already been synthesized and reported,[13] it had not been fully characterized thus we collected further spectroscopic data. The $^{13}C\{^{1}H\}$ NMR is consistent with the proposed composition. One of the chemical shifts observed at 118.26 ppm, a singlet, is attributable to the deuterated acetonitrile solvent used to make the NMR sample. Acetonitrile displays another resonance at approximately 1.39 ppm which is a septet. It is not observed in this spectrum because the spectral width is too

narrow. The resonance observed due to the methyl groups on trimethylphosphonium iodide is a doublet a 5.75 ppm. This is distinct from the chemical shift of trimethyl phosphine, which displays a chemical shift of 14.3 ppm. The doublet splitting pattern is due to the one-bond coupling of the carbons to phosphorus, which is quantified at 55.6Hz.

Since this compound has not been crystallographically characterized before, X-ray diffraction was performed on a sample recrystallized by slow evaporation of acetonitrile. The crystallographic data provides further insight into the bonding nature of this compound. The bond lengths found in this structure for P-C1 and P-C2 of ca. 1.783Å and the P-H bond distance of ca. 1.52Å are in good agreement with those previously reported for trimethyl phosphonium cations.[14] Figure 2.5 displays the structure of trimethylphosphonium iodide.

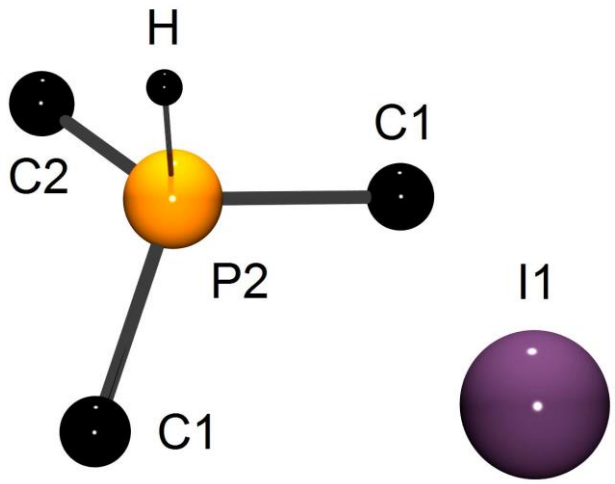

Figure 2.5: Crystal structure (ball and stick) of $[HPMe_3][I]$ with selected bond lengths (Å) and angles (º): P2-C2, 1.7827(10); P2-C(1), 1.7831(6); P2-H, 1.52(3)Å; C2-P2-C1, 110.13(3); C1-P2-C1, 111.25(4); C2-P2-H, 112.7(9); C1-P2-H, 106.3(5). Hydrogen atoms not bound to phosphorus are omitted for clarity.

Tri(n-butyl)phosphonium Iodide

The successful synthesis of both $[PMe_4][I]$ and $[HPMe_3][I]$ via protonation and alkylation of PMe_3 prompted us to probe similar reactions with tri(n-butyl)phosphine. For the protonation, tri(n-butyl)phosphine was dissolved in toluene and HI was added dropwise in the same manner as with the synthesis of $[HPMe_3][I]$. The toluene was removed via vacuum after 24h, leaving an orange oil. This oil was further pumped on, and after 6h a pale pink solid was collected. The percent yield of this reaction was 96.0%. Although no crystals were obtained for this reaction, NMR spectroscopy confirmed that the product created was indeed the target tri(n-butyl)phosphonium iodide. A single resonance in the $^{31}P\{^1H\}$ NMR at 12.98 ppm indicated that there was only one phosphorus species in the product mixture. There was no peak at -32.4 ppm, which would indicate the presence of the starting tri(n-butyl)phosphine.[15,16]

^1H and $^{13}C\{^1H\}$ NMR are also consistent with the synthesis of tri(n-butyl)phosphonium. A doublet of septets at 7.40 ppm indicates that the phosphine was protonated. This shift, which corresponds to Environment A in Figure 2.6, represents the coupling of the lone proton to the phosphorus atom and the six protons of Environment B. The strong one-bond coupling between proton A and the phosphorus atom (489Hz) is similar in magnitude to the one reported for trimethylphosphonium iodide by Bellachioma et al.[13] (496.4Hz). Environments B, C, and D have shifts of 2.35 ppm, 1.62 ppm, and 1.49 ppm, respectively and appear as multiplets with unresolved coupling. The coupling is unresolved because each of the environments is coupled to many similar but different environments and as a result the couplings are ambiguous and the splitting patterns are convoluted. Environment E is a triplet at 0.95 ppm, which is in the typical range for a

terminal methyl group. The three-bond coupling of these protons to Environment D is similar to those observed in trimethylphosphonium iodide.[13] The ^{1}H NMR chemical shifts, multiplicities, integrations, and coupling constants are shown in Table 2.1.

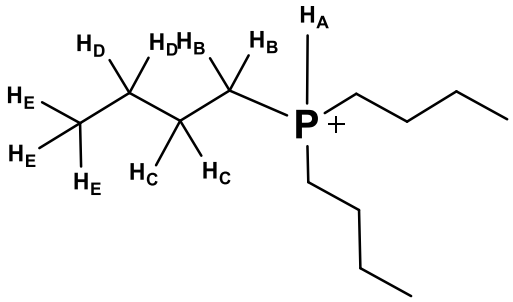

Figure 2.6: ^{1}H Environments in Tri(n-butyl)phosphonium Iodide

Table 2.1: Summary of the ^{1}H NMR Spectrum of [HP(n-butyl)$_3$][I] in CD_3CN

Environment	Chemical Shift (ppm)	Multiplicity	Integration	Coupling (Hz)
A	7.40	Dsept	1H	$^{1}J_{PH}$ = 489 $^{3}J_{HH}$ = 5.5
B	2.35	M	6H	Unres.
C	1.62	M	6H	Unres.
D	1.49	M	6H	Unres.
E	0.95	T	9H	$^{3}J_{HH}$ = 7

The ^{13}C{^{1}H} NMR spectrum served as further confirmation that tri(n-butyl)phosphonium iodide was synthesized. Figure 2.7 depicts the ^{13}C environments observed in this phosphonium salt. Environments A, B, and C appear as doublets due to coupling to phosphorus. The one-bond coupling between phosphorus and Environment A is 47.2Hz, the two-bond coupling to Environment B is 15.5Hz, and the three-bond coupling to Environment C is 4.7Hz. The two-bond coupling is reminiscent of the $^{2}J_{PC}$ present in tetramethylphosphonium iodide, which is quantified at 56Hz.[17] The one-bond coupling

observed in this spectrum is like that observed in trimethylphosphonium iodide.[13] Environment D, the terminal methyl environment, is a singlet at 12.70 ppm. It does not couple to the phosphorus atom since it is four bonds away. It is also worthwhile to note that the carbon environments do not experience observable coupling to each other because the ^{13}C nucleus is in such low abundance. The chemical shifts, multiplicities, and coupling of the ^{13}C NMR of tri(n-butyl)phosphonium iodide are summarized in Table 2.2.

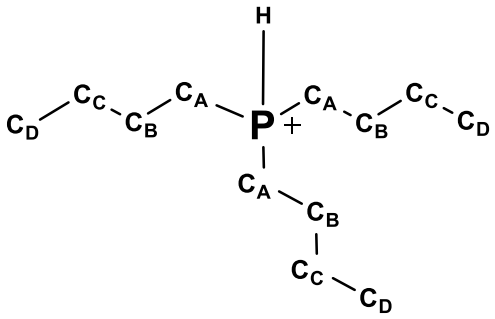

Figure 2.7: ^{13}C Environments in Tri(n-butyl)phosphonium iodide.

Table 2.2 Summary of the ^{13}C Spectrum of [HP(n-butyl)$_3$][I] in CD_3CN.

Environment	Chemical Shift (ppm)	Multiplicity	Coupling (Hz)
A	16.10	D	$^1J_{PC}$ = 47.2
B	23.36	D	$^2J_{PC}$ = 15.5
C	24.20	D	$^3J_{PC}$ = 4.7
D	12.70	S	N/A

Tri(n-butyl)methylphosphonium Iodide

Tri(n-butyl)phosphine was also alkylated with iodomethane in a similar fashion to trimethylphosphine. The resulting phosphonium salt is tri(n-butyl)methylphosphonium iodide. This compound has been synthesized and characterized before,[16,18,19] however the synthesis used in this thesis is different than those that have been previously reported. Tri(n-butyl)methylphosphonium iodide was first accessed as a byproduct in a ^{31}P NMR-monitored Mitsunobu reaction by Guthrie et al.[16] It was then made for further reactions

with tri(n-butyl)phosphine and MeI stirring in THF for 12h at room temperature by Takeshi et al.[19] It was also made by Yuzhen et al.[18] as the target compound by heating a solution of tri(n-butyl)phosphine in ethyl acetate to 33-37℃ and adding MeI in a dropwise fashion under stirring. This mixture was stirred for 1-3h after the addition of MeI at elevated temperature and then cooled to room temperature to obtain the product.

For this thesis, tri(n-butyl)methylphosphonium iodide was synthesized in a similar way to that of Takeshi et al.[19] Because of the improved preparations of the other phosphonium salts described above using toluene as a solvent, we chose to employ it for this reaction as opposed to the THF that had been used in the literature method. Thus, tri(n-butyl)phosphonium iodide was dissolved in toluene and MeI was added in a dropwise fashion. After 16h, the toluene was pumped off and a white powder was collected. A $^{31}P\{^{1}H\}$ NMR spectrum of the white powder displayed a single resonance at 32.95 ppm, which is similar to the resonance observed by Guthrie et al.[16] (31.8 ppm) for this compound. The $^{13}C\{^{1}H\}$ spectrum further confirmed that tri(n-butyl)methylphosphonium was created since there were five resonances displayed apart from the DMSO-d_6 solvent peak. The ^{13}C environments in this phosphonium salt are shown in Figure 2.8.

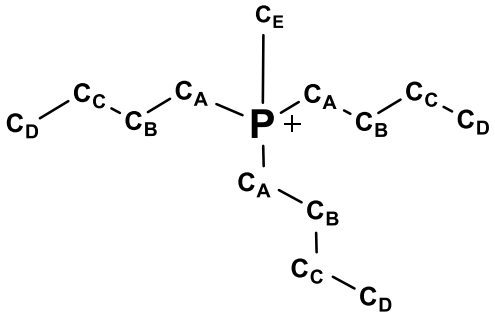

Figure 2.8: ^{13}C Environments in Tri(n-butyl)methylphosphonium Iodide

The terminal methyl group in the n-butyl chains in Environment D resonate as a singlet at 13.25 ppm, which is a typical chemical shift for this environment.[20] Environment E, which is directly bound to the phosphorus, was observed as a doublet at 18.89 ppm due to coupling to the phosphorus. The one-bond coupling constant was found to be 49.4Hz, which is close to that of the one-bond phosphorus-carbon coupling constant reported in tetramethylphosphonium iodide.[17] Environment A, which is also directly bound to the phosphorus is also a doublet at 22.55 ppm, however the one-bond coupling to phosphorus is much smaller than that of Environment A. Environments B and C have very similar chemical shifts at 23.33 and 23.20 ppm, respectively, because they are both in the middle of the n-butyl chain. Both carbon environments resonate as singlets because they are too far away to couple to the phosphorus.

To complete the characterization of this phosphonium salt, a ^{1}H NMR spectrum of tri(n-butyl)methylphosphonium iodide was collected. It revealed the five different proton resonances according to Figure 2.9. Environment A appeared on the spectrum as a doublet at 1.798 ppm whose two-bond coupling to phosphorus is quantified at 13.5Hz. The peak integration matched the expected number of protons (i.e. 3) that belong to this environment. Environment B should appear as a triplet of doublets due to the coupling of this environment to phosphorus and Environment C, alas only a broad triplet at 2.17 ppm was observed. The two-bond coupling of these protons to phosphorus is valued at 14.5Hz, however the three-bond coupling of Environment B to Environment C is not resolvable. Since DMSO-d_6 was used to collect this spectrum, the broadness of the triplet and the absence of the doublets within it could be attributable to solvent effects.

The solvent effects of using deuterated DMSO also affected the determination of coupling constants for Environments C and D. Environment C, which should appear as a triplet of triplets due to coupling to environments B and D, appears as a multiplet at 1.46 ppm. Similarly, Environment D resonated as a multiplet despite the predicted splitting pattern being a triplet of quartets. The protons in this environment resonated at 1.41 ppm. Neither of the three-bond coupling constants to other protons could be resolved. The terminal methyl group in the n-butyl chains manifested as a triplet at 0.93 ppm, which is a characteristic shift of methyl protons.[20] The three-bond coupling of these protons in Environment E to those in Environment D was found to be 7Hz.

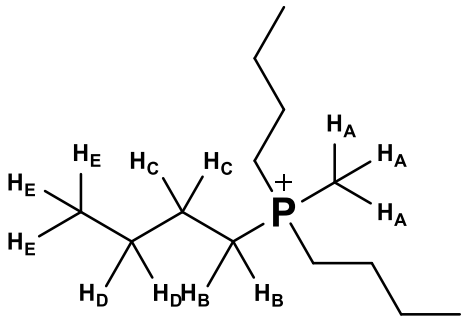

Figure 2.9: The ^{1}H NMR Environments of tri(n-butyl)methylphosphonium iodide.

2.2.2 Synthesis of Diphosphonium Salts

Bis(dimethylphosphonio)ethane Iodide

Given the successful synthesis of monophosphonium iodide salts by protonation and alkylation of various phosphines, the synthesis of diphosphonium iodide salts was also attempted using the same methods. The first diphosphine ligand used was bis(dimethylphosphino)ethane, or dmpe. This ligand was protonated to make (bisdimethylphosphonio)ethane iodide by adding two equivalents of hydroiodic acid to a

solution of dmpe in iodide according to Scheme 2.4. Two equivalents of acid were added to ensure that both phosphorus atoms were protonated in the reaction. At first, dropwise addition of the HI produced a brown solution, suggesting that the HI did not initially react with the diphosphine. However, after approximately two minutes of stirring, the solution turned pale yellow with some white precipitate on the sides of the flask. After 16h of continuous stirring, the solution was colourless with a white precipitate.

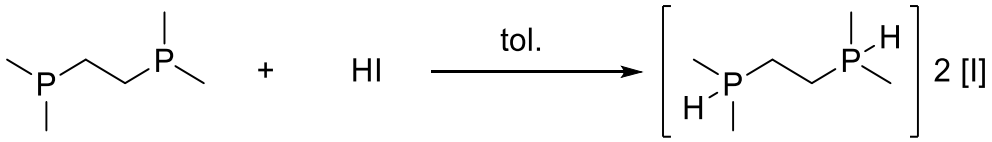

Scheme 2.5: Protonation of dmpe.

Once the toluene and water from the hydroiodic acid solution was pumped off, a white solid remained. The white solid was dissolved in acetonitrile and a $^{31}P\{^{1}H\}$ NMR spectrum was collected. A singlet was observed at 5.55 ppm, indicating that there is only one phosphorus environment and suggesting that the desired product was created. Moreover, this chemical shift is similar to that of other phosphoniums[13,17] previously synthesized and not close to that of the starting material (dmpe, -48.7 ppm).[21] Although the ^{1}H and $^{13}C\{^{1}H\}$ NMR spectra have yet to be collected, the single phosphorus environment observed provides good encouragement that bis(dimethylphosphonio)ethane iodide was indeed prepared. Attempts at recrystallization with various solvents via slow evaporation, including acetonitrile, DCM, and THF, did not produce a crystal.

Bis(trimethylphosphonio)ethane Iodide

Dmpe was also alkylated with two equivalents of iodomethane, yielding bis(trimethylphosphonio)ethane iodide. The phosphine was dissolved in toluene and the

MeI was added to the solution in a dropwise fashion. A white precipitate formed at the surface as the MeI was introduced to the phosphine. The reaction mixture was left to stir for 18h, after which a white precipitate was present in the flask. The volatiles were pumped off, and the white solid that remained was collected and analyzed via NMR spectroscopy.

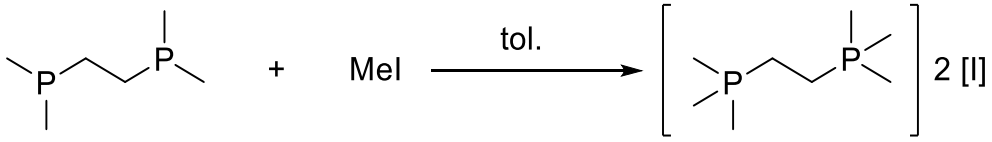

Scheme 2.6: Methylation of dmpe.

The $^{31}P\{^{1}H\}$, ^{1}H, and $^{13}C\{^{1}H\}$ are consistent with the formation of the desired product, bis(trimethylphosphonio)ethane iodide. The $^{31}P\{^{1}H\}$ NMR showed one phosphorus environment, a singlet at 32.49 ppm, suggesting that both phosphorus atoms were methylated as intended. The ^{1}H NMR displayed two environments aside from the deuterium oxide solvent resonance; a doublet at 1.99 ppm and a doublet at 2.65 ppm from coupling of the proton environments to the phosphorus atoms. The resonance at 1.99 ppm is attributable to the 18 methyl protons, while the resonance at 2.65 ppm is due to the four protons of the ethylene bridge. The two-bond coupling constant from the methyl protons to phosphorus was found to be 13.8Hz and the three-bond coupling constant from the bridge protons to the phosphorus was 6Hz. These values are similar to those reported by Yuan et al.,[22] as they observed coupling constants of 15Hz and 7Hz for two-bond and three-bond coupling, respectively in their diphosphonium salts. The $^{13}C\{^{1}H\}$ spectrum also contained two environments other than the solvent signals: a triplet at 6.92 ppm and a singlet at 15.24 ppm. The former shift is consistent with the methyl carbons, whereas the latter shift represents the carbon atoms of the ethylene bridge. The one-bond coupling

constant from the phosphorus atoms to the methyl protons was calculated to be 26.2Hz. This falls on the lower end of the literature range for $^{1}J_{PC}$ coupling constants (18Hz-89Hz).[17,23–25] Although no crystals suitable for X-Ray diffraction were obtained, the NMR spectra of the product give conclusive evidence that bis(trimethylphosphonio)ethane iodide was made.

[(Diphenylphosphino)methyl]methyldiphenylphosphonium Iodide

Dppm was also methylated to build the library of phosphonium salts for this thesis. Although this reaction has been carried out before and the products fully characterized,[27,28] it was re-synthesized for the purposes of this thesis. In the literature preparation, dppm is dissolved in toluene at 80°C and the iodomethane, which is in excess, is added to this solution.[27] The product, which is a white solid, is collected via filtration. In this thesis we have slightly modified the literature method by reacting the diphosphine and MeI at room temperature and allowing it to stir for 18h as opposed to 4h. In addition, the product was isolated by pumping off the toluene instead of by filtration. Furthermore, crystals of the product were obtained from acetonitrile, whereas in the literature[28] crystals were obtained from chloroform.

The $^{31}P\{^{1}H\}$ NMR provided evidence that this reaction did not go as initially planned. Instead of having only one phosphorus environment, which would be observed if both phosphorus atoms were methylated, two phosphorus environments were present in the NMR. This suggests that only one of the two phosphine centers were methylated. One phosphorus environment was observed at -28.06 ppm as a doublet with a two-bond P-P coupling constant of 64.2Hz. This is similar to the literature chemical shift of dppm (-21.78

ppm),[26] suggesting that the phosphorus atom in this environment experiences shielding similar to that of the phosphine and not a phosphonium. Another doublet was present at 23.39 ppm, which suggests that this resonance belongs to a phosphonium environment given that the shift is similar to other monophosphonium ions that have previously been reported.[17] The two-bond coupling between the phosphonium and phosphine phosphorus environments was determined to be 64Hz. The literature methylation of dppm also reports two $^{31}P\{^{1}H\}$ NMR environments at a similar shift; one at -22.3 ppm and another at 26.7 ppm, with both two-bond coupling constants equal to 59.7Hz.[28] Figure 2.10 shows the predicted product based on the $^{31}P\{^{1}H\}$ NMR spectrum, [(Diphenylphosphino)methyl]methyldiphenylphosphonium iodide. This salt will be referred to as ***Compound 2.3.8*** for the remainder of this chapter.

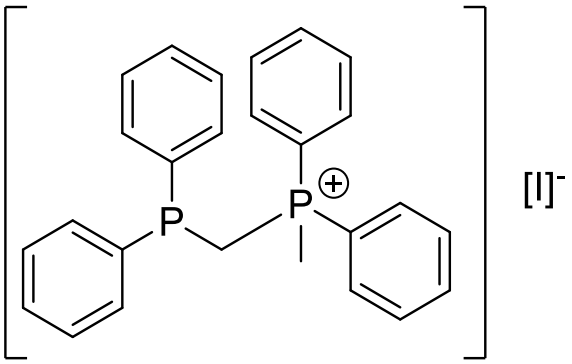

Figure 2.10: [(Diphenylphosphino)methyl]methyldiphenylphosphonium iodide, Compound 2.3.8.

^{1}H NMR of the product made in this thesis was also compared to the literature. There were eight resonances in the spectrum. Two doublets at 2.42 and 3.71 ppm represented the three methyl protons and the two protons of the methyl bridge, respectively. In the literature these shifts were found to be 2.72 ppm and 4.15 ppm,[28] indicating that the products match. The discrepancies in chemical shift between the synthesized product and

the literature could be due to the differences in solvent used to make the sample, since this thesis used deuterated acetonitrile and the literature used deuterated chloroform. The two-bond coupling of the methyl protons to phosphorus was found to be 13.5Hz, which matches the analogous literature coupling constant[28] exactly. The two-bond coupling of the methane bridge protons to phosphorus matched the literature closely as well (15Hz *cf.* 14.7Hz).[28] The other six resonances observed correspond to the six different aromatic proton environments. Their chemical shifts range from 7.18-7.72 ppm, which is comparable to the literature shifts that range from 7.20-7.78 ppm.[28]

Although the $^{13}C\{^{1}H\}$ NMR spectrum for the material produced has not yet been obtained, X-Ray crystallography drew further parallels between the structure reported in the literature and the one presented herein. The crystal of [(diphenylphosphino)methyl]methyldiphenylphosphonium iodide reported in this thesis was obtained by slow evaporation from acetonitrile, while the literature crystal[28] was grown from chloroform. A comparison of bond lengths between the the two compounds, illustrated in Figure 2.11, is outlined in Table 2.3. Since there was disorder at the phosphine site in the literature structure,[28] there is no assigned bond length for P1-C(Ph) and P1-C1, and no assigned angle for P1-C1-P2. Thus, the structure reported in this thesis more completely elucidates the key bond lengths and angles for Compound 2.3.8.

The bond lengths of the phosphonium site in Compound 2.3.8 were first compared to the literature structure. In Table 2.3, the average of the phosphonium phosphorus (P2) to phenyl carbon (C211, C221) bond length is reported. This value, 1.7942(12)Å, is similar to that of the literature (1.792(5)Å)[28] since the estimated standard deviations (ESDs) overlap. The P2-C1 bond, which is the bond between the phosphonium phosphorus and the

methane bridge carbon, is also close to the literature value within experimental error based on the ESDs (1.7888(13)Å cf. 1.782(5)Å).[28] Furthermore, the P2-C2 bond which is 1.8066(12)Å (*cf.* 1.802(5)Å)[28] also resembles the literature value within an accepted ESD.

The remaining key metrical parameters of this crystal structure were compared to those of other dppm-derived monophosphonium salts. A crystal structure of ethylated dppm served as a good model for comparing the bond lengths of the phosphine phosphorus to the two phenyl carbons and the bridging methane group. The average value of the P1-C111 and P1-C121 bond lengths was found to be 1.8300(13)Å, while the average value reported in the literature[28] was 1.832(2)Å. Once again, ESDs confirm that these bonds are crystallographically similar. The P1-C1-P2 bond angle in this crystal structure was found to be 117.30(7)˚, which falls within the literature range for dppm-templated monophosphonium salts and ylides.[28–31]

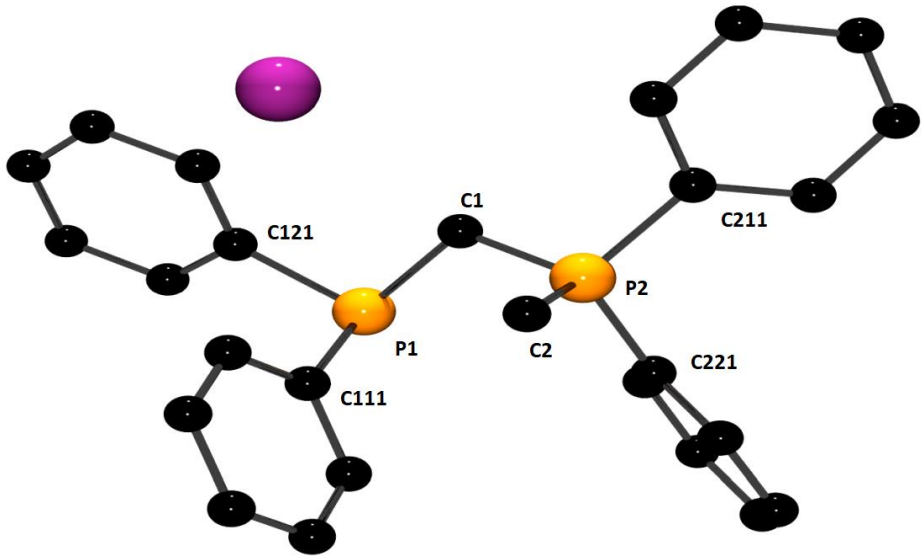

Figure 2.11 Crystal structure (ball and stick) of Compound 2.3.8 with selected bond lengths (Å) and angles (º): P2-C2, 1.7888(13); P2-C1, 1.8066(12); P1-C1, 1.8656(12); P1-C1-P2, 117.30(7). Hydrogen atoms are omitted for clarity.

Table 2.3 Selected Metrical Parameters of Compound 2.3.8.

Parameter	Value (Å/˚)	Literature Value(Å/˚)[28]
P1-C(Ph)	1.8300(13)*	N/A
P1-C1	1.8656(12)	N/A
P2-C(Ph)	1.7942(12)†	1.792(5)
P2-C1	1.7888(13)	1.782(5)
P2-C2	1.8066(12)	1.802(5)
P1-C1-P2	117.30(7)	N/A

*= this bond length is the average of P1-C121 and P1-C111; †= this bond length is the average of P2-C221 and P2-C211.

Even though excess iodomethane was used in this reaction, the desired demethylated product was not obtained. This could be due to the steric bulk of the phosphine not allowing the methylation of the phosphine sites. This supposition is supported by a study conducted on various phosphine ligands by Clavier and Nolan.[32] They compared numerous phosphines based on the percent buried volume, which is defined by the total volume of a sphere occupied by a chelating ligand with a metal at the center of the sphere. This helps assess the steric pressures brought on by a ligand. Clavier and Nolan found that dppm has the largest % buried volume among the bis(diphenylphosphines) with an alkyl bridge.[32] Although this ligand property is often discussed in terms of chelation, it can give insight into the steric bulk around the phosphine centers and thus help to assess the difficulty of methylating both sites. The larger the percent buried volume, the more difficult it may be to methylate both sites of a diphosphine.

Bis(methyldiphenylphosphonio)propane Iodide

To probe the hypothesis about steric prevention of reactivity, bis(diphenylphosphino)propane (dppp) was reacted with iodomethane to determine if mono- or dimethylated products are formed. The diphosphine was dissolved in toluene and MeI was added to the flask in a dropwise manner while the solution was stirring. Shortly after the MeI had been added, a white precipitate started to form in the flask. After 12h of stirring, the solvent was evaporated by vacuum and a white solid was collected. $^{31}P\{^{1}H\}$ NMR analysis was immediately carried out on the white powder to check if one or both phosphine sites had been methylated in the reaction. According to the literature, dppp has a chemical shift of -19.4 ppm.[33] Interestingly, the $^{31}P\{^{1}H\}$ NMR of the product showed only one peak at 24.8 ppm, which indicates that there is only one phosphorus environment in the product, and it is not a phosphine environment. The similarity in chemical shift between this product and other tetraalkylphosphonium environments presented in this thesis, especially tetramethylphosphonium (23.65 ppm) and the phosphonium site of Compound 2.3.8 (23.39 ppm), is evident. This shift is also close to PMe_4 cations previously reported in the literature.[17,23] Thus, based on the $^{31}P\{^{1}H\}$ NMR, it is reasonable to conclude that dppp was methylated at both phosphine sites. The reaction scheme along with the proposed product based on NMR is depicted in Scheme 2.7.

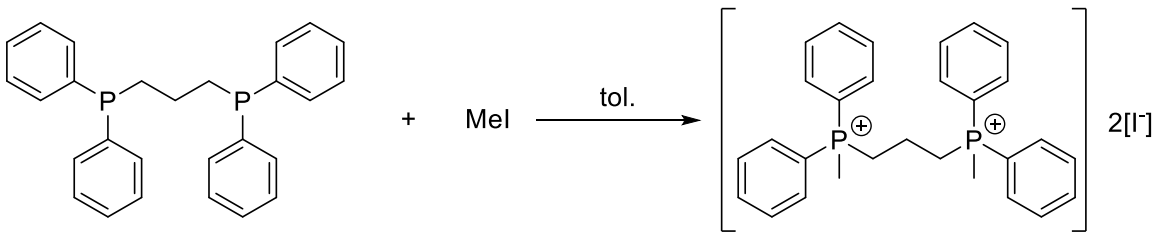

Scheme 2.7: The Methylation of dppp.

To further characterize this product, ^{1}H and $^{13}C\{^{1}H\}$ NMR spectra were collected. Five proton environments, which are labelled according to Figure 2.12, were observed. Environment C, which should resonate as a doublet of quintets due to coupling to phosphorus and Environment B, appeared as a multiplet at 1.74 ppm. Coupling constants that would represent the two-bond coupling to phosphorus and the three-bond coupling to Environment B were unable to be resolved. Environment A resonates just upfield from Environment C at 2.68 ppm. As predicted, this environment appears as a doublet due to the two-bond coupling of the methyl protons to the phosphorus. The coupling constant was quantified at 15.5Hz, which is similar to the $^{2}J_{PH}$ values observed in the literature.[22,28] Environment B appears as a doublet of triplets due to coupling to Environment C and phosphorus, with the two-bond coupling constant equal to 13Hz and the three-bond coupling constant equal to 8.5Hz. Environments D, E, and F appear downfield from the other shifts in the aromatic region of the spectrum since they are attached to the phenyl rings. Environments E and F could not be distinguished from each other since they occur at virtually the same shift. Their chemical shift range is 7.80-7.88 ppm. Environment D appeared further upfield at 7.69 ppm and showed a clear triplet of doublets splitting pattern. The three-bond coupling from Environment D to the phosphorus atom was found to be 3Hz, while the three-bond coupling from Environment D to the protons of Environment E is 8Hz.

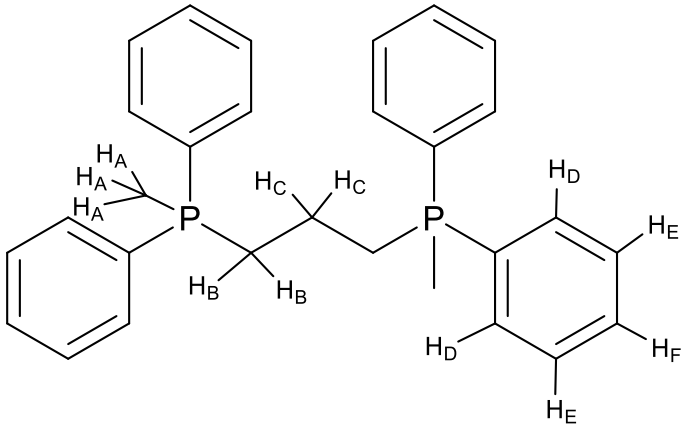

Figure 2.12: ^{1}H NMR Environments of bis(methyldiphenylphosphonio)propane iodide.

Table 2.4: Summary of ^{1}H NMR Shifts in Dimethylated dppp

Environment	Chemical Shift (ppm)	Multiplicity	Integration	Coupling Constant (Hz)
A	2.69	D	6	$^{2}J_{PH}$=15.5
B	3.27	Dt	4	$^{2}J_{PH}$=13.0 $^{3}J_{HH}$=8.5
C	1.74	M	2	Unresolved
D	7.69	Td	8	$^{3}J_{PH}$=3 $^{3}J_{HH}$=8
E,F	7.80-7.88	M	12	unresolved

The ^{13}C{^{1}H} further confirmed the demethylation of dppp. There were six carbon environments present in the spectrum, labelled according to Figure 2.13. The peak of the methyl carbons in Environment A was displayed as a doublet due to coupling to phosphorus at 4.94 ppm. The one-bond coupling constant of this carbon environment to phosphorus was quantified at 54.5Hz and falls in the middle of the literature range for one-bond carbon to phosphorus coupling.[17,23–25] Environment B also resonated as a doublet due to coupling to phosphorus at 21.9 ppm. The one-bond coupling constant of this environment to phosphorus was found to be 70.9Hz. Environment C appears as a singlet at 15.1 ppm, which is a common shift for bridging alkyl groups in these diphosphines.[28] The

ipso-carbon of the phenyl groups, Environment D, is a doublet at 119.7 ppm due to coupling to phosphorus. It has a $^{1}J_{PH}$ of 85.8Hz, which is at the upper end of the literature range for these coupling constants.[17,23–25] Environment E is the *ortho*-carbon on the phenyl groups and it experiences coupling to phosphorus as well, producing a doublet at 132.14 ppm and a coupling constant of 5.2Hz, which is weak coupling in comparison to the literature.[25] The *meta*-carbon, Environment F, experiences a similar coupling to phosphorus despite it being three bonds away. It appears as a doublet at 129.99 ppm with a calculated coupling constant of 6.2Hz. Finally, Environment G appears as a singlet at 134.63 ppm. It is four bonds away from phosphorus and thus does not experience any coupling to it.

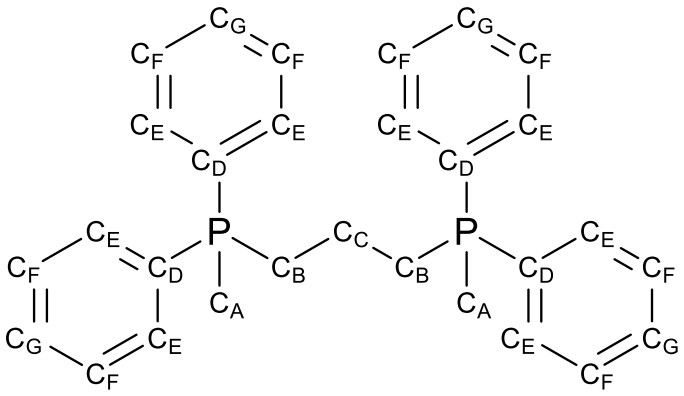

Figure 2.13: ^{13}C NMR Environments of Dimethylated dppp.

NMR analysis of the product point towards the synthesis of bis(methyldiphenylphosphonio)propane iodide. Since both phosphine sites were methylated, it is reasonable to conclude that this phosphine is less sterically encumbered than dppm. This is undoubtedly attributable to the longer alkyl bridge in dppp.

Bis(methyldiisopropylphosphonio)propane Iodide

Another phosphine with a propylene bridge, bis(diisopropylphosphino)propane was also reacted with iodomethane. This ligand will be called dippp for the remainder of this chapter. Like the other phosphines in this chapter, dippp was dissolved in toluene and MeI was added to this solution in a dropwise fashion. A white precipitate started to form just two minutes after adding the iodomethane. The reaction mixture was left to stir for 16h, after which the toluene was pumped off. A white solid was collected and analyzed via NMR spectroscopy. Figure 2.14 shows the predicted product.

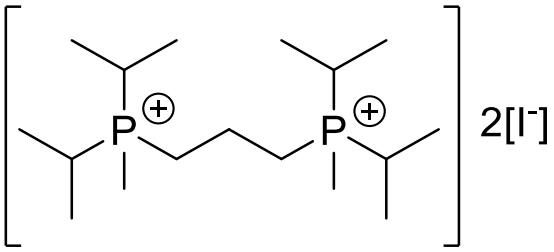

Figure 2.14: Bis(methyldiisopropylphosphonio)propane iodide

A $^{31}P\{^{1}H\}$ NMR spectrum was collected to see if the phosphine was methylated at both sites. The spectrum showed a single peak at 42.5 ppm, which is downfield from the literature shift of dippp at 3.13 ppm.[34] Since only one phosphorus environment was present, this suggests that both phosphine sites were indeed methylated. A ^{1}H NMR spectrum was also taken to observe the proton environments of this species, which are depicted in Figure 2.15. A summary of the spectrum is presented in Table 2.5. Environments A, B, and C appear in the spectrum as predicted. Environment A is a doublet of doublets at 1.31 ppm due to coupling to the ipso protons of the isopropyl groups as well as coupling to phosphorus. Both environments are three bonds away from Environment A, however the

three-bond coupling due to phosphorus (17Hz) is stronger than the three-bond coupling to Environment C (7Hz). The methyl protons of Environment B also show the predicted doublet splitting pattern due to coupling to phosphorus. These protons resonate at 1.80 ppm and have a two-bond coupling constant of 12Hz. The ipso proton (Environment C) resonates as a doublet of septets at 1.52 ppm due to coupling to phosphorus and the Environment A protons. The two-bond coupling constant to phosphorus, 363Hz, is much larger than the others observed in similar phosphonium salts. The coupling to the Environment A protons was not able to be resolved. Environment D, which should have appeared on the spectrum as a doublet of triplets, resonated as a multiplet at 2.44 ppm. Hence, the two-bond and three-bond coupling to phosphorus and the protons of Environment E, respectively, were not able to be resolved. Similarly, Environment E was a multiplet when it should have appeared as a doublet of quintets due to coupling to phosphorus and the four protons of Environment D. This coupling was also unresolvable.

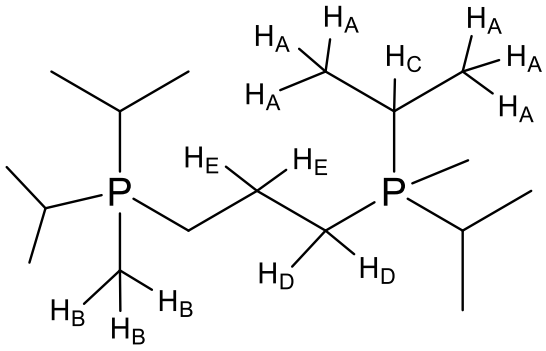

Figure 2.15: ^{1}H NMR Environments of Bis(methyldiisopropylphosphonio)propane iodide.

Table 2.5: A Summary of the ^{1}H NMR Spectrum of Bis(methyldiisopropylphosphonio)propane iodide.

Environment	Chemical Shift (ppm)	Multiplicity	Integration	Coupling Constant (Hz)
A	1.31	Dd	24H	$^{3}J_{PH}$= 17Hz $^{3}J_{HH}$= 7Hz
B	1.80	D	6H	$^{2}J_{PH}$= 12Hz
C	1.52	Dsept	4H	$^{2}J_{PH}$=363Hz $^{3}J_{HH}$= unresolved
D	2.44	M	4H	Unresolved
E	2.69	M	2H	Unresolved

2.2.3 Chapter Conclusions

This chapter explored the synthesis of various phosphonium iodide salts as potential precursors to phosphonium-templated perovskites. To achieve this, organic monophosphines and diphosphines were protonated and methylated using hydoiodic acid and iodomethane, respectively. Ten phosphonium salts were synthesized in good yield and characterized via NMR spectroscopy. Five monophosphonium iodide salts were synthesized, including [(Diphenylphosphino)methyl]methyldiphenylphosphonium iodide, which was intended to be a diphosphonium salt. Its crystal structure, along with that of tetramethylphosphonium iodide and trimethylphosphonium iodide, was crystallographically elucidated and compared to the current literature. Five diphosphonium salts were synthesized and characterized by NMR spectroscopy. Thus, a library of phosphonium iodide salts with varying substituent size was built for eventual reaction with group 14 halides with the goal of forming a phosphonium-templated perovskite.

2.3 Experimental

General Procedures

All manipulations were carried out using standard inert atmosphere techniques. All chemicals and reagents were purchased from Sigma-Aldrich, except for tri(n-butyl)phosphine which was purchased from Strem Chemicals, and used without further purification. Deuterated solvents were dried according to literature procedure when necessary, and all other solvents were dried over a series of Grubbs'-type columns and degassed prior to use. NMR spectra were recorded at room temperature on a Bruker Avance III 500 MHz, Bruker Avance Ultrashield 300 MHz or Bruker Avance DPX 300 MHz spectrometers. Chemical shifts are reported in ppm relative to internal standards for ^{1}H and ^{13}C (the given deuterated solvent) and the external standard for ^{31}P (85% H_3PO_4). Coupling constants |J| are given in Hz. Elemental Analysis was performed by the University of Windsor Mass Spectrometry Service Laboratory using Perkin Elmer 2400 combustion CHN analyzer.

X-Ray Crystallography

Crystals for investigation were covered in Paratone®, mounted into a goniometer head, and then rapidly cooled under a stream of cold N2 of the low-temperature apparatus (Oxford Cryostream) attached to the diffractometer. The data were then collected using the APEXII software suite[35] on a Bruker Photon 100 CMOS diffractometer using a graphite monochromator with MoKα (λ = 0.71073 Å) or CuKα (λ = 1.54178 Å) radiation. For each sample, data were collected at low temperature. APEXII software was used for data reductions and SADABS[36] was used for absorption corrections (multi-scan; semi-empirical

from equivalents). XPREP was used to determine the space group and the structures were solved and refined using the SHELX[37] software suite as implemented in the WinGX[38] or OLEX2[39] program suites. Validation of the structures was conducted using PLATON.[40]

2.3.1 Tetramethylphosphonium iodide

To a 100mL Schlenk flask was added trimethylphosphine (0.75mL, 7.5mmol) and dissolved in ca. 30mL of toluene. Iodomethane (0.47mL, 7.50mmol) was added to the Schlenk flask in a dropwise fashion under stirring and nitrogen atmosphere. Upon addition of MeI, a white precipitate formed. After approximately 24h of stirring, the toluene was pumped off and a white solid was collected. Some of this solid was dissolved in acetonitrile and left for slow evaporation, bestowing crystals suitable for X-ray diffraction. Yield: 78.0% (1.275 g, 5.84 mmol). $^{31}P\{^{1}H\}$ NMR (D_2O) δ: 23.65 (s). $^{13}C\{^{1}H\}$ NMR (CD_3CN) δ: 9.98 (d, P*C*H_3, $^{1}J_{CP}$ = 56.3Hz). ^{1}H NMR (CD_3CN) δ: 1.84 (d, 12H, PC***H*****3**, $^{2}J_{HP}$=15Hz). Elemental analysis: calc. for $C_4H_{12}PI$·0.33 tol: C, 30.51; H, 5.94; N, 0.00, found: C, 30.42; H, 5.73; N, 0.21.

2.3.2 Trimethylphosphonium iodide

0.5mL of trimethylphosphine was dissolved in toluene in a Schlenk flask. Hydroiodic acid (0.64mL) was added dropwise to the Schleck flask containing trimethylphosphine solution under stirring, forming a white precipitate. The solution was allowed to stir for 24 hours, after which the solvent was pumped off. The solid was dissolved in acetonitrile and left to recrystallize by slow evaporation, granting colourless crystals suitable for X-ray diffraction. Yield: 70% (0.758 g, 3.71 mmol). $^{31}P\{^{1}H\}$ NMR (CD_3CN) δ: 2.089 (s). $^{13}C\{^{1}H\}$ NMR (CD_3CN) δ: 5.75 (d, P*C*H_3, $^{1}J_{CP}$ = 55.6). ^{1}H NMR

(CD_3CN) δ: 1.85 (dd, 9H, PC***H₃***, $^2J_{HP}$=16.5Hz., $^3J_{HH}$=6.3Hz), 6.423 (ddec, 1H, P***H***, $^1J_{HP}$= 513Hz, $^3J_{HH}$=5.7Hz.) . Elemental analysis: calc. for $C_3H_{10}PI$: C, 17.66; H, 5.13; N, 0.00, found: C, 18.13; H, 5.13; N, 0.04.

2.3.3 Tri(n-butyl)phosphonium iodide

Tri-n-butylphosphine (0.75mL, 3.0mmol) was added to a 100mL Schlenk flask with ca. 30mL of toluene. Under stirring, hydroiodic acid (0.41mL, 3.0mmol) was added dropwise to the flask under nitrogen atmosphere. After 24h, the toluene was pumped off and an orange oily substance was left in the flask. The orange substance was placed under vacuum, and after 6h a pale pink solid was collected. Yield: 96% (1.566 g, 4.74 mmol). $^{31}P\{^1H\}$ NMR (CD_3CN) δ: 12.98 (s). $^{13}C\{^1H\}$ NMR (CD_3CN) δ: 12.70 (s, PCCC***C***H_3), 16.10 (d, P***C***H_2CCC,$^1J_{CP}$=47.2Hz), 23.36 (d, PC***C***H_2CC, $^2J_{PC}$ =15.5Hz), 24.20 (d, PCC***C***H_2C, $^3J_{PC}$= 4.7Hz). ^1H NMR (CD_3CN) δ: 0.95 (t, 9H, PCCCC***H₃***, $^3J_{HH}$=7.0Hz), 1.49 (m, 6H, PCCC***H₂***C, unresolved coupling), 1.62 (m, 6H, PCC***H₂***CC, unresolved coupling), 2.35 (m, 6H, PC***H₂***CCC, unresolved coupling), 7.40 (dsept, 1H, P***H***, $^1J_{HP}$= 489Hz, $^3J_{HH}$=5.5Hz.). Elemental analysis: calc. for $PC_{12}H_{28}I$: C, 43.65; H, 8.55; N, 0.00, found: C, 43.36; H, 8.54; N, 0.02.

2.3.4 Tri(n-butyl)methylphosphonium iodide

0.75mL (3.0mmol) of tri(n-butyl)phosphine was added to a 100mL Schlenk flask along with ca. 30mL of toluene. Iodomethane (0.43mL, 3.0mmol) was added dropwise to the flask under nitrogen atmosphere. A white precipitate formed immediately upon introduction of MeI to the solution and the reaction was left to stir for 16h. After 16h, the toluene was pumped off and a white solid was collected. Yield: 66% (0.403 g, 1.17 mmol).

$^{31}P\{^{1}H\}$ NMR (DMSO-d_6) δ: 32.95 (s). $^{13}C\{^{1}H\}$ NMR (DMSO-d_6, 125.77MHz) δ: 13.25 (s, PCCC***C***H_3), 18.89 (d, P***C***H_3 $^{1}J_{CP}$ = 49.4Hz), 22.55(d, P***C***H_2CCC, $^{1}J_{CP}$= 4.3Hz), 23.21(s, PCC***C***H_2C), 22.33(s, PC***C***H_2CC). ^{1}H NMR (DMSO-d_6) δ: 1.80 (d, 3H, PC***H₃***, $^{2}J_{PH}$=13.5Hz.), 2.17 (m, 2H, PC***H₂***CCC, $^{2}J_{PH}$=14.5Hz), 1.46 (m, 2H, PCC***H₂***CC, unresolved coupling), 1.41 (m, 2H, PCCC***H₂***C, unresolved coupling), 0.93 (t, 3H, PCCCC***H₃***, $^{3}J_{HH}$ = 7Hz). Elemental analysis: calc. for $PC_{13}H_{30}I$: C, 45.36; H, 8.78; N, 0.00, found: C, 44.57; H, 8.66; N, 0.01.

2.3.5 Bis(dimethylphosphonio)ethane iodide

2.61mL (15.9mmol) of dmpe was added to a Schlenk flask and dissolved in ca. 10mL of toluene. Hydroiodic acid (4.19mL, 31.9mmol) was added to the flask containing dmpe in a dropwise fashion under stirring, producing a brown solution. After approx. 2mins, the solution turned pale yellow and a small amount of white precipitate was visible in the flask. The reaction mixture was left to stir for 16h, after which a white precipitate was observed in a colourless solution. The toluene was pumped off and a white solid was collected. Yield: 55% (1.273 g, 8.26 mmol). $^{31}P\{^{1}H\}$ NMR (MeCN, 121.5MHz) δ: 5.55 (s). Elemental analysis: calc. for $P_2C_6H_{18}I_2$: C, 17.75; H, 4.47; N, 0.00, found: C, 17.81; H, 3.51; N, 0.01.

2.3.6 Bis(trimethylphosphonio)ethane iodide

Dmpe (0.25mL, 1.53mmol) was dissolved in ca. 10mL of toluene in a Schlenk flask. Two equivalents of MeI (0.19mL, 3.06mmol) was added to the flask in a dropwise fashion under stirring. A white precipitate was observed at the surface of the solution upon addition of the first drops of MeI. The reaction mixture was left to stir for 18h and the solvent was pumped off. A white powder was collected. Yield: 78% (0.515 g, 1.19 mmol). $^{31}P\{^{1}H\}$

NMR (DMSO-d_6) δ: 32.49 (s). $^{13}C\{^1H\}$ NMR (D_2O) δ: 6.92 (t, P(***C***$H_3)_3$, $^1J_{CP}$ = 26.2Hz), 15.24(s, P(μ-***C***H_2). ^1H NMR (D_2O) δ: 1.99 (d, 18H, P(C***H₃***$)_3$, $^2J_{PH}$=13.8Hz.), 2.65 (d, 4H, P(μ-C***H₂***$)_2$, $^3J_{PH}$ = 6Hz). Elemental analysis: calc. for $P_2C_8H_{22}I_2$•tol: C, 34.24; H, 5.75; N, 0.00, found: C, 33.93; H, 5.48; N, -0.03.

2.3.7 [(Diphenylphosphino)methyl]methyldiphenylphosphonium iodide

0.100g (0.26mmol) of dppm was dissolved in toluene in a Schlenk flask and 0.1mL (1.6mmol) of MeI was added dropwise under stirring. No immediate colour change was observed upon addition of MeI, however after approx. 20 minutes a clear solution with a white precipitate was observed. The reaction mixture was left to stir for 18h. The reaction mixture was filtered through a frit and a white solid was collected and pumped on to remove any lingering solvent. The white solid was dissolved in MeCN and produced crystals suitable for X-ray diffraction. Yield: 88% (0.092g, 0.23 mmol). $^{31}P\{^1H\}$ NMR (CD_3CN, 202.45MHz) δ: -28.06 (d, ***P***$(Ph)_2$, $^2J_{PP}$ = 64.2Hz), 23.39 (d, Me***P***$(Ph)_2$, $^2J_{PP}$ = 64Hz). ^1H NMR (CD_3CN, 500MHz) δ: 2.42 (d, 3H, PC***H₃***, $^2J_{PH}$=13.5Hz.), 3.71 (d, 2H, PC***H₂***P, $^1J_{PH}$ = 15Hz), 7.18-7.25 (m, 2H, H-Ph, unresolved coupling), 7.30-7.32 (m, 2H, H-Ph, unresolved coupling), 7.33-7.36 (m, 4H, H-Ph, unresolved coupling), 7.41-7.44(m, 4H, H-Ph, unresolved coupling), 7.53-7.57(m, 4H, H-Ph, unresolved coupling), 7.67-7.72(m, 4H, H-Ph, unresolved coupling). Elemental analysis: calc. for $P_2C_{26}H_{25}I_2$•1.5tol: C, 55.39; H, 4.71; N, 0.00, found: C, 55.51; H, 4.51; N, 0.00.

2.3.8 Bis(methyldiphenylphosphonio)propane iodide

Bis(diphenylphosphino)propane (0.100g, 0.24mmol) was added to a Schlenk flask and dissolved in ca. 20mL of toluene. 0.15mL of iodomethane (2.42mmol) was added dropwise

to the flask containing the phosphine under stirring. After a few minutes, a white precipitate was present in the reaction flask and the mixture was left to stir for 12h. The toluene was pumped off and a white powder was collected. Yield: 56% (0.094 g, 0.14 mmol). $^{31}P\{^{1}H\}$ NMR (DMSO-d_6) δ: 24.58 (s). $^{13}C\{^{1}H\}$ NMR (DMSO-d_6) δ: 4.94 (d, 2C, P***C***H_3, $^{1}J_{CP}$ = 54.5Hz), 15.13 (s, 1C, PC***C***CP), 119.72 (d, 4C, P$\boldsymbol{C_{ipso}}$, $^{1}J_{CP}$ =85.8Hz), 129.99 (d, 8C, $\boldsymbol{C_{meta}}$, $^{3}J_{CP}$ = 6.2Hz.), 132.14 (d, 8C, $\boldsymbol{C_{ortho}}$, $^{2}J_{CP}$ = 5.2Hz.), 134.63 (s, 4C, $\boldsymbol{C_{para}}$). ^{1}H NMR (DMSO-d_6) δ: 1.74 (m, 2H, PCC$\boldsymbol{H_2}$CP, unresolved coupling), 2.68 (d, 6H, PC$\boldsymbol{H_3}$, $^{2}J_{PH}$=15.5Hz.), 3.27 (dt, 4H, PC$\boldsymbol{H_2}$, $^{2}J_{PH}$=13Hz, $^{3}J_{HH}$=8.5Hz), 7.69 (td, 8H, PCC(***H-ortho)***$_2$, $^{3}J_{PH}$ = 3Hz., $^{3}J_{HH}$ = 8Hz.), 7.80-7.88 (m, 12H, ***H-meta (2) & H-para***, unresolved coupling). Elemental analysis: calc. for $P_2C_{29}H_{32}I_2$•0.75tol: C, 53.74; H, 5.00; N, 0.00, found: C, 53.64; H, 4.95; N, -0.01.

2.3.9 Bis(methyldiisopropylphosphonio)propane iodide

0.29g (1.03mmol) of dippp was added to a Schlenk flask and dissolved in toluene. Two equivalents of iodomethane (0.13mL, 2.06mmol) were added to the Schlenk flask containing dippp in a dropwise fashion under stirring. Approximately two minutes following the addition of the MeI, a white precipitate started to form. The reaction mixture was left to stir for 16h, after which the toluene was pumped off and a white solid was collected. Yield: 83% (0.357 g, 0.85 mmol). $^{31}P\{^{1}H\}$ NMR (D_2O) δ: 42.15 (s). ^{1}H NMR (DMSO-d_6) δ: 1.31 (dd, 24H, PCCC$\boldsymbol{H_3}$, $^{3}J_{PH}$=17Hz, $^{3}J_{HH}$=7Hz), 1.80 (d, 6H, PC$\boldsymbol{H_3}$, $^{2}J_{PH}$= 12Hz), 1.52 (dsept, 4H, PC***H***, $^{2}J_{PH}$= 363Hz), 2.44 (m, 4H, PC$\boldsymbol{H_2}$CC$\boldsymbol{H_2}$P, unresolved coupling), 2.69 (m, 1H, PCC$\boldsymbol{H_2}$CP, unresolved coupling). Elemental analysis: calc. for $P_2C_{17}H_{40}I_2$•0.75tol: C, 42.46; H, 7.37; N, 0.00, found: C, 42.08; H, 8.01; N, -0.05.

2.4 References

(1) Crabtree, R. H. The Organometallic Chemistry of the Transition Metals, Fifth.; John Wiley & Sons, Inc.: New Haven, **2009**.

(2) Burt, J.; Levason, W.; Reid, G. Coordination Chemistry of the Main Group Elements with Phosphine, Arsine and Stibine Ligands. *Coord. Chem. Rev.* **2014**, *260* (1), 65–115.

(3) Downing, J. H.; Smith, M. B. Phosphorus Ligands. In Comprehensive Coordination Chemistry II; Elsevier, **2003**; pp 253–296.

(4) Tolman, C. A. Steric Effects of Phosphorus Ligands in Organometallic Chemistry and Homogeneous Catalysis. *Chem. Rev.* **1977**, *77* (3), 313–348.

(5) Tolman, C. A. Phosphorus Ligand Exchange Equilibriums on Zerovalent Nickel. Dominant Role for Steric Effects. *J. Am. Chem. Soc.* **1970**, *92* (10), 2956–2965.

(6) Corbridge, D. E. C. Phosphorus: An Outline of Its Chemistry, Biochemistry, and Uses; Elsevier, **1995**.

(7) Stoumpos, C. C.; Malliakas, C. D.; Kanatzidis, M. G. Semiconducting Tin and Lead Iodide Perovskites with Organic Cations: Phase Transitions, High Mobilities, and Near-Infrared Photoluminescent Properties. *Inorg. Chem.* **2013**, *52* (15), 9019–9038.

(8) Stoumpos, C. C.; Frazer, L.; Clark, D. J.; Kim, Y. S.; Rhim, S. H.; Freeman, A. J.; Ketterson, J. B.; Jang, J. I.; Kanatzidis, M. G. Hybrid Germanium Iodide Perovskite

Semiconductors: Active Lone Pairs, Structural Distortions, Direct and Indirect Energy Gaps, and Strong Nonlinear Optical Properties. *J. Am. Chem. Soc.* **2015**, *137* (21), 6804–6819.

(9) Grätzel, M. The Light and Shade of Perovskite Solar Cells. *Nat. Mater.* **2014**, *13* (9), 838–842.

(10) Weber, D. $CH_3NH_3PbX_3$, a Pb(II)-System with Cubic Perovskite Structure. *Zeitschrift für Naturforsch. B.* **1978**, *33*, 1443–1445.

(11) Herrmann, F.; Kuhn, N. Ein Einfacher Zugang Zu Tetramethylphosphoniumiodid / A Simple Access to Tetramethylphosphonium Iodide. *Zeitschrift für Naturforsch. B.* **2012**, *67* (8), 853–854.

(12) Kornath, A.; Neumann, F.; Oberhammer, H. Tetramethylphosphonium Fluoride: "Naked" Fluoride and Phosphorane. *Inorg. Chem.* **2003**, *42* (9), 2894–2901.

(13) Bellachioma, G.; Cardaci, G.; Macchioni, A.; Venturi, C.; Zuccaccia, C. Reductive Elimination of Halogens Assisted by Phosphine Ligands in $Fe(CO)_4X_2$ (X=I,Br) Complexes. *J. Organomet. Chem.* **2006**, *691* (18), 3881–3888.

(14) Kociok-Köhn, G.; Winter, J. G.; Filippou, A. C. Trimethylphosphonium Trichlorogermanate(II). *Acta Crystallogr. Sect. C Cryst. Struct. Commun.* **1999**, *55* (3), 351–353.

(15) Pusztai, Z.; Vlád, G.; Bodor, A.; Horváth, I. T.; Laas, H. J.; Halpaap, R.; Richter, F. U. In Situ NMR Spectroscopic Observation of a Catalytic Intermediate in

Phosphine-Catalyzed Cyclo-Oligomerization of Isocyanates. *Angew. Chemie Int. Ed.* **2006**, *45* (1), 107–110.

(16) Guthrie, R.; Jenkins, I. The Mechanism of the Mitsunobu Reaction. A ^{31} P N.M.R. Study. *Aust. J. Chem.* **1982**, *35* (4), 767.

(17) Herrmann, F.; Kuhn, N. Ein Einfacher Zugang Zu Tetramethylphosphoniumiodid A Simple Access to Tetramethylphosphonium Iodide. *Z. Naturforsch.* **2012**, *67*, 853–854.

(18) Liu, Y.; Liu, Y.; Huang, S.; Li, Z.; Liu, Q.; Liu, Y. Synthetic Method of Tributylmethylphosphonium Iodide. CN 105330694, **2016**.

(19) Aoyagi, N.; Endo, T. Manufacture of Cyclic Carbonates from Epoxides, Carbon Dioxide, Phosphonium Salts, and Epoxy-Reactive Compounds. WO 2014034936, **2014**.

(20) Pavia, D. L.; Lampman, G. M.; Kriz, G. S.; Vyvyan, J. R. Introduction to Spectroscopy, 5th ed.; Cengage Learning: Stamford, CT, **2015**.

(21) Burt, R. J.; Chatt, J.; Hussain, W.; Leigh, G. J. A Convenient Synthesis of 1,2-Bis(Dichlorophosphino)Ethane, 1,2-Bis(Dimethylphosphino)Ethane and 1,2-Bis(Diethylphosphino)Ethane. *J. Organomet. Chem.* **1979**, *182* (2), 203–206.

(22) Yuan, B.; Hu, W.; Lv, S.; Huang, J.; Huang, K. Synthesis of Aliphatic Symmetric Diphosphonium Salts and Bactericidal Activity of Selected Products. *Chem. J. Mold.* **2017**, *12* (1), 81–86.

(23) Kornath, A.; Neumann, F.; Oberhammer, H. Tetramethylphosphonium Fluoride: "Naked" Fluoride and Phosphorane. *Inorg. Chem.* **2003**, *42* (9), 2894–2901.

(24) Burford, N.; Ragogna, P. J.; McDonald, R.; Ferguson, M. J. Homoatomic P - P Coordination: A Versatile Synthetic Approach to Polyphosphorus Dications. *Chem. Commun.* **2003**, No. 16, 2066.

(25) Jia, Y.-X.; Yang, X.-Y.; Tay, W. S.; Li, Y.; Pullarkat, S. A.; Xu, K.; Hirao, H.; Leung, P.-H. Computational and Carbon-13 NMR Studies of Pt–C Bonds in P–C–P Pincer Complexes. *Dalt. Trans.* **2016**, *45* (5), 2095–2101.

(26) Xu, Q.; Kwon, O. 1,2-Bis(Diphenylphosphino)Methane. In Encyclopedia of Reagents for Organic Synthesis; John Wiley & Sons, Ltd: Chichester, UK, **2012**.

(27) Schmidbaur, H.; Deschler, U. Die Atomsequenz PCPCP Als Grundstrukturelement Für Phosphoniumsalze, Ylide Und Deren Alkalikomplexe. *Chem. Ber.* **1983**, *116* (4), 1386–1392.

(28) Langer, J.; Meyer, S.; Dündar, F.; Schowtka, B.; Görls, H.; Westerhausen, M. Dppm-Derived Phosphonium Salts and Ylides as Ligand Precursors for s-Block Organometallics. *Issue Honor Prof. Rainer Beckert Ark.* **2012**, 210–225.

(29) Petz, W.; Dehnicke, K.; Neumüller, B. About the Reaction of $BeCl_2$ with the Carbodiphosphorane Addition Compound $O_2C{\leftarrow}C(PPh_3)_2$ and Its Hydrolysis Product $Ph_3PCHP(O)Ph_2$. *Zeitschrift für Anorg. und Allg. Chemie.* **2011**, *637* (12), 1761–1768.

(30) Petz, W.; Fahlbusch, M.; Gromm, E.; Neumüller, B. The Ylide Adduct $SOC_2(PPh_3)_2$ as Complex Ligand. Reaction with $[Mn_2(CO)_{10}]$ and $InCl_3$; Crystal Structures of $[(CO)_4Mn(SOC_2\{PPh_3\}_2)_2][Mn(CO)_5]$ and $(H_2C\{PPh_3\}_2)[InCl_4]_2$. *Zeitschrift für Anorg. und Allg. Chemie*. **2008**, *634* (4), 682–687.

(31) Petz, W.; Neumüller, B. Reaction of $(PPh_3)_2C{\rightarrow}CO_2$ with Halogenated Hydrocarbons; Formation and Crystal Structure of a Cationic Ester with 1, 2-Dichloroethane. *Zeitschrift für Anorg. und Allg. Chemie.* **2012**, *638* (6), 987–991.

(32) Clavier, H.; Nolan, S. P. Percent Buried Volume for Phosphine and N-Heterocyclic Carbene Ligands: Steric Properties in Organometallic Chemistry. *Chem. Commun.* **2010**, *46* (6), 841.

(33) Dean, P. A. W. Nuclear Magnetic Resonance Studies of the Solvation of Phosphorus(V) Selenides, 1,2-Bis(Diphenylphosphino)Ethane, and Tris(Dimethylamino)Phosphine Telluride by Sulfur Dioxide. *Can. J. Chem.* **1979**, *57* (7), 754–761.

(34) Dillon, K. B.; Goeta, A. E.; Howard, J. A. K.; Monks, P. K.; Shepherd, H. J.; Thompson, A. L. Alkyl and Aryl Dicationic Derivatives of Cyclic Triphosphenium Ions. *Dalton Trans.* **2008**, No. 9, 1144.

(35) APEX II. Bruker AXS Inc. APEX II. Bruker AXS Inc.: Madison, WI p Madison, WI, 2012.

(36) SADABS. Bruker AXS Inc. SADABS. Bruker AXS Inc.: Madison, WI p Madison, WI, 2008.

(37) Sheldrick, G. M. A Short History of SHELX. *Acta Crystallogr. A.* **2008**, *64* (Pt 1), 112–122.

(38) Farrugia, L. J. WinGX Suite for Small-Molecule Single-Crystal Crystallography. *J. Appl. Crystallogr.* **1999**, *32* (4), 837–838.

(39) Dolomanov, O. V.; Bourhis, L. J.; Gildea, R. J.; Howard, J. A. K.; Puschmann, H. OLEX2 : A Complete Structure Solution, Refinement and Analysis Program. *J. Appl. Crystallogr.* **2009**, *42* (2), 339–341.

(40) Spek, A. L. Single-Crystal Structure Validation with the Program PLATON. *J. Appl. Crystallogr.* **2003**, *36* (1), 7–13.

CHAPTER 3: Phosphonium-Templated Iodoplumbates

3.1 Introduction

In the past two decades, lead(II) iodide-organic hybrids (iodoplumbates) have emerged as promising materials for a myriad of applications ranging from photovoltaics and non-linear optics to semiconductors and dielectric materials.[1] This great diversity of applications is a consequence of their variable and interesting optical and electronic properties. The topology of the anionic lead(II) iodide component (which largely determines the electronic and optical properties) is controlled by the packing of the cationic organic components.[1,2] Typically, small cations like methylammonium and formamidinium yield three-dimensional perovskites which make useful light-harvesting materials.[1,3] Larger polycationic organic components give rise to two-dimensional and one-dimensional iodoplumbate networks[4,5], which can exhibit interesting optical properties (e.g. efficient photoluminescence[6], non-linear optics) or magnetic properties[7], respectively. Nitrogen centered organic cations are components in most examples of iodoplumbate materials, with there being only a few examples containing phosphorus centered organic cations.[8] This chapter presents the reactions of four monophosphoniums and one diphosphonium with lead (II) iodide and demonstrates the potential applications of these products.

3.2 Results & Discussion

3.2.1 Monophosphonium-Templated Iodoplumbates

Group 14 iodometalates have demonstrated the ability to form perovskitic structures of the formula ABI_3, where 'A' is a monocation and 'BI_3' is a monoanion.[3] Historically, the 'A' cation site is occupied by a larger alkali metal such as Rb or Cs[2,9,10] or an alkylammonium.[11–14] These cations render 3D perovskite structures due to their smaller size. When a larger cation is used, a 2D- or 1D- perovskitic structure is observed with possible formulae of the general form ABI_3, A_2BI_4, and A_3BI_5.[13–17] Given that different-sized alkylammonium cations produce different dimensionalities of anion connectivity, and in light of the interesting structures obtained with trimethyl sulfonium cations,[17] we sought to elucidate the structures obtained using alkyl- and arylphosphonium cations. Trimethylphosphonium, tetramethylphosphonium, tri(n-butyl)phosphonium and methyltriphenylphosphonium iodide salts were used to react with lead (II) iodide in the hopes of obtaining distorted perovskitic structures.

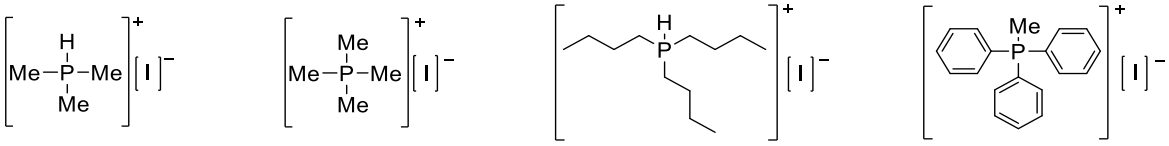

Figure 3.1 Monophosphoniums Reacted with PbI_2.

The new family of phosphonium-templated perovskite was initiated by reacting trimethylphosphonium iodide with lead (II) iodide. A recent paper by Saidaminov et al.[18] demonstrated the creation of perovskite crystals by inverse temperature crystallization (ITC), a method that takes advantage of the decrease in solubility of products in certain

solvents as the temperature increases. Thus, trimethylphosphonium iodide and PbI_2 were dissolved in DMSO, creating a yellow solution and heated at 120℃ for 16h to evaporate the solvent. A brown substance coated the bottom and sides of the vial in a thin layer after this time and could not be recovered for analysis. Given these results, another method of obtaining crystals was attempted.

Since high-performing perovskites have been synthesized via a ball-milling[6,19], the reaction of trimethylphosphonium iodide and PbI_2 was attempted mechanochemically. $[HPMe_3]$ [I], a colourless salt, and PbI_2, a pale-yellow solid, were placed in a ball mill for one hour at a milling frequency of 30Hz, yielding a golden-yellow powder. Since the colour of the mixture changed after milling, there is reason to believe that a reaction did occur. The powder was analyzed via $^{31}P\{^1H\}$ and ^1H NMR spectroscopy. The $^{31}P\{^1H\}$ NMR displayed a lone singlet at -0.27 ppm, which is similar to the shift observed for trimethylphosphonium iodide in this thesis (2.09 ppm) as well as that observed by Bellachioma et al. (-0.44 ppm[20]). The absence of other phosphorus environments and the similarities between this shift and the literature shift[20] support the persistence of the phosphonium in the product mixture. The ^1H NMR gave further evidence for the presence of the phosphonium since there was a doublet of multiplets observed at 6.33 ppm, representing the lone proton attached to the phosphorus atom. As previously determined in Chapter 2 of this thesis, the lone proton should appear as a doublet of decets due to coupling to phosphorus and the nine methyl protons. The one-bond coupling of the proton to the phosphorus atom was resolved at 119Hz, whereas the three-bond coupling of the proton to the methyl protons could not be resolved. This could be due to solvent effects since DMSO was used to prepare the sample. A doublet of doublets, which represents the nine methyl

protons, was observed at 1.63 ppm. The larger splitting, 119Hz, is due to the coupling of the methyl protons to the phosphorus atom that is two bonds away and the smaller splitting, 16.2Hz, results from coupling to the lone proton three bonds away. Attempts at obtaining crystals suitable for X-Ray diffraction from this powder were unsuccessful, however the colour change as the reaction progressed and the NMR evidence of the phosphonium indicate that new products were accessed.

Although ITC[18] did not work for the reaction of trimethylphosphonim iodide with PbI_2 and elevated temperatures caused decomposition of the reactants, crystals of the reaction of tetramethylphosphonium iodide with lead(II) iodide were successfully obtained. For tetramethylphosphonium, the starting materials were combined in DMSO and heated at 120˚C to drive off the solvent. After two days mustard-yellow crystals suitable for X-Ray diffraction ($[PMe_4][PbI_3]$) were collected directly from the product. Alternatively, crystals for the reaction of lead(II) iodide with tri(n-butyl)phosphonium ($[PH(n\text{-}butyl)_3][PbI_3]$) and methyltriphenylphosphonium iodide ($[PPh_3Me][PbI_3]$) were obtained by slow evaporation from acetonitrile. The reaction of $[PPh_3Me][I]$ and lead(II) iodide was carried out in the same manner as the reaction with $[PMe_4][I]$, however a yellow powder was created as opposed to crystals. This yellow powder was then dissolved in MeCN, which granted crystals for X-Ray Diffraction.

A different preparative method was used for $[PH(n\text{-}butyl)_3]$ $[PbI_3]$. Since HI was used to make the reactant phosphonium and elevated temperatures had previously caused these protonated phosphoniums to decompose, the reactants were dissolved in acetonitrile and allowed to react. A yellow solution was produced immediately upon combination of the two reactants and after 24h of stirring a yellow precipitate in yellow solution was present.

The solution was separated from the precipitate and set up for slow recrystallization. Yellow crystals suitable for X-Ray diffraction were obtained.

NMR data revealed that the phosphonium cations, whose spectra were previously elucidated in Chapter 2, persisted in the product mixture. Interestingly, the single-crystal X-Ray diffraction data of the monophosphonium-lead iodide reactions did not yield traditional perovskites of the form ABI_3 but provided instead an extended 1-D network of PbI_3^- fragments in which each lead atom is coordinated octahedrally and the resultant octahedra are linked to each other in a face-sharing fashion. The anionic fragments were charged-balanced with the monophosphonium cation. The 1-D $[PbI_3^-]_\infty$ network is pictured in Figure 3.2. Figure 3.3 shows the face-sharing octahedra demonstrated by the lead-iodide fragments.

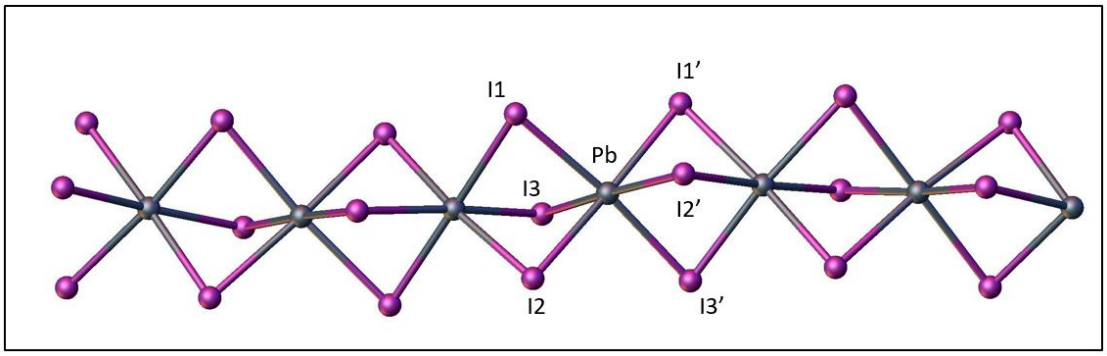

Figure 3.2: The $[PbI_3]_\infty$ chain of **[PMe$_4$][PbI$_3$]**. The iodine atoms labelled with a prime symbol indicate the symmetry-generated iodine atoms.

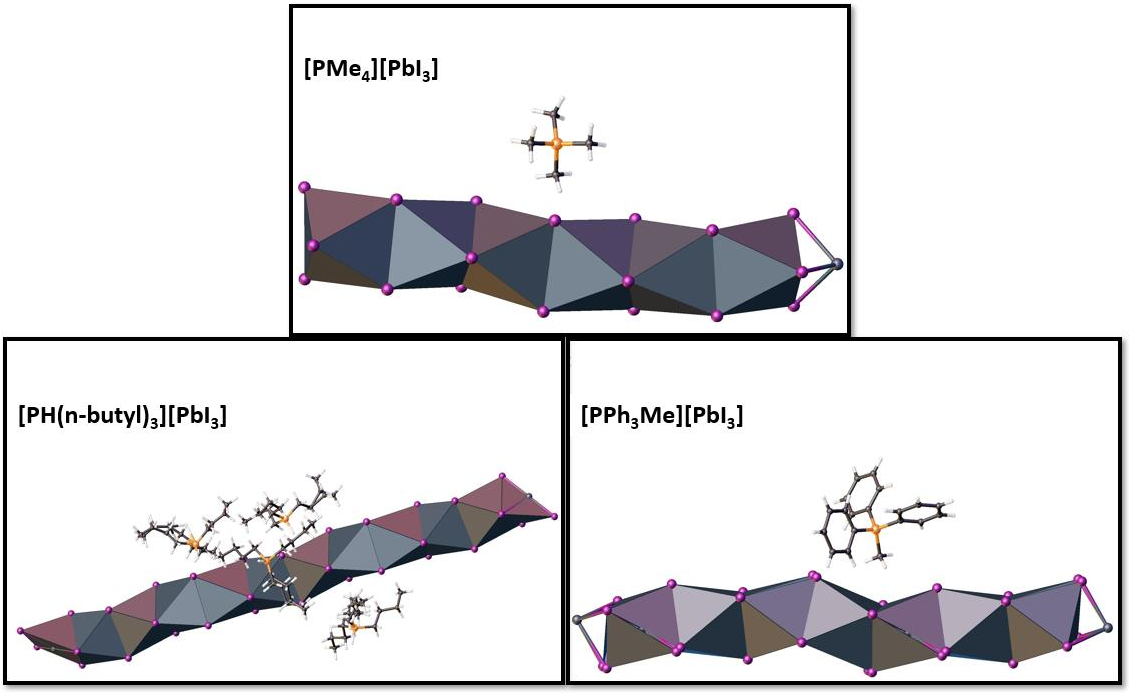

Figure 3.3: Diagrams of the Monophosphonium-Templated Iodoplumbates highlighting the face-sharing octahedra of the $[PbI_3]_\infty$ chains.

A CSD search indicated that the P-C bond lengths and angles in the cations are typical of those reported in other phosphoniums, ranging from 1.781-1.793Å and 108.97˚(10)-109.5˚(2), respectively. The bond lengths of the PbI_3^- fragments in the 1-D network range from 3.1379(4)Å to 3.398(3)Å, which is similar to the iodoplumbate networks that have been previously examined.[4,5,11,14,16,17,21] Interestingly, the bond angles in this network deviate from those normally observed in an octahedral network. One would expect the average *trans* I-Pb-I bond angles to be 180˚, however this 1-D network had an average bond angle of 175.37(4) ˚. By the same token, the bond angle of *cis* iodine atoms in the molecule should be 90˚ in an ideal octahedral network, but this network had an average of 90.96(3)˚ with the minimum at 81.93(3)˚ and the maximum at 96.90(2)˚. It is not surprising that the bond angles are slightly off the ideal, since $[PbI_3^-]_\infty$ networks observed in the past have cross-molecule and adjacent bond angles of less than 180˚ and

greater or less than 90˚, respectively.[4,5,14,17,21–23] The crystal packing of each of the monophosphonium-iodoplumbates is depicted in Figure 3.4.

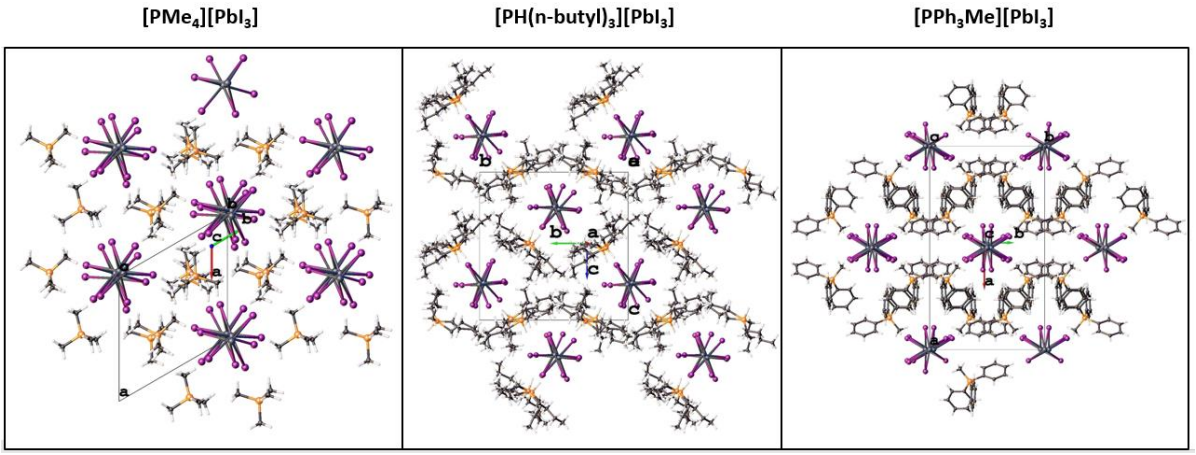

Figure 3.4: The crystal packing of the Monophosphonium-Templated Iodoplumbates.

3.2.2 Diphosphonium-Templated Iodoplumbates

Given that the monophosphonium cations did not generate the 3-D corner-sharing octahedra structure characteristic of a perovskite but instead produced interesting 1-D networks, a diphosphonium cation was reacted with lead (II) iodide to observe the effect of a dication in templating the lead iodide. Bis(trimethylphosphonio)ethane iodide was dissolved in DMSO with lead iodide, producing a yellow solution, and evaporation of the DMSO yielded pale yellow crystals ($[P_2C_8H_{22}]$ $[Pb_2I_6]$). NMR spectroscopy revealed that the phosphonium persisted in the product and single crystal X-Ray diffraction showed an extended 1-D face-sharing network of octahedral PbI_3^- fragments charge-balanced with the diphosphonium in the same manner as the monophosphonium-templated iodoplumbates.

The average P-C bond length is 1.792(12)Å, which is typical of other P-C bond lengths in phosphoniums in the CSD. Furthermore, the C-P-C bond angles average at

109.6(9) ˚, indicating a tetrahedral coordination environment around the phosphorus atoms. As for the 1-D iodoplumbate network, the average Pb-I bond length is 3.219(4)Å, which is in agreement with our monophosphonium iodoplumbate networks as well as those that have been previously reported.[4,5,14,17,21–25] The I-Pb-I bond angles are close to that of the ideal for an octahedral network, with the angle between *cis* iodides averaging at 90.0(10)˚, the minimum angle being 83.644(12)˚, and the maximum angle being 96.356(12)˚. The angles between *trans* iodides were all 180.0(0) ˚. Figure 3.5 shows the face-sharing octahedra of the 1-D iodoplumbate network in $[P_2C_8H_{22}]$ $[Pb_2I_6]$, whereas Figure 3.6 depicts its crystal packing.

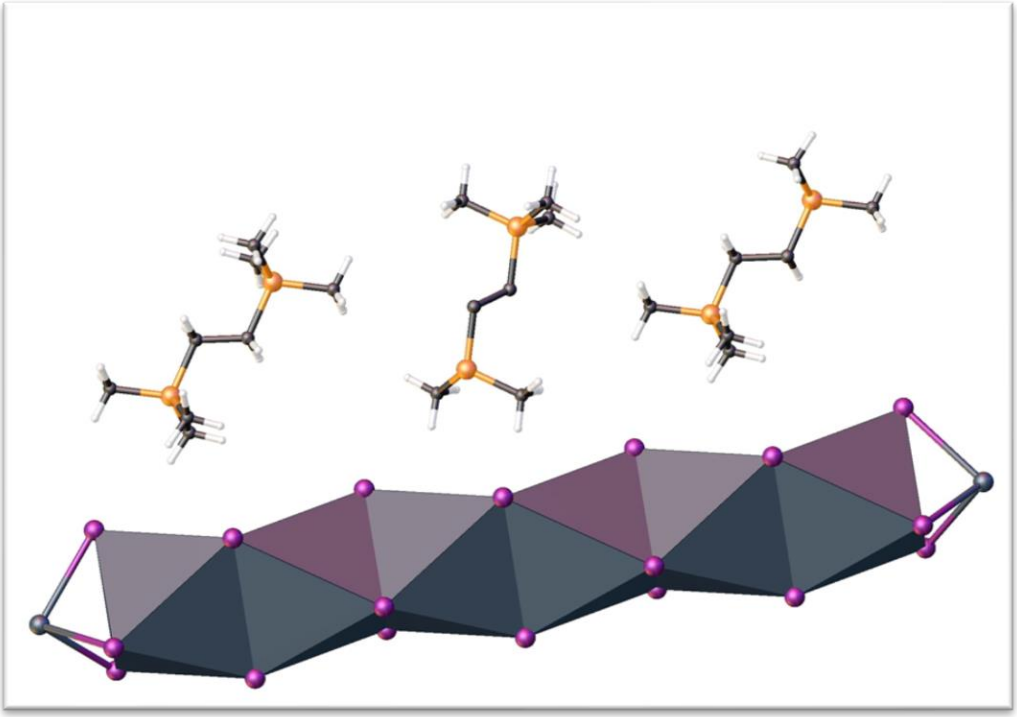

Figure 3.5: Face-sharing octahedra of the $[PbI_3]_\infty$ chain in **$[P_2C_8H_{22}][Pb_2I_6]$**.

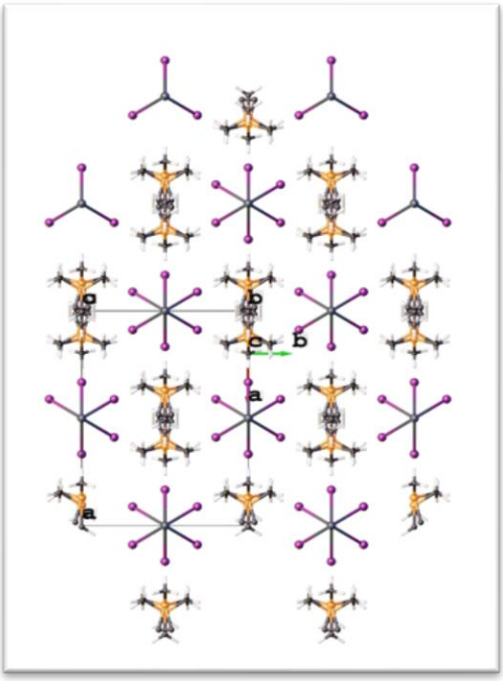

Figure 3.6: The crystal packing of $[P_2C_8H_{22}][Pb_2I_6]$.

3.2.3 Absorption Spectra

Absorption spectra of all phosphonium-templated iodoplumbates except for the one containing trimethylphosphonium were obtained. UV-Vis spectroscopy showed that all compounds have a strong absorbance in the 370nm region which corresponds to band gaps ranging from 2.4eV to 2.7eV. These bandgaps are slightly greater than that of bulk PbI_2, which has a bandgap of 2.3eV.[7] The organic moiety of the phosphonium-templated iodoplumbates appear to have an effect on the bandgap of the compound, with $[PH(n\text{-}butyl)_3][PbI_3]$ having the smallest bandgap (2.4eV) and $[PMe_4][PbI_3]$ having the largest bandgap. Although these bandgaps are much greater than the 1.54eV bandgap of the methylammonium-PbI_3^- perovskite reported by Stoumpos et al.[3], these results indicate that phosphonium-templated iodoplumbates could have material applications as wide-bandgap

semiconductors in the solution state. Further UV-Vis studies in the solid state need to be conducted in order to relate the bandgaps of the phosphonium-templated iodoplumbates to those of the perovskites.

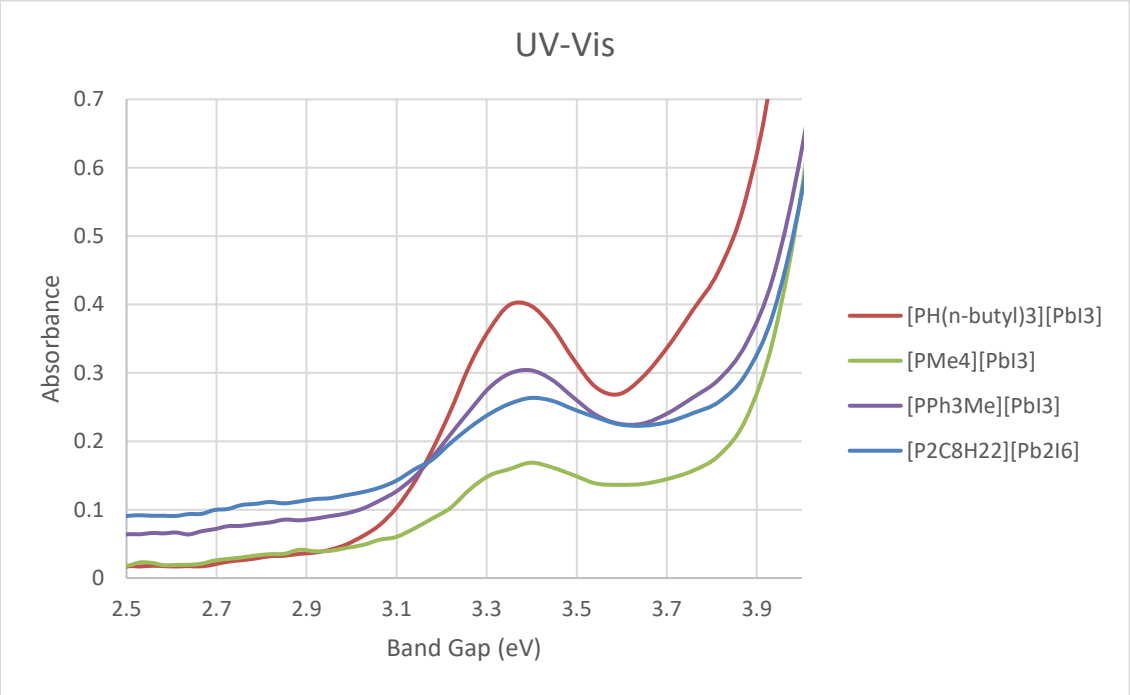

Figure 3.7: UV-Vis Spectra of the Phosphonium-Templated Iodoplumbates.

3.2.4 Thermogravimetric Analysis

Thermogravimetric analysis (TGA) was performed to assess the thermal stability of the phosphonium iodoplumbates, excluding the one containing trimethylphosphonium. The TGA curves are outlined in Figure 3.8. We observed that the monophosphoniums and the diphosphonium with methyl substituents afforded the best stability at higher temperatures, with $[PMe_4][PbI_3]$ having no significant mass loss up to 400°C and $[P_2C_8H_{22}][Pb_2I_6]$ having lost approximately 8% of its original mass. Conversely, the

phosphoniums with longer alkyl and aryl substituents showed decomposition and significant mass loss at much lower temperatures. The TGA curves for [PH(n-butyl)$_3$] [PbI$_3$] and [PPh$_3$Me][PbI$_3$] display two events with the first occurring at approximately 129℃, which can be attributed to evaporation of toluene used to make the starting material. The second event at approximately 300℃ for [PH(n-butyl)$_3$] [PbI3] and 325℃ for [PPh$_3$Me][PbI$_3$] represents a significant mass loss due to decomposition of the product, with [PH(n-butyl)$_3$][PbI$_3$] losing approximately 25% of its original mass and [PPh$_3$Me][PbI$_3$] losing 34% of its original mass.

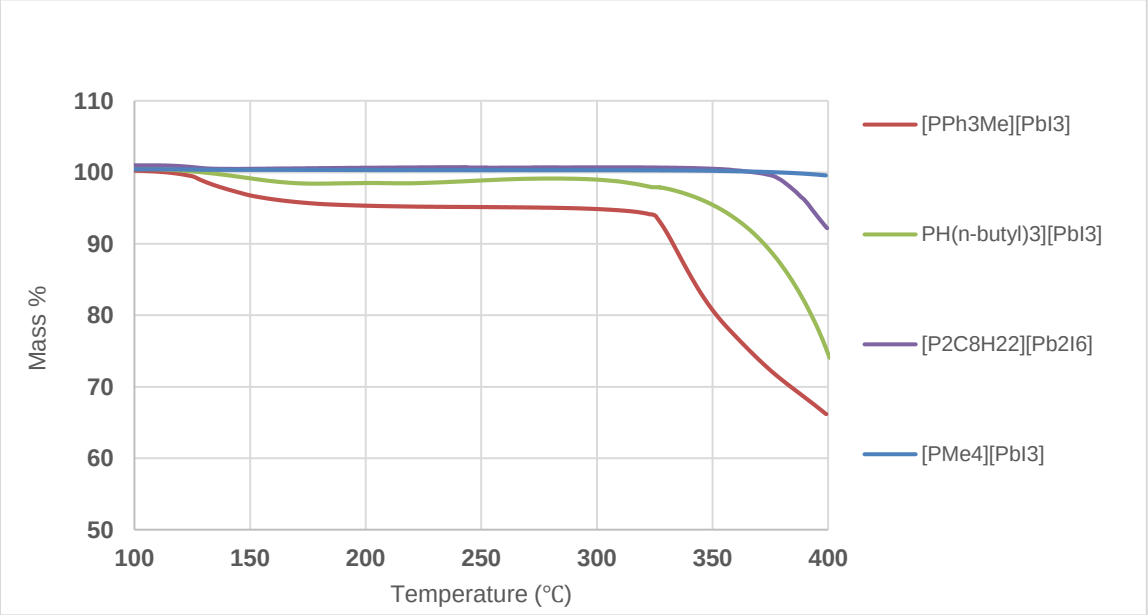

Figure 3.8: The TGA Curves of Phosphonium-Templated Iodoplumbates

The TGA curves of these phosphonium-templated iodoplumbates show increased thermal stability in comparison to the previously reported amide-templated iodoplumbates, which show complete decomposition between 120-130℃[4], which is significantly lower than the decomposition temperature of any phosphonium-templated compounds. Conversely, the transition metal-templated iodoplumbates decompose at approximately

270°C[7], which is just below the decomposition temperature of our compounds. Most notably, the phosphonium-templated iodoplumbates' decomposition pattern resembles that of the methylammonium-PbI_3^- perovskite, which initiates decomposition after 300°C[3]. Both the phosphonium-templated iodoplumbates and the methylammonium-PbI_3^- perovskite display a one-step decomposition which likely corresponds to the loss of the organic cation and iodide content. These similarities between perovskites and our compounds with respect to thermal stability point towards a potential for making functional organic-inorganic hybrid materials from phosphonium-templated iodoplumbates.

3.2.5 Chapter Conclusions

This chapter investigated the reaction of phosphonium cations with lead(II) iodide with the target of synthesizing a phosphonium-based perovskite. Although a perfect perovskite structure was not observed, this work has demonstrated that phosphonium-templated iodoplumbates may be synthesized via direct addition of a phosphonium salt to lead(II) iodide in solution. Four phosphonium-templated iodoplumbate materials have been crystallographically characterized, revealing an extended network of anionic lead iodide fragments charge-balanced with a phosphonium cation. Through UV-Visible spectroscopy and thermogravimetric analysis we have shown that these compounds are wide-bandgap semiconductors that exhibit remarkable thermal stability. Therefore, it is evident that phosphonium-templated iodoplumbates have potential applications as semiconducting materials.

3.3 Experimental

General Procedures

All manipulations were carried out using standard inert atmosphere techniques. All chemicals and reagents were purchased from Sigma-Aldrich and used without further purification. Deuterated solvents were dried according to literature procedure when necessary, and all other solvents were dried over a series of Grubbs'-type columns and degassed prior to use. NMR spectra were recorded at room temperature on a Bruker Avance III 500 MHz, Bruker Avance Ultrashield 300 MHz or Bruker Avance DPX 300 MHz spectrometers. Chemical shifts are reported in ppm relative to internal standards for ^{1}H and ^{13}C (the given deuterated solvent) and the external standard for ^{31}P (85% H_3PO_4). Coupling constants |J| are given in Hz. Elemental Analysis was performed by the University of Windsor Mass Spectrometry Service Laboratory using Perkin Elmer 2400 combustion CHN analyzer. UV-Vis absorption spectra were recorded on a Varian Cary 50 Conc UV-Vis spectrophotometer. All samples were run in a quartz cuvette with path length of 1cm. Thermogravimetric analysis was conducted on a Mettler Toledo TGA SDTA 851e. Helium (99.99%) was used to purge the system at a flow rate of 60mL/min. Samples were held at 25˚C for 30min before heated to 400˚C at a rate of 5˚C/min. All samples were run in aluminum crucibles.

X-Ray Crystallography

Crystals for investigation were covered in Paratone®, mounted into a goniometer head, and then rapidly cooled under a stream of cold N_2 of the low-temperature apparatus (Oxford Cryostream) attached to the diffractometer. The data were then collected using the APEXII software suite[26] on a Bruker Photon 100 CMOS diffractometer using a graphite

monochromator with MoKα (λ = 0.71073 Å) or CuKα (λ = 1.54178 Å) radiation. For each sample, data were collected at low temperature. APEXII software was used for data reductions and SADABS[27] was used for absorption corrections (multi-scan; semi-empirical from equivalents). XPREP was used to determine the space group and the structures were solved and refined using the SHELX[28] software suite as implemented in the WinGX[29] or OLEX2[30] program suites. Validation of the structures was conducted using PLATON.[31]

3.3.1 Trimethylphosphonium lead triiodide

Trimethylphosphonium iodide (67mg, 0.33mmol) and lead (II) iodide (151mg, 0.33mmol) were combined in a 20mL scintillation vial. The contents of the vial were ball-milled for 1h at 30Hz milling frequency. A golden yellow powder was observed after 1h of milling. Yield: 46% (75 mg, 0.12 mmol). $^{31}P\{^{1}H\}$ NMR (DMSO-d_6, 121.5MHz) δ: -0.27 (s). ^{1}H NMR (DMSO-d_6, 300 MHz); δ: 1.63 (PC***H*****$_3$**, dd, 9H, $^{2}J_{PH}$ = 119Hz,), 6.33 (***H***P, dm, $^{1}J_{PH}$=516Hz, $^{3}J_{HH}$= unresolved coupling). EA calculated for $C_3H_{10}PPbI_3$: C, 5.42; H, 1.52; N 0.00%; found: C, 4.98; H 0.94; N, -0.05%.

3.3.2 Tetramethylphosphonium lead triiodide

A 20 mL scintillation vial was charged with tetramethylphosphonium iodide (50 mg, 0.23 mmol) and (106 mg, 0.23 mmol) of PbI_2 and then dissolved in DMSO (ca. 5 mL). The vial was placed in an oil bath set at 120˚C and the solvent was left to evaporate from the vial with the cap off. After 48 h mustard-yellow crystals suitable for X-ray diffraction formed at the bottom of the vial. Yield: 76% (118 mg, 0.17 mmol). $^{31}P\{^{1}H\}$ NMR (DMSO-d_6, 121.5MHz) δ: 22.88 (s). ^{1}H NMR (DMSO-d_6, 300 MHz); δ: 1.82 (PC***H*****$_3$**, d, 12H, $^{2}J_{PH}$ = 15.3Hz). $^{13}C\{^{1}H\}$ NMR (DMSO-d_6, 75.5MHz); δ: 9.70 (P***C***H_3, d,$^{1}J_{PC}$ = 55Hz). EA

calculated for $C_4H_{12}PPbI_3$: C, 7.08; H, 1.78; N 0.00%; found: C, 7.08; H 1.19; N, -0.05%. UV-Vis Absorption Peak: 364.9 nm.

3.3.3 Tri(n-butyl)phosphonium lead triiodide

To 50mg (0.151mmol) of tri-n-butylphosphonium iodide was added 70mg of PbI_2 in a 20mL scintillation vial with approximately 10mL of acetonitrile, creating a yellow solution. The mixture was left to stir for 24h, after which time a yellow solution with a pale yellow precipitate was observed. The yellow solution was separated and left for recrystallization by slow evaporation. Yellow crystals suitable for X-Ray diffraction were collected. Yield: 55% (33 mg, 41.7 mmol). $^{31}P\{^1H\}$ NMR (CD_3CN, 202.5MHz); δ: 12.72 (s). ^1H NMR (CD_3CN, 500MHz); δ: 0.95 (PCCCC***H₃***, t, 9H, $^3J_{HH}$ = 7Hz), 1.48 (PCCC***H₂***C, m, 6H, unresolved coupling), 1.62 (PCC***H₂***CC, m, 6H, unresolved coupling), 2.23 (PC***H₂***CCC, m, 6H, unresolved coupling) . $^{13}C\{^1H\}$ NMR (CD_3CN, 125.8MHz); δ: 12.65 (PCCC***C***H_3, s), δ: 16.10 (P***C***H_2CCC, d,$^1J_{PC}$ = 47Hz), δ: 12.65 (PC***C***H_2CC, d,$^2J_{PC}$ = 16Hz), δ: 12.65 (PCC***C***H_2C, d,$^3J_{PC}$ = 4.5Hz). EA calculated for $[HP(n\text{-}bu)_3]^+[PbI_3]^-$·0.5 toluene: C, 22.23; H, 3.85; N 0.00%; found: C, 21.99; H 3.88; N, -0.06%. UV-Vis Absorption Peak: 364.9nm.

3.3.4 Methyltriphenylphosphonium lead triiodide

Methyltriphenyl phosphonium iodide (50 mg, 0.12 mmol) and lead (II) iodide (57 mg, 0.12 mmol) were combined in a 20 mL scintillation vial and dissolved in ca. 5 mL of DMSO, forming a yellow solution. The vial was placed in an oil bath and the solvent was left to evaporate. After 24h a pale yellow solid was found at the bottom of the vial and collected. The solid product was dissolved in acetonitrile and yellow crystals suitable for

X-Ray diffraction were collected upon evaporation of the MeCN. Yield: 70% (74 mg, 0.085 mmol). $^{31}P\{^{1}H\}$ NMR (DMSO-d_6, 121.5MHz); δ: 22.590 (s). ^{1}H NMR (DMSO-d_6, 300 MHz) δ: 3.12 (PC***H*****$_3$**, d, 3H, $^{2}J_{PH}$ = 14.4Hz), 7.71-7.86 (aromatic protons, m, 15H). $^{13}C\{^{1}H\}$ NMR (DMSO-d_6, 75.5MHz) δ: 7.89 (P***C***H_3, d, 1C,$^{1}J_{PC}$ = 58Hz), 120.43 (***C*****$_{ipso}$**, d, 3C, $^{1}J_{PC}$ = 88.3Hz), 133.77 (***C*****$_{ortho}$**, d, 6C, $^{2}J_{PC}$ = 10.8Hz), 130.66 (***C*****$_{meta}$**, d, 6C, $^{3}J_{PC}$ = 12.7Hz), 135.34(***C*****$_{para}$**, s, 3C). EA calculated for $[PMePh_3]^{+}[PbI_3]^{-}\cdot$MeCN: C, 25.95; H, 2.06; N 1.59%; found: C, 25.94; H 1.99; N, 1.58%. UV-Vis Absorption Peak: 364.9 nm.

3.3.5 Bis(trimethylphosphonio)ethane lead triiodide

To a 20mL scintillation vial was added 50mg (0.12mmol) of bis-(trimethylphosphonio-) ethane iodide and two equivalents of lead (II) iodide (106mg, 0.23mmol) in ca. 5mL of DMSO, which generated a pale-yellow solution. The vial was placed in an oil bath and the solvent was allowed to evaporate. After 24h a pale-yellow crystals were found at the bottom of the vial and collected for X-Ray diffraction. Yield: 86.5% (135 mg, 85 μmol). $^{31}P\{^{1}H\}$ NMR (DMSO-d_6, 121.5MHz) δ: 32.86 (s). ^{1}H NMR (DMSO-d_6, 500MHz); δ: 1.89 (P(C***H*****$_3$**$)_3$, d, 18H, $^{2}J_{PH}$= 15Hz), 2.55 (P(C***H*****$_2$**$)_2$, d, 4H, $^{2}J_{PH}$=6.5Hz). $^{13}C\{^{1}H\}$ NMR (DMSO-d_6, 125.8MHz); δ: 7.13 (P***C***H_3, t,$^{1}J_{PC}$ = 26.7Hz), 15.42 (P***C***H_2, t,$^{1}J_{PC}$ =25.0Hz). EA calculated for $C_8H_{22}P_2Pb_2I_6$: C, 7.09; H, 1.64; N 0.00%; found: C, 6.78; H 1.13; N, -0.06%. UV-Vis Absorption Peak: 364.9nm.

3.4 References

(1) Zhao, Y.; Zhu, K. Organic–inorganic Hybrid Lead Halide Perovskites for Optoelectronic and Electronic Applications. *Chem. Soc. Rev.* **2016**, 45 (3), 655–689.

(2) Li, Z.; Yang, M.; Park, J. S.; Wei, S. H.; Berry, J. J.; Zhu, K. Stabilizing Perovskite Structures by Tuning Tolerance Factor: Formation of Formamidinium and Cesium Lead Iodide Solid-State Alloys. *Chem. Mater.* **2016**, 28 (1), 284–292.

(3) Stoumpos, C. C.; Malliakas, C. D.; Kanatzidis, M. G. Semiconducting Tin and Lead Iodide Perovskites with Organic Cations: Phase Transitions, High Mobilities, and Near-Infrared Photoluminescent Properties. *Inorg. Chem.* **2013**, 52 (15), 9019–9038.

(4) Eppel, S.; Fridman, N.; Frey, G. Amide-Templated Iodoplumbates: Extending Lead-Iodide Based Hybrid Semiconductors. *Cryst. Growth Des.* **2015**, 15 (9), 4363–4371.

(5) Li, H.-H.; Chen, Z.-R.; Cheng, L.-C.; Wang, Y.-J.; Feng, M.; Wang, M. Hybrid Polymeric Iodoplumbates Constructed from Morpholine and Its Derivatives: Structures and Properties. *Dalt. Trans.* **2010**, 39 (45), 11000.

(6) Dohner, E. R.; Jaffe, A.; Bradshaw, L. R.; Karunadasa, H. I. Intrinsic White-Light Emission from Layered Hybrid Perovskites. *J. Am. Chem. Soc.* **2014**, 136 (38), 13154–13157.

(7) Zhang, Z. J.; Xiang, S. C.; Zhang, Y. F.; Wu, A. Q.; Cai, L. Z.; Guo, G. C.; Huang, J. S. A New Type of Hybrid Magnetic Semiconductor Based upon Polymeric Iodoplumbate and Metal-Organic Complexes as Templates. *Inorg. Chem.* **2006**, 45 (5), 1972–1977.

(8) Bartlett, P. N.; Burt, J.; Hasan, M. M.; Hector, A. L.; Levason, W.; Reid, G.; Richardson, P. W. Haloplumbate Salts as Reagents for the Non-Aqueous Electrodeposition of Lead. *RSC Adv.* **2016**, 6 (77), 73323–73330.

(9) Tan, Z.-K.; Moghaddam, R. S.; Lai, M. L.; Docampo, P.; Higler, R.; Deschler, F.; Price, M.; Sadhanala, A.; Pazos, L. M.; Credgington, D.; et al. Bright Light-Emitting Diodes Based on Organometal Halide Perovskite. *Nat. Nanotechnol.* **2014**, 9 (9), 687–692.

(10) Saidaminov, M. I.; Mohammed, O. F.; Bakr, O. M. Low-Dimensional-Networked Metal Halide Perovskites: The Next Big Thing. *ACS Energy Lett.* **2017**, 2 (4), 889–896.

(11) Aamir, M.; Shah, Z. H.; Sher, M.; Iqbal, A.; Revaprasadu, N.; Malik, M. A.; Akhtar, J. Enhanced Photocatalytic Activity of Water Stable Hydroxyl Ammonium Lead Halide Perovskites. *Mater. Sci. Semicond. Process.* **2017**, 63, 6–11.

(12) Stoumpos, C. C.; Mao, L.; Malliakas, C. D.; Kanatzidis, M. G. Structure-Band Gap Relationships in Hexagonal Polytypes and Low-Dimensional Structures of Hybrid Tin Iodide Perovskites. *Inorg. Chem.* **2017**, 56 (1), 56–73.

(13) Stoumpos, C. C.; Frazer, L.; Clark, D. J.; Kim, Y. S.; Rhim, S. H.; Freeman, A. J.; Ketterson, J. B.; Jang, J. I.; Kanatzidis, M. G. Hybrid Germanium Iodide Perovskite Semiconductors: Active Lone Pairs, Structural Distortions, Direct and Indirect Energy Gaps, and Strong Nonlinear Optical Properties. *J. Am. Chem. Soc.* **2015**, 137 (21), 6804–6819.

(14) Liu, G.; Liu, J.; Sun, Z.; Zhang, Z.; Chang, L.; Wang, J.; Tao, X.; Zhang, Q. Thermally Induced Reversible Double Phase Transitions in an Organic–Inorganic Hybrid Iodoplumbate $C_4H_{12}NPbI_3$ with Symmetry Breaking. *Inorg. Chem.* **2016**, 55 (16), 8025–8030.

(15) Cao, D. H.; Stoumpos, C. C.; Farha, O. K.; Hupp, J. T.; Kanatzidis, M. G. 2D Homologous Perovskites as Light-Absorbing Materials for Solar Cell Applications. *J. Am. Chem. Soc.* **2015**, 137 (24), 7843–7850.

(16) Huang, Z. J.; Cheng, H. J.; Dai, M.; Ni, C. Y.; Li, H. X.; Hou, K. P.; Ren, Z. G.; Lang, J. P. Solvothermal Syntheses and Crystal Structures of One 1D and Two 3D $[Pb_xI_y]$-Based Coordination Polymers. *Inorg. Chem. Commun.* **2013**, 31, 33–36.

(17) Kaltzoglou, A.; Stoumpos, C. C.; Kontos, A. G.; Manolis, G. K.; Papadopoulos, K.; Papadokostaki, K. G.; Psycharis, V.; Tang, C. C.; Jung, Y.-K.; Walsh, A.; et al. Trimethylsulfonium Lead Triiodide: An Air-Stable Hybrid Halide Perovskite. *Inorg. Chem.* **2017**, 56 (11), 6302–6309.

(18) Saidaminov, M. I.; Abdelhady, A. L.; Murali, B.; Alarousu, E.; Burlakov, V. M.; Peng, W.; Dursun, I.; Wang, L.; He, Y.; Maculan, G.; et al. High-Quality Bulk Hybrid Perovskite Single Crystals within Minutes by Inverse Temperature Crystallization. *Nat. Commun.* **2015**, 6 (May), 1–6.

(19) Solis-Ibarra, D.; Smith, I. C.; Karunadasa, H. I. Post-Synthetic Halide Conversion and Selective Halogen Capture in Hybrid Perovskites. *Chem. Sci.* **2015**, 6 (7), 4054–4059.

(20) Bellachioma, G.; Cardaci, G.; Macchioni, A.; Venturi, C.; Zuccaccia, C. Reductive Elimination of Halogens Assisted by Phosphine Ligands in $Fe(CO)_4X_2$ (X=I,Br) Complexes. *J. Organomet. Chem.* **2006**, 691 (18), 3881–3888.

(21) Tang, Z.; Guloy, A. M. A Methylviologen Lead(II) Iodide: Novel $[PbI_3^-]_\infty$ Chains with Mixed Octahedral and Trigonal Prismatic Coordination. *J. Am. Chem. Soc.* **1999**, 121 (2), 452–453.

(22) Liu, J.-J.; Guan, Y.-F.; Jiao, C.; Lin, M.-J.; Huang, C.-C.; Dai, W.-X. A Panchromatic Hybrid Crystal of Iodoplumbate Nanowires and J-Aggregated Naphthalene Diimides with Long-Lived Charge-Separated States. *Dalt. Trans.* **2015**, 44.

(23) Krautscheid, H.; Lode, C.; Vielsack, F.; Vollmer, H. Synthesis and Crystal Structures of Iodoplumbate Chains, Ribbons and Rods with New Structural Types. *J. Chem. Soc. Dalt. Trans.* **2001**, 1099–1104.

(24) Bedlivy, D.; Mereiter, K. The Structures of Potassium Lead Triiodide Dihydrate and Ammonium Lead Triiodide Dihydrate. *Acta Crystallogr. Sect. B Struct. Crystallogr. Cryst. Chem.* **1980**, 36 (4), 782–785.

(25) Vincent, B. R.; Robertson, K. N.; Cameron, T. S.; Knop, O. Alkylammonium Lead Halides. Part 1. Isolated PbI_6^{4-} Ions in $(CH_3NH_3)_4PbI_6 \cdot 2H_2O$. *Can. J. Chem.* **1987**, 65 (5), 1042–1046.

(26) APEX II. Bruker AXS Inc. APEX II. Bruker AXS Inc.: Madison, WI p Madison, WI, 2012.

(27) SADABS. Bruker AXS Inc. SADABS. Bruker AXS Inc.: Madison, WI p Madison, WI, 2008.

(28) Sheldrick, G. M. A Short History of SHELX. *Acta Crystallogr. A.* **2008**, *64* (Pt 1), 112–122.

(29) Farrugia, L. J. WinGX Suite for Small-Molecule Single-Crystal Crystallography. *J. Appl. Crystallogr.* **1999**, *32* (4), 837–838.

(30) Dolomanov, O. V.; Bourhis, L. J.; Gildea, R. J.; Howard, J. A. K.; Puschmann, H. OLEX2 : A Complete Structure Solution, Refinement and Analysis Program. *J. Appl. Crystallogr.* **2009**, *42* (2), 339–341.

(31) Spek, A. L. Single-Crystal Structure Validation with the Program PLATON. *J. Appl. Crystallogr.* **2003**, *36* (1), 7–13.

CHAPTER 4: Synthesis of a Novel Iodotin Trianion

4.1 Introduction

Main group halometallate perovskites, especially those consisting of group 14 halides, have exploded onto the scene in recent years due to their fascinating properties and broad range of applications ranging from photovoltaics to dielectric materials.[1] Perovskites of the form ABX_3 where B = Pb and X = I have been proven to possess light-harvesting properties, however the inherent toxicity and carcinogenic nature of lead(II) iodide poses a risk to the environment.[2] Therefore, in order for PSCs to be used on a widespread basis, it is necessary to explore lead-free perovskitic materials. Since tin is a group 14 metal and has a comparable ionic radius to lead, it was the first metal considered in the quest to replace lead in PSCs.[3] The substitution of lead for tin in PSCs was initiated by the synthesis of $CH_3NH_3Sn_xPb_{1-x}I_3$.[4] This perovskite demonstrated a reduced bandgap with a higher concentration of tin, which showed promise for tin's presence in PSCs. The first completely lead-free perovskite, $CsSnI_3$, was reported in 2012 and was classified as a semiconductor.[5] In 2014, the first lead-free perovskite with an organic 'A' cation was synthesized: $CH_3NH_3SnI_3$.[6,7] Like the analogous lead perovskite, this perovskite demonstrated a high PCE and a low bandgap,[3] which was proven to be ideal for semiconducting applications. Unfortunately, Sn(II) is readily oxidized to Sn(IV) in ambient air in these materials, which calls for further investigation of these systems.[3] Given that the methylammonium tin perovskite has shown similar properties to the lead perovskites in terms of photovoltaic applications, this chapter of this thesis seeks to elucidate whether alkyl- and arylphosphonium-based perovskites are accessible. The reactions of various phosphonium salts with tin(II) and tin(IV) halides are presented, along with three novel crystal structures.

4.2 Results & Discussion

4.2.1 Reactions of Phosphonium Salts with Tin(II) Halides

A Novel Iodotin Trianion

Trimethylphosphonium iodide served as a reactant with tin(II) iodide in an attempt to make a perovskite structure similar to those reported by Kanatzidis.[5,8,9] The predicted structure would consist of SnI_3^- anions occupying the corners of the unit cell, with the trimethylphosphonium cation occupying the centre of the cell, making for a charge-balanced compound. If the product had this structure, it could be considered a perovskite since it would theoretically adopt the ABX_3 structural formula characteristic of perovskites.

The reaction of trimethylphosphonium iodide with tin(II) iodide was done by dissolving both in MeCN and adding trimethylphosphonium iodide to the tin(II) iodide with stirring and in a dropwise manner to ensure complete reaction. Upon addition of the colourless trimethylyphosphonium iodide solution, the orange tin(II) iodide solution turned deep red. This colour change is good evidence that a reaction occurred. Interestingly, this deep red colour changed to orange as the reaction progressed, and after 72h of stirring the solution was pale yellow. Some of the acetonitrile solvent was pumped off at this point and the solution was placed in the freezer for slow recrystallization. After two weeks of recrystallization, some garnet red crystals were formed. Though these were taken for X-ray analysis, but no structure was obtained because of severe twinning of the crystals. The mother liquor was left to slowly evaporate at room temperate, which remarkably yielded a batch of dark yellow/orange crystals, which were harvested for NMR and crystallographic study.

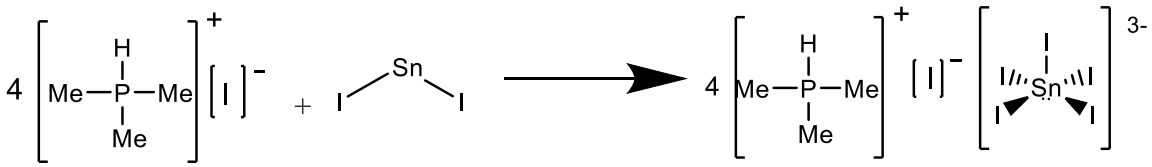

Scheme 4.1: Reaction Scheme of the Synthesis of $[HPMe_3]_4[SnI_5][I]$

$^{31}P\{^1H\}$ NMR was run to compare the phosphorus environment of the product to the phosphorus environment of the starting material, trimethylphosphonium iodide. A singlet was observed at -0.71 ppm, which is slightly different than the shift for trimethylphosphonium iodide found by Bellachioma et al. (-0.44 ppm)[10] and the one found in this thesis (2.09 ppm). In addition to this, the ^1H NMR and $^{13}C\{^1H\}$ NMR were also typical of trimethylphosphonium iodide as reported by Bellachioma et al.[10] and in Chapter 2 of this thesis. NMR spectroscopy points towards the creation of a charge-balanced compound with a phosphonium ion.

While the NMR experiments confirmed the assignment of the phosphonium ion in solution, the crystal structure showed a much more interesting result. Instead of adopting a corner-sharing octahedron crystal structure that is characteristic of perovskites, the unit cell contained three ions; eight trimethyl phosphonium ions, two iodide anions, as well as a previously unreported SnI_5 species. The species has a square-pyramidal geometry suggesting an anion with a -3 charge, as would be expected if the oxidation state of tin were +2. Two of these anions were observed in the unit cell, which is depicted in Figure 4.1. This assignment is further confirmed by the charge balanced unit cell.

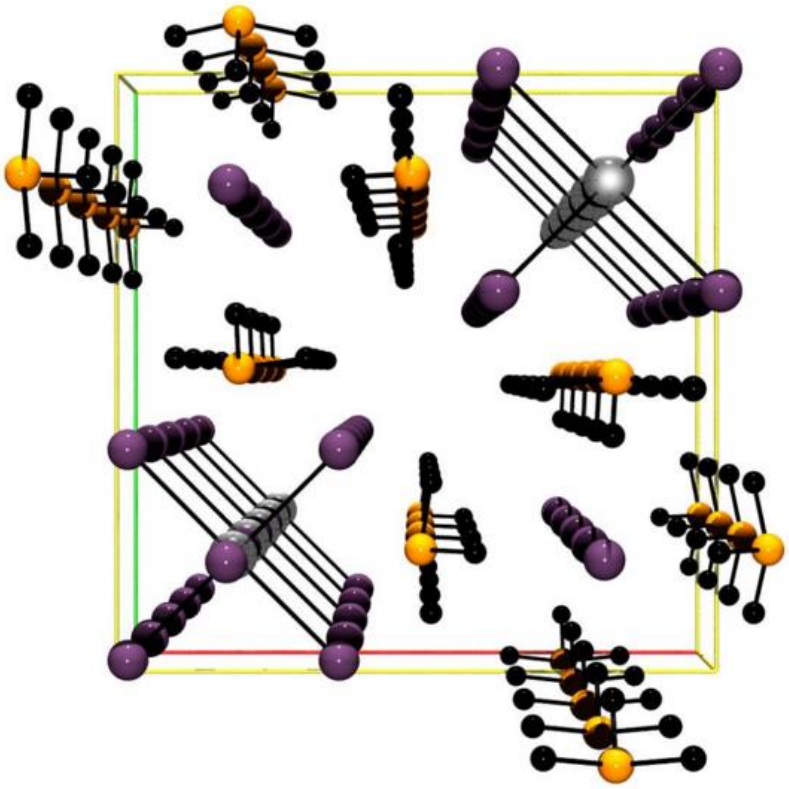

Figure 4.1: Unit cell contents of $[HPMe_3]_4[I][SnI_5]$ normal to (001). The orange balls represent phosphorus, the black balls represent carbon, the silver balls represent tin, and the purple balls represent iodine. Hydrogen atoms are omitted for clarity.

The I(1)-Sn-I(2) bond angle of 93.62° is characteristic of a square pyramidal geometry. Although there is precedence for this geometry in some vertex linked networks of Sn_xI_x,[11–13] this trianion has never been observed as a discrete species. Examination of the bond lengths of the trianion, show that they are in close agreement with those reported for tin(II) iodide,[14] but not for tin(IV) iodide.[15] The Sn-I(1) bond distance was found to be 2.949Å and the Sn-I(2) distance was found to be 3.211Å. The long Sn-I(2) bond distance could be due to tin(II) being less positively charged than tin(IV), rendering the iodide atoms less attracted to the tin center.

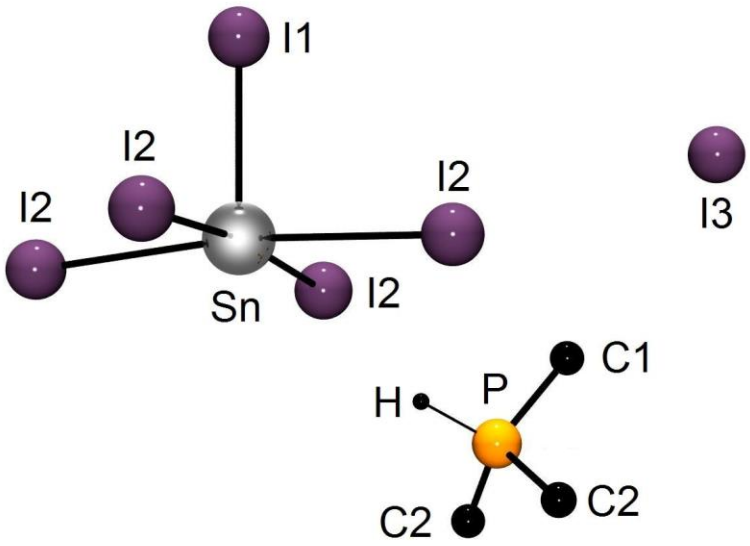

Figure 4.2: Crystal structure (ball and stick) of $[HPMe_3]_4[I][SnI_5]$ with selected bond lengths (Å) and angles (º): Sn-I1, 2.9487(8); Sn-I2, 3.2111(3); P-C2, 1.770(4); P-C1, 1.779(4); P-H, 1.33(5); I1-Sn-I2, 93.619(11); I2-Sn-I2(adjacent), 89.772(1); I2-Sn-I2(across), 172.76(2); C2-P-C1, 109.01(18); C2-P-C2, 111.1(3); C1-P-H, 106(2); C2-P-H, 110.6(11). Hydrogen atoms not bound to phosphorus are omitted for clarity.

Other Reactions with Tin(II) Halides

Given the interesting results displayed by the reaction of trimethylphosphonium iodide with tin(II) iodide, a similar reaction with tetraphenylphosphonium iodide was carried out. The goal of this reaction was to see if the larger tetraphenylphosphonium cation would behave similarly to the smaller trimethylphosphonium cation in its reaction with tin(II) iodide. The white tetraphenylphosphonium iodide powder was dissolved in acetonitrile and added dropwise to a solution of tin(II) iodide in acetonitrile. Upon addition of tetraphenylphosphonium iodide, the tin(II) iodide solution changed colour from orange to deep red. This colour change is similar to the one observed when trimethylphosphonium iodide was added to tin(II) iodide, suggesting that a similar reaction may be taking place. However, in contrast to the reaction with trimethylphosphonium iodide, the

tetraphenylphosphonium iodide reaction solution with tin(II) iodide remained red after two days of stirring. When the acetonitrile was pumped off, a purple-brown solid was left. This was dissolved in acetonitrile and left for recrystallization.

A $^{31}P\{^{1}H\}$ NMR sample was made approximately 30 minutes after all the tetraphenylphosphonium iodide had been added to the tin(II) iodide. The spectrum observed displayed a single resonance at 24.3 2 ppm. The previously reported spectrum for tetraphenylphosphonium iodide exhibits a singlet at 24.0 ppm.[16] The close correspondence between the reaction mixture and the literature value could indicate that the phosphorus environment of the product is very similar to the phosphorus environment of tetraphenylphosphonium iodide.

^{1}H and $^{13}C\{^{1}H\}$ NMR spectra were also collected and further pointed towards the presence of the tetraphenylphosphonium ion in solution. All proton resonances, except for that of the solvent, appear in the aromatic region of the spectrum ranging from 7.67-7.94 ppm. There are three distinct proton environments arising from the protons attached to the *ortho*-, *meta*-, and *para*- carbons, and they are pictured in Figure 4.3. Environment A, the *ortho*- protons, appeared as a doublet of triplets due to coupling to the phosphorus atom as well as the protons of Environment B. It resonated at 7.69 ppm and had a three-bond coupling constant to phosphorus valued at 7Hz. The three-bond coupling constant to the *meta*- protons of Environment B was quantified at 1.5Hz. Environment B resonated at 7.75 ppm as a triplet of doublets, which is expected due to coupling to the *ortho*- and *para*- protons. The coupling to the two protons in Environment A (8.2Hz) is observed to be larger than the coupling to the proton of Environment C (3.5Hz). The *para*- proton of

Environment C has a chemical shift of 7.93 ppm. It is displayed as a triplet due to coupling to the *meta*- protons of Environment B and has a three-bond coupling constant of 7.5Hz.

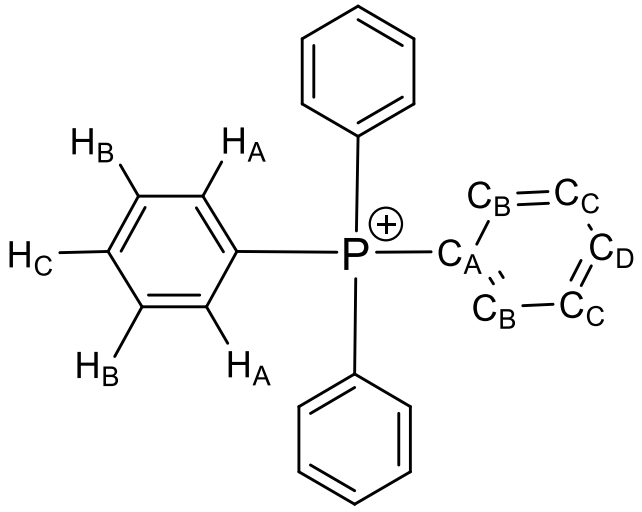

Figure 4.3: ^{1}H and ^{13}C Environments in Tetraphenylphosphonium Iodide.

Four different carbon-13 environments were observed in the $^{13}C\{^{1}H\}$ spectrum, corresponding to the *ipso*-, *ortho*-, *meta*-, and *para*- carbons on the phenyl rings as depicted in Figure 4.3. Each of these environments appeared as doublets due to coupling to phosphorus. The *ipso*-carbon's (Environment A) chemical shift was the furthest upfield at 118.89 ppm. The one-bond coupling to phosphorus, which was found to be 88.2Hz, agreed well with the literature values for this type of coupling.[17–19] The *meta*-carbon of Environment C, which shows coupling to phosphorus three bonds away, resonates at 131.27 ppm. The three-bond coupling constant was found to be 13Hz. Environment B, which is two bonds away from phosphorus, has a chemical shift of 132.66 ppm and a two-bond coupling constant equal to 10.6Hz. Finally, the *para*-carbon of Environment D has a chemical shift of 136.33 ppm and a four-bond coupling constant of 2.8Hz. This is consistent with other four-bond phosphorus to carbon coupling constants reported in the

literature.[20] The NMR spectra show that the tetraphenylphosphonium ion persists in solution, giving insight into the potential product. Attempts to produce crystals suitable for X-Ray diffraction so that the structure of the product may be elucidated are ongoing.

In light of the recent discovery in perovskite research, trimethylsulfonium lead triiodide described in the last chapter,[21] it seemed appropriate to react tetramethylphosphonium iodide with tin (II) iodide to investigate whether or not it would produce similar results. Thus, $[PMe_4][I]$ was reacted with tin(II) iodide in the same manner as $[HPMe_3][I]$ and $[PPh_4][I]$, producing a dark red solution upon combination of the two reactants. This solution was set up for recrystallization by slow evaporation, however no crystals suitable for X-Ray diffraction were formed. Rather, a flaky black solid was isolated.

$^{31}P\{^1H\}$, ^1H, and $^{13}C\{^1H\}$ NMR studies of this solid showed persistence of the tetramethylphosphonim ion in solution. The $^{31}P\{^1H\}$ NMR showed a singlet at 24.51 ppm, which is very comparable to the shifts reported by Herrmann et al.[22] and Kornath et al.[17] for the tetramethylphosphonium ion. Furthermore, a doublet at 9.98 ppm in the $^{13}C\{^1H\}$ NMR spectrum provided evidence for tetramethylphosphonium since the four methyl carbons couple to the phosphorus atom. This shift is in the expected range for methyl groups[23] and the two-bond coupling constant is very close to that observed by Herrmann et al.[22] (56.3Hz *cf.* 56Hz). Finally, the ^1H NMR of this reaction mixture showed that tetramethylphosphonium was in solution due to a doublet at 1.82 ppm. Once again, this shift matches that of the literature for this ion,[22] and the two-bond coupling constant is also close to that of the literature (14.5Hz *cf.* 15Hz).

Although the crystal structure of this compound could not be obtained, recrystallizations by slow evaporation of the product in DCM and acetonitrile are currently underway. The very dark colour of this compound is promising for potential applications as a light-harvesting material since it would be able to absorb most wavelengths of light. In addition to this, the material can withstand prolonged exposure to ambient air, which is a necessary quality in any material used in a solar cell. Interestingly, another reaction including a diphosphonium iodide salt with tin(II) iodide appeared as a black solid.

The reaction of bis(trimethylphosphonio)ethane iodide with tin(II) iodide was carried out in the same manner as the previous three reactions. Upon dissolution in acetonitrile, a black precipitate was formed. After overnight stirring, the reaction mixture appeared as an orange solution with a black precipitate. The orange solution was set up for recrystallization by slow evaporation, however it did not yield any crystals. The black precipitate was analyzed via NMR spectroscopy. The compound was only sparingly soluble in acetonitrile, however solution-NMR spectra were still able to be collected. The $^{31}P\{^{1}H\}$ NMR showed a singlet at 32.4 3 ppm, suggesting that the phosphorus environment in the precipitate is similar to that of bis(trimethylphosphonio)ethane iodide. The ^{1}H NMR spectrum showed further encouragement that the parent phosphonium was part of the product mixture. A doublet due to the coupling of the eighteen methyl protons to phosphorus was observed at 1.92 ppm, which is within the range of expected shifts for this type of proton environment.[23] The two-bond coupling constant between these protons and phosphorus was found to be 36 Hz, which is also within the literature range for this coupling.[23] A doublet representing the protons of the ethane bridge was observed at 2.53 ppm. The coupling of these protons to phosphorus is weaker than the coupling of the methyl

protons to phosphorus, but it is similar to the coupling found in the diphosphonium starting material, which was discussed in Chapter 2 of this thesis (6.5Hz *cf.* 6Hz). Unfortunately, given the low solubility of the product in MeCN, no $^{13}C\{^{1}H\}$ NMR spectrum was obtained.

Like the product created from the reaction of $[PMe_4][I]$ and SnI_2, this product is remarkably stable in air. After prolonged exposure to air there was no considerable change in the chemical shift in the $^{31}P\{^{1}H\}$ NMR (32.17 *cf.* 32.43 ppm), which bodes well for a potential light-harvesting material. However, the product is soluble in water, which is not ideal for the light-harvesting portion of a solar cell since solar cells must withstand exposure to water. Nevertheless, the dark colour of the solid means that it could have useful applications in photovoltaics and it is a material that deserves further study, particularly in UV-Visible spectroscopy. Crystal structure elucidation of this solid would be the next step in its characterization, and a recrystallization from acetonitrile is currently underway.

Thus far, all the reactions with phosphoniums and group 14 halides have been with phosphonium iodides and group 14 iodides. Since there have been perovskites created with group 14 bromides,[24–28] it seemed pertinent to investigate whether or not a phosphonium-templated perovskite could be created with tin(II) bromide. Tetramethylphosphonium bromide and tin(II) bromide were combined in DCM, and after 20h of stirring a milky white suspension was observed. The reaction mixture was centrifuged, and the colourless supernatant was placed in a vial for recrystallization by slow evaporation. The white pellet was dried and kept for analysis. No material was present in the vial containing the supernatant after the solvent had evaporated, suggesting that the product must be in the pellet. Although both reactants as well as the product are colourless solids, it is reasonable

to conclude that the pellet consists of a separate material than the two reactants since it is insoluble in DCM.

As with the previous reactions, NMR spectroscopy was useful in determining whether the phosphonium ion is present in the product mixture. Although the halide counterion in this tetramethylphosphonium salt is different than the previous tetramethylphosphonium salt discussed in this chapter, there should be no appreciable difference in chemical shift between the cations. The $^{31}P\{^{1}H\}$NMR showed a singlet at 25.60 ppm, which is similar to the tetramethylphosphonium shifts found in the literature[17,22] and previously in this thesis. Both the $^{13}C\{^{1}H\}$ and ^{1}H spectra showed a doublet for the methyl group within the expected range.[23] The methyl carbons resonated at 8.88 ppm in the $^{13}C\{^{1}H\}$ NMR and the one-bond coupling to phosphorus was found to be 55.3Hz (*cf.* 56Hz[22]). The methyl protons resonated at the same frequency as the analogous reaction with tin(II) iodide (1.82 ppm), and the two-bond coupling constant between the protons and phosphorus was calculated to be 15.5Hz. Although NMR provides good evidence for the phosphonium cation in the pellet, it cannot give insight as to what the anion is in the product. X-Ray crystallography studies would be able to elucidate exactly what the anion might be. Attempts to recover crystals for this product are currently underway.

4.2.2 Reactions of Phosphonium Salts with Tin(IV) Iodides

Synthesis of $[O{=}PMe_3SnI_3][SnI_6]$

As mentioned in the Oxidation State section of Chapter 1 of this thesis, the group 14 elements can occur in a variety of oxidation states. In particular, tin is found in nature

as having a +2 or +4 oxidation state.[29] Given the interesting results of the reaction of phosphoniums with tin(II) halides, it seemed necessary to investigate how these species interacted with the tin(IV) halides. Thus, two reactions with two different phosphoniums and tin(IV) iodide were carried out to investigate the reactivity of these compounds with each other.

The first phosphonium to be reacted with tin (IV) iodide was trimethylphosphonium iodide. The two reactants were dissolved in acetonitrile in separate vials and the SnI_4 was added to the phosphonium in a dropwise manner. The solution quickly changed colour to dark red when the reactants were added together, indicating that a reaction took place. The dark red solution persisted after 24h of stirring and was set up for recrystallization via slow evaporation, granting black crystals suitable for X-Ray diffraction. $^{31}P\{^{1}H\}$ NMR of an aliquot of the product mixture showed two singlets; one at -1.02 ppm and another at 86.56 ppm. The peak at -1.02 ppm is reminiscent of the chemical shift reported by Bellachioma et al.[10] for trimethylphosphonium iodide, indicating that this cation must be present in solution. The peculiar peak at 86.56 ppm did not resemble any phosphonium environments and had a much lower intensity than the peak at -1.02 ppm, suggesting that the phosphorus environment it represents is less abundant in solution than the phosphonium environment. Figure 4.4 shows the $^{31}P\{^{1}H\}$ spectrum of the reaction of trimethylphosphonium iodide with SnI_4 to highlight the differences in intensity between the two peaks mentioned above.

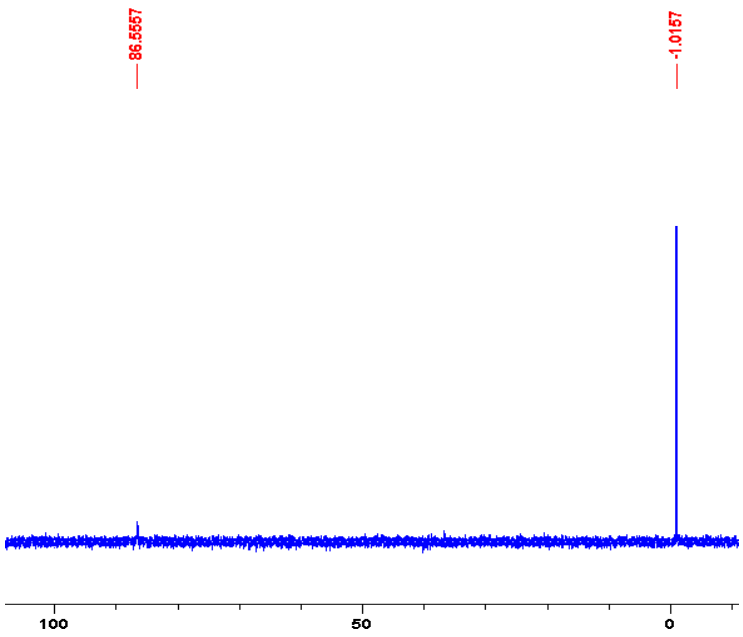

Figure 4.4: $^{31}P\{^{1}H\}$ NMR Spectrum of the Product Mixture in the Reaction of Trimethylphosphonium iodide with SnI_4. The peak at -1.0157 ppm represents the trimethylphosphonium ion, while the peak at 86.5557 ppm represents trimethylphosphine oxide.

The mysterious peak at 86.56 ppm was able to be identified on the basis of the results of a crystal structure elucidated by X-Ray crystallography. The crystal did not include a phosphonium ion with a BX_3^- anion as expected in a traditional perovskite,[1,5,8,9] but rather it consisted of a tin(IV) species surrounded by three phosphine oxide ligands and three iodides along with a $[SnI_6]^{2-}$ anion. The crystal structure is presented in Figure 4.5. The phosphine oxide ligands coordinated to the tin(IV) metal centre was an unexpected result, as the reaction took place in inert atmosphere conditions. It is possible that some unreacted trimethylphosphine in the starting material was exposed to air when trimethylphosphonium iodide was analyzed by NMR and Elemental Analysis, causing the trimethylphosphine oxide ligands to be in the reaction mixture.

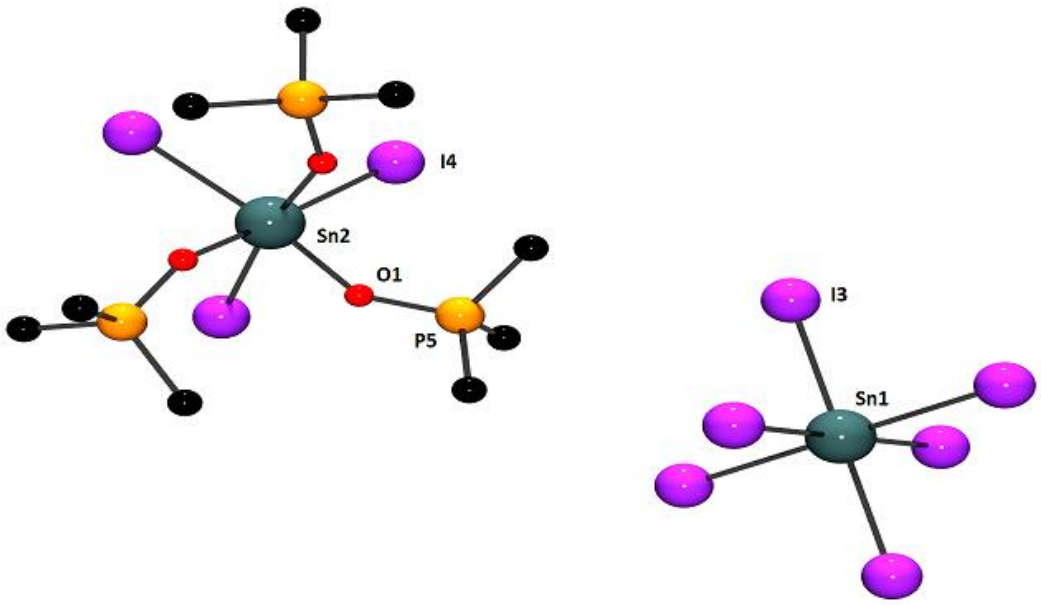

Figure 4.5: Crystal structure (ball and stick) of $[(O{=}PMe_3)_3SnI_3]_2[SnI_6]$ with selected bond lengths (Å) and angles (º): Sn-I3, 2.8431(7); Sn2-I4, 2.7912(9); Sn2-O1, 2.064(7); P5-O1, 1.521(7); I4-Sn2-I4, 94.26(3); I3-Sn1-I3(adjacent), 90.0(3); I3-Sn1-I3(across), 180.0; O1-Sn2-O1, 82.9(3). Hydrogen atoms are omitted for clarity.

Although this crystal does not represent the bulk material, it is still worthy of discussion as a novel complex. There are two $[(O{=}PMe_3)_3SnI_3]$ cations for every $[SnI_6]$ dianion. A CSD search revealed that there have been no previously reported species consisting of both aforementioned ions, however there are compounds in the literature with a $[SnI_6]$ anion as well as complexes in which a phosphine oxide coordinates to a tin atom. It is valuable to compare bond lengths and angles of these previously reported compounds to the one synthesized in order to understand the geometry of the molecule made. The $[SnI_6]$ moiety has been isolated before as a dianion in tropylium tin iodide[30] and as an attempt to make an adduct of Ph_2PH and SnI_4.[31] The labels in Figure 4.5 will be used to compare the $[SnI_6]$ ion synthesized in this thesis to the other $[SnI_6]$ ions found in the literature.

On average, the Sn1-I3 bonds in the literature are slightly larger than the analogous bonds in this structure. We report a bond length of 2.8431(7)Å for all Sn1-I3 bonds in this structure since it is a symmetry-generated octahedron. In contrast, the average Sn-I bond in this moiety in tropylium tin iodide[30] and $[Ph_2PH_2]_2[SnI_6]$[31] is 2.88(1)Å and 2.858(1)Å, respectively, which renders them crystallographically distinct from the $[SnI_6]$ ion in this thesis. The bond angles in $[SnI_6]$ match those of the same ion in $[Ph_2PH_2]_2[SnI_6]$.[31] The bond angle between adjacent iodine atoms was found to average at 90.0(3)˚, while the symmetry-generated I-Sn-I bond angles were 180.0˚. This is consistent with the ideal octahedral VSEPR geometry around the tin(IV) atom.

Since the $[(O{=}PMe_3)_3SnI_3]$ cation has never been observed before, the Sn-I, Sn-O, and P-O bond angles were compared to the crystal structure of $[SnI_3]^-$ elucidated by Lode et al.[32] and a bidentate phosphine oxide ligand that coordinated to tin reported by Wirth et al.[33] Once again, the labels in Figure 4.5 will identify which bonds are being compared. In comparison to the $[SnI_3]$ anion,[32] the Sn2-I4 bonds in $[(O{=}PMe_3)_3SnI_3]$ are much shorter (2.7912(9) *cf.* 2.898(8)Å). This can be explained by the additional coordination of the phosphine oxide ligands to the tin(IV) centre in $[(O{=}PMe_3)_3SnI_3]$. The I4-Sn2-I4 angle in $[(O{=}PMe_3)_3SnI_3]$ was found to be 94.26(3)˚, whereas this angle in $[SnI_3]$ is 96.69(3)˚.[32] Once again, this could be attributed to the phosphine oxide ligands also being present in $[(O{=}PMe_3)_3SnI_3]$, which causes the iodide X-ligands to come closer together. In terms of Sn-O bond lengths, the Sn2-O1 distance is also much shorter than the one reported in the chelating diphosphine oxide ligand[33] (2.064(7)Å *cf.* 2.2057(13)Å). Unsurprisingly, the O1-Sn2-O1 angle in $[(O{=}PMe_3)_3SnI_3]$, which was found to be 82.9(3)˚, is less than that of the literature, which reports an average of 90.0(6)˚ for these angles.[33] This suggests that the

geometry around the Sn(IV) centre in the cation is not perfectly octahedral. Lastly, the P5-O1 bond distance in the cation closely resembles that of the literature, suggesting that the oxygen and phosphorus are indeed connected by a double bond. $[(O=PMe_3)_3SnI_3]$ has a P=O distance of 1.521(7)Å and the phosphine oxide ligand coordinating to tin in the literature has a similar bond length of 1.512(9)Å.[33] A summary of the key metrical parameters discussed for this crystal structure can be found in Table 4.1 and a diagram of the crystal packing can be found in Figure 4.6.

Table 4.1: Summary of the Key Metrical Parameters in $[(O=PMe_3)_3SnI_3]_2[SnI_6]$

Parameter	Value (Å/°)	Literature Value (Å/°)
Sn1-I3	**2.8431(7)**	**2.88(1)**[30] **2.858(1)**[31]
Sn2-I4	**2.7912(9)**	**2.898(8)**[32]
Sn2-O1	**2.064(7)**	**2.2057(13)**[33]
P5-O1	**1.521(7)**	**1.512(9)**[33]
I3-Sn1-I3	**90.0(3), 180.0**	**90.5(3), 175.0(5)**[30] **90.0, 180.0**[31]
I4-Sn2-I4	**94.26(3)**	**96.69(3)**[32]
O1-Sn2-O1	**82.9(3)**	**90.0(6), 180.0**[33]

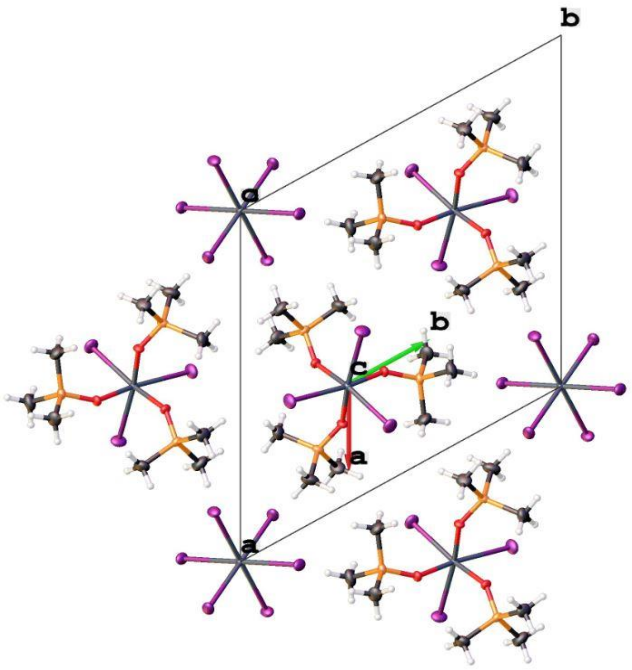

Figure 4.6: Crystal Packing of $[(O=PMe_3)_3SnI_3]_2[SnI_6]$ normal to (001) in the form of thermal ellipsoids. The orange ellipsoids represent phosphorus, the black represent carbon, the red represent oxygen, the grey represent tin, and the purple represent iodine.

The unprecedented coordination of trimethylphosphine oxide (TMPO) to the Sn(IV) centre was further investigated by exploring its Lewis acidity via the Gutmann-Beckett method.[34–36] By comparing the $^{31}P\{^1H\}$ NMR chemical shift of the coordinated phosphine to the chemical shift of the free phosphine, this method can assess the Lewis Acidity of a particular species. Using the literature shift of TMPO[37] (-48 ppm), the equation in Figure 4.7 was employed to make an estimate of the Acceptor Number (AN) of the SnI_3 centre for Lewis acidity. The higher the AN, the stronger the Lewis acidity of a species. Also, the change in chemical shift in the $^{31}P\{^1H\}$ NMR between free TMPO and coordinated TMPO was calculated. Once again, the greater the $\Delta\delta^{31}P\{^1H\}$, the better the Lewis acid. The AN for the SnI_3 cation reported in this thesis was found to be 85.2, while the $\Delta\delta^{31}P\{^1H\}$ was found to be 38.6 ppm.

$$AN = 2.21 \times (\delta_{sample} - 48)$$

Figure 4.7: The Equation for the Gutmann-Beckett Method.[34-36]

Although the Gutmann-Beckett acceptor number is dependent on the solvent used, it is beneficial to provide some literature examples of the AN and $\Delta\delta^{31}P\{1H\}$ of well-known Lewis acids for comparison. The boron trihalides are some of the best Lewis-acidic compounds on record. BI_3 boasts the highest AN of 114.9, with BBr_3 and BCl_3 having ANs of 109 and 106, respectively.[34,38] Another well-studied Lewis acid, $B(C_6F_5)_3$, has an AN of 82 and a $\Delta\delta^{31}P\{^1H\}$= 26.6 ppm.[39,40] More recently, silylium[41] and iodonium[42] cations have been investigated as Lewis acids, having $\Delta\delta^{31}P\{^1H\}$ ranges of 39-45 and 22.6-57.6, respectively. Given these literature values the SnI_3 cation falls right in the mix of having good Lewis acidity, exceeding the $\Delta\delta^{31}P\{^1H\}$ of $B(C_6F_5)_3$[39,40] and similar to the $\Delta\delta^{31}P\{^1H\}$ range of silylium[41] and iodonium[42] cations.

It is not a surprise that the Sn(IV) species in the $[(O{=}PMe_3)_3SnI_3]$ moiety displays Lewis acidity. There have been multiple instances of tin (IV)[43–45] as well as tin(II)[46] Lewis acid catalysts in the literature. For example, Yamanaka et al.[45] have shown that another tin(IV) halide, $SnCl_4$, demonstrates Lewis acid activity in a carbonyl-ene reaction. The discovery of the Lewis acidity of the SnI_3 cation in $[(O{=}PMe_3)_3SnI_3]$ and the application for tin(IV) species in catalysis shows that tin(IV) iodide deserves further investigation as a potential Lewis acid catalyst.

Synthesis of [PMePh$_3$][SnI$_5$]

Although the Lewis acidity of the tin(IV) centre is fascinating, this thesis is still focused on creating phosphonium-templated perovskite materials. Methyltriphenylphosphonium iodide was the next phosphonium reacted with tin(IV) iodide. Equimolar amounts of the two solids were combined in a vial. After a few minutes a reaction was observed in the solid state, since a red solid appeared at the interface of the white and orange solids. Acetonitrile was used to dissolve the solids, making a dark red solution, and the reaction was left to stir for 48h. After this time, the solution was set up for recrystallization and a small aliquot was taken for $^{31}P\{^1H\}$ NMR analysis. Eventually, dark red crystals grew from acetonitrile.

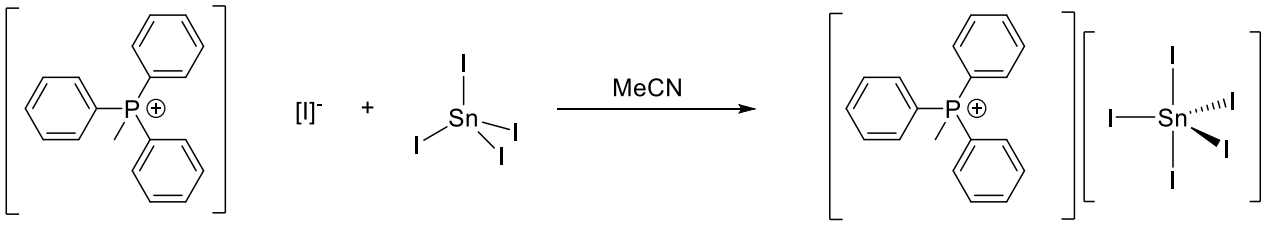

Scheme 4.2: The Reaction of Methyltriphenylphosphonium iodide with SnI_4

The phosphorus NMR showed a singlet at 21.86 ppm, which is indicative of a single phosphorus environment in solution. This chemical shift is similar to that of the starting material [PMePh$_3$][I], which resonates at 21.5 ppm,[47] suggesting that the phosphorus environment in the product mixture is like that of methyltriphenylphosphonium iodide. To further confirm the presence of this ion in solution, ^1H and $^{13}C\{^1H\}$ NMR spectra were collected of the dark red crystals of this material. The ^1H NMR showed evidence of methyltriphenylphosphonium in solution since four distinct proton environments were observed. A doublet at 2.79 ppm was representative of the three methyl protons. The two-

bond coupling constant from this environment's coupling to phosphorus was calculated to be 14Hz, which is similar to the literature value of this coupling at 14.6Hz.[47] The aromatic *ortho*-, *meta*-, and *para*- proton environments had chemical shifts of 7.66, 7.71, and 7.86 ppm, respectively. The six *ortho*- protons appeared as a doublet of triplets due to coupling to phosphorus and the *meta*- protons. The *meta*- proton environment couples to both the *ortho*- and *para*- proton environments and therefore appears as a triplet of doublets. Lastly, the *para*- protons appear as a triplet due to coupling to the *meta*- protons. The chemical shifts of these aromatic protons, as well as their coupling constants match closely with the literature[47] and are outlined in Table 4.2.

Table 4.2: Summary of the ^{1}H NMR Spectrum of $[PMePh_3][I] + SnI_4$

Environment	Chemical Shift (ppm)	Multiplicity	Integration	Coulping Constant (Hz)
Methyl	**2.79**	**D**	**3H**	**$^{2}J_{PH}$ =14**
***Ortho*-H(Ph)**	**7.66**	**Dt**	**6H**	**$^{3}J_{PH}$ =7 $^{1}J_{HH}$ =1.5**
***Meta*-H(Ph)**	**7.71**	**Td**	**6H**	**$^{3}J_{HH\text{-}ortho}$= 8 $^{3}J_{HH\text{-}para}$=3.5**
***Para*-H(Ph)**	**7.86**	**T**	**3H**	**$^{3}J_{HH}$ = 6.5**

The $^{13}C\{^{1}H\}$ NMR of methyltriphenylphosphonium iodide reported in the literature also closely matched that of the material left after slow evaporation. Five distinct carbon environments were observed in the spectrum, each of them appearing as a doublet because of coupling to phosphorus. The carbon representing the methyl group appeared the furthest upfield at 9.39 ppm, with a one-bond coupling to phosphorus of 58.5Hz. This value is very similar to that of the literature, which is reported at 57.3Hz.[48] The *ipso*-carbon, which is

directly bound to the phosphorus, resonated at 120.33 ppm and had a one-bond coupling constant of 89Hz. This is at the higher end of the literature range for one-bond phosphorus to carbon coupling.[17–19] The *meta-*, *ortho-*, and *para-* carbons displayed chemical shifts of 131.16, 134.23, and 136.10 ppm respectively. Chemical shifts in this range are common in aromatic carbons[23] and closely matched the chemical shifts reported in the literature[48] which solidifies the presence of the methyltriphenylphosphonium ion in solution. A full summary of the $^{13}C\{^{1}H\}$ NMR spectrum of the reaction of methyltriphenylphosphonium iodide with tin(IV) iodide, including coupling constants, is given in Table 4.3.

Table 4.3: Summary of the $^{13}C\{^{1}H\}$ NMR Spectrum of $[PMePh_3][I] + SnI_4$

Environment	Chemical Shift (ppm)	Multiplicity	Coupling Constant (Hz)
Methyl	**9.39**	**D**	**$^{1}J_{PC}$ = 58.5**
Ipso-C(Ph)	**12.33**	**D**	**$^{1}J_{PC}$ = 89**
Meta-C(Ph)	**131.16**	**D**	**$^{3}J_{PC}$ = 13**
Ortho-C(Ph)	**134.23**	**D**	**$^{2}J_{PC}$ = 10.7**
Para-C(Ph)	**136.10**	**D**	**$^{4}J_{PC}$ = 2.8**

Single-crystal X-Ray diffraction determined the identity of the anion in this product. It was discovered that the product consisted of $[PMePh_3]$ as the cation and $[SnI_5]$ as the anion, making a charge-balanced compound. The asymmetric unit of this compound, as well as the atom labels that will be used in the following discussion of the structure, can be found in Figure 4.8. A $[PMePh_3]$ ion found in the literature as the counter-ion to $[CdI_4]$[49] was used to crystallographically compare the two ions in terms of their metrical parameters. An average of the P1-C2 bond lengths in both the literature structure and the structure reported in this thesis was calculated. In $[PMePh_3][SnI_5]$, the average P1-C2 bond is 1.791(4)Å, while in $[PMePh_3][CdI_4]$ this value is 1.77(2)Å.[49] The average C-P-C in both

structures indicates a tetrahedral geometry around the phosphonium ion, with the average in $[PMePh_3][SnI_5]$ being 109.48(18)˚ and the average in $[PMePh_3][CdI_4]$ at 109.45(5)˚.[49] The ESDs of the metrical parameters in both structures overlap, which suggests that they are crystallographically indistinguishable within statistical error.

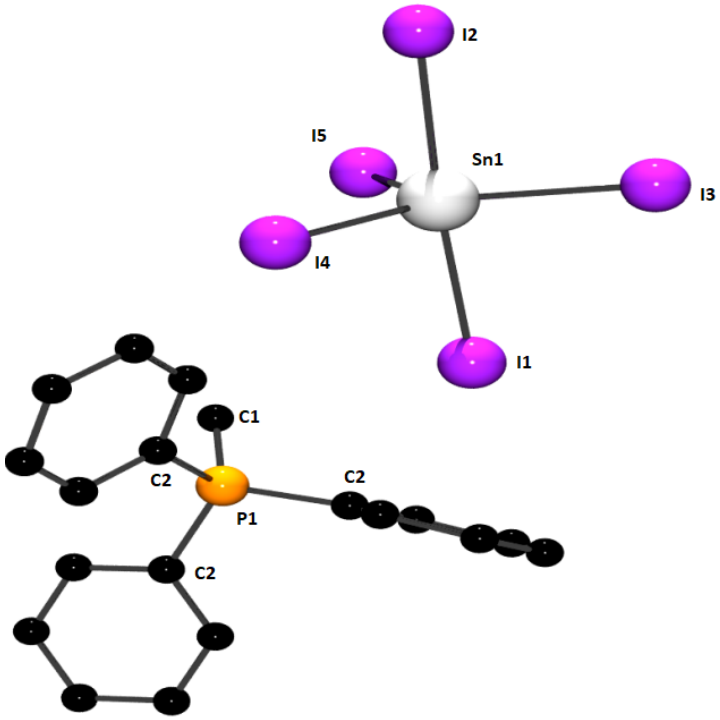

Figure 4.8: Crystal structure (ball and stick) of $[PMePh_3][SnI_5]$ with selected bond lengths (Å) and angles (º): Sn1-I1, 2.8378(4); Sn1-I2, 2.8617(4); Sn1-I3, 2.7267(4); Sn1-I4, 2.7255(4); Sn1-I5, 2.7391(4); P1-C2, 1.791(4); P1-C1, 1.791(4); I1-Sn1-I2, 175.869(11); I3-Sn1-I1, 90.519(11); I3-Sn1-I2, 90.989(11); I3-Sn1-I5, 128.017(14); I4-Sn1-I1, 90.973(14); I4-Sn1-I2, 92.030(14); I4-Sn1-I3, 111.931(14); I4-Sn1-I5, 120.052(14); I5-Sn1-I1, 88.670(11); I5-Sn1-I2, 87.372(11); C-P1-C, 109.48(18). Hydrogen atoms are omitted for clarity.

The $[SnI_5]$ anion was compared to a similar anion in the compound $[IPCy_3][SnI_5]$, which was reported by Apostolico et al.[31] This compound was made in a similar fashion to that of $[PMePh_3][SnI_5]$ in that it was synthesized from SnI_4. At first glance, both anions appear to adopt a trigonal bipyramidal structure, which would constitute a 120˚ angle

between the equatorial iodines, a 90˚ angle between the axial and equatorial iodines, and a 180˚ angle between the two axial iodines. Geometrically, this is much different than the $[SnI_5]^{3-}$ ion discussed earlier in this chapter and this difference can be due to the difference in oxidation state of the tin centre. A closer examination of the present species reveals that the equatorial I-Sn-I angles deviate from trigonal bipyramidal geometry, with the lowest angle being between I3 and I4 at 111.931(14)˚ and the largest angle being between I3 and I5 at 128.017(14)˚. The average of the equatorial I-Sn-I angles in $[PMePh_3][SnI_5]$ is 120.00(14)˚, which matches the ideal geometry and that of the $[SnI_5]$ ion reported by Apostolico et al.[31] The angles between the axial and equatorial iodine atoms in $[PMePh_3][SnI_5]$ are also close to that of a trigonal bipyramid, with the smallest angle being 87.372(11)˚ and the largest angle being 92.030(14)˚. A similar range for these angles was observed in $[IPCy_3][SnI_5]$, with the smallest angle being 87.92(2)˚ and the largest being 91.70(3)˚.[31] Finally, the I1-Sn-I2 angle was compared in both $[PMePh_3][SnI_5]$ and $[IPCy_3][SnI_5]$. Both structures demonstrate an angle close to the ideal 180˚, with $[PMePh_3][SnI_5]$ having an angle of 175.869(11)˚ and $[IPCy_3][SnI_5]$ having an angle of 177.43(3)˚.[31] Thus, it is conclusive that the $[SnI_5]$ component in $[PMePh_3][SnI_5]$ adopts a trigonal bipyramidal geometry similar to that of $[SnI_5]$ anion in $[IPCy_3][SnI_5]$.

The bond lengths in the $[SnI_5]$ anion in this structure are very similar to the $[SnI_5]$ anion in $[IPCy_3][SnI_5]$. In general, the equatorial Sn-I bonds are shorter than the axial Sn-I bonds due to repulsion from the atoms in the equatorial position. The average of the axial Sn-I bonds in $[IPCy_3][SnI_5]$ is 2.8507(7)Å,[31] whereas in $[PMePh_3][SnI_5]$ this average is 2.8498(4)Å. The overlapping ESDs between the two parameters shows that the Sn-I axial bonds in both structures are the same within the estimated error. The ESDs of the average

equatorial Sn-I bond length, however, do not overlap since this average in $[PMePh_3][SnI_5]$ is 2.7304(4)Å and the analogous average bond in $[IPCy_3][SnI_5]$ is 2.7345(8)Å.[31] This means that the equatorial Sn-I bond lengths in $[IPCy_3][SnI_5]$ are slightly longer than those of $[PMePh_3][SnI_5]$, however the overall geometry of the anions are still the same.

4.2.3 Chapter Conclusions

This chapter explored the reactivity of various phosphonium cations with both tin(II) and tin(IV) halides via direct addition of the starting materials to each other in solution. Although the goal of creating a phosphonium-templated perovskite was not achieved, three new crystal structures of phosphonium-templated iodostannates were characterized. The crystal structure of the reaction between trimethylphosphonium iodide and tin(II) iodide produced a novel iodotin trianion, $[SnI_5]^{3-}$. Two tin trianion species exist in the unit cell with eight phosphonium cations and two iodides to make a novel charge-balanced compound. Furthermore, an unprecedented oxidation of some of the phosphine starting material in $[HPMe_3][I]$ in its reaction with SnI_4 produced a crystal structure of the new salt $[(O{=}PMe_3)_3SnI_3]_2[SnI_6]$, which exhibits Lewis acidic properties. Lastly, a stoichiometric reaction of $[PMePh_3]$ with SnI_4 produced a novel charged-balanced compound, $[PMePh_3][SnI_5]$, whose anion has a trigonal bipyramidal structure with precedence in the literature. Five other reactions with phosphoniums and tin(II) or tin(IV) halides were carried out and NMR spectroscopy showed persistence of the phosphonium cation in solution. The dark colour of the product of the reactions with tin(II) and tin(IV) iodide show that these compounds deserve further investigation as potential light-harvesting materials.

4.3 Experimental

General Procedures

All manipulations were carried out using standard inert atmosphere techniques. All chemicals and reagents were purchased from Sigma-Aldrich and used without further purification. Deuterated solvents were dried according to literature procedure when necessary, and all other solvents were dried over a series of Grubbs'-type columns and degassed prior to use. NMR spectra were recorded at room temperature on a Bruker Avance III 500 MHz, Bruker Avance Ultrashield 300 MHz or Bruker Avance DPX 300 MHz spectrometers. Chemical shifts are reported in ppm relative to internal standards for ^{1}H and ^{13}C (the given deuterated solvent) and the external standard for ^{31}P (85% H_3PO_4). Coupling constants |J| are given in Hz. Elemental Analysis was performed by the University of Windsor Mass Spectrometry Service Laboratory using Perkin Elmer 2400 combustion CHN analyzer.

X-Ray Crystallography

Crystals for investigation were covered in Paratone®, mounted into a goniometer head, and then rapidly cooled under a stream of cold N_2 of the low-temperature apparatus (Oxford Cryostream) attached to the diffractometer. The data were then collected using the APEXII software suite[34] on a Bruker Photon 100 CMOS diffractometer using a graphite monochromator with MoKα (λ = 0.71073 Å) or CuKα (λ = 1.54178 Å) radiation. For each sample, data were collected at low temperature. APEXII software was used for data reductions and SADABS[35] was used for absorption corrections (multi-scan; semi-empirical from equivalents). XPREP was used to determine the space group and the structures were solved and refined using the SHELX[36] software suite as implemented in the WinGX[37] or OLEX2[38] program suites. Validation of the structures was conducted using PLATON.[39]

4.3.1 Synthesis of $[HPMe_3]_4[I][SnI_5]$

0.327g of $[HPMe_3]^+[I]^-$ and 0.600g of SnI_2 were dissolved in acetonitrile in separate vials. Under stirring, the $[HPMe_3]^+[I]^-$ solution was transferred dropwise to the SnI_2 solution. The solution turned deep red immediately upon addition of the phosphonium iodide with this colour turning to orange 20 minutes after addition was complete. After 72 hours, the solution was pale yellow. Some of the acetonitrile solvent was pumped off at this point and the solution was placed in the freezer for slow recrystallization. After two weeks of recrystallization in a freezer, garnet red crystals were formed and the mother liquor was decanted, and allowed to slowly evaporate at room temperature, yielding orange crystals of $[HPMe_3][I][SnI_5]$. $^{31}P\{^1H\}$ NMR (CD_3CN, 121.5MHz) δ: -0.711 (s). $^{13}C\{^1H\}$ NMR (CD_3CN) δ: 5.696 (d, P*C*H_3, $^1J_{CP}$ = 55.3Hz). ^1H NMR (CD_3CN) δ: 1.841 (dd, 9H, PC***H*****3**, $^2J_{HP}$= 15.9Hz. , $^3J_{HH}$=5.4Hz.), 6.360 (ddec, 1H, P***H***, $^1J_{HP}$=510Hz, $^3J_{HH}$=5.4Hz). Elemental analysis: calc. for $PC_{12}H_{40}SnI_6$•1 tol: C, 11.09; H, 3.10; N, 0.00, found: C, 12.13; H, 3.39; N, 0.03.

4.3.2 Reaction of $[PPh_4][I]$ with SnI_2

0.195g of $[PPh4]^+[I]^-$ and 0.196g of SnI_2 were dissolved in acetonitrile in separate vials. Under stirring, the $[PPh4]^+[I]^-$ solution was transferred dropwise to the SnI_2 solution. The solution turned deep red immediately upon addition of the phosphonium. After 72 hours, the solution was red with a mustard yellow precipitate. The solution was centrifuged and the red supernatant was cannula transferred to a Schlenk flask. The solvent was pumped off, and a purple-brown solid was left behind. This was redissolved in acetonitrile and left for slow recrystallization. $^{31}P\{^1H\}$ NMR (CD_3CN) δ: 24.322 (s). ^1H NMR (CD_3CN, 500

MHz); δ: 7.69 (***H*****$_{ortho}$**-Ph, dt, 8H, $^{3}J_{PH}$ = 7Hz, $^{3}J_{HH}$ = 1.5Hz), 7.75 (***H*****$_{meta}$**- Ph, td, 8H, $^{3}J_{HH\text{-}ortho}$ = 8.2Hz, $^{3}J_{HH\text{-}para}$ = 3.5Hz), 7.93(***H*****$_{para}$** – Ph, t, 4H, $^{3}J_{HH}$ = 7.5Hz). $^{13}C\{^{1}H\}$ NMR (CD_2Cl_2, 125.7MHz): δ: 118.89 (***C*****$_{ipso}$**, d, $^{1}J_{PC}$=88.2Hz), 131.27 (***C*****$_{meta}$**, d, $^{3}J_{PC}$ = 13Hz), 135.66 (***C*****$_{ortho}$**, d, $^{2}J_{PC}$ = 10.6Hz), 136.33 (***C*****$_{para}$**, d, $^{4}J_{PC}$ = 2.8Hz).

4.3.3 Reaction of [PMe$_4$][I] with SnI$_2$

Tetramethylphosphonium iodide (50mg, 0.23mmol) was placed in a 20mL scintillation vial along with an equivalent of tin (II) iodide (85mg, 0.23mmol). The two solids were dissolved in ca. 10mL of acetonitrile, producing a deep red solution. The reaction was left to stir for 20h, after which time the deep red solution was left for recrystallization via slow evaporation. $^{31}P\{^{1}H\}$ NMR (CD_3CN, 202.5MHz) δ: 24.51 (s). $^{13}C\{^{1}H\}$ NMR (CD_3CN, 125.8MHz) δ: 9.98 (d, P***C***H_3, $^{1}J_{CP}$ = 56.3Hz). ^{1}H NMR (CD_3CN, 500MHz) δ: 1.82 (d, 12H, PC***H*****$_3$**, $^{2}J_{HP}$= 14.5Hz).

4.3.4 Reaction of [Me$_3$PC$_2$H$_4$PMe$_3$] 2[I] with SnI$_2$

50mg (0.12mmol) of bis(trimethylphosphonio)ethane iodide was placed in a 20mL scintillation vial along with 86mg (0.23mmol) of tin (II) iodide. Acetonitrile was added to the vial slowly under stirring. Upon addition of the solvent, a black precipitate started to form. The reaction mixture was left to stir for 20h after which time an orange solution with a black precipitate was observed. The precipitate was separated from the solution. The orange solution was set up for recrystallization via slow evaporation, however no crystals were isolated. The black precipitate was analyzed. $^{31}P\{^{1}H\}$ NMR (CD_3CN, 202.5MHz) δ: 32.43 (s). $^{31}P\{^{1}H\}$ NMR (DMSO-*d*$_6$, 202.5MHz) δ: 32.17(s). ^{1}H NMR (CD_3CN, 500MHz)

δ: 1.93 (d, 18H, PC***H₃***, $^{2}J_{HP}$= 36Hz), 2.53 (d, 4H, μ-(C***H₂***)$_2$, $^{2}J_{HP}$=6.5Hz). Elemental analysis: calc. for $P_2C_8H_{22}I_6Sn_2$: C, 8.15; H, 1.88; N, 0.00, found: C, 8.73; H, 1.81; N, 0.04.

4.3.5 Reaction of [PMe₄][Br] with SnBr₂

A 20mL scintillation vial was charged with 50mg (0.29mmol) tetramethylphosphonium bromide and 81mg (0.29mmol) tin (II) bromide. The solids were dissolved in approx. 10mL DCM and produced an opaque white suspension that was left to stir for 20h. After this time, the white suspension persisted. The suspension was centrifuged for 5mins and a colourless solution with a white pellet was observed. The clear solution was set up for recrystallization via slow evaporation, but it did not produce any crystals or other solid upon complete evaporation of the solvent. The pellet was analyzed. $^{31}P\{^{1}H\}$ NMR (CD_3CN, 202.5MHz) δ: 25.60(s). $^{13}C\{^{1}H\}$ NMR (CD_3CN, 125.8MHz) δ: 8.88 (d, P*C*H_3, $^{1}J_{CP}$ = 55.3Hz). ^{1}H NMR (CD_3CN, 500MHz) δ: 1.82 (d, 12H, PC***H₃***, $^{2}J_{HP}$= 15.5Hz).

4.3.6 Synthesis of [(O=PMe₃)₃SnI₃]₂[SnI₆]

Trimethylphosphonium iodide (50mg, 0.25mmol) and tin (IV) iodide (154mg, 0.25mmol) were dissolved separately in two 20mL scintillation vials in approx. 10mL acetonitrile. The SnI_4 was added to the phosphonium salt under stirring in a dropwise manner. Upon introduction of the SnI_4, the colour of the solution went from colourless/orange to very dark red. The reaction was left to stir for 24h, after which time the dark red solution persisted. The solution was set up for recrystallization via slow evaporation and afforded black crystals suitable for X-Ray diffraction. $^{31}P\{^{1}H\}$ NMR (CD_3CN, 121.5MHz) δ: -1.02 (s, H***P***Me_3), 86.56 (s, O=***P***Me_3).

4.3.7 Synthesis of [$PMePh_3$][SnI_5]

Methyltriphenylphosphonium iodide (50mg, 0.12mmol) was placed in a 20mL scintillation vial with an equimolar amount of SnI_4 (77mg). After a few minutes of the white and orange solids being in the vial a red solid started to form, indicating reaction in the solid state. Ca. 10mL of acetonitrile was added to the vial containing the two reactants and the solution was dark red. The reaction was left to stir for 48h. Dark red crystals suitable for X-Ray diffraction were grown from acetonitrile. $^{31}P\{^1H\}$ NMR (CD_3CN, 202.5MHz) δ: 21.86(s). ^1H NMR (CD_3CN, 500 MHz); δ: 2.79 (PC***H*****$_3$**, d, 3H, $^2J_{PH}$ = 14Hz), 7.66 (***H*****$_{ortho}$*****-Ph,*** dt, 6H, $^3J_{PH}$ = 7Hz, $^3J_{HH}$= 1.5Hz), 7.71(***H*****$_{meta}$*****- Ph***, td, 6H, $^3J_{HH\text{-}ortho}$ = 8Hz, $^3J_{HH\text{-}para}$= 3.5Hz), 7.86 (***H*****$_{para}$*****-Ph***, t, 3H, $^3J_{HH}$= 6.5Hz). $^{13}C\{^1H\}$ NMR (CD_3CN, 125.8MHz): δ: 9.39 (P-***C***H_3, d, $^1J_{PC}$ = 58.5Hz), 120.33 (***C*****$_{ipso}$**, d, $^1J_{PC}$=89Hz), 131.16 (***C*****$_{meta}$**, d, $^3J_{PC}$ = 13Hz), 134.23 (***C*****$_{ortho}$**, d, $^2J_{PC}$ = 10.7Hz), 136.10 (***C*****$_{para}$**, d, $^4J_{PC}$ = 2.8Hz).

4.4 References

(1) Zhao, Y.; Zhu, K. Organic–inorganic Hybrid Lead Halide Perovskites for Optoelectronic and Electronic Applications. *Chem. Soc. Rev.* **2016**, *45* (3), 655–689.

(2) Grätzel, M. The Light and Shade of Perovskite Solar Cells. *Nat. Mater.* **2014**, *13* (9), 838–842.

(3) Boix, P. P.; Agarwala, S.; Koh, T. M.; Mathews, N.; Mhaisalkar, S. G. Perovskite Solar Cells: Beyond Methylammonium Lead Iodide. *J. Phys. Chem. Lett.* **2015**, *6* (5), 898–907.

(4) Ogomi, Y.; Morita, A.; Tsukamoto, S.; Saitho, T.; Fujikawa, N.; Shen, Q.; Toyoda, T.; Yoshino, K.; Pandey, S. S.; Ma, T.; et al. $CH_3NH_3Sn_xPb_{(1-x)}I_3$ Perovskite Solar Cells Covering up to 1060 Nm. *J. Phys. Chem. Lett.* **2014**, *5* (6), 1004–1011.

(5) Chung, I.; Lee, B.; He, J.; Chang, R. P. H.; Kanatzidis, M. G. All-Solid-State Dye-Sensitized Solar Cells with High Efficiency. *Nature* **2012**, *485* (7399), 486–489.

(6) Noel, N. K.; Stranks, S. D.; Abate, A.; Wehrenfennig, C.; Guarnera, S.; Haghighirad, A.-A.; Sadhanala, A.; Eperon, G. E.; Pathak, S. K.; Johnston, M. B.; et al. Lead-Free Organic–inorganic Tin Halide Perovskites for Photovoltaic Applications. *Energy Environ. Sci.* **2014**, *7* (9), 3061–3068.

(7) Hao, F.; Stoumpos, C. C.; Cao, D. H.; Chang, R. P. H.; Kanatzidis, M. G. Lead-Free Solid-State Organic–inorganic Halide Perovskite Solar Cells. *Nat. Photonics* **2014**, *8* (6), 489–494.

(8) Stoumpos, C. C.; Frazer, L.; Clark, D. J.; Kim, Y. S.; Rhim, S. H.; Freeman, A. J.; Ketterson, J. B.; Jang, J. I.; Kanatzidis, M. G. Hybrid Germanium Iodide Perovskite Semiconductors: Active Lone Pairs, Structural Distortions, Direct and Indirect Energy Gaps, and Strong Nonlinear Optical Properties. *J. Am. Chem. Soc.* **2015**, *137* (21), 6804–6819.

(9) Stoumpos, C. C.; Malliakas, C. D.; Kanatzidis, M. G. Semiconducting Tin and Lead Iodide Perovskites with Organic Cations: Phase Transitions, High Mobilities, and Near-Infrared Photoluminescent Properties. *Inorg. Chem.* **2013**, *52* (15), 9019–9038.

(10) Bellachioma, G.; Cardaci, G.; Macchioni, A.; Venturi, C.; Zuccaccia, C. Reductive Elimination of Halogens Assisted by Phosphine Ligands in $Fe(CO)_4X_2$ (X=I,Br) Complexes. *J. Organomet. Chem.* **2006**, *691* (18), 3881–3888.

(11) Mitzi, D. B.; Medeiros, D. R.; Malenfant, P. R. L. Intercalated Organic−Inorganic Perovskites Stabilized by Fluoroaryl−Aryl Interactions. *Inorg. Chem.* **2002**, *41* (8), 2134–2145.

(12) Mitzi, D. B.; Feild, C. a.; Harrison, W. T. a.; Guloy, A. M. Conducting Tin Halides with a Layered Organic-Based Perovskite Structure. *Nature.* **1994**, *369* (6480), 467– 469.

(13) Lode, C.; Krautscheid, H.; Müller, U. $[C_3H_7N(C_2H_4)_3NC_3H_7]_2\infty^1[Sn_4I_{12}]$ - Ein Iodostannat Aus Verknöpften SnI_5^-Pyramiden. *Zeitschrift für Anorg. und Allg. Chemie.* **2005**, *631* (2–3), 587–591.

(14) Howie, R. A.; Moser, W.; Trevena, I. C. The Crystal Structure of Tin(II) Iodide. *Acta Crystallogr. Sect. B Struct. Crystallogr. Cryst. Chem.* **1972**, *28* (10), 2965–2971.

(15) Dickinson, R. G. THE CRYSTAL STRUCTURE OF TIN TETRA-IODIDE. *J. Am. Chem. Soc.* **1923**, *45* (4), 958–962.

(16) Kwong, F. Y.; Lai, C. W.; Yu, M.; Chan, K. S. Application of Palladium-Catalyzed Pd–aryl/P–aryl Exchanges: Preparation of Functionalized Aryl Phosphines by Phosphination of Aryl Bromides Using Triarylphosphines. *Tetrahedron.* **2004**, *60* (26), 5635–5645.

(17) Kornath, A.; Neumann, F.; Oberhammer, H. Tetramethylphosphonium Fluoride: "Naked" Fluoride and Phosphorane. *Inorg. Chem.* **2003**, *42* (9), 2894–2901.

(18) Burford, N.; Ragogna, P. J.; McDonald, R.; Ferguson, M. J. Homoatomic P - P Coordination: A Versatile Synthetic Approach to Polyphosphorus Dications. *Chem. Commun.* **2003**, No. 16, 2066.

(19) Jia, Y.-X.; Yang, X.-Y.; Tay, W. S.; Li, Y.; Pullarkat, S. A.; Xu, K.; Hirao, H.; Leung, P.-H. Computational and Carbon-13 NMR Studies of Pt–C Bonds in P–C–P Pincer Complexes. *Dalt. Trans.* **2016**, *45* (5), 2095–2101.

(20) Krudy, G. A.; Macomber, R. S. Phosphorus Coupling in ^{13}C and ^{1}H NMR. *J. Chem. Educ.* **1979**, *56* (2), 109.

(21) Kaltzoglou, A.; Stoumpos, C. C.; Kontos, A. G.; Manolis, G. K.; Papadopoulos, K.; Papadokostaki, K. G.; Psycharis, V.; Tang, C. C.; Jung, Y.-K.; Walsh, A.; et al. Trimethylsulfonium Lead Triiodide: An Air-Stable Hybrid Halide Perovskite. *Inorg. Chem.* **2017**, *56* (11), 6302–6309.

(22) Herrmann, F.; Kuhn, N. Ein Einfacher Zugang Zu Tetramethylphosphoniumiodid A Simple Access to Tetramethylphosphonium Iodide. *Z. Naturforsch.* **2012**, *67*, 853–854.

(23) Pavia, D. L.; Lampman, G. M.; Kriz, G. S.; Vyvyan, J. R. Introduction to Spectroscopy, 5th ed.; Cengage Learning: Stamford, CT, **2015**.

(24) Gonzalez-Carrero, S.; Schmidt, L. C.; Rosa-Pardo, I.; Martínez-Sarti, L.; Sessolo, M.; Galian, R. E.; Pérez-Prieto, J. Colloids of Naked $CH_3NH_3PbBr_3$ Perovskite

Nanoparticles: Synthesis, Stability, and Thin Solid Film Deposition. *ACS Omega*. **2018**, *3* (1), 1298–1303.

(25) Luo, B.; Pu, Y.-C.; Lindley, S. A.; Yang, Y.; Lu, L.; Li, Y.; Li, X.; Zhang, J. Z. Organolead Halide Perovskite Nanocrystals: Branched Capping Ligands Control Crystal Size and Stability. *Angew. Chemie Int. Ed.* **2016**, *55* (31), 8864–8868.

(26) Schmidt, L. C.; Pertegás, A.; González-Carrero, S.; Malinkiewicz, O.; Agouram, S.; Mínguez Espallargas, G.; Bolink, H. J.; Galian, R. E.; Pérez-Prieto, J. Nontemplate Synthesis of $CH_3NH_3PbBr_3$ Perovskite Nanoparticles. *J. Am. Chem. Soc.* **2014**, *136* (3), 850–853.

(27) Jeon, N. J.; Noh, J. H.; Yang, W. S.; Kim, Y. C.; Ryu, S.; Seo, J.; Seok, S. Il. Compositional Engineering of Perovskite Materials for High-Performance Solar Cells. *Nature*. **2015**, *517* (7535), 476–480.

(28) Li, C.; Lu, X.; Ding, W.; Feng, L.; Gao, Y.; Guo, Z. Formability of ABX_3 (X = F, Cl, Br, I) Halide Perovskites. *Acta Crystallogr. Sect. B Struct. Sci.* **2008**, *64* (6), 702–707.

(29) Henderson, W. Main Group Chemistry, 3rd ed.; Abel, E. W., Ed.; The Royal Society of Chemistry: Cambridge, **2000**.

(30) Maughan, A. E.; Kurzman, J. A.; Neilson, J. R. Hybrid Inorganic–Organic Materials with an Optoelectronically Active Aromatic Cation: $(C_7H_7)_2SnI_6$ and $C_7H_7PbI_3$. *Inorg. Chem.* **2015**, *54* (1), 370–378.

(31) Apostolico, L.; Kociok-Köhn, G.; Molloy, K. C.; Blackman, C. S.; Carmalt, C. J.; Parkin, I. P. The Reaction of Tin(IV) Iodide with Phosphines: Formation of New Halotin Anions. *Dalt. Trans.* **2009**, No. 47, 10486.

(32) Lode, C.; Krautscheid, H. Schwache Sn…I-Wechselwirkungen in Den Kristallstrukturen Der Iodostannate $[SnI_4]^{2-}$ Und $[SnI_3]^-$. *Zeitschrift für Anorg. und Allg. Chemie*. **2000**, *626* (2), 326–331.

(33) Wirth, A.; Moers, O.; Blaschette, A.; Jones, P. G. Die Ersten Röntgenstrukturen Kationischer Diorganylzinn(IV)-Dichelate $[R_2Sn(L\text{-}L)_2]_2$ Mit Zweizähnigen Phosphanoxid-Liganden: Di(Methansulfonyl)amid Als Nichtkoordinierendes Gegenion. *Zeitschrift für Anorg. und Allg. Chemie*. **1999**, *625* (6), 982–988.

(34) APEX II. Bruker AXS Inc. APEX II. Bruker AXS Inc.: Madison, WI p Madison, WI, 2012.

(35) SADABS. Bruker AXS Inc. SADABS. Bruker AXS Inc.: Madison, WI p Madison, WI, 2008.

(36) Sheldrick, G. M. A Short History of SHELX. *Acta Crystallogr. A.* **2008**, *64* (Pt 1), 112–122.

(37) Farrugia, L. J. WinGX Suite for Small-Molecule Single-Crystal Crystallography. *J. Appl. Crystallogr.* **1999**, *32* (4), 837–838.

(38) Dolomanov, O. V.; Bourhis, L. J.; Gildea, R. J.; Howard, J. A. K.; Puschmann, H. OLEX2 : A Complete Structure Solution, Refinement and Analysis Program. *J. Appl. Crystallogr.* **2009**, *42* (2), 339–341.

(39) Spek, A. L. Single-Crystal Structure Validation with the Program PLATON. *J. Appl. Crystallogr.* **2003**, *36* (1), 7–13.

CHAPTER 5: Phosphonium-Templated Halogermanates

5.1 Introduction

The discovery of lead- and tin-based perovskites prompted the investigation of germanium-based perovskites. $CsGeX_3$ perovskites, where X = Cl, Br, or I, demonstrated nonlinear optical properties as well as the capacity to be photovoltaic absorbers.[1,2] Furthermore, these perovskites have similar bandgaps to their lead counterparts.[3] The advent of germanium-containing inorganic/organic hybrid perovskites came when Stoumpos et al.[4] synthesized a family in which the 'A' cation consisted of alkylammonium cations of various sizes. The properties of these species showed a dependence on cation size. Smaller alkylammonium cations produced a 3D perovskite framework, while larger cations produced infinite 1D chains.[4] Furthermore, the smaller cations showed direct bandgaps and larger cations showed indirect bandgaps.[4] Given these interesting properties exhibited by the alkylammonium germanium perovskites, this chapter investigates the species created when germanium(II) and germanium(IV) halides are combined with alkyl- and arylphosphonium halide salts. Kociok-Köhn et al.[5] have reported a distorted perovskite structure of the formula $[HPMe_3][GeC1_3]$, which serves as encouragement that the germanium halides could form perovskitic structures with a phosphonium as the central 'A' cation. This chapter presents the reactions of six phosphoniums with germanium(II) halides and the crystal structures of two of the products. It also discusses the reactions of four phosphoniums with germanium(IV) iodide and three of their crystal structures.

5.2 Results & Discussion

5.2.1 Reactions with Germanium(II) Halides

Trimethylphosphonium Triiodogermanate

Since germanium(II) iodide was used to synthesize cesium[1] and alkylammonium-based perovskites[4] with important optical properties, it follows that it was the first germanium halide reacted with phosphonium salts for this thesis. Furthermore, given that Kociok-Kohn inadvertently created a perovskite containing trimethylphosphonium as the central 'A' cation,[5] it seemed prudent to react trimethylphosphonium iodide with germanium(II) iodide first. The two starting materials were combined in acetonitrile, producing a bright orange solution. After 12h stirring the reaction solution turned pale yellow, indicating that a new product had been formed. The pale-yellow solution was set up for recrystallization and orange crystals suitable for X-Ray diffraction grew from acetonitrile.

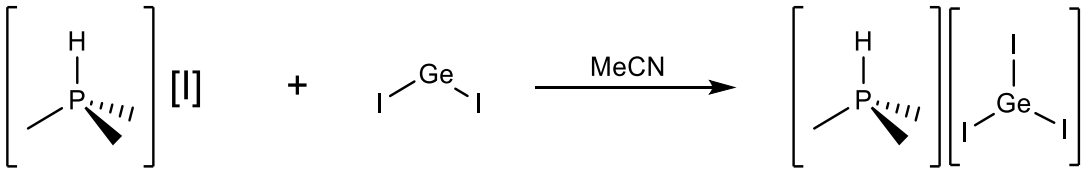

Scheme 5.1: Reaction of $[HPMe_3][I]$ with GeI_2.

To examine the product in solution, $^{31}P\{^1H\}$, ^1H, and $^{13}C\{^1H\}$ NMR spectroscopy on the orange crystals was carried out. The $^{31}P\{^1H\}$ NMR showed a singlet at -0.98 ppm, which is in good agreement with the starting material made in this thesis (2.09 ppm) and the literature shift reported by Bellachioma et al.[6] This preliminary spectrum suggests that the trimethylphosphonium ion persists in the product. The ^1H NMR spectrum displays a

doublet of doublets at 1.80 ppm and a doublet of decets at 6.15 ppm, which is also similar to the shifts observed in the starting material. The doublet of doublets is due to the methyl protons coupling to phosphorus and the lone proton, while the doublet of decets is a result of the lone proton coupling to phosphorus and the nine methyl protons. The values of the coupling constants are close to those reported for trimethylphosphonium iodide, similarly suggesting that the phosphonium ion is present in the product mixture. $^{13}C\{^{1}H\}$ provided further evidence for the phosphonium in solution, as the spectrum showed only one environment; a doublet due to the methyl carbons coupling to phosphorus. Once again, the chemical shift (4.64 *cf.* 5.75 ppm) and one-bond coupling constant (55.4 *cf.* 55.6Hz) agree well with the chemical shifts reported for the starting material.

Single crystal X-Ray diffraction of the orange crystals obtained from the reaction mixture confirmed that the phosphonium ion does indeed persist in the final product. It also revealed the formation of a $[GeI_3]$ anion, which is charge-balanced with the phosphonium cation. Thus, this compound was characterized as trimethylphosphonium triiodogermanate. The asymmetric unit is depicted in Figure 5.1, and the atomic labels in this figure will be used in the following discussion. The bond lengths and angles of the trimethylphosphonium cation were compared to the same species in Kociok-Kohn's work.[5] It was found that the average P-C bond length in this structure was within the estimated standard deviation of Kociok-Kohn's trimethylphosphonium cation (1.759(13) *cf.* 1.769(3)Å).[5] Furthermore, the P5-H5 bond length was found to be 1.4(1)Å, which is crystallographically similar to the value reported by Kociok-Kohn[5] of 1.28(3)Å. The average C-P-C bond angles of trimethylphosphonium triiodogermanate, 111.5(8)˚ are slightly larger than those of the trichlorogermanate analogue,[5] which average at

110.55(16)˚. The ESDs of this metrical parameter in both compounds barely overlap each other, suggesting that the C-P-C angle in trimethylphosphonium triiodogermanate is indeed larger.

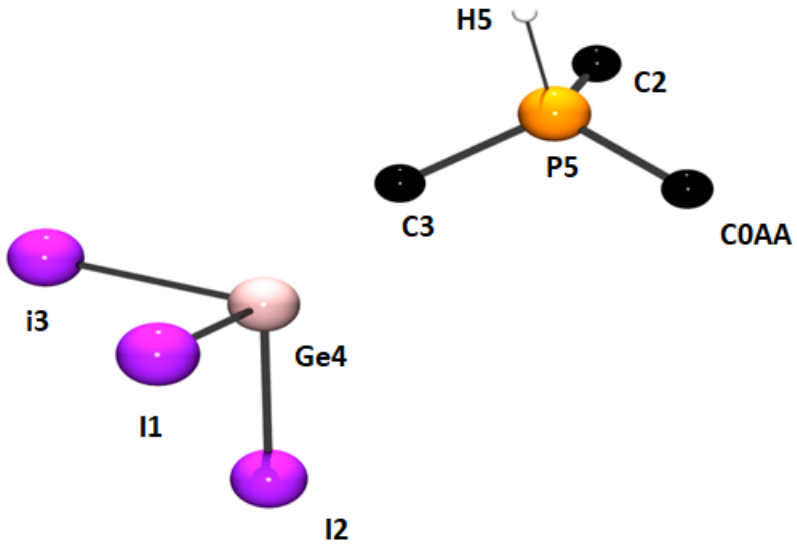

Figure 5.1: Crystal structure (ball and stick) of $[HPMe_3][GeI_3]$. The orange balls represent phosphorus, the black balls represent carbon, the pink balls represent germanium, and the purple balls represent iodine. Hydrogen atoms not bound to phosphorus are omitted for clarity.

The $[GeI_3]$ anion was compared to two different literature sources, one being a perovskite reported by Stoumpos et al.,[4] whose asymmetric unit contained trimethylammonium and the same anion. The other instance of this anion in the literature occurred in the reaction of germanium(II) iodide with an imidazolium salt, which was reported by Bartlett et al.[7] The average Ge-I bond length in $[HPMe_3][GeI_3]$ was found to be 2.8345(10)Å, which is larger than that reported by Stoumpos et al.[4] (2.7526(8)Å) and Bartlett et al.[7] (2.775(5)Å). The average of the I-Ge-I angles for the compound reported in this thesis is 95.37(3), which is less than that of the perovskite reported by Stoumpos et al.[4] at 96.60(5)˚. These differences in bond lengths and angles between trimethylphosphonium

triiodogermanate and the perovskite could be due to the difference in crystal packing between the two compounds. Although the asymmetric unit of the species reported in this thesis matches the ABX_3 general formula, it does not adopt the corner-sharing octahedra and twelve-fold coordination sphere characteristic of a perovskite.[8] Rather, it forms columns of trimethylphosphonium charge-balanced with an adjacent triiodogermanate. The $[GeI_3]$ ions alternate their orientation in the crystal in the direction perpendicular to (100) as shown in Figure 5.2. Interestingly $[HPMe_3][GeI_3]$ crystallizes in the $P2_12_12_1$ orthorhombic space group, which is the same as that of $[EMIM][GeI_3]$ reported by Bartlett et al.,[7] where EMIM = 1-ethyl-3-methylimidazolium.

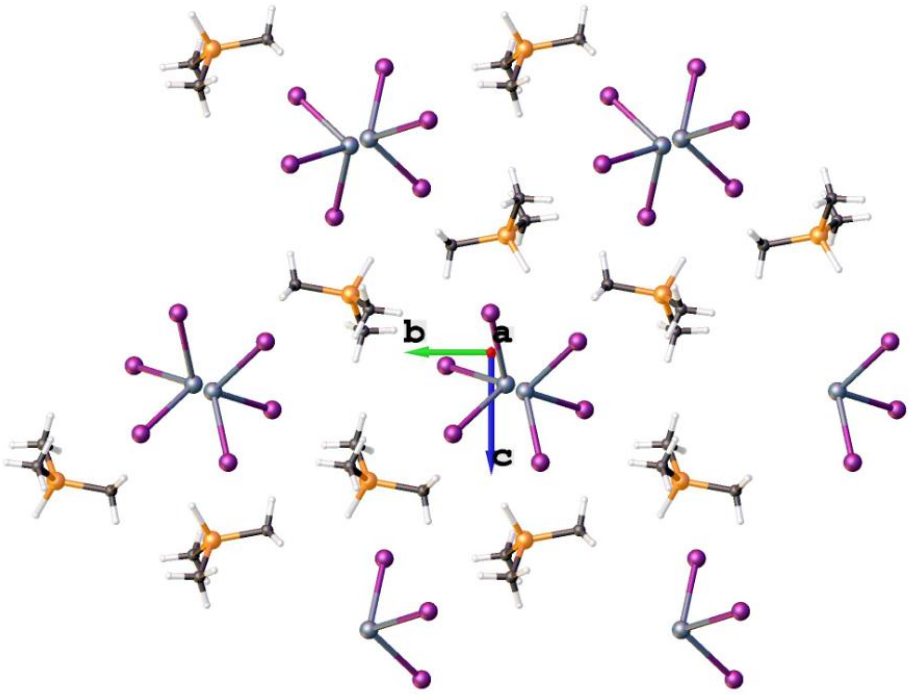

Figure 5.2: Unit cell contents of $[HPMe_3][GeI_3]$ normal to (100). The orange balls represent phosphorus, the black balls represent carbon, the white balls represent hydrogen, the silver balls represent germanium, and the purple balls represent iodine.

Although $[HPMe_3][GeI_3]$ does not have a perovskitic structure, its crystallographic similarity to $[EMIM][GeI_3]$ suggests that it could possess interesting properties. Cyclic

voltammetry experiments performed by Bartlett et al.[7] showed that germanium(II) compounds that contained iodide as a co-ligand with a non-coordinating cation are good candidates for electrodeposition. Trimethylphosphonium triiodogermanate fits these criteria, suggesting a possible electrochemical application for this material. Furthermore, the colour of this compound suggests that it could be a wide-bandgap semiconductor like the inorganic/organic hybrid materials reported by Stoumpos et al.[4] Therefore, UV-Visible studies on this material are necessary to evaluate its potential semiconducting properties.

Other Reactions with GeI_2

The results of the reaction between trimethylphosphonium iodide prompted the reaction of other phosphonium iodides with GeI_2. Tetramethylphosphonium iodide and GeI_2 were combined in a vial and dissolved in MeCN. The solution turned bright orange upon dissolution in MeCN, suggesting that a reaction had taken place in solution. After two days of stirring, the solution appeared darker orange and was set up for recrystallization via slow evaporation. The material recovered from this attempted recrystallization did not yield any crystals suitable for X-Ray diffraction, thus it was analyzed by NMR spectroscopy to observe the phosphorus, proton, and carbon environments in solution. The NMR spectra of the various nuclei showed a large resemblance to that of $[PMe_4][I]$, which suggests that the phosphonium ion endures in the product. The $^{31}P\{^1H\}$ NMR shows a singlet at 25.51 ppm, showing that there is only one phosphorus environment in solution. The similarity of this shift to the shift for $[PMe_4]$ reported by Herrmann et al.[9] (25.51 *cf.* 22.8 ppm) suggests that the $[PMe_4]$ cation is present in the product.

The ^1H and $^{13}C\{^1H\}$ NMR spectra of this product also closely resemble that of $[PMe_4][I]$. The ^1H NMR shows that the methyl protons resonate as a doublet at 1.81 ppm

due to coupling to phosphorus, with the two-bond coupling constant being 14.7Hz. In comparison, the same doublet in the $[PMe_4][I]$ spectrum reported by Herrmann et al.[9] resonated at 1.93 ppm with a coupling constant of 15Hz. Lastly, a doublet in the $^{13}C\{^1H\}$ NMR spectrum that represents the methyl carbons resonated at 9.33 ppm with a calculated carbon-phosphorus one-bond coupling constant of 72.6Hz. The $[PMe_4][I]$ $^{13}C\{^1H\}$ shift reported by Herrmann et al.[9] was similar (9.2 ppm), however the one-bond coupling constant was slightly less at 56Hz. This could be due to a difference in solvent since CD_3CN was used in this thesis instead of D_2O, which was used as the NMR solvent in the starting material. It is not uncommon to see a $^1J_{PC}$ as large as 72.6Hz, however, as there have been P-C couplings reported upwards of 88Hz.[10] Since the other shifts and coupling constants matched closely with the literature, it is reasonable to conclude that the cation in the product is $[PMe_4]$. Further studies of this compound are necessary, and recrystallization attempts from both acetonitrile and DCM are currently underway.

Germanium(II) iodide was also reacted with an aryl-monophosphonium, $[PMePh_3][I]$. NMR studies similar to the one discussed above were carried out since no crystals suitable for X-Ray diffraction were obtained for this reaction. For the reaction of $[PMePh_3][I]$ with GeI_2, the reactants were combined in a vial and a solid-state reaction was observed upon their combination. The pale yellow GeI_2 and white phosphonium solids turned garnet red at their interfaces. When acetonitrile was added to the vial, an orange solution was formed. After 3h of stirring the orange colour persisted and the solution was set up for recrystallization. The solid orange material left in the vial after all the acetonitrile had evaporated was analyzed via NMR spectroscopy, which showed that the phosphonium environment in the product solution is similar to that of methyltriphenylphosphonium

iodide. The $^{31}P\{^{1}H\}$, ^{1}H, and $^{13}C\{^{1}H\}$ NMR spectra were very similar to that of the literature,[11,12] which suggests that the phosphonium ion persists in solution. The different ^{13}C NMR environments are depicted in Figure 5.3, and the results of the NMR spectrum are summarized in Table 5.1.

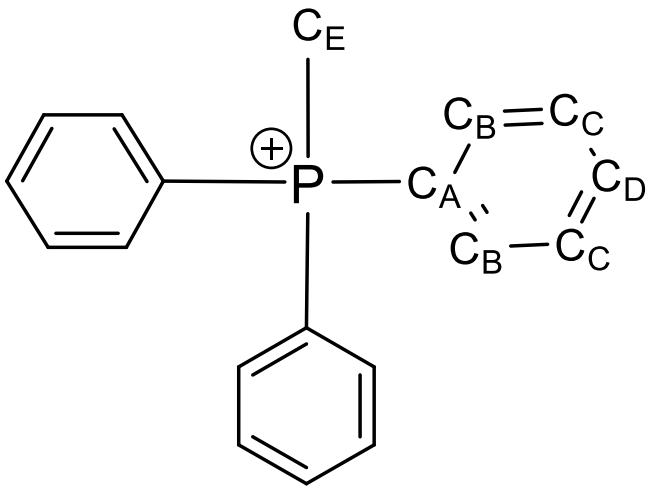

Figure 5.3: ^{13}C NMR Environments in $[PMePh_3][I]$.

Table 5.1 Summary of the $^{13}C\{^{1}H\}$ NMR Spectrum of the Reaction of $[PMePh_3][I]$ with GeI_2

Environment	Chemical Shift (ppm)	Multiplicity	Coupling Constant (Hz)
A	119.04	D	$^{1}J_{PC}$= 89
B	133.54	D	$^{2}J_{PC}$= 10.8
C	130.75	D	$^{3}J_{PC}$= 12.9
D	135.64	D	$^{4}J_{PC}$= 2.9
E	11.36	D	$^{1}J_{PC}$= 58

Tetramethylphosphonium Tribromogermanate

Given that perovskites have been obtained from the group 14 bromides,[2,13–17] the next reaction included germanium(II) bromide and tetramethylphosphonium bromide. The reactants were combined in a vial and dissolved in DCM, producing a pale pink solution.

After 16h of stirring, the solution was colourless and was set up for recrystallization via slow evaporation. Colourless crystals were obtained when all of the DCM had evaporated and these were analyzed by NMR spectroscopy.

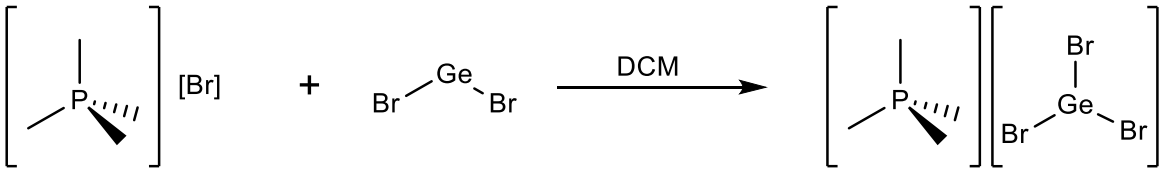

Scheme 5.2: Reaction of $[PMe_4][I]$ with $GeBr_2$.

As previously stated in this thesis, NMR spectroscopy only offers a glimpse into the structure of a compound in solution. The three different nuclei used, ^{31}P, ^{1}H, and ^{13}C, only occur in the phosphonium salt, therefore the only conclusions that can be drawn are whether or not the phosphonium cation is present in the product mixture. A $^{31}P\{^{1}H\}$ NMR experiment of the colourless crystals obtained from this reaction revealed that the $[PMe_4]$ cation is in the product due to a lone singlet in the spectrum at 24.6 3 ppm. This is much like the shift for $[PMe_4]$ reported by Herrmann et al.[9] and Kornath et al.[18], suggesting that this cation persists in the product. ^{1}H NMR and $^{13}C\{^{1}H\}$ NMR provide similar evidence for the phosphonium in the product solution. These results give good insight as to what the phosphonium environment is in the product, however they do not give a clue about the structure of the anion.

As shown previously, single crystal X-Ray crystallography is an excellent tool for chemists to determine exactly what the structure of a product is in the solid state. As mentioned before, the metrical parameters of bond length and bond angles and their comparison to other similar structures in the literature can give insight into the geometry

of the synthesized compound. In this particular reaction, X-Ray crystallography showed that the product created was tetramethylphosphonium triboromogermanante, $[PMe_4][GeBr_3]$, whose asymmetric unit is depicted in Figure 5.4. This compound, like $[HPMe_3][GeI_3]$, has the ABX_3 formula like other perovskites, however it does not adopt a corner-sharing octahedral crystal structure characteristic of the other germanium perovskites. Rather, the ions pack in columns in an alternating fashion, as shown in Figure 5.5 and Figure 5.6.

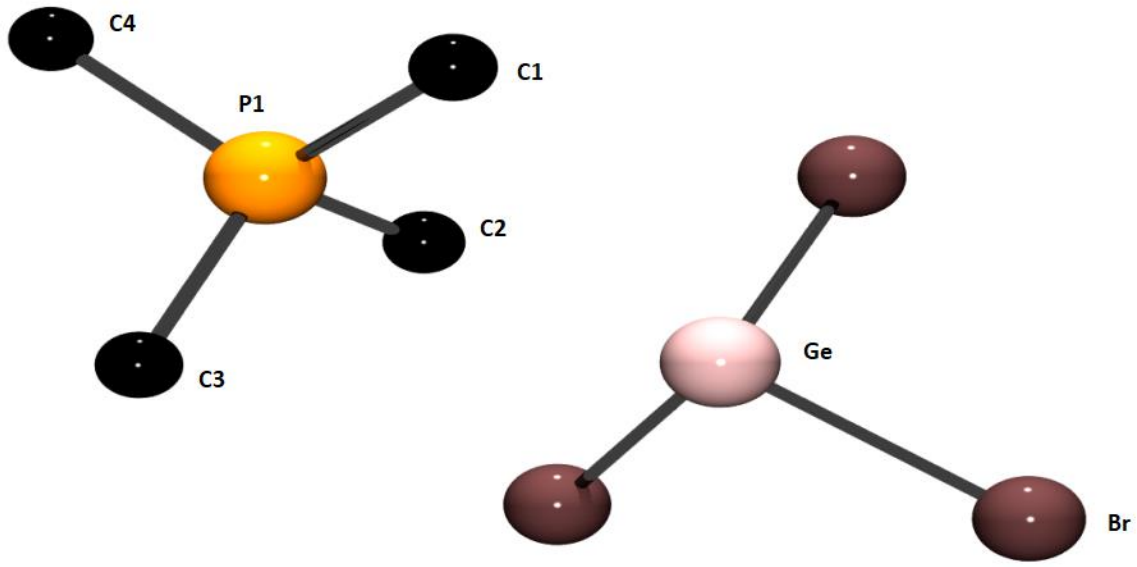

Figure 5.4: Crystal structure (ball and stick) of $[PMe_4][GeBr_3]$. The orange balls represent phosphorus, the black balls represent carbon, the pink balls represent germanium, and the brown balls represent bromine. Hydrogen atoms are omitted for clarity.

The bond lengths and angles of $[PMe_4][GeBr_3]$ were compared to literature structures. The $[PMe_4]$ cation, which has been previously reported multiple times, was related to the $[PMe_4]$ cation in $[PMe_4][F]$,[18] and the values were found to match closely with that of the literature. The ESDs of the literature and thesis metrical parameters overlap, suggesting that the $[PMe_4]$ cation adopts a tetrahedral geometry like that of $[PMe_4][F]$.

The [$GeBr_3$] anion was compared to literature structures containing the same species. Ruthe et al.[19] worked with bromotrialkylphosphonium tribromogermanates, while Bandyopadhyay et al.[20] synthesized a crown ether complex of germanium(II) bromide. The Ge-Br bond lengths in these two structures were averaged and compared with the Ge-Br bond length in [PMe_4][$GeBr_3$]. Since the [$GeBr_3$] ion is symmetry-generated, there is only one Ge-Br bond length present in this structure, 2.4681(8)Å. This bond distance is shorter than the bond distances reported for the triboromogermanate made by Ruthe et al.[19] (2.506(1)Å) and Bandyopadhyay et al.[20] (2.472Å). The Br-Ge-Br bond angle in [PMe_4][$GeBr_3$] is also greater than the averages of the comparable literature structures (96.10(3)˚ *cf.* 95.10˚, 95.69(4)˚).[19,20] Although the bond lengths and angles of these structures are similar, they cannot be classified as crystallographically indistinguishable. The difference in the metrical parameters between the [$GeBr_3$] species could be due to the corresponding cation since each of the cations vary in the compounds discussed.

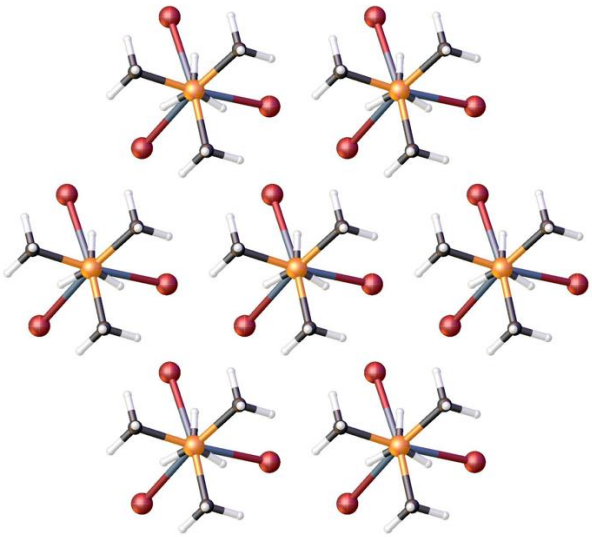

Figure 5.5: Unit cell contents of [PMe_4][$GeBr_3$] normal to (001). The orange balls represent phosphorus, the black balls represent carbon, the white balls represent hydrogen, the silver balls represent germanium, and the red balls represent bromine.

This new compound adds to the understanding of how phosphonium salts and germanium(II) halides interact with each other. In contrast to $[HPMe_3][GeI_3]$, this compound is colourless and packs with the anions all facing the same way. This difference in packing could be due to the size of the phosphonium cation used or, more likely, due to the different halide. The colour of the final product may also be due to the difference in halogen used. Further studies are required on this material to discover potential applications for $[PMe_4][GeBr_3]$. Although it is unlikely that this compound can behave as a light absorber since it is colourless, UV-Vis experiments should be conducted to see if any electronic transitions occur. In addition to this, cyclic voltammetry (CV) analysis conducted by Bartlett et al.[7] found that materials containing $[GeBr_3]$ could have electrochemical applications. Thus, it would be useful to perform CV on $[PMe_4][GeBr_3]$ as well.

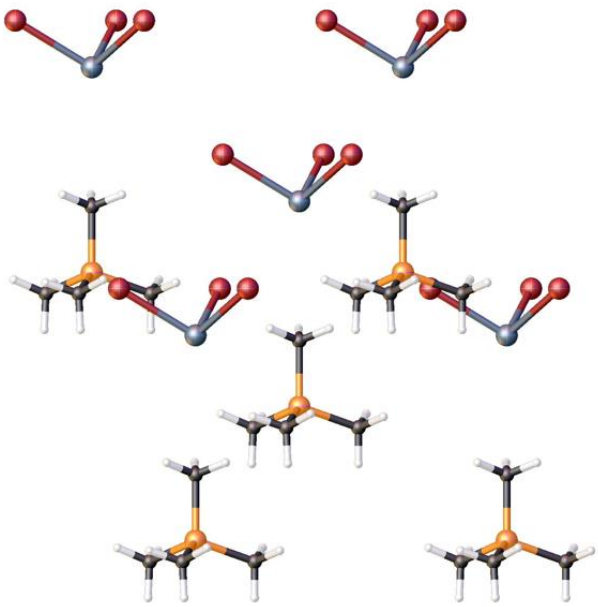

Figure 5.6: Unit cell contents of $[PMe_4][GeBr_3]$ normal to (001). The orange balls represent phosphorus, the black balls represent carbon, the white balls represent hydrogen, the silver balls represent germanium, and the red balls represent bromine.

Other Reactions with $GeBr_2$

Germanium(II) bromide was also reacted with tetraphenylphosphonium bromide to see how the difference in cation might impact the structure of the product. The reactants were combined in DCM according to Scheme 5.3, producing a colourless solution with a white precipitate. The mixture was left to stir for 16h, after which time it was centrifuged to separate the precipitate from the solution. The mother liquor was set up for recrystallization via slow evaporation, granting a white crystalline solid that was analyzed by NMR.

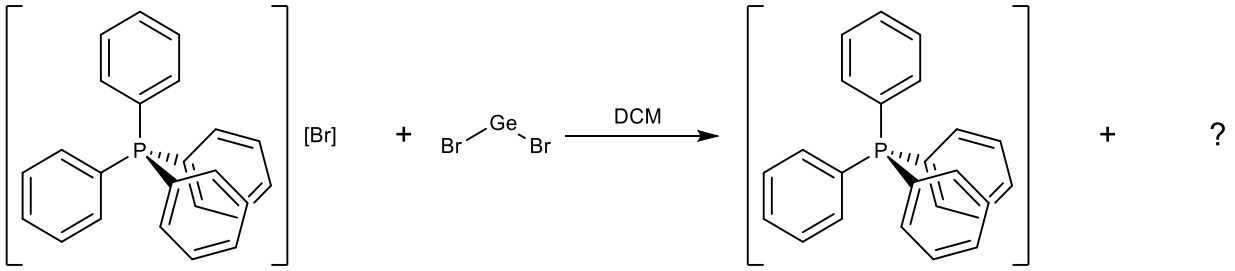

Scheme 5.3: The reaction of $[PPh_4][Br]$ with $GeBr_2$.

The $^{31}P\{^1H\}$, ^1H, and $^{13}C\{^1H\}$ NMR spectra provided insight on the behaviour of the phosphonium cation in solution. A singlet at 23.48 ppm in the $^{31}P\{^1H\}$ NMR supported the presence of the $[PPh_4]$ ion in the mother liquor, as the literature shift for this ion is 24 ppm.[21] The ^1H and $^{13}C\{^1H\}$ NMR are also indicative of this ion, as the spectra match closely to that of the literature.[22] Three proton environments, representing the *ortho-*, *meta*, and *para-* protons, were observed in the aromatic region of the NMR spectrum[23] and their shifts, multiplicities and coupling constants are summarized in Table 5.2. Similarly, the $^{13}C\{^1H\}$ NMR spectrum was close to that of the literature in both chemical shift and

coupling constants. A summary of the carbon-13 environments observed can be found in Table 5.3.

Table 5.2: A Summary of the ^{1}H NMR Spectrum of $[PPh_4][Br] + GeBr_2$

^{1}H Environment	Chemical Shift (ppm)	Multiplicity	Integration	Coupling Constants
Ortho	7.69	Dt	8H	$^{3}J_{PH}$= 8Hz $^{3}J_{HH}$= 1.5Hz
Meta	7.75	Td	8H	$^{3}J_{HH\text{-}ortho}$= 8Hz $^{3}J_{HH\text{-}para}$= 4Hz
Para	7.92	T	4H	$^{3}J_{HH}$= 7.5Hz

Table 5.3: A Summary of the $^{13}C\{^{1}H\}$ NMR Spectrum of $[PPh_4][Br] + GeBr_2$

^{13}C Environment	Chemical Shift (ppm)	Multiplicity	Coupling Constants
Ipso	118.78	D	$^{1}J_{PC}$= 89.8Hz
Meta	131.18	D	$^{3}J_{PC}$= 12.9Hz
Ortho	135.56	D	$^{2}J_{PC}$= 10.2Hz
Para	136.24	D	$^{4}J_{PC}$= 2.8Hz

NMR spectroscopy of the product showed that the phosphonium cation was present, however it cannot tell what the anion is in solution. It is possible that the solid isolated is recrystallized starting material, and further studies are required to determine whether or not this is the case. X-Ray crystallography, bromine-NMR, and elemental analysis would provide absolute information on the structure of the material obtained.

5.2.2 Reactions with Germanium(IV) Iodide

Tetramethylphosphonium iodide

The reactions of phosphonium salts with germanium(II) iodide prompted the analogous reactions with germanium(IV) iodide. The first phosphonium up for reaction

with Ge(IV) was tetramethylphosphonium iodide, which was used previously in reaction with lead and tin halides. The phosphonium salt was combined in a vial with GeI_4 and dissolved in acetonitrile. The white and orange solids formed a deep red solution when combined, suggesting that a reaction had taken place. This solution paled in colour after 16h of stirring and was set up for recrystallization. Although no crystals suitable for XRD were obtained, a dark red solid left after the evaporation of MeCN was analyzed via NMR.

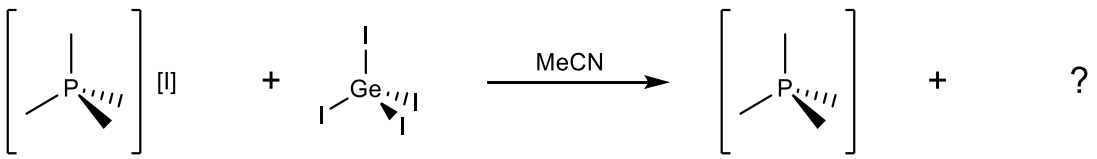

Scheme 5.4: Reaction of $[PMe_4][I]$ with GeI_4.

As stated previously, for the reactions for which no crystals are obtained, NMR can only determine whether or not the phosphonium ion is present in the product mixture; it cannot give any insight into the structure of the anion. The spectra obtained were compared to the literature spectra for $[PMe_4][I]$ reported by Herrmann et al.[9] The $^{31}P\{^1H\}$ showed a single peak in the spectrum at 24.22 ppm, which is a characteristic peak for the $[PMe_4]$ cation. Also, the absence of other peaks in the spectrum and the colour change upon addition of MeCN suggests that the reaction went to completion and no side products were obtained. ^1H NMR offered further confirmation that tetramethylphosphonium is in the product due to a doublet appearing in the methyl proton region of the spectrum at 2.07 ppm. The doublet splitting pattern for this proton environment is observed due to coupling to phosphorus. The calculated two-bond coupling constant was 14Hz, which closely matches the literature coupling constant of 15Hz.[9] The final clue that the $[PMe_4]$ ion persisted in the product solution came in the $^{13}C\{^1H\}$ NMR spectrum. A doublet at 11.62

ppm falls within the expected range of shifts for methyl carbons. The splitting of the resonance into a doublet is due to the four methyl environments coupling to phosphorus which is one bond away. The one bond phosphorus-to-carbon coupling constant was found to be 56.2Hz, which is very similar to the literature value of 56Hz.[9]

The dark colour of the solid product material obtained is promising for its potential applications. UV-Vis experiments could shed light on its abilities as a light absorber and possible semiconductor. Also, to completely understand the structure of this material, XRD studies must be performed. Alternative methods of recrystallization such as using a different solvent and putting the solution in a freezer are currently underway.

Tetraphenylphosphonium iodide

Since arylphosphoniums produced different structural motifs in reactions with both lead(II) iodide and tin(IV) iodide, it was of interest to react an arylphosphonium with GeI_4 as well. Tetraphenylphosphonium iodide was added to a vial with germanium(IV) iodide and, interestingly, the white and orange solids starting materials produced a dark red solid at their interfaces, indicating that a reaction occurred in the solid state. The solids were dissolved in acetonitrile and the deep red solution was left to stir for 16h. After this time, a recrystallization of the red solution was prepared, eventually granting red crystals suitable for X-Ray diffraction.

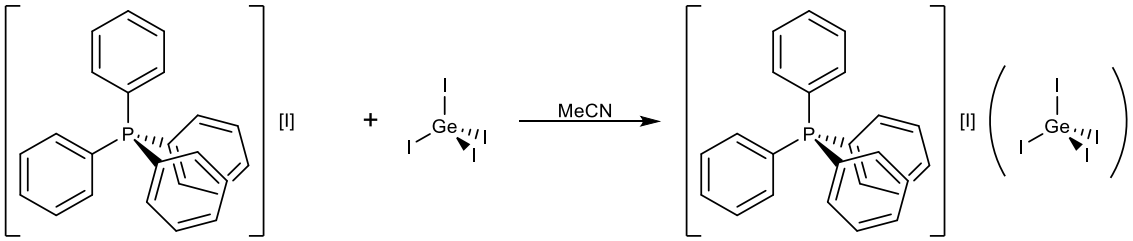

Scheme 5.5: Reaction of $[PPh_4][I]$ with GeI_4.

NMR studies on the red crystals revealed that the tetraphenylphosphonium ion persisted in the product solution. As a result, the $^{31}P\{^1H\}$, ^1H, and $^{13}C\{^1H\}$ spectra were very similar to that of the reaction of $[PPh_4][Br]$ with $GeBr_2$. The $^{31}P\{^1H\}$ NMR showed a singlet at 24.22 ppm, which is close to the literature value for $[PPh_4]$ at 24 ppm.[21] Resonances in the ^1H NMR spectrum of the product were also typical of the $[PPh_4]$ cation. A summary of the chemical shifts and coupling constants of the various proton environments for this compound can be found in Table 5.4. The $^{13}C\{^1H\}$ NMR was also similar to the spectrum obtained for the $[PPh_4]$ ion in the previous reactions. Each of the four different carbon environments, which are outlined in Table 5.5, appear as a doublet due to coupling to the phosphorus atom. All of the carbon-phosphorus coupling constants reported in Table 5.5 are within the acceptable literature range for this type of coupling.[10,18,21,22,24,25]

Table 5.4: A Summary of the ^1H NMR Spectrum of $[PPh_4][I](GeI_4)$

^1H Environment	Chemical Shift (ppm)	Multiplicity	Integration	Coupling Constants
Ortho	7.63	Dt	8H	$^3J_{PH}$= 6.5Hz $^3J_{HH}$= 5Hz
Meta	7.76	Td	8H	$^3J_{HH\text{-}ortho}$= 5Hz $^3J_{HH\text{-}para}$= 4Hz
Para	7.93	T	4H	$^3J_{HH}$= 5Hz

Table 5.5: A Summary of the $^{13}C\{^{1}H\}$ NMR Spectrum of $[PPh_4][I](GeI_4)$

^{13}C Environment	Chemical Shift (ppm)	Multiplicity	Coupling Constants
Ipso	117.89	D	$^{1}J_{PC}$= 89.7Hz
Meta	131.06	D	$^{3}J_{PC}$= 12.8Hz
Ortho	134.87	D	$^{2}J_{PC}$= 10.2Hz
Para	136.14	D	$^{4}J_{PC}$= 2.9Hz

Single-Crystal XRD of the red crystals indicated that $[PPh_4][I]$ and GeI_4 crystallized together, forming a cocrystal. A cocrystal is defined as two or more crystalline, solid, non-solvated compounds that occupy the same crystalline lattice.[26] The unit cell is depicted in Figure 5.7. The metrical parameters of the $[PPh_4]^+$ ion in tetraphenylphosphonium hexachlorogermanate bis(dichloromethane) solvate[27] are compared to the $[PPh_4]^+$ ion reported in this thesis. A co-crystallization of a similar nature with GeI_4 and tetraethylammonium iodide has been previously reported[28] and is used to draw a comparison between the two GeI_4 molecules. A summary of the key metrical parameters and their analogous literature values can be found in Table 5.6. All bond lengths and angles are named according to Figure 5.7.

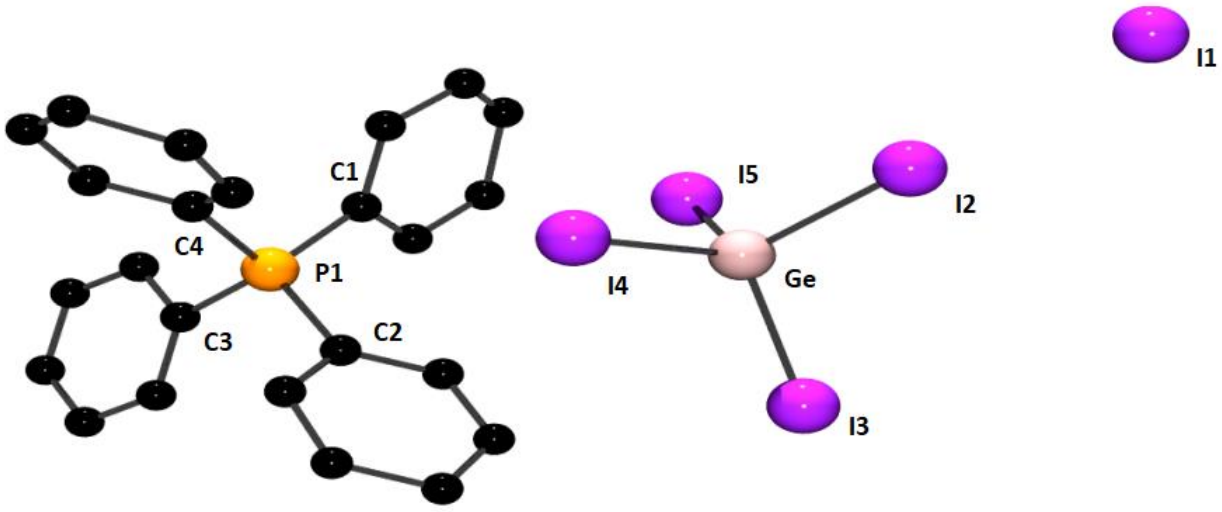

Figure 5.7: Crystal structure (ball and stick) of $[PPh_4][I](GeI_4)$. Hydrogen atoms are omitted for clarity.

The X-Ray Data showed that the $[PPh_4]$ ion persisted in the product in the solid state, as indicated by the solution NMR spectra. The bond distances and angles for $[PPh_4]$ in this product suggest that the cation adopts a tetrahedral geometry similar to that reported in the literature for this ion.[27] Moreover, the GeI_4 moiety in this crystal structure matches well with that of the literature, confirming a tetrahedral structure around the germanium(IV) centre. Similarly, average Ge-I bond distances and I-Ge-I angles for $[PPh_4][I](GeI_4)$ were calculated and compared to those of the GeI_4 molecule in a cocrystal with tetraethylammonium iodide.[28] The average Ge-I bond distance is 2.523(12)Å in the co-crystal with $[PPh_4][I]$ and 2.518(2)Å in the $[NEt_4][I]$ co-crystal. Furthermore, the average I-Ge-I angle in the structure reported in this thesis was found to be109.46(4) ˚, which indicates that the geometry of the GeI_4 molecule is tetrahedral in this co-crystal. The $[NEt_4][I](GeI_4)$ co-crystal shows the same geometry, as the average I-Ge-I bond is reported at 109.5(1)˚. Once again, the overlapping ESDs indicate the crystallographic similarity between the GeI_4 moieties in these two different systems.

Table 5.6: A Summary of the Key Metrical Parameters in $[PPh_4][I](GeI_4)$

Metrical Parameter	Value (Å/°)	Literature Value(Å/°)
P1-C	1.795(10)	1.794(3)[27]
C-P-C	109.5(4)	109.5(1)[27]
Ge-I	2.523(12)	2.518(2)[28]
I-Ge-I	109.46(4)	109.5(1)[28]
I1····I2	3.564	3.660(2)[28]
Ge-I2····I1	176.96	177.42[30] 174.4[28]

The nature of the crystal packing suggests a potential σ-hole interaction between the GeI_4 molecules and the iodide anions. Sigma-hole interactions typically occur between an atom from Group IV-VII that is covalently bonded and a site of negative charge.[31] This site of negative charge can be either be a Lewis base or an anion. Halogen bonds are a specific subset of σ-hole interactions that occur in halogenated systems. More specifically, a halogen bond is defined by IUPAC as "a net attractive interaction between an electrophilic region associated with a halogen atom in a molecular entity and a nucleophilic region in another, or the same, molecular entity".[32]

Halogen bonds are similar to the more well-known hydrogen bonds in that there exists an electron donor/acceptor relationship, however there is a difference in which species acts as the donor or acceptor.[33] In hydrogen bonding (H-bonds), the H-atom accepts electron density from an electron-rich species, whereas in halogen bonding (X-bonds) a halogen atom accepts electron density. This shortens the covalent bond between the X-bond donor and the halogen atom to within the sum of the Van der Waals radii and creates a region of electropositivity.[31,33,34] Halogen bonds also tend to be stronger than H-bonds and form at 180˚ angles.[31,33,34] A simplified halogen bonding interaction is depicted in Figure 5.8. 'A' represents the X-bond acceptor, which donates electron density, 'X'

denotes the halogen associated with the molecule in question, and 'D' represents the donor of the X-bond that accepts electron density from 'A'.[31]

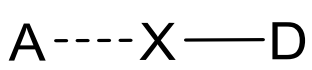

Figure 5.8: A Halogen Bond Interaction.[31]

In $[PPh_4][I](GeI_4)$, a halogen bond between Ge-I fragments of the GeI_4 molecule and the iodide anion is observed. Referring to Figure 5.7, the I1····I2 distance is 3.564Å, which is shorter than the sum of the Van der Waals radii for iodine, 3.96Å.[35] The I1····I2 distance in this structure is also shorter than the 3.660(2)Å distance reported for $[NEt_4][I](GeI_4)$,[28] suggesting that the X-bond in $[PPh_4][I](GeI_4)$ is stronger. The Ge-I2····I1 angle in the structure reported in this thesis is close to the ideal X-bond angle of 180˚at 176.96˚.[31,33,34] To compare, a structure reported by Ruthe et al.[30] as a CSD Private Communication that contained a similar X-bond interaction has a Ge-I····I angle of 177.42˚. This same angle in $[NEt_4][I](GeI_4)$ is 174.4˚.[28] Figure 5.9 shows the X-bonding in $[PPh_4][I](GeI_4)$. It is worthwhile to note that the Ge-I distance associated with the halogen bond is in good agreement with the average value, and this was also observed in $[NEt_4][I](GeI_4)$.[28]

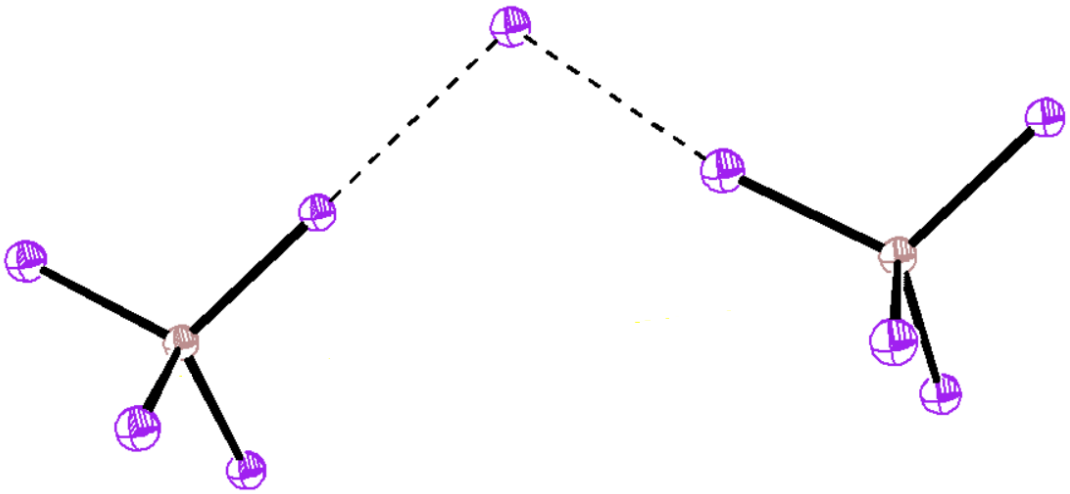

Figure 5.9: Halogen Bonding Interaction in $[PPh_4][I](GeI_4)$. The purple ellipsoids represent iodine and the pink ellipsoids represent germanium. The $[PPh_4]$ ions have been omitted for clarity.

Methyltriphenylphosphonium iodide

A similar structure to that of $[PPh_4][I](GeI_4)$ was isolated when an analogous reaction was carried out between methyltriphenylphosphonium iodide and germanium(IV) iodide. This reaction also began in the solid state, with the white phosphonium and orange GeI_4 forming a dark red species at the interface of the two reactants. This mixture was then dissolved in acetonitrile and left to stir for 16h, after which time a red solution persisted. The solution was set up for recrystallization via slow evaporation, yielding red crystals suitable for X-Ray diffraction after the MeCN had evaporated. NMR studies show that the methyltriphenylphosphonium ion persists in the product, as is the case for all of the previous germanium(II) and germanium(IV) halide reactions reported in this thesis.

Single-crystal XRD revealed that a co-crystal similar to the one formed with $[PPh_4][I]$ and GeI_4 was formed in this reaction as well. One key difference in this structure is that the asymmetric unit consists of two GeI_4 molecules as opposed to one as seen in

$[PPh_4][I](GeI_4)$. As a result, the chemical formula becomes $[PMePh_3][I](GeI_4)_2$. The bond lengths and angles of the $[PMePh_3]$ ion are compared to those of the same ion in bis(methyltriphenylphosphonium) tetraiodocadmate[36] and $[MePh_3P][BF_4]$.[37] The GeI_4 moieties are compared to the same species in $[NEt_4][I](GeI_4)$,[28] which was also used in the discussion of $[PPh_4][I](GeI_4)$. The atomic labels in Figure 5.10, which shows the asymmetric unit of $[PMePh_3][I](GeI_4)_2$, are used to refer to particular bond lengths and angles in the following discussion.

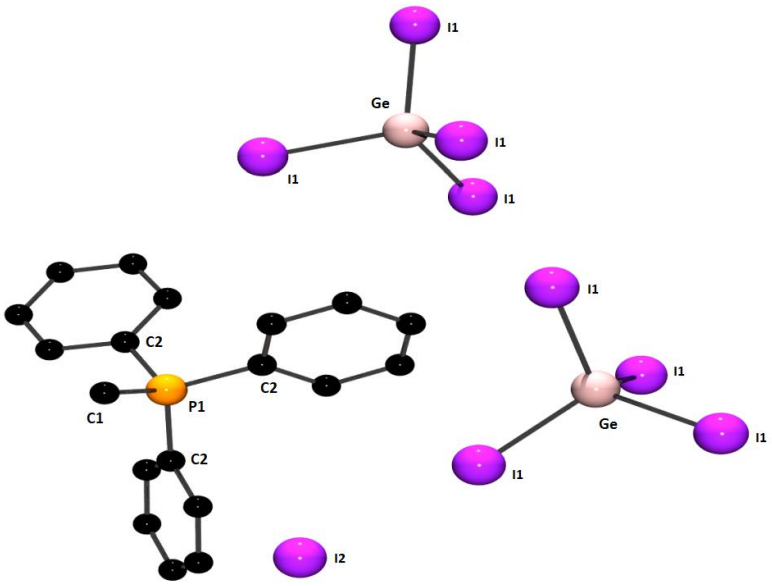

Figure 5.10: Crystal structure (ball and stick) of $[PMePh_3][I](GeI_4)_2$. The orange balls represent phosphorus, the black balls represent carbon, the pink balls represent germanium, and the purple balls represent iodine. Hydrogen atoms are omitted for clarity.

The P-C bonds and C-P-C bond angles indicate that $[PMePh_3]$ in this structure is similar to the $[PMePh_4]$ ions that have been previously reported.[36,37] The P1-C1 bond length was found to be 1.798(6)Å in this structure. Similar bond distances were observed in $[PMePh_3]_2[CdI_4]$[36] and $[PMePh_3][BF4]$,[37] their values being 1.83(3) and 1.791(4)Å, respectively. The P1-C2 distance, which is reported as an average of the phosphorus to

phenyl carbon bond distances, was found to be 1.792(6)Å. In $[PMePh_3][BF_4]$ this distance was found to be 1.780(5)Å,[37] whereas in the $[CdI_4]$ analogue the average distance was 1.77(2)Å.[36] Since the ESDs of $[PMePh_3][I](GeI_4)_2$ overlap with the ESDs reported for the same bond lengths in the literature, it is reasonable to conclude that the bond distances are crystallographically indistinguishable from each other. The average of the P-C angles in the phosphonium ion suggest a tetrahedral geometry around the phosphorus atom since the average (109.5(3)˚) meets the standard angle for a tetrahedral system according to VSEPR theory.[29] The two literature compounds[36,37] also meet this standard angle when ESDs are taken into account, suggesting that the $[PMePh_3]$ cation adopts tetrahedral geometry.

The GeI_4 molecule in this co-crystal adopts a nearly tetrahedral geometry, as the average I1-Ge-I1 angle was found to be 109.45(3)˚. As discussed previously, the literature value from $[NEt_4][I](GeI_4)$ for the average Ge-I bond is 109.5(1)˚. The overlap in estimated standard deviations suggest that both GeI_4 moieties have tetrahedral geometry around the germanium centre. The average of all of the Ge-I1 bonds in $[PMePh_3][I](GeI_4)_2$ is 2.5179(8)Å, which matches closely to the literature value of 2.518(2)Å.[28] Thus, the GeI_4 component of this co-crystal is much like that of the GeI_4 component in the $[NEt_4][I](GeI_4)$ co-crystal. Once again, the Ge-I distance associated with the σ-hole interaction is very similar to that of the average.

A closer look at the asymmetric unit of the $[PMePh_3][I](GeI_4)_2$ co-crystal suggests that a similar σ-hole type interaction could be occurring between the GeI_4 molecule and the iodide anion. This was observed in the $[PPh_4][I](GeI_4)$ crystal discussed above, as well as in the $[NEt_4][I](GeI_4)$[28] and $[HP(t\text{-}bu)_3][Ge_2I_9]$.[30] The I1···I2 distance was measured to be 3.537(2)Å, which is within the sum of the Van der Waals radii[35] for iodine and thus fits

the criteria for a halogen bond.[31,33,34] The Ge-I1···I2 angle is significantly less than the ideal 180˚ for a halogen bond at 173.23(2)˚. There have been X-bonds less than 180˚ reported in the past with some being as low as 169˚.[31] This can be attributed to other non-covalent interactions present in the compound as it is difficult to separate the effects of each individual type of interaction.[31]

Bis(trimethylphosphonio)ethane iodide

Given that crystals for the reaction of monophosphonium iodide salts with GeI_4 generated co-crystals, it was of interest to see what would occur if a diphosphonium salt were used. Bis(trimethylphosphonio)ethane iodide was combined with GeI_4 in a 1:2 molar ratio, producing a red solid before the solvent was introduced in a similar fashion to the previous reactions with GeI_4. When acetonitrile was added to the vial, a dark red solution was formed. This was left to stir for 16h before the product solution was set up for recrystallization by slow evaporation. Red crystals suitable for X-Ray diffraction were grown from this solution and these were examined by NMR spectroscopy.

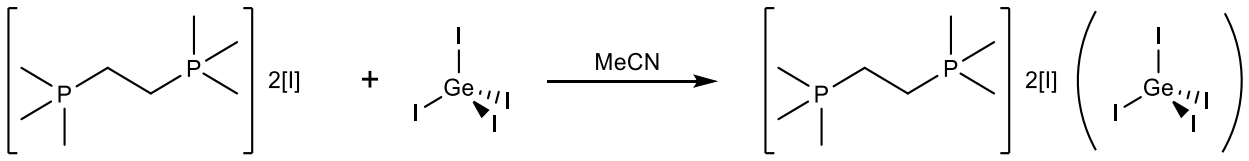

Scheme 5.6: Reaction of bis(trimethylphosphonio)ethane iodide with GeI_4.

The $^{31}P\{^1H\}$ NMR showed a singlet at 32.28 ppm, which is very similar to the chemical shift of the starting material. This shows that there is only one phosphorus environment in solution and it is representative of the bis(trimethylphosphonio)ethane ion. ^1H NMR further confirmed this assignment of the phosphorus peak to the phosphonium

ion. Two proton environments, one at 1.94 ppm that represents the methyl protons, and another at 2.58 ppm that represents the ethane bridge protons, were observed in the spectrum. Both environments resonated as doublets due to coupling to the phosphorus atom two bonds away. The coupling constants were calculated to be 18.3Hz for the methyl protons and 6.6 Hz for the ethane bridge protons. $^{13}C\{^{1}H\}$ NMR studies have yet to be done, however the ^{1}H and $^{31}P\{^{1}H\}$ NMR spectra give conclusive evidence that the diphosphonium cation exists in the product mixture.

Crystallographic examination of the product revealed that another co-crystal of a phosphonium with germanium(IV) iodide was indeed synthesized. The asymmetric unit consists of one diphosphonium cation, two iodide anions, and one GeI_4 molecule. As a result, the chemical formula of this co-crystal is $[C_8H_{22}P_2][I]_2(GeI_4)$. A diagram of the asymmetric unit is shown in Figure 5.11. It should be noted that the diphosphonium is shown as two monophosphonium fragments since the other half of the cation is symmetry-generated. To gain an understanding of the geometry of the diphosphonium ion in this crystal, a comparison will be drawn between it and a bis(dimethylphosphonio)ethane cation ($[C_6H_{18}P_2]$) reported by Davis et al.[38] The $[NEt_4][I](GeI_4)$ co-crystal that was previously used to relate to the GeI_4 moiety in this thesis will be used again to compare bond lengths and angles.

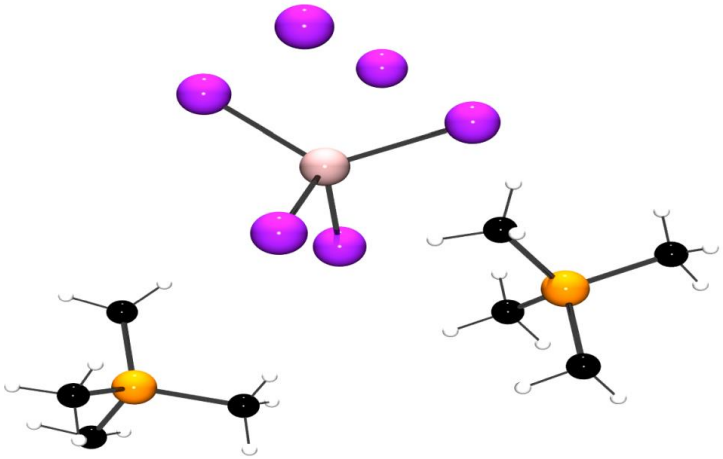

Figure 5.11: Crystal structure (ball and stick) of $[C_8H_{22}P_2][I]_2(GeI_4)$. The orange balls represent phosphorus, the black balls represent carbon, the white balls represent hydrogen, the pink balls represent germanium, and the purple balls represent iodine. The other half of each diphosphonium cation is symmetry-generated.

The diphosphonium in $[C_8H_{22}P_2][I]_2(GeI_4)$ contains similar bond lengths and angles to that of the diphosphonium in the literature,[38] which suggests that the substituents arrange tetrahedrally around the phosphonium centre in the $[C_8H_{22}P_2][I]_2(GeI_4)$ co-crystal. The GeI_4 moieties of $[C_8H_{22}P_2][I]_2(GeI_4)$ show great structural similarity to the same species in the $[NEt_4][I](GeI_4)$ co-crystal. The ESDs of the average Ge-I bond distances overlap almost completely (2.526(12)Å *cf.* 2.523(12)Å),[28] suggesting that this parameter in GeI_4 molecule of this co-crystal is crystallographically equal to that of the literature within statistical error. Upon examination of the individual Ge-I distances, it can be seen that the three Ge-I bonds within the GeI_4 molecule that are associated with the σ-hole are shorter than the Ge-I distance that is not associated with an X-bond interaction (2.5263(12), 2.5166(12), 2.5275(12)Å *cf.* 2.5366(12)Å).

In a comparison of the average I-Ge-I bond angles in $[C_8H_{22}P_2][I]_2(GeI_4)$ and $[NEt_4][I](GeI_4)$ it was found that the ESDs do not overlap, which indicates that the

geometry around GeI_4 is slightly different in both co-crystals. In $[C_8H_{22}P_2][I]_2(GeI_4)$, the average I-Ge-I angle is 109.24(4)˚, which is less than the standard angle for a tetrahedral geometry based on VSEPR theory.[29] To contrast, the same angle in the $[NEt_4][I](GeI_4)$ co-crystal is 109.5(1)˚, suggesting that the literature system adopts a tetrahedral geometry.[28] It is possible that the way in which the GeI_4 packs with the larger diphosphonium cation prevents it from having tetrahedral geometry or that the nature of the sigma hole donor-acceptor interactions has a marked effect on the geometry.

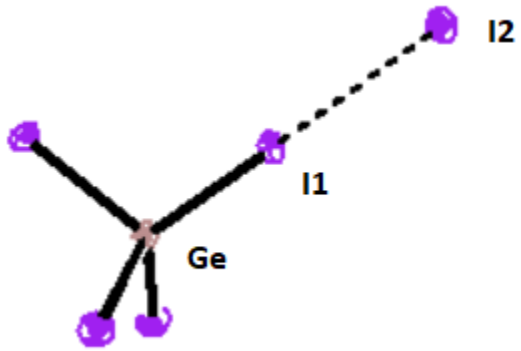

Figure 5.12: The Halogen Bonding Interaction in $[C_8H_{22}P_2][I]_2(GeI_4)$.

Despite the difference in I-Ge-I bond angle between the GeI_4 molecules in the structure reported here and the literature, the I1····I2 distances are very similar. In the $[C_8H_{22}P_2][I]_2(GeI_4)$, this distance was found to be 3.657(12)Å, whereas in the literature it was found to be 3.660(2)Å.[28] Both of these distances are within the sum of the Van der Waals radii for iodine,[35] suggesting a possible halogen bonding interaction. The Ge-I1····I2 angle for the $[C_8H_{22}P_2][I]_2(GeI_4)$ co-crystal, 171.61(3)˚, is less than the typical 180˚ for this type of interaction, however there have been halogen bonds reported that have had angles less than this.[31,33,34]

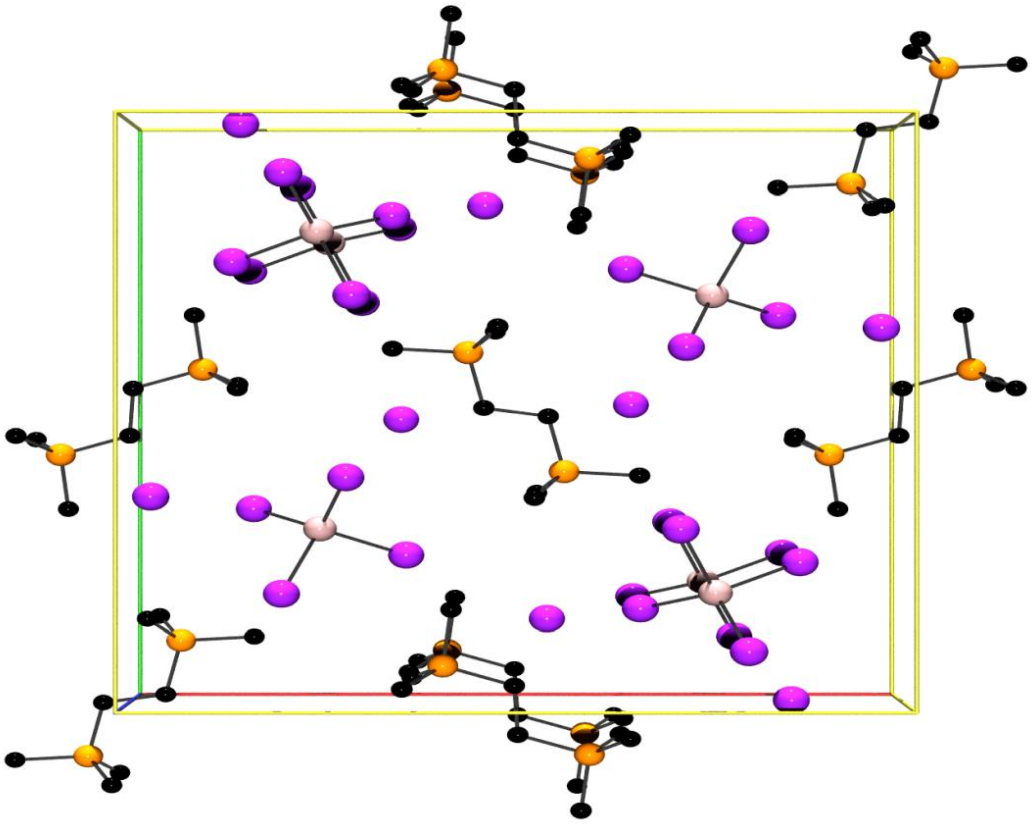

Figure 5.13: Unit cell contents of $[C_8H_{22}P_2][I]_2(GeI_4)$ normal to (001). The orange balls represent phosphorus, the black balls represent carbon, the pink balls represent germanium, and the purple balls represent iodine. Hydrogen atoms are omitted for clarity.

The three co-crystals synthesized by reaction of phosphonium salts with GeI_4 are compounds that certainly deserve further study. There are numerous techniques that have been used in the past to affirm the presence of halogen bonding. Microwave spectroscopy, IR spectroscopy, NQR, SSNMR, and UV-Vis have been used in the past to confirm a halogen bond interaction in different materials.[34] It would certainly be worthwhile to employ these techniques on the co-crystals of phosphoniums and GeI_4 to confirm that a halogen bond exists. In addition to this, computational studies can calculate an electrostatic potential map of this interaction. An area of electropositivity along the halogen bond would be a definitive indication of a σ-hole interaction.[31] Furthermore, since the crystalline

material appeared dark red, it would be beneficial to conduct UV-Vis studies to assess the band-gap of these materials and examine whether they could behave as semiconductors.

5.2.3 Chapter Conclusions

Multiple phosphonium iodide salts were reacted with germanium(II) and germanium(IV) halides, producing the phosphonium-templated halogermanate family. Although none of the synthesized compounds possess a perovskitic structure, their synthesis has increased the understanding of the reactivity between germanium halides and phosphonium salts. The phosphonium ion persists in the product for each of the reactions reported. For the reactions of germanium(II) iodide with $[HPMe_3][I]$ and germanium(II) bromide with $[PMe_4][Br]$, novel charge-balanced compounds of the general formula $[PR_4][GeX_3]$ were created. In the reactions of $[PPh_4][I]$, $[PMePh_3][I]$, and $[C_8H_{22}P_2][I]$ with GeI_4, a series of co-crystals that exhibit potential halogen bonding behaviour were synthesized. This family of compounds could act as semiconducting materials, however more studies are required to investigate this.

5.3 Experimental

General Procedures

All manipulations were carried out using standard inert atmosphere techniques. All chemicals and reagents were purchased from Sigma-Aldrich and used without further purification. Deuterated solvents were dried according to literature procedure when necessary, and all other solvents were dried over a series of Grubbs'-type columns and degassed prior to use. NMR spectra were recorded at room temperature on a Bruker Avance III 500 MHz, Bruker Avance Ultrashield 300 MHz or Bruker Avance DPX 300

MHz spectrometers. Chemical shifts are reported in ppm relative to internal standards for ^{1}H and ^{13}C (the given deuterated solvent) and the external standard for ^{31}P (85% H_3PO_4). Coupling constants |J| are given in Hz. Elemental Analysis was performed by the University of Windsor Mass Spectrometry Service Laboratory using Perkin Elmer 2400 combustion CHN analyzer.

X-Ray Crystallography

Crystals for investigation were covered in Paratone®, mounted into a goniometer head, and then rapidly cooled under a stream of cold N_2 of the low-temperature apparatus (Oxford Cryostream) attached to the diffractometer. The data were then collected using the APEXII software suite[39] on a Bruker Photon 100 CMOS diffractometer using a graphite monochromator with MoKα (λ = 0.71073 Å) or CuKα (λ = 1.54178 Å) radiation. For each sample, data were collected at low temperature. APEXII software was used for data reductions and SADABS[40] was used for absorption corrections (multi-scan; semi-empirical from equivalents). XPREP was used to determine the space group and the structures were solved and refined using the SHELX[41] software suite as implemented in the WinGX[42] or OLEX2[43] program suites. Validation of the structures was conducted using PLATON.[44]

5.3.1 Trimethylphosphonium triiodogermanate

50mg (0.25mmol) of trimethylphosphonium iodide was dissolved in acetonitrile as was 80mg (0.25mmol) of germanium (II) iodide in a separate vial. Under stirring, the GeI_2 was added to the phosphonium solution, which changed in colour from colourless to bright orange upon introduction of GeI_2. The mixture was left to stir for 12h, after which the solution had turned pale yellow. The solution was set up for recrystallization by slow

evaporation, granting orange crystals suitable for X-Ray diffraction. $^{31}P\{^{1}H\}$ NMR (CD_3CN, 121.5MHz) δ: -0.98 (s). ^{1}H NMR (CD_3CN, 300 MHz); δ: 1.80 (PC***H*****$_3$**, dd, 9H, $^{2}J_{PH}$ = 15.9Hz, $^{3}J_{HH}$ = 5.7Hz), 6.15(***H***P, ddec, $^{1}J_{PH}$=509Hz, $^{3}J_{HH}$= 5.4Hz). $^{13}C\{^{1}H\}$ NMR(CD_3CN, 75.5MHz): δ: 4.64 (P***C***H_3, d, $^{1}J_{PC}$=55.4Hz). EA calculated for $C_3H_{10}PGeI_3$•0.1 MeCN•0.1 tol: C, 8.61; H, 2.06; N 0.26%; found: C, 8.78; H 2.12; N, 0.17%.

5.3.2 Tetramethylphosphonium iodide + GeI_2

Tetramethylphosphonium iodide (50mg, 0.23mmol) and germanium (II) iodide (75mg, 0.23mmol) were placed in a 20mL scintillation vial and dissolved in MeCN under stirring. The reaction mixture immediately turned bright orange and the solution was left to stir for 48h. After this time, the solution turned a darker orange. $^{31}P\{^{1}H\}$ NMR (CD_3CN, 121.5MHz) δ: 25.51 (s). ^{1}H NMR (CD_3CN, 300 MHz); δ: 1.81 (PC***H*****$_3$**, d, 12H, $^{2}J_{PH}$ = 14.7Hz). $^{13}C\{^{1}H\}$ NMR (CD_3CN, 75.5MHz): δ: 9.33 (P***C***H_3, d, $^{1}J_{PC}$=72.6Hz). EA calculated for $C_4H_{12}PGeI_3$•0.5 MeCN: C, 10.63; H, 2.41; N 1.24%; found: C, 10.30; H 2.40; N, 0.04%.

5.3.3 Methyltriphenylphosphonium iodide + GeI_2

[$PMePh_3$][I] (50mg, 0.12mmol) and germanium (II) iodide (40mg, 0.12mmol) were placed in a 20mL scintillation vial and dissolved in acetonitrile. Prior to dissolution in acetonitrile, the white phosphonium powder and the pale yellow germanium iodide reacted in the solid state, showing a garnet colour. When the acetonitrile was added to the reactants under stirring, the solution turned orange. After 3h of stirring the colour of the solution persisted. $^{31}P\{^{1}H\}$ NMR (CD_2Cl_2, 202.46MHz) δ: 21.83(s). ^{1}H NMR (CD_2Cl_2, 500 MHz); δ: 3.03 (PC***H*****$_3$**, d, 3H, $^{2}J_{PH}$ = 13Hz), 7.67-7.86(***H*****-Ph**, m, 15H, unresolved coupling).

$^{13}C\{^{1}H\}$ NMR (CD_2Cl_2, 125.8MHz): δ: 11.36 (P***C***H_3, d, $^{1}J_{PC}$=58Hz), 119.04(***C*****$_{ipso}$**, d, $^{1}J_{PH}$= 89Hz), 130.75(***C*****$_{meta}$**, d, $^{3}J_{PC}$= 12.9Hz), 133.54(***C*****$_{ortho}$**, d, $^{2}J_{PC}$= 10.8Hz), 135.64(***C*****$_{para}$**, d, $^{4}J_{PC}$= 2.9Hz).

5.3.4 Tetramethylphosphonium tribromogermanate

50mg (0.29mmol) of tetramethylphosphonium bromide and germanium (II) bromide (68mg, 0.29mmol) were combined in a 20mL scintillation vial and dissolved in approx. 10mL of DCM. This produced a pale salmon-coloured solution. The mixture was left to stir for 16h, after which time the solution turned colourless. Colourless crystals suitable for X-Ray diffraction were harvested from this solution. $^{31}P\{^{1}H\}$ NMR (CD_3CN, 202.5MHz) δ: 24.63 (s). ^{1}H NMR (CD_3CN, 500 MHz); δ: 1.78 (PC***H*****$_3$**, d, 12H, $^{2}J_{PH}$ = 14.5Hz). $^{13}C\{^{1}H\}$ NMR (CD_3CN, 125.8MHz): δ: 9.88 (P***C***H_3, d, $^{1}J_{PC}$=54.4Hz).

5.3.5 Tetraphenylphosphonium bromide + $GeBr_2$

Tetraphenylphosphonium bromide (50mg, 0.12mmol) and germanium (II) bromide (28mg, 0.12mmol) were placed in a 20mL scintillation vial and dissolved in ca. 10mL of MeCN. This produced a colourless solution with a white precipitate. The mixture was left to stir for 16h and then centrifuged to separate the precipitate from the solution. The colourless mother liquor was analyzed. $^{31}P\{^{1}H\}$ NMR (CD_3CN, 202.5MHz) δ: 23.48 (s). ^{1}H NMR (CD_3CN, 500 MHz); δ: 7.69 (***H*****$_{ortho}$**-Ph, dt, 8H, $^{3}J_{PH}$ = 8Hz, $^{3}J_{HH}$ = 1.5Hz), 7.75 (***H*****$_{meta}$**- Ph, td, 8H, $^{3}J_{HH\text{-}ortho}$ = 8.5Hz, $^{3}J_{HH\text{-}para}$ = 4Hz), 7.92(***H*****$_{para}$** – Ph, t, 4H, $^{3}J_{HH}$ = 7.5Hz). $^{13}C\{^{1}H\}$ NMR (CD_3CN, 125.8MHz): δ: 118.78 (***C*****$_{ipso}$**, d, $^{1}J_{PC}$=89.8Hz), 131.18 (***C*****$_{meta}$**, d, $^{3}J_{PC}$ = 12.9Hz), 135.56(***C*****$_{ortho}$**, d, $^{2}J_{PC}$ = 10.2Hz), 136.24 (***C*****$_{para}$**, d, $^{4}J_{PC}$ = 2.8Hz).

5.3.6 Tetramethylphosphonium iodide + GeI_4

Tetramethylphosphonium iodide (50mg, 0.23mmol) was added to a 20mL scintillation vial containing 133mg (0.23mmol) germanium (IV) iodide and both reactants were dissolved in ca. 10mL of acetonitrile. Upon the addition of MeCN, the solution turned dark red and was left to stir for 16h. After this time, a lighter red solution was observed in the flask. $^{31}P\{^{1}H\}$ NMR (CD_2Cl_2, 202.5MHz) δ: 23.65(s). ^{1}H NMR (CD_2Cl_2, 500 MHz); δ: 2.07 (PC***H*****$_3$**, d, 12H, $^{2}J_{PH}$ = 14Hz). $^{13}C\{^{1}H\}$ NMR (CD_2Cl_2, 75.5MHz): δ: 11.62 (P***C***H_3, d, $^{1}J_{PC}$=56.2Hz).

5.3.7 Tetraphenylphosphonium iodide + GeI_4

Tetraphenylphosphonium iodide (50mg, 0.11mmol) and germanium (IV) iodide (62mg, 0.11mmol) were combined in a 20mL scintillation vial. Prior to dissolving these two species in ca. 10mL MeCN, the white and orange solids reacted in the solid state to form a red species. When the MeCN was added, a dark red solution formed. The reaction was left to stir for 16h, after which time the red solution was set up for recrystallization via slow evaporation. This granted red crystals suitable for X-Ray diffraction. $^{31}P\{^{1}H\}$ NMR (CD_2Cl_2, 202.5MHz) δ: 24.22 (s). ^{1}H NMR (CD_2Cl_2, 500 MHz); δ: 7.63 (***H*****$_{ortho}$**-Ph, dt, 8H, $^{3}J_{PH}$ = 6.5Hz, $^{3}J_{HH}$ = 1.5Hz), 7.76 (***H*****$_{meta}$**- Ph, td, 8H, $^{3}J_{HH\text{-}ortho}$ = 5Hz, $^{3}J_{HH\text{-}para}$ = 4Hz), 7.93(***H*****$_{para}$** – Ph, t, 4H, $^{3}J_{HH}$ = 5Hz). $^{13}C\{^{1}H\}$ NMR (CD_2Cl_2, 125.7MHz): δ: 117.89 (***C*****$_{ipso}$**, d, $^{1}J_{PC}$=89.7Hz), 131.06 (***C*****$_{meta}$**, d, $^{3}J_{PC}$ = 12.8Hz), 134.87 (***C*****$_{ortho}$**, d, $^{2}J_{PC}$ = 10.2Hz), 136.14 (***C*****$_{para}$**, d, $^{4}J_{PC}$ = 2.9Hz).

5.3.8 Methyltriphenylphosphonium iodide + GeI_4

Methyltriphenylphosphonium iodide (50mg, 0.12mmol) and GeI_4 (71mg, 0.12mmol) wetre combined in a 20mL scintillation vial. The white and orange solids

showed reaction in the solid state, as a red substance was observed shortly after combining the reactants. The species were dissolved in ca. 10mL of MeCN, producing a dark red solution. The reaction was left to stir for 16h, and the solution was set up for recrystallization by slow evaporation. Red crystals suitable for X-Ray diffraction were collected. $^{31}P\{^{1}H\}$ NMR (CD_2Cl_2, 202.5MHz) δ: 21.85(s). ^{1}H NMR (CD_2Cl_2, 500 MHz); δ: 2.99 (PC***H₃***, d, 3H, $^{2}J_{PH}$ = 13Hz), 7.66-7.73 (***H*** *ortho* ***& H*** *meta* ***- Ph,*** m, 12H, unresolved coupling), 7.86 (***H*** *para* ***-Ph***, t, 3H, 5Hz). $^{13}C\{^{1}H\}$ NMR (CD_2Cl_2, 125.7MHz): δ: 11.37 (P-***C***H_3, d, $^{1}J_{PC}$ = 58.1Hz), 118.99 (***C*** *ipso*, d, $^{1}J_{PC}$=88.9Hz), 130.85 (***C*** *meta*, d, $^{3}J_{PC}$ = 13Hz), 133.55 (***C*** *ortho*, d, $^{2}J_{PC}$ = 10.8Hz), 135.74 (***C*** *para*, d, $^{4}J_{PC}$ = 2.9Hz). EA calculated for $PC_{19}H_{18}I_9Ge_2$: C, 14.58; H, 1.16; N 0.00%; found: C, 15.05; H 1.19; N, 0.00%.

5.3.9 Bis(trimethylphosphonio)ethane iodide + GeI_4

Bis(trimethylphosphonio)ethane iodide (50mg, 0.12mmol) and germanium (IV) iodide (139mg, 0.24mmol) were placed in a 20mL scintillation vial. The white and orange powders showed some reaction in the solid state before solvent was introduced, producing a red solid. The reactants were dissolved in ca. 10mL of MeCN and left to react for 16h under stirring. After this time, a red solution was observed and set up for recrystallization via slow evaporation. Dark red crystals suitable for X-Ray diffraction were collected. $^{31}P\{^{1}H\}$ NMR (CD_2Cl_2, 202.5MHz) δ: 32.28(s). ^{1}H NMR (CD_3CN, 300 MHz); δ: 1.94 (PC***H₃***, d, 18H, $^{2}J_{PH}$ = 18.3Hz), 2.58(μ-(C***H₂***)$_2$, d, 4H, $^{2}J_{PH}$ = 6.6Hz).

5.4 References

(1) Tang, L.-C.; Chang, C.-S.; Tang, L.-C.; Huang, J. Y. Electronic Structure and Optical Properties of Rhombohedral $CsGeI_3$ Crystal. *J. Phys. Condens. Matter.* **2000**, *12* (43), 9129–9143.

(2) Tang, L. C.; Huang, J. Y.; Chang, C. S.; Lee, M. H.; Liu, L. Q. New Infrared Nonlinear Optical Crystal $CsGeBr_3$: Synthesis, Structure and Powder Second-Harmonic Generation Properties. *J. Phys. Condens. Matter.* **2005**, *17* (46), 7275–7286.

(3) Boix, P. P.; Agarwala, S.; Koh, T. M.; Mathews, N.; Mhaisalkar, S. G. Perovskite Solar Cells: Beyond Methylammonium Lead Iodide. *J. Phys. Chem. Lett*. **2015**, *6* (5), 898–907.

(4) Stoumpos, C. C.; Frazer, L.; Clark, D. J.; Kim, Y. S.; Rhim, S. H.; Freeman, A. J.; Ketterson, J. B.; Jang, J. I.; Kanatzidis, M. G. Hybrid Germanium Iodide Perovskite Semiconductors: Active Lone Pairs, Structural Distortions, Direct and Indirect Energy Gaps, and Strong Nonlinear Optical Properties. *J. Am. Chem. Soc*. **2015**, *137* (21), 6804–6819.

(5) Kociok-Köhn, G.; Winter, J. G.; Filippou, A. C. Trimethylphosphonium Trichlorogermanate(II). *Acta Crystallogr. Sect. C Cryst. Struct. Commun.* **1999**, *55* (3), 351–353.

(6) Bellachioma, G.; Cardaci, G.; Macchioni, A.; Venturi, C.; Zuccaccia, C. Reductive Elimination of Halogens Assisted by Phosphine Ligands in $Fe(CO)_4X_2$ (X=I,Br) Complexes. *J. Organomet. Chem.* **2006**, *691* (18), 3881–3888.

(7) Bartlett, P. N.; Cummings, C. Y.; Levason, W.; Pugh, D.; Reid, G. Halometallate Complexes of Germanium(II) and (IV): Probing the Role of Cation, Oxidation State and Halide on the Structural and Electrochemical Properties. *Chem. - A Eur. J.* **2014**, *20* (17), 5019–5027.

(8) Navrotsky, A. Energetics and Crystal Chemical Systematics among Ilmenite, Lithium Niobate, and Perovskite Structures. *Chem. Mater.* **1998**, *10* (10), 2787–2793.

(9) Herrmann, F.; Kuhn, N. Ein Einfacher Zugang Zu Tetramethylphosphoniumiodid A Simple Access to Tetramethylphosphonium Iodide. *Z. Naturforsch.* **2012**, *67*, 853–854.

(10) Burford, N.; Ragogna, P. J.; McDonald, R.; Ferguson, M. J. Homoatomic P - P Coordination: A Versatile Synthetic Approach to Polyphosphorus Dications. *Chem. Commun.* **2003**, No. 16, 2066.

(11) Lichtenberg, C.; Elfferding, M.; Sundermeyer, J. Unexpected Oxidative Dimerisations of a Cyclopentadienyl-Phosphane - Formation of Unprecedented, Structurally Remarkable Phosphacyclic Compounds. *Eur. J. Inorg. Chem.* **2010**, *2010* (20), 3117–3124.

(12) Sekhri, L.; Bebba, A. A.; Hassini, Z. Synthesis, Applications and Comparison of Some Phosphine Oxides and Their Salts with the Nitrogen Containing Compounds. *Asian J. Chem.* **2005**, *17* (4), 2455–2462.

(13) Butler, K. T.; Frost, J. M.; Walsh, A. Band Alignment of the Hybrid Halide Perovskites $CH_3NH_3PbCl_3$, $CH_3NH_3PbBr_3$ and $CH_3NH_3PbI_3$. *Mater. Horizons*. **2015**, *2* (2), 228–231.

(14) Gonzalez-Carrero, S.; Schmidt, L. C.; Rosa-Pardo, I.; Martínez-Sarti, L.; Sessolo, M.; Galian, R. E.; Pérez-Prieto, J. Colloids of Naked $CH_3NH_3PbBr_3$ Perovskite Nanoparticles: Synthesis, Stability, and Thin Solid Film Deposition. *ACS Omega.* **2018**, *3* (1), 1298–1303.

(15) Schmidt, L. C.; Pertegás, A.; González-Carrero, S.; Malinkiewicz, O.; Agouram, S.; Mínguez Espallargas, G.; Bolink, H. J.; Galian, R. E.; Pérez-Prieto, J. Nontemplate Synthesis of $CH_3NH_3PbBr_3$ Perovskite Nanoparticles. *J. Am. Chem. Soc.* **2014**, *136* (3), 850–853.

(16) Luo, B.; Pu, Y.-C.; Lindley, S. A.; Yang, Y.; Lu, L.; Li, Y.; Li, X.; Zhang, J. Z. Organolead Halide Perovskite Nanocrystals: Branched Capping Ligands Control Crystal Size and Stability. *Angew. Chemie Int. Ed.* **2016**, *55* (31), 8864–8868.

(17) Mosconi, E.; Amat, A.; Nazeeruddin, M. K.; Grätzel, M.; De Angelis, F. First-Principles Modeling of Mixed Halide Organometal Perovskites for Photovoltaic Applications. *J. Phys. Chem. C.* **2013**, *117* (27), 13902–13913.

(18) Kornath, A.; Neumann, F.; Oberhammer, H. Tetramethylphosphonium Fluoride: "Naked" Fluoride and Phosphorane. *Inorg. Chem.* **2003**, *42* (9), 2894–2901.

(19) Ruthe, F. 'Soft–soft' Halogen–halogen Interactions in Solid Ion Pairs of Solvent-Free Pri_3PCl_2 and CH_2Cl_2-Solvated Pri_3PBr_2: Structural Features of Chloro- and Bromo-Triisopropylphosphonium Salts. *Chem. Commun.* **1997**, *113* (20), 1947.

(20) Bandyopadhyay, R.; Nguyen, J. H.; Swidan, A.; Macdonald, C. L. B. Water and Ammonia Complexes of Germanium(II) Dications. *Angew. Chemie Int. Ed.* **2013**, *52* (12), 3469–3472.

(21) Kwong, F. Y.; Lai, C. W.; Yu, M.; Chan, K. S. Application of Palladium-Catalyzed Pd–aryl/P–aryl Exchanges: Preparation of Functionalized Aryl Phosphines by Phosphination of Aryl Bromides Using Triarylphosphines. *Tetrahedron.* **2004**, *60* (26), 5635–5645.

(22) Krudy, G. A.; Macomber, R. S. Phosphorus Coupling in ^{13}C and ^{1}H NMR. *J. Chem. Educ.* **1979**, *56* (2), 109.

(23) Pavia, D. L.; Lampman, G. M.; Kriz, G. S.; Vyvyan, J. R. Introduction to Spectroscopy, 5th ed.; Cengage Learning: Stamford, CT, **2015**.

(24) Jia, Y.-X.; Yang, X.-Y.; Tay, W. S.; Li, Y.; Pullarkat, S. A.; Xu, K.; Hirao, H.; Leung, P.-H. Computational and Carbon-13 NMR Studies of Pt–C Bonds in P–C–P Pincer Complexes. *Dalt. Trans.* **2016**, *45* (5), 2095–2101.

(25) Bartlett, P. N.; Burt, J.; Hasan, M. M.; Hector, A. L.; Levason, W.; Reid, G.; Richardson, P. W. Haloplumbate Salts as Reagents for the Non-Aqueous Electrodeposition of Lead. *RSC Adv.* **2016**, *6* (77), 73323–73330.

(26) Aitipamula, S.; Banerjee, R.; Bansal, A. K.; Biradha, K.; Cheney, M. L.; Choudhury, A. R.; Desiraju, G. R.; Dikundwar, A. G.; Dubey, R.; Duggirala, N.; et al. Polymorphs, Salts, and Cocrystals: What's in a Name? *Cryst. Growth Des.* **2012**, *12* (5), 2147–2152.

(27) Gruber, H.; Müller, U. Crystal Structure of Tetraphenylphosphonium Hexachlorogermanate Bis(Dichloromethane) Solvate, $(P(C_6H_5)_4)_2GeCl_6$ $2CH_2Cl_2$. *Zeitschrift für Krist. - New Cryst. Struct.* 1997, *212* (JG), 497–498.

(28) Müller, U.; Krug, V. Tetraethylammoniumiodid–Germaniumtetraiodid (1/2), Eine Struktur Mit Einem von Acht Iodatomen Koordinierten Iodidion. *Acta Crystallogr. Sect. C Cryst. Struct. Commun.* **1990**, *46* (4), 523–525.

(29) Tro, N. J. Chemistry: A Molecular Approach, 2nd ed.; Folchetti, N., Ed.; Pearson Education, Inc.: Upper Saddle River, **2011**.

(30) Jones, P. G.; Ruthe, F. Experimental Crystal Structure Determination. *CSD Private Communication*, **2014**.

(31) Politzer, P.; Murray, J. S.; Clark, T. Halogen Bonding and Other σ-Hole Interactions: A Perspective. *Phys. Chem. Chem. Phys.* **2013**, *15* (27), 11178.

(32) Desiraju, G. R.; Ho, P. S.; Kloo, L.; Legon, A. C.; Marquardt, R.; Metrangolo, P.; Politzer, P.; Resnati, G.; Rissanen, K. Definition of the Halogen Bond (IUPAC Recommendations 2013). *Pure Appl. Chem.* **2013**, *85* (8), 1711–1713.

(33) Metrangolo, P.; Resnati, G. Halogen Bonding: A Paradigm in Supramolecular Chemistry. *Chem. - A Eur. J.* **2001**, *7* (12), 2511–2519.

(34) Cavallo, G.; Metrangolo, P.; Milani, R.; Pilati, T.; Priimagi, A.; Resnati, G.; Terraneo, G. The Halogen Bond. *Chem. Rev.* **2016**, *116* (4), 2478–2601.

(35) Batsanov, S. S. Van Der Waals Radii of Elements. *Inorg. Mater.* **2001**, *37* (9), 871–885.

(36) Couldwell, C.; Prout, K. Bis(Methyltriphenylphosphonium) Tetraiodocadmate. *Acta Crystallogr. Sect. B Struct. Crystallogr. Cryst. Chem.* **1978**, *34* (7), 2312–2313.

(37) Blachnik, R.; Reuter, H.; Wiest, T.; Eickmeier, H. Crystal Structures and DSC Investigations of Trimethylphenylammonium Perchlorate, Trimethyl-Phenylammonium Tetrafluoroborate, Methyltriphenyl-Phosphonium Perchlorate, and Methyltriphenyl-Phosphonium Tetrafluoroborate, $[Me_3PhN][ClO_4]$, $[Me_3PhN][BF_4]$, $[MePh_3]$. *Zeitschrift für Krist. - Cryst. Mater.* **2000**, *215* (1).

(38) Davis, M. F.; Levason, W.; Reid, G.; Webster, M. Complexes of Germanium(Iv) Fluoride with Phosphane Ligands: Structural and Spectroscopic Authentication of Germanium(Iv) Phosphane Complexes. *Dalt. Trans.* **2008**, No. 17, 2261.

(39) APEX II. Bruker AXS Inc. APEX II. Bruker AXS Inc.: Madison, WI p Madison, WI, 2012.

(40) SADABS. Bruker AXS Inc. SADABS. Bruker AXS Inc.: Madison, WI p Madison, WI, 2008.

(41) Sheldrick, G. M. A Short History of SHELX. *Acta Crystallogr. A.* **2008**, *64* (Pt 1), 112–122.

(42) Farrugia, L. J. WinGX Suite for Small-Molecule Single-Crystal Crystallography. *J. Appl. Crystallogr.* **1999**, *32* (4), 837–838.

(43) Dolomanov, O. V.; Bourhis, L. J.; Gildea, R. J.; Howard, J. A. K.; Puschmann, H. OLEX2 : A Complete Structure Solution, Refinement and Analysis Program. *J. Appl. Crystallogr.* **2009**, *42* (2), 339–341.

(44) Spek, A. L. Single-Crystal Structure Validation with the Program PLATON. *J. Appl. Crystallogr.* **2003**, *36* (1), 7–13.

CHAPTER 6: Conclusions & Future Work

6.1 Conclusions

This thesis has outlined and discussed the findings of research into the reactivity of phosphonium salts with group 14 halides towards synthesizing phosphonium-templated inorganic-organic hybrid perovskites. Inorganic-organic hybrid perovskite materials have lately been of great interest due to their semiconducting and light-harvesting abilities.[1–5] Since only one phosphonium-containing perovskite had been synthesized thus far,[6] this research sought to add to the library of these type perovskite materials.

Ten new phosphonium iodide salts were synthesized with the intention of using them as precursors for the phosphonium-containing perovskites. Although some of the phosphonium salts have been accessed before,[7–11] the phosphonium salts made in this work were synthesized in a novel manner via protonation and methylation of various organic mono- and diphosphines in toluene. Their structures were confirmed by NMR spectroscopy. Trimethylphosphonium iodide, tetramethylphosphonium iodide, and [(Diphenylphosphino)methyl]methyldiphenylphosphonium iodide were crystallographically characterized. The new mono- and diphosphonium salts were synthesized in good yield.

The novel phosphonium salts were first reacted with lead (II) iodide, targeting a phosphonium-based lead perovskite. Although a perovskite structure was not observed, this work has demonstrated that phosphonium-templated iodoplumbates may be synthesized via direct addition of a phosphonium salt to lead(II) iodide in solution. Four

phosphonium-templated iodoplumbate materials have been crystallographically characterized, revealing an extended face-sharing octahedral network of anionic lead iodide fragments charge-balanced with a phosphonium cation. Through UV-Visible spectroscopy and thermogravimetric analysis it was shown that these compounds are wide-bandgap semiconductors that exhibit remarkable thermal stability.

Reactions of tin(II) and tin(IV) halides with phosphonium salts do not produce perovskitic structures, however three novel crystal structures of phosphonium-templated iodostannates were characterized. The reaction between trimethylphosphonium iodide and tin(II) iodide produced an iodotin trianion of the chemical formula $[SnI_5]^{3-}$, which adopts a trigonal pyramidal geometry. An unplanned oxidation of the phosphine starting material in the reaction of $[HPMe_3][I]$ with SnI_4 created a new salt, $[(O{=}PMe_3)_3SnI_3]_2[SnI_6]$, whose cation displays Lewis acidic properties. Furthermore, a reaction of $[PMePh_3][I]$ with tin(IV) iodide produced a salt with the phosphonium cation and a $[SnI_5]^-$ anion. The three anions elucidated by X-Ray crystallography have precedence in previous structures,[12–17] however the cation-anion combination in each of these species has not been reported before.

Germanium(II) and germanium(IV) halides were the last of the group 14 halides reacted with phosphonium salts as part of this research. For the reactions of germanium(II) iodide with $[HPMe_3][I]$ and germanium(II) bromide with $[PMe_4][Br]$, novel charge-balanced compounds of the general formula $[A][GeX_3]$ were created and crystallographically characterized. The trihalogermanate anions in both of these species have precedence in perovskite materials[4] and in other organic-inorganic hybrid

materials.[18–20] In the reactions of $[PPh_4][I]$, $[PMePh_3][I]$, and $[C_8H_{22}P_2][I]$ with GeI_4, a series of co-crystals that exhibit potential halogen bonding behaviour were synthesized.

6.2 Future Work

The research presented in this dissertation strengthens the understanding of the behaviour of phosphonium salts with group 14 halides, however it is far from complete. Most of the products discussed need further characterization to fully understand their potential applications. Many of the reactions done in this thesis only show persistence of the phosphonium ion in the NMR spectrum of the product and there is no elucidation of the anion without crystallographic data. Other methods such as ^{207}Pb, ^{119}Sn, and ^{73}Ge NMR could be used to determine the oxidation state and coordination geometry of the anion. Furthermore, mass spectrometry and infrared spectroscopy could be used. UV-Visible spectroscopy and TGA studies were carried out for the iodoplumbate species but not for the iodostannates or iodogermanates. These experiments are key in understanding the potential semiconducting abilities of a material. Furthermore, the electronic structure of all the materials presented in this thesis can be determined via synchrotron radiation. Patwardhan et al.[21] have demonstrated that a solar cell can be fabricated and the photovoltage of the cell can be measured quite easily. This would be the next test for the phosphonium-templated iodoplumbate materials and an eventual test for the iodostannates and iodogermanates if they are classified as semiconductors by UV-Vis. Lastly, even though ten new phosphonium salts were made for reactions with group 14 halides, not all of them had the opportunity to be reacted as part of the research presented in this thesis. It would be worthwhile to perform these reactions to discover what kind of compounds they may make.

The perovskite materials have generated a lot of interest due to their tunability.[22] The general formula for perovskites (ABX_3)[23] has three different components that can be changed up. Choosing different 'A' site cations could prove useful to creating novel perovskitic materials. The recent discovery of $(CH_3)_3SPbI_3$ as an alternative to ammonium cations[1] has opened the door for chalcogen-templated semiconducting materials. This perovskite does not undergo hydrolysis in ambient air like ammonium cations do and its bandgap is similar to that of the phosphonium-templated iodoplumbates reported in this dissertation. The sulfonium-based perovskite suggests that oxonium, selenonium, or telluronium-based perovskites should be considered.

To continue to build the phosphonium-templated materials family towards making perovskites, the 'B' and 'X' components of this formula can be tuned. The 'B' site cation can be substituted as demonstrated by the Kanatzidis group[2,4,24] and the research presented in this thesis. Bismuth-based perovskites where group I metals such as rubidium and cesium have acted as the 'A' site cations have shown similar optoelectronic performance to the lead-halide perovskites.[25] It would be beneficial to explore whether or not a phosphonium-templated bismuth perovskite could be synthesized, as it would be the first perovskite in which both the 'A' and 'B' cations contain group 15 elements. Finally, the 'X' component of the perovskite structure can be tuned to created novel phosphonium-based perovskites using different phosphonium halide salts. Following Kociok-Kohn's[6] discovery of trimethylphosphonium tricholorgermanate(II), which demonstrated a distorted perovskite structure, it would make most sense to explore the reaction of phosphonium chlorides with group 14 chlorides in future studies. Furthermore, Noh et al.[26] demonstrated that the bandgap of the $MAPbI_3$ was lowered with gradual incorporation of

bromine at the ‘X’ site. Given this result, it would be useful to investigate the effect on the electronic properties of these materials if a mix of halogens were used in the phosphonium-based hybrids.

6.3 References

(1) Kaltzoglou, A.; Stoumpos, C. C.; Kontos, A. G.; Manolis, G. K.; Papadopoulos, K.; Papadokostaki, K. G.; Psycharis, V.; Tang, C. C.; Jung, Y.-K.; Walsh, A.; et al. Trimethylsulfonium Lead Triiodide: An Air-Stable Hybrid Halide Perovskite. *Inorg. Chem.* **2017**, *56* (11), 6302–6309.

(2) Chung, I.; Lee, B.; He, J.; Chang, R. P. H.; Kanatzidis, M. G. All-Solid-State Dye-Sensitized Solar Cells with High Efficiency. *Nature* **2012**, *485* (7399), 486–489.

(3) Hao, F.; Stoumpos, C. C.; Chang, R. P. H.; Kanatzidis, M. G. Anomalous Band Gap Behavior in Mixed Sn and Pb Perovskites Enables Broadening of Absorption Spectrum in Solar Cells. *J. Am. Chem. Soc.* **2014**, *136* (22), 8094–8099.

(4) Stoumpos, C. C.; Frazer, L.; Clark, D. J.; Kim, Y. S.; Rhim, S. H.; Freeman, A. J.; Ketterson, J. B.; Jang, J. I.; Kanatzidis, M. G. Hybrid Germanium Iodide Perovskite Semiconductors: Active Lone Pairs, Structural Distortions, Direct and Indirect Energy Gaps, and Strong Nonlinear Optical Properties. *J. Am. Chem. Soc.* **2015**, *137* (21), 6804–6819.

(5) Hao, F.; Stoumpos, C. C.; Cao, D. H.; Chang, R. P. H.; Kanatzidis, M. G. Lead-Free Solid-State Organic–inorganic Halide Perovskite Solar Cells. *Nat. Photonics* **2014**, *8* (6), 489–494.

(6) Kociok-Köhn, G.; Winter, J. G.; Filippou, A. C. Trimethylphosphonium Trichlorogermanate(II). *Acta Crystallogr. Sect. C Cryst. Struct. Commun.* **1999**, *55* (3), 351–353.

(7) Bellachioma, G.; Cardaci, G.; Macchioni, A.; Venturi, C.; Zuccaccia, C. Reductive Elimination of Halogens Assisted by Phosphine Ligands in $Fe(CO)_4X_2$ (X=I,Br) Complexes. *J. Organomet. Chem.* **2006**, *691* (18), 3881–3888.

(8) Herrmann, F.; Kuhn, N. Ein Einfacher Zugang Zu Tetramethylphosphoniumiodid/ A Simple Access to Tetramethylphosphonium Iodide. *Zeitschrift für Naturforsch. B.* **2012**, *67* (8), 853–854.

(9) Guthrie, R.; Jenkins, I. The Mechanism of the Mitsunobu Reaction. A ^{31}P N.M.R. Study. *Aust. J. Chem.* **1982**, *35* (4), 767.

(10) Aoyagi, N.; Endo, T. Manufacture of Cyclic Carbonates from Epoxides, Carbon Dioxide, Phosphonium Salts, and Epoxy-Reactive Compounds. WO 2014034936, **2014**.

(11) Langer, J.; Meyer, S.; Dündar, F.; Schowtka, B.; Görls, H.; Westerhausen, M. Dppm-Derived Phosphonium Salts and Ylides as Ligand Precursors for s-Block ` Organometallics. *Issue Honor Prof. Rainer Beckert Ark.* **2012**, 210–225.

(12) Mitzi, D. B.; Feild, C. a.; Harrison, W. T. a.; Guloy, A. M. Conducting Tin Halides with a Layered Organic-Based Perovskite Structure. *Nature* **1994**, *369* (6480), 467–469.

(13) Mitzi, D. B.; Medeiros, D. R.; Malenfant, P. R. L. Intercalated Organic−Inorganic Perovskites Stabilized by Fluoroaryl−Aryl Interactions. *Inorg. Chem.* **2002**, *41* (8), 2134–2145.

(14) Lode, C.; Krautscheid, H.; Müller, U. $[C_3H_7N(C_2H_4)_3NC_3H_7]_2\infty^1[Sn_4I_{12}]$ - Ein Iodostannat Aus Verknöpften SnI_5-Pyramiden. *Zeitschrift für Anorg. und Allg. Chemie*. **2005**, *631* (2–3), 587–591.

(15) Lode, C.; Krautscheid, H. Schwache Sn…I-Wechselwirkungen in Den Kristallstrukturen Der Iodostannate $[SnI_4]^{2-}$ Und $[SnI_3]^-$. *Zeitschrift für Anorg. und Allg. Chemie*. **2000**, *626* (2), 326–331.

(16) Maughan, A. E.; Kurzman, J. A.; Neilson, J. R. Hybrid Inorganic–Organic Materials with an Optoelectronically Active Aromatic Cation: $(C_7H_7)_2SnI_6$ and $C_7H_7PbI_3$. *Inorg. Chem.* **2015**, *54* (1), 370–378.

(17) Apostolico, L.; Kociok-Köhn, G.; Molloy, K. C.; Blackman, C. S.; Carmalt, C. J.; Parkin, I. P. The Reaction of Tin(IV) Iodide with Phosphines: Formation of New Halotin Anions. *Dalt. Trans.* **2009**, No. 47, 10486.

(18) Bartlett, P. N.; Cummings, C. Y.; Levason, W.; Pugh, D.; Reid, G. Halometallate Complexes of Germanium(II) and (IV): Probing the Role of Cation, Oxidation

State and Halide on the Structural and Electrochemical Properties. *Chem. - A Eur. J.* **2014**, *20* (17), 5019–5027.

(19) Ruthe, F. 'Soft–soft' Halogen–halogen Interactions in Solid Ion Pairs of Solvent-Free Pri_3PCl_2 and CH_2Cl_2-Solvated Pri_3PBr_2: Structural Features of Chloro- and Bromo-Triisopropylphosphonium Salts. *Chem. Commun.* **1997**, *113* (20), 1947.

(20) Bandyopadhyay, R.; Nguyen, J. H.; Swidan, A.; Macdonald, C. L. B. Water and Ammonia Complexes of Germanium(II) Dications. *Angew. Chemie Int. Ed.* **2013**, *52* (12), 3469–3472.

(21) Patwardhan, S.; Cao, D. H.; Hatch, S.; Farha, O. K.; Hupp, J. T.; Kanatzidis, M. G.; Schatz, G. C. Introducing Perovskite Solar Cells to Undergraduates. *J. Phys. Chem. Lett.* **2015**, *6* (2), 251–255.

(22) Li, Z.; Yang, M.; Park, J. S.; Wei, S. H.; Berry, J. J.; Zhu, K. Stabilizing Perovskite Structures by Tuning Tolerance Factor: Formation of Formamidinium and Cesium Lead Iodide Solid-State Alloys. *Chem. Mater.* **2016**, *28* (1), 284–292.

(23) Navrotsky, A. Energetics and Crystal Chemical Systematics among Ilmenite, Lithium Niobate, and Perovskite Structures. *Chem. Mater.* **1998**, *10* (10), 2787–2793.

(24) Stoumpos, C. C.; Malliakas, C. D.; Kanatzidis, M. G. Semiconducting Tin and Lead Iodide Perovskites with Organic Cations: Phase Transitions, High

Mobilities, and Near-Infrared Photoluminescent Properties. *Inorg. Chem.* **2013**, *52* (15), 9019–9038.

(25) Fabini, D. H.; Labram, J. G.; Lehner, A. J.; Bechtel, J. S.; Evans, H. A.; Van Der Ven, A.; Wudl, F.; Chabinyc, M. L.; Seshadri, R. Main-Group Halide Semiconductors Derived from Perovskite: Distinguishing Chemical, Structural, and Electronic Aspects. *Inorg. Chem.* **2017**, *56* (1), 11–25.

(26) Jeon, N. J.; Noh, J. H.; Yang, W. S.; Kim, Y. C.; Ryu, S.; Seo, J.; Seok, S. Il. Compositional Engineering of Perovskite Materials for High-Performance Solar Cells. *Nature 2015*, *517* (7535), 476–480.

APPENDICES

Appendix A: Crystallographic Data and Refinement Parameters from Chapter 2

A1: Tetramethylphosphonium Iodide

Table A1: Crystal data and structure refinement for $[PMe_4][I]$.

Identification code	mo_EO36_0m
Empirical formula	$C_4H_{12}IP$
Formula weight	218.01
Temperature/K	170.0
Crystal system	tetragonal
Space group	P4/nmm
a/Å	8.1978(10)
b/Å	8.1978(10)
c/Å	6.0037(8)
α/°	90
β/°	90
γ/°	90
Volume/$Å^3$	403.47(11)
Z	2
$\rho_{calc}g/cm^3$	1.794
μ/mm^{-1}	4.061
F(000)	208.0
Crystal size/mm^3	0.2 × 0.1 × 0.015
Radiation	MoKα (λ = 0.71073)
2Θ range for data collection/°	6.786 to 65.036
Index ranges	$-12 \leq h \leq 10$, $-12 \leq k \leq 12$, $-9 \leq l \leq 9$
Reflections collected	7940
Independent reflections	448 [R_{int} = 0.0702, R_{sigma} = 0.0253]
Data/restraints/parameters	448/0/13
Goodness-of-fit on F^2	1.232
Final R indexes [I>=2σ (I)]	R_1 = 0.0423, wR_2 = 0.0914
Final R indexes [all data]	R_1 = 0.0501, wR_2 = 0.0962
Largest diff. peak/hole / e $Å^{-3}$	2.90/-1.04

A2: Trimethylphosphonium Iodide

Table A2: Crystal data and structure refinement for [$HPMe_3$][I].

Identification code	EO24
Empirical formula	$C_3H_{10}IP$
Formula weight	203.98
Temperature/K	100.01
Crystal system	monoclinic
Space group	$P2_1/m$
a/Å	5.9233(3)
b/Å	8.3560(4)
c/Å	7.0360(4)
α/°	90
β/°	100.9631(17)
γ/°	90
Volume/Å^3	341.89(3)
Z	4
ρ_{calc}g/cm^3	3.963
μ/mm^{-1}	9.571
F(000)	384.0
Crystal size/mm^3	0.254 × 0.239 × 0.171
Radiation	MoKα (λ = 0.71073)
2Θ range for data collection/°	5.898 to 125.772
Index ranges	$-14 \leq h \leq 14$, $-20 \leq k \leq 20$, $-17 \leq l \leq 15$
Reflections collected	58355
Independent reflections	5780 [R_{int} = 0.0288, R_{sigma} = 0.0134]
Data/restraints/parameters	5780/0/33
Goodness-of-fit on F^2	1.303
Final R indexes [I>=2σ (I)]	R_1 = 0.0171, wR_2 = 0.0362
Final R indexes [all data]	R_1 = 0.0199, wR_2 = 0.0369
Largest diff. peak/hole / e Å^{-3}	0.80/-2.67

A3: [(Diphenylphosphino)methyl]methyldiphenylphosphonium iodide

Table A3: Crystal data and structure refinement for $[C_{26}H_{25}P_2][I]$.

Identification code	mo_EO98_0m
Empirical formula	$C_{26}H_{25}IP_2$
Formula weight	526.30
Temperature/K	149.99
Crystal system	triclinic
Space group	P-1
a/Å	8.8787(5)
b/Å	10.7167(6)
c/Å	13.5092(7)
α/°	74.5892(18)
β/°	73.6728(18)
γ/°	79.5436(19)
Volume/Å^3	1181.27(11)
Z	2
ρ_{calc}g/cm^3	1.480
μ/mm^{-1}	1.501
F(000)	528.0
Crystal size/mm^3	0.242 × 0.147 × 0.07
Radiation	MoKα (λ = 0.71076)
2Θ range for data collection/°	5.61 to 66.45
Index ranges	$-13 \leq h \leq 13$, $-16 \leq k \leq 16$, $-20 \leq l \leq 20$
Reflections collected	102260
Independent reflections	9066 [R_{int} = 0.0409, R_{sigma} = 0.0223]
Data/restraints/parameters	9066/0/263
Goodness-of-fit on F^2	1.037
Final R indexes [I>=2σ (I)]	R_1 = 0.0229, wR_2 = 0.0461
Final R indexes [all data]	R_1 = 0.0334, wR_2 = 0.0498
Largest diff. peak/hole / e Å^{-3}	0.44/-0.58

Appendix B: Crystallographic Data and Refinement Parameters from Chapter 3

B1: Tetramethylphosphonium Lead Triiodide

Table B1: Crystal data and structure refinement for $[PMe_4][PbI_3]$.

Identification code	[PMe4][PbI3]
Empirical formula	$C_4H_{12}I_3PPb$
Formula weight	679.00
Temperature/K	170(2)
Crystal system	hexagonal
Space group	$P6_5$
a/Å	10.0382(8)
b/Å	10.0382(8)
c/Å	23.738(2)
α/°	90
β/°	90
γ/°	120
Volume/Å^3	2071.5(4)
Z	6
ρ_{calc}g/cm^3	3.266
μ/mm^{-1}	18.987
F(000)	1752.0
Crystal size/mm^3	0.600 × 0.280 × 0.150
Radiation	MoKα (λ = 0.71073)
2Θ range for data collection/°	5.808 to 61.136
Index ranges	$-14 \leq h \leq 13$, $-14 \leq k \leq 14$, $-33 \leq l \leq 33$
Reflections collected	36416
Independent reflections	4194 [R_{int} = 0.0620, R_{sigma} = 0.0314]
Data/restraints/parameters	4194/1/88
Goodness-of-fit on F^2	1.108
Final R indexes [I>=2σ (I)]	R_1 = 0.0471, wR_2 = 0.1125
Final R indexes [all data]	R_1 = 0.0489, wR_2 = 0.1144
Largest diff. peak/hole / e Å^{-3}	4.45/-4.16
Flack parameter	0.491(10)

B2: Tri(n-butyl)phosphonium Lead Triiodide

Table B2: Crystal data and structure refinement for $[PHBu_3][PbI_3]$.

Identification code	[PHBu3][PbI3]
Empirical formula	$C_{12}H_{28}I_3PPb$
Formula weight	791.20
Temperature/K	170(2)
Crystal system	monoclinic
Space group	$P2_1$
a/Å	16.0770(7)
b/Å	16.3313(9)
c/Å	16.9952(9)
α/°	90
β/°	107.066(2)
γ/°	90
Volume/Å^3	4265.7(4)
Z	8
ρ_{calc}g/cm^3	2.464
μ/mm^{-1}	12.313
F(000)	2848.0
Crystal size/mm^3	0.420 × 0.200 × 0.200
Radiation	MoKα (λ = 0.71073)
2Θ range for data collection/°	5.728 to 61.136
Index ranges	$-22 \leq h \leq 21$, $-23 \leq k \leq 23$, $-24 \leq l \leq 24$
Reflections collected	208613
Independent reflections	25712 [R_{int} = 0.0807, R_{sigma} = 0.0565]
Data/restraints/parameters	25712/105/608
Goodness-of-fit on F^2	1.113
Final R indexes [I>=2σ (I)]	R_1 = 0.0552, wR_2 = 0.1097
Final R indexes [all data]	R_1 = 0.1017, wR_2 = 0.1364
Largest diff. peak/hole / e Å^{-3}	3.76/-4.03
Flack parameter	0.260(7)

B3: Methyltriphenylphosphonium Lead Triiodide

Table B3: Crystal data and structure refinement for $[PMePh_3][PbI_3]$.

Identification code	[PHPh3][PbI3]
Empirical formula	$C_{40}H_{39}I_6NP_2Pb_2$
Formula weight	1771.44
Temperature/K	170(2)
Crystal system	monoclinic
Space group	C2/c
a/Å	24.560(2)
b/Å	13.0686(11)
c/Å	16.1499(14)
α/°	90
β/°	110.037(2)
γ/°	90
Volume/$Å^3$	4869.8(7)
Z	4
$\rho_{calc}g/cm^3$	2.416
μ/mm^{-1}	10.802
F(000)	3192.0
Crystal size/mm^3	0.530 × 0.500 × 0.470
Radiation	MoKα (λ = 0.71073)
2Θ range for data collection/°	5.932 to 66.52
Index ranges	$-37 \leq h \leq 37$, $-20 \leq k \leq 20$, $-24 \leq l \leq 24$
Reflections collected	76614
Independent reflections	9334 [R_{int} = 0.0564, R_{sigma} = 0.0331]
Data/restraints/parameters	9334/0/254
Goodness-of-fit on F^2	1.154
Final R indexes [I>=2σ (I)]	R_1 = 0.0371, wR_2 = 0.0783
Final R indexes [all data]	R_1 = 0.0522, wR_2 = 0.0854
Largest diff. peak/hole / e $Å^{-3}$	2.50/-4.19

B4: Bis(trimethylphosphonio)ethane Lead Triiodide

Table B4: Crystal data and structure refinement for $[Me_3PC_2H_4PMe_3][PbI3]_2$.

Identification code	[Me3PC2H4PMe3][PbI3]2
Empirical formula	$C_8H_{22}I_6P_2Pb_2$
Formula weight	1355.97
Temperature/K	170(2)
Crystal system	monoclinic
Space group	C2/m
a/Å	15.3593(6)
b/Å	11.1506(4)
c/Å	7.9441(3)
α/°	90
β/°	100.8890(10)
γ/°	90
Volume/$Å^3$	1336.05(9)
Z	2
$\rho_{calc}g/cm^3$	3.371
μ/mm^{-1}	19.626
F(000)	1164.0
Crystal size/mm^3	0.5 × 0.4 × 0.3
Radiation	MoKα (λ = 0.71073)
2Θ range for data collection/°	6.526 to 66.356
Index ranges	$-22 \leq h \leq 23$, $-17 \leq k \leq 15$, $-12 \leq l \leq 12$
Reflections collected	33343
Independent reflections	2676 [R_{int} = 0.0498, R_{sigma} = 0.0228]
Data/restraints/parameters	2676/18/71
Goodness-of-fit on F^2	1.062
Final R indexes [I>=2σ (I)]	R_1 = 0.0296, wR_2 = 0.0661
Final R indexes [all data]	R_1 = 0.0409, wR_2 = 0.0718
Largest diff. peak/hole / e $Å^{-3}$	3.19/-3.02

Appendix C: Crystallographic Data and Refinement Parameters from Chapter 4

C1: $[HPMe_3]_4[I][SnI_5]$

Table C1: Crystal data and structure refinement for $[HPMe_3]_4[I][SnI_5]$.

Identification code	mo_EO20_ye
Empirical formula	$C_{12}H_{40}I_6P_4Sn$
Formula weight	1188.41
Temperature/K	173.2
Crystal system	tetragonal
Space group	P4/nmm
a/Å	15.7178(6)
b/Å	15.7178(6)
c/Å	6.8796(2)
α/°	90
β/°	90
γ/°	90
Volume/Å^3	1699.60(14)
Z	2
ρ_{calc}g/cm^3	2.322
μ/mm^{-1}	6.389
F(000)	1080.0
Crystal size/mm^3	0.33 × 0.216 × 0.16
Radiation	MoKα (λ = 0.71073)
2Θ range for data collection/°	5.922 to 72.676
Index ranges	$-26 \leq h \leq 26$, $-26 \leq k \leq 26$, $-11 \leq l \leq 10$
Reflections collected	36211
Independent reflections	2266 [R_{int} = 0.0341, R_{sigma} = 0.0125]
Data/restraints/parameters	2266/0/41
Goodness-of-fit on F^2	1.221
Final R indexes [I>=2σ (I)]	R_1 = 0.0313, wR_2 = 0.0724
Final R indexes [all data]	R_1 = 0.0368, wR_2 = 0.0755
Largest diff. peak/hole / e Å^{-3}	0.92/-2.68

C2: [(O=PMe$_3$)$_3$SnI$_3$]$_2$[SnI$_6$]

Table C2: Crystal data and structure refinement for [(O=PMe$_3$)$_3$SnI$_3$]$_2$[SnI$_6$].

Identification code	EO33
Empirical formula	$C_{18}H_{54}I_{12}O_6P_6Sn_3$
Formula weight	2431.41
Temperature/K	170.2
Crystal system	trigonal
Space group	P-3
a/Å	14.6186(9)
b/Å	14.6186(9)
c/Å	8.0358(5)
α/°	90
β/°	90
γ/°	120
Volume/Å^3	1487.21(16)
Z	1.00002
ρ_{calc}g/cm^3	2.7146
μ/mm^{-1}	7.664
F(000)	1080.3
Crystal size/mm^3	N/A × N/A × N/A
Radiation	Mo Kα (λ = 0.71073)
2Θ range for data collection/°	6 to 72.78
Index ranges	$-24 \leq h \leq 24$, $-24 \leq k \leq 24$, $-13 \leq l \leq 13$
Reflections collected	41240
Independent reflections	4706 [R_{int} = 0.0456, R_{sigma} = 0.0303]
Data/restraints/parameters	4706/0/72
Goodness-of-fit on F^2	1.010
Final R indexes [I>=2σ (I)]	R_1 = 0.0742, wR_2 = 0.1905
Final R indexes [all data]	R_1 = 0.0886, wR_2 = 0.1990
Largest diff. peak/hole / e Å^{-3}	6.73/-5.20

C3: [PMePh$_3$][SnI$_5$]

Table C3: Crystal data and structure refinement for [PMePh$_3$][SnI$_5$].

Identification code	EO88_P-1
Empirical formula	$C_{19}H_{18}I_5PSn$
Formula weight	1030.49
Temperature/K	169.9
Crystal system	triclinic
Space group	P-1
a/Å	8.7605(6)
b/Å	11.4468(8)
c/Å	14.5308(10)
α/°	108.587(2)
β/°	90.102(2)
γ/°	108.424(2)
Volume/Å^3	1301.80(16)
Z	2
ρ_{calc}g/cm^3	2.629
μ/mm^{-1}	6.975
F(000)	924.0
Crystal size/mm^3	0.26 × 0.24 × 0.09
Radiation	MoKα (λ = 0.71073)
2Θ range for data collection/°	5.72 to 61.184
Index ranges	$-12 \leq h \leq 12$, $-16 \leq k \leq 16$, $-20 \leq l \leq 20$
Reflections collected	115514
Independent reflections	7958 [R_{int} = 0.0615, R_{sigma} = 0.0223]
Data/restraints/parameters	7958/0/236
Goodness-of-fit on F^2	1.063
Final R indexes [I>=2σ (I)]	R_1 = 0.0300, wR_2 = 0.0667
Final R indexes [all data]	R_1 = 0.0398, wR_2 = 0.0730
Largest diff. peak/hole / e Å^{-3}	1.24/-1.81

Appendix D: Crystallographic Data and Refinement Parameters from Chapter 5

D1: Trimethylphosphonium Triiodogermanate

Table D1: Crystal data and structure refinement for $[HPMe_3][GeI_3]$.

Identification code	mo_EO31_0m
Empirical formula	$C_3H_{10}GeI_3P$
Formula weight	530.37
Temperature/K	170.0
Crystal system	orthorhombic
Space group	$P2_12_12_1$
a/Å	7.6701(3)
b/Å	9.9946(5)
c/Å	15.7148(7)
α/°	90
β/°	90
γ/°	90
Volume/Å^3	1204.69(9)
Z	4
ρ_{calc}g/cm^3	2.924
μ/mm^{-1}	10.300
F(000)	936.0
Crystal size/mm^3	0.24 × 0.222 × 0.18
Radiation	MoKα (λ = 0.71073)
2Θ range for data collection/°	5.91 to 63.048
Index ranges	$-11 \leq h \leq 11$, $-14 \leq k \leq 14$, $-23 \leq l \leq 23$
Reflections collected	21820
Independent reflections	4031 [R_{int} = 0.0334, R_{sigma} = 0.0258]
Data/restraints/parameters	4031/0/80
Goodness-of-fit on F^2	1.213
Final R indexes [I>=2σ (I)]	R_1 = 0.0298, wR_2 = 0.0752
Final R indexes [all data]	R_1 = 0.0320, wR_2 = 0.0759
Largest diff. peak/hole / e Å^{-3}	1.25/-1.51
Flack parameter	0.056(9)

D2: Tetramethylphosphonium Tribromogermanate

Table D2: Crystal data and structure refinement for $[PMe_4][GeBr_3]$.

Identification code	EO116_R3
Empirical formula	$C_4H_{12}Br_3GeP_{0.33}$
Formula weight	382.78
Temperature/K	170.0
Crystal system	trigonal
Space group	R3
a/Å	9.7407(6)
b/Å	9.7407(6)
c/Å	10.8858(8)
α/°	90
β/°	90
γ/°	120
Volume/Å^3	894.48(13)
Z	3
ρ_{calc}g/cm^3	2.132
μ/mm^{-1}	12.601
F(000)	534.0
Crystal size/mm^3	0.308 × 0.122 × 0.118
Radiation	MoKα (λ = 0.71073)
2Θ range for data collection/°	6.11 to 58.292
Index ranges	$-13 \leq h \leq 13$, $-13 \leq k \leq 13$, $-14 \leq l \leq 14$
Reflections collected	7301
Independent reflections	1078 [R_{int} = 0.0447, R_{sigma} = 0.0319]
Data/restraints/parameters	1078/1/30
Goodness-of-fit on F^2	1.069
Final R indexes [I>=2σ (I)]	R_1 = 0.0239, wR_2 = 0.0503
Final R indexes [all data]	R_1 = 0.0302, wR_2 = 0.0522
Largest diff. peak/hole / e Å^{-3}	0.52/-0.62
Flack parameter	0.030(11)

D3: [PPh_4][I](GeI_4)

Table D3: Crystal data and structure refinement for [PPh_4][I](GeI_4)$_2$.

Identification code	EO128 _P21n_a
Empirical formula	$C_{96}H_{80}Ge_4I_{20}P_4$
Formula weight	4185.3
Temperature/K	170.0
Crystal system	monoclinic
Space group	P21/n
a/Å	9.6682(5)
b/Å	15.2669(7)
c/Å	20.8344(10)
α/°	90
β/°	101.009
γ/°	90
Volume/Å^3	3018.6
Z	1
ρ_{calc}g/cm^3	2.303
μ/mm^{-1}	6.192
F(000)	1904.0
Crystal size/mm^3	0.33 × 0.22 × 0.11
Radiation	MoKα (λ = 0.71073)
2Θ range for data collection/°	5.696 to 66.502
Index ranges	$-14 \leq h \leq 14$, $-23 \leq k \leq 23$, $-32 \leq l \leq 32$
Reflections collected	95509
Independent reflections	11582 [R_{int} = 0.0402, R_{sigma} = 0.0274]
Data/restraints/parameters	11582/0/125
Goodness-of-fit on F^2	2.424
Final R indexes [I>=2σ (I)]	R_1 = 0.0966, wR_2 = 0.3019
Final R indexes [all data]	R_1 = 0.1248, wR_2 = 0.3244
Largest diff. peak/hole / e Å^{-3}	11.69/-11.76

D4: [PMePh$_3$][I](GeI$_4$)$_2$

Table D4: Crystal data and structure refinement for [PMePh$_3$][I](GeI$_4$)$_2$.

Identification code	mo_EO79_0m
Empirical formula	$C_{19}H_{18}Ge_2I_9P$
Formula weight	1564.58
Temperature/K	150.0
Crystal system	triclinic
Space group	P-1
a/Å	10.5704(11)
b/Å	13.4412(12)
c/Å	14.2976(14)
α/°	110.046(3)
β/°	95.418(3)
γ/°	105.634(3)
Volume/Å^3	1798.1(3)
Z	2
ρ_{calc}g/cm^3	2.890
μ/mm^{-1}	9.451
F(000)	1376.0
Crystal size/mm^3	0.333 × 0.207 × 0.074
Radiation	MoKα (λ = 0.71076)
2Θ range for data collection/°	5.418 to 69.056
Index ranges	$-16 \leq h \leq 16$, $-21 \leq k \leq 21$, $-22 \leq l \leq 22$
Reflections collected	153104
Independent reflections	15146 [R_{int} = 0.0659, R_{sigma} = 0.0355]
Data/restraints/parameters	15146/0/281
Goodness-of-fit on F^2	1.135
Final R indexes [I>=2σ (I)]	R_1 = 0.0481, wR_2 = 0.0981
Final R indexes [all data]	R_1 = 0.0799, wR_2 = 0.1188
Largest diff. peak/hole / e Å^{-3}	2.83/-3.37

D5: $[C_8H_{22}P_2][I]_2(GeI_4)$

Table D5: Crystal data and structure refinement for $[C_8H_{22}P_2][I]_2(GeI_4)$.

Identification code	mo_EO65_0m
Empirical formula	$C_8H_{22}GeI_6P_2$
Formula weight	1014.18
Temperature/K	170.0
Crystal system	orthorhombic
Space group	Pnn2
a/Å	18.6739(9)
b/Å	18.674
c/Å	6.7970(4)
α/°	90
β/°	90
γ/°	90
Volume/Å^3	2370.21(18)
Z	4
ρ_{calc}g/cm^3	2.842
μ/mm^{-1}	9.229
F(000)	1800.0
Crystal size/mm^3	? × ? × ?
Radiation	MoKα (λ = 0.71073)
2Θ range for data collection/°	6.17 to 72.884
Index ranges	$-29 \leq h \leq 31$, $-30 \leq k \leq 30$, $-11 \leq l \leq 10$
Reflections collected	50964
Independent reflections	11232 [R_{int} = 0.1521, R_{sigma} = 0.0786]
Data/restraints/parameters	11232/1/160
Goodness-of-fit on F^2	1.035
Final R indexes [I>=2σ (I)]	R_1 = 0.0635, wR_2 = 0.1482
Final R indexes [all data]	R_1 = 0.0799, wR_2 = 0.1570
Largest diff. peak/hole / e Å^{-3}	2.81/-6.12
Flack parameter	0.03(3)

VITA AUCTORIS

NAME:	Emily Helen Omahen
PLACE OF BIRTH:	Windsor, ON
YEAR OF BIRTH:	1994
EDUCATION:	St. Anne Catholic High School, Lakeshore, ON, 2012
	University of Windsor, B.Sc., Windsor, ON, 2016
	University of Windsor, M.Sc., Windsor, ON, 2018 (pending)